Structural analysis of the multi-layer bellows in the ball valves

Von der Fakultät Energie-, Verfahrens- und Biotechnik der Universität Stuttgart zur Erlangung der Würde eines Doktors der Ingenieurwissenschaften (Dr.-Ing.) genehmigte Abhandlung

vorgelegt von
Dipl.-Ing. Andrey Oleynikov

Geboren in Wolgograd, Russland

Vorsitzender:	Prof. Dr.-Ing. Ulrich Nieken
Hauptberichter:	Prof. Dr.-Ing. habil. Clemens Merten
Mitberichter:	Prof. Dr.-Ing. Thomas Maier

Tag der mündlichen Prüfung: 11.10.2023
Institut für Chemische Verfahrenstechnik der Universität Stuttgart

Oktober 2023

Vorwort

Diese Doktorarbeit entstand im Rahmen meiner Tätigkeit als wissenschaftlicher Mitarbeiter an der Universität Stuttgart im Institut für Chemische Verfahrenstechnik und an der Staatlichen Technischen Universität Wolgograd im Institut für Apparate und Verfahren der Chemischen Industrie.

Ich bedanke mich herzlich bei Professor Dr.-Ing. habil. Clemens Merten für die Unterstützung und Betreuung der Arbeit und für die Möglichkeit am Institut für Chemische Verfahrenstechnik als wissenschaftlicher Mitarbeiter tätig zu sein. Ein besonderer Dank geht an Professor Dr.-Ing. Maier, Leiter des Forschungs- und Lehrgebiets Technisches Design, für die umfassende Unterstützung und die Begleitung dieser Arbeit. Ich danke Professor Alexander Golovanchikov für die Zusammenarbeit bei den ersten Schritten und seinem Interesse an diesem Thema.

Ich bedanke mich bei Professor Ulrich Nieken, Leiter des Instituts für Chemische Verfahrenstechnik. Mein Dank geht an Thomas Lorenz, Boris Binder und Holger Aschenbrenner für die technische Unterstützung beim Aufbau der Versuchsanlage. Ich danke den Mitarbeiterinnen und Mitarbeitern des Instituts für ihr Vertrauen und freundschaftliche Unterstützung.

Ich bedanke mich bei Matthias Konstantin, Yao Wang, Leticia Ninzeko, Jasmin Kaiser, Julian Lauff, Florian Vogt, Michael Rauter, Thobias Thiemt, Francis Wamy, Linda Werneck, Georg von Blumental, Birgit Salzmann, Marc Buschlüter und Felix Weinhardt, die durch ihre Abschlussarbeiten, Semester-Projektarbeiten und wissenschaftlichen-Tätigkeiten zu dieser Doktorarbeit beigetragen haben.

Ich danke meinen Kollegen Navid Ghavami und Umer Afzal, die mich in die ICVT-Tätigkeiten eingearbeitet und mir geholfen haben.

Noch ein besonderer Dank gilt Dr.-Ing. Thomas Böhmer, Peter Pilapl, Georg Schreiner, Helmut Ringel, Eicke Kobbe, Dr.-Ing. Wolfgang Radisch, Mathias Dragojlovic, Dr.-Ing. Jan Hommel, Dr.-Ing. Christian Sivers und vielen anderen Mitarbeiterinnen und Mitarbeitern des Unternehmens Böhmer GmbH für die gute Einführung in den Armaturenbau und das neue Wissen, welches ich aus meiner Tätigkeit in diese Doktorarbeit einbringen konnte.

Ich danke meinen Eltern, Natalia Oleynikova und Vladimir Oleynikov, für die Motivation und die finanzielle Unterstützung während meines Studiums, durch die diese Arbeit erst möglich wurde. Ein besonderer Dank gilt meiner Freundin Gina Günther, die mich viel bei der Doktorarbeit unterstützt hat.

Zusammenfassung

Armaturen sind unentbehrliche Komponenten der Industrierohrleitungen und Industrieanlagen. Bekannt sind verschiedene Grundtypen und Konstruktionsformen wie Ventile, Hähne, Schieber und Klappen, die für unterschiedliche Funktionen (wie regeln, absperren und dosieren), Betriebsbedingungen (wie Druck- und Temperaturbereiche) und Fluide (Gase, Flüssigkeiten und Dämpfe) eingesetzt werden.

Auf dem Markt für Armaturen erscheinen immer wieder neue Typen von Armaturen, die von der modernen Industrie benötigt werden. Abhängig von den spezifischen Anforderungen wird die zum Einsatz kommende Armatur bestimmt. Spezifische Anforderungen ergeben sich z. B. aus einem hohen Betriebsdruck, hohen oder niedrigen Betriebstemperaturen oder aggressiven Medien, wie z. B. Ethanol und Säuren.

Eine Möglichkeit, die Anzahl der Ausführungen zu reduzieren, ist die Entwicklung von Armaturen, welche möglichst viele Betriebsbedingungen, z. B. Hoch- und Tieftemperaturbereiche als auch aggressive Medien, abdecken. Um hierbei die Kosten nicht zu hoch werden zu lassen, ist die Armatur möglichst effizient zu gestalten. Entscheidend hierfür sind das Design und die Auswahl der eingesetzten Materialien.

Die Armaturen haben meistens eine Spindel, die mit einem Antriebsmechanismus, z. B. mit einer Kupplung, einem Getriebe, einem Handrad oder -griff betätigt wird. Die Dichtheit der Spindel und ihre Schaltbarkeit zur Änderung der Stellung des Durchgangs (geschlossen/geöffnet) muss sichergestellt bleiben. Die Dichtelemente sorgen für die Abdichtung der Spindel. Die Dichtelemente, wie z. B. Dichtringe und O-Ringe sind aus Kunststoff und werden oft aus Polymeren, Elastomeren oder Gummi hergestellt. Diese Materialien können aufgrund ihrer mechanischen und chemischen Eigenschaften weder für Hoch- noch für Tieftemperaturanwendungen und nur eingeschränkt für aggressive Medien eingesetzt werden.

Entscheidend für den Beginn dieser Arbeit war, dass bei den praktischen Erfahrungen im Chemiewerk „Nikochem Group“ in Wolgograd, Russland, festgestellt wurde, dass viele Armaturen nach mehrmonatigem Betrieb aufgrund nachlassender technischer Leistungsfähigkeit ausgetauscht werden mussten. Die Polymer- oder Elastomer-Dichtelemente konnten aggressiven Medien nicht widerstehen und wurden nach einiger Zeit entweder beschädigt oder vollständig verschwanden. Die konstruktiven metallischen Elemente der

Armaturen waren funktionsfähig, aber es traten die Leckagen in den Flanschen, den Spindeln und den Kugeln auf. Daher erfüllten die Armaturen ihre Anwendungsaufgaben nicht mehr. Die Reparatur erforderte hohe Kosten, folglich war der Austausch der Armaturen eine billigere und schnellere Lösung.

Um dieses Problem zu lösen, war es notwendig, ein Armaturdesign zu entwickeln, welches nichtmetallische Dichtungselemente enthält und die Möglichkeit hat, in einem breiten Spektrum von aggressiven Medien und Temperaturverhältnissen zu funktionieren.

Damit die Dichtheitsprobleme der Kunststoffdichtungen und O-Ringe in diesem Armaturbereich gelöst werden können, wurden folgende drei Gebrauchsmuster entwickelt: Gebrauchsmuster № 107836 „Ventil“, 29.03.2011, Gebrauchsmuster № 123877 „Ventil mit Kompensator“, 10.01.2013; Gebrauchsmuster № 139949 „Kugelhahn mit Ratschengetriebe“, 03.27.2014. In den genannten Gebrauchsmustern sind alle drucktragenden Bauteile nach außen hin verschweißt. Der Kompensator dient als Hauptdichtelement in den Konstruktionen. Dies garantiert ihre absolute Dichtheit und macht die Notwendigkeit der Kunststoffdichtungen und O-Ringe in dem Spindelbereich obsolet.

Die genannten Konstruktionen der Armaturen widerstehen hohen und niedrigen Temperaturen, haben eine Korrosionsbeständigkeit für ein breites Spektrum von Medien und eine lange Lebensdauer.

Im Rahmen dieser Arbeit wird stellvertretend der „Kugelhahn mit Ratschengetriebe“, Gebrauchsmuster № 139949, 03.27.2014, in Funktion und Auslegung näher untersucht. Die anderen entwickelten Ventilkonstruktionen „Ventil“, Gebrauchsmuster № 107836, 29.03.2011, und „Ventil mit Kompensator“ Gebrauchsmuster № 123877, 10.01.2013, werden wegen ihrer komplizierten Konstruktion, den hohen Produktionskosten und ihrer spezifischen Ausführung in dieser Arbeit nicht näher betrachtet.

Die entwickelte Konstruktion des Kugelhahns mit Ratschengetriebe, Gebrauchsmuster № 139949, wird umfassend betrachtet, ausgelegt und dimensioniert. Ebenfalls wird eine Produktionsserie des Kugelhahns mit Nenndurchmesser 100 mm, 150 mm, 200 mm und 300 mm ausgelegt und nachgewiesen.

Um die Leistungsfähigkeit, die Funktionalität und die Dichtheit für die entwickelte Konstruktion des Kugelhahns mit Ratschengetriebe nachzuweisen, werden die analytischen Berechnungen, die experimentellen Versuche und die Finite Elemente Analyse (FEA) bereitgestellt.

Eingangs werden die analytischen Berechnungen der gesamten Konstruktion des Kugelhahns einschließlich Ratschengetriebe durchgeführt. Während dieser analytischen Betrachtung werden die Schwachpunkte der Konstruktion ermittelt, die später genauer analysiert werden. Für detaillierte Ergebnisse der belasteten Elemente der Konstruktion werden verschiedene Konstruktionsparameter berücksichtigt. Für das Ratschengetriebe werden geometrische Eigenschaften wie der Durchmesser der Zahnräder, deren Breite, die Anzahl der Zähne und die Größe der Klinke ausgelegt.

Für die ein- und mehrlagigen Kompensatoren mit U-förmigem Balgprofil werden Berechnungen mit Spannungsnachweisen durchgeführt und die geometrischen Eigenschaften für den entsprechenden Betriebsfall optimiert. Für die Kompensatoren werden ebenfalls geometrische Eigenschaften berücksichtigt, wie z. B. die Anzahl der Balgwellen, der innere und äußere Durchmesser und die Anzahl der Schichten der Balgwelle.

Deswegen sind die Sicherheit und Leistung des Kugelhahns mit Ratschengetriebe direkt an die Betriebsbelastungen für die ein- und mehrlagigen Kompensatoren mit U-förmigem Balgprofil gebunden, wie z. B. Betriebstemperatur und Innendruck.

Die möglichen Betriebsfälle, geometrischen Eigenschaften und Spannungsnachweise für die ein- und mehrlagigen Kompensatoren mit U-förmigem Balgprofil werden in Kapitel 3 diskutiert. Diese Analyse basiert auf der Berechnungsmethode für die Kompensatoren nach der Norm EN ISO DIN 13445 Teil 3 [21].

Die Belastung mit dem Innendruck wird mit den genannten Berechnungsmethoden analysiert und die Ergebnisse werden mit den experimentellen Untersuchungen und den Simulationsergebnissen der Finite Elemente Methode (FEM) verglichen.

Die Konstruktion des Kugelhahns mit Ratschengetriebe wird in Kapitel 3 beschrieben. Um die Lasten der Kompensatoren zu analysieren, wird nachfolgend die exakte Funktionalität der Ratschengetriebe mit dem Kompensator erklärt. Die Spindel ist mit einem Zweiflach an der Kugel eingesetzt. Damit die Kugel rotiert werden die Ratschenzahnräder mit Hilfe einer Passfeder an der Spindel angesetzt. Die Klinken rotieren die Zahnräder und sind an dem Hebelarm mit einer Verschraubung befestigt. Der Hebelarm bewegt sich in einem Winkel (circa 10 °), sodass die Klinke permanent einen Kontakt zum Zahnrad hat. Wenn der Kontakt zwischen Klinke und Zahnrad verloren ist, bewegt sich der Hebel auf die Null-Position. Danach wiederholen sich die Zyklen, bis die Kugel entweder die geschlossene oder die geöffnete Position in dem Durchgang des Kugelhahnes erreicht hat.

Der Kompensator ist auf das Gehäuse des Ratschengetriebes und auf den Hebelarm geschweißt. Deswegen biegt sich der Kompensator durch die zyklischen Bewegungen des Hebelarmes zu dem entsprechenden Winkel. Außerdem verbindet sich der Hebelarm mit dem Gelenkkopf, welcher in der Mitte der Horizontalen des Rohrteils des Gehäuses des Ratschengetriebes angeschweißt ist. Wegen diesem Lagerungsfall kann der Biegungsfall des Kompensators nur eingeschränkt analytisch betrachtet werden. Deshalb können die genannten Berechnungsmethoden für den Biegefall des Kompensators nicht eindeutig herangezogen werden. Hierfür werden von zwei Biegungsfällen Vergleichsspannungen nach der DIN EN ISO 13445 Teil 3 ermittelt, welche Lateral- und Angular-Bewegungen sind. Die ermittelten Werte werden aus den experimentellen Untersuchungen und den Simulationsergebnissen der Finite-Elemente-Methode (FEM) bestimmt.

Um diese komplizierte Methode für die entwickelten Gebrauchsmuster zu vermeiden, wird im nächsten Schritt für eine genauere und schnellere Analyse von ein- und mehrlagigen Kompensatoren mit U-förmigem Balgprofil eine neue Berechnungsmethode entwickelt. Damit kann die Vergleichsspannung auf jedem Punkt des Kompensatorbalges berücksichtigt werden.

Die neue Berechnungsmethode basiert auf der Theorie von R. A. Clark „On the theory of thin toroidal shells“. Mit dieser neuen Berechnungsmethode werden die kritischen Stellen der ein- und mehrlagigen Kompensatorbalge mit U-förmigem Profil ermittelt und darauf basierend eine analytische Optimierung der Geometrie des Faltenbalg-Kompensators vorgenommen. Diese beinhaltet die Ermittlung ihrer Abmessung beim maximalen Belastungsfall. Die Optimierung der Kompensatorabmessungen wird im Folgenden detaillierter mit FEM überprüft und verbessert.

Die Laborversuche werden in zwei Schritten durchgeführt. Zuerst wird die Funktionsweise des Kugelhahnes mit Ratschengetriebe und zweilagigem Faltenbalg-Kompensator untersucht. Hierbei werden die Lebenszyklen des Ratschengetriebes und des zweilagigen Kompensators mit U-förmigen Balgprofil getestet. Außerdem wird die Biegung des Faltenbalg-Kompensators betrachtet und ermittelt, die anschließend analytisch und mit Hilfe der FEM berechnet wird.

Der zweite Schritt beinhaltet die experimentelle Untersuchung des zweilagigen Faltenbalg-Kompensators unter Innendruck sowie bei Biegung. Die Spannungs-Messungen am äußeren Kompensatorbalg werden mit Dehnungsmessstreifen durchgeführt. Der innere Kompensatorbalg, an dem die höchsten Spannungen auftreten, wird analytisch und mit FEM Simulationen untersucht.

Die Funktionalität des Gesamtmechanismus des Kugelhahns mit dem Ratschengetriebe, Faltenbalg-Kompensator und Hebel wird berechnet. Mit der FEM Simulation wird ebenfalls das Ratschengetriebe im Zusammenspiel mit ein- und mehrlagigen U-förmigen Kompensatoren untersucht und überprüft. Hierbei werden als Schwachstellen das Ratschengetriebe und der Kompensator identifiziert. Außerdem wird das Worst-Case-Szenario für das Ratschengetriebe und den Kompensator betrachtet. Dafür wird das Verhalten des Gehäuses, der Zahnräder und der Klinke unter maximaler Last untersucht.

Für die Bestimmung der maximalen Lasten des Ratschengetriebes und der Faltenbalg-Kompensatoren wird die Gestaltänderungsenergiehypothese (GEH) angewandt. Die, durch die FEM berechneten, Vergleichsspannungen werden an den kritischen Stellen und unter angenommenen Festigkeitsbedingungen linearisiert. Dadurch können die elastischen Grenzlasten bestimmt werden.

In den FEM Simulationen wird das Verhalten der ein-, zwei- und dreilagigen Faltenbalg-Kompensatoren mit U-förmigem Profil für verschiedene Lastbedingungen untersucht.

Die Lastbedingungen, welche auf die Faltenbalg-Kompensatoren aufgebracht werden, sind i) Temperaturen von 20 bis 500 °C, ii) Innendruck von 0,3 bis 2 MPa gemäß DIN EN ISO 1333 und API 6D und iii) Biegungen bis zu 10 °. Die Auswirkungen dieser Lasten werden jeweils einzeln ermittelt und als Worst-Case-Szenario wird das gleichzeitige Einwirken der jeweiligen Maximallasten untersucht.

Am Ende werden die Ergebnisse der verschiedenen Berechnungsmethoden, der Versuche und FEM Simulationen miteinander verglichen. Dabei werden zwischen den Ergebnissen der verschiedenen Methoden (theoretisch, experimentell und simulativ) keine signifikanten Abweichungen festgestellt. Die untersuchten zwei- und dreilagigen Faltenbalg-Kompensatoren können unter den zuvor beschriebenen maximalen Lastbedingungen eingesetzt werden.

Als Standard für das genannte Gebrauchsmuster № 139949 „Kugelhahn mit Ratschengetriebe“ wird der zweilagige Kompensator mit U-förmigem Profil gewählt, welcher zufriedenstellend bei dem untersuchten Innendruck, hohen und tiefen Temperaturen und der Biegung funktioniert. Für den zweilagigen Kompensator mit U-förmigem Profil werden Lebenszyklen, für normale Bedingungen (hohe Temperatur und Biegung) und für das Worst-Case-Szenario, mit maximalem Innendruck, Biegung und hoher Temperatur berechnet.

Der einlagige Faltenbalg-Kompensator kann wegen der mechanischen Eigenschaften der Biegung nicht widerstehen. Die drei-, vier- und fünflagigen Kompensatoren werden aufgrund

ihrer Kosten verworfen.

Abschließend wird eine Serie neuer Kugelhähne mit Ratschenantrieb in den Nenndurchmessern 100 mm, 150 mm, 200 mm und 300 mm nach EN 1983:2013 „Industriearmaturen-Kugelhähne aus Stahl“ ausgelegt und nachgewiesen, dies entspricht nach API 6D 4”, 6”, 8” und 12”. In dieser genannten Konstruktionsserie wird der zuvor untersuchte zweilagige Kompensator mit U-förmigem Profil verwendet.

Die Neuentwicklung kann für Hoch- und Tieftemperaturanwendungen, als auch für aggressive Medien eingesetzt werden, sowie für die Nuklear-, Chemische-, Öl-, Gasindustrie und im Wasserstoffbereich.

Content

Glossary

Abbreviation

FEA	Finite element analysis
ANSYS®	Finite element software package
3D	Three dimensional
CAD	Computer assisted design
MatLab®	Matrix Laboratory software package
Ltd.	Limited company
Inventor®	CAD software package
Creo Parametric®	CAD software package
SG	Strain gauges
Gantner Instruments®	Test and measurement technology systems (modules)
RGM	Ratchet Gear Mechanism
ABAQUS	Finite element software package
ETS	Equivalent tensile stress

Latin symbols

A	$[mm^2]$	Cross-sectional area of the material of a bellows corrugation
$A_{SeatArea}$	$[mm^2]$	Pressure influencing area of the seat
A_{fS}	$[mm^2]$	Ball valve's body stress loaded cross section area
A_{pS}	$[mm^2]$	Ball valve body pressure loaded area
A_{fb}	$[mm^2]$	Nozzle stress loaded cross section area
A_{pb}	$[mm^2]$	Nozzle pressure loaded area
A_{fW}	$[mm^2]$	Cross section area of filled weld seam between ball valve's body and nozzle

$A_{f,VS}$	[mm^2]	RGM vertical shell stress loaded cross section area
$A_{p,VS}$	[mm^2]	RGM vertical shell pressure loaded cross section area
$A_{f, Hb}$	[mm^2]	RGM horizontal shell stress loaded cross section area
$A_{p, Hb}$	[mm^2]	RGM horizontal shell pressure loaded cross section area
A_{fWRGM}	[mm^2]	Cross section area of filled weld seam between vertical and horizontal shells of RGM
A_G	[mm^2]	Cross section of ratchet wheel tooth
A_b	[°]	Angle of pawl's body
A_t	[°]	Angle of pawl's tooth
a, a´	[mm]	Radius from middle line to the centre of investigated bellows corrugation
a_G	[mm]	Length of the ratchet wheel tooth
a_p	[mm]	Length of the pawl's tooth
b	[mm]	Internal radius of bellows corrugation
b_K	[-]	Conical calculation coefficient
b_{GK}	[mm]	Width of the key's pass for ratchet wheel
b_G	[mm]	Width of the ratchet wheel
b_p	[mm]	Width of the pawl
B	[mm]	Width of the rod end bearing's ball ring
C_1, C_2	[-]	Coefficients for determining C_P, C_f, C_d
$C_{1RB\ max}$	[mm]	Width of the rod end bearing's head
C_p, C_f, C_d	[-]	Coefficients for determining the stresses in bellows
C_r	[mm]	Thickness of the rod end bearing's head
c_{1i}	[-]	Stem square shape torsion factor 1 for analysis of

		polar section modulus
c_{2i}	[-]	Stem square shape torsion factor 2i for analysis of polar section modulus
c_1	[-]	Tolerance coefficient of ball valve's body
c_2	[-]	Corrosion and wear coefficient of ball valve's body
d	[mm]	Diameter of a rod end bearing's ball
d_k	[mm]	Head ball diameter of rod end bearing
d_{seat}	[mm]	Diameter of the seat
$d_{seat\ contact}$	[mm]	Diameter of seat contact to ball
DN	[mm]	Nominal diameter of a valve
D_{ball}	[mm]	Diameter of the ball (obturator)
d_1	[mm]	Diameter of stem section 1
d_{1r}	[mm]	Diameter of stem section 1 without key seats
d_2	[mm]	Diameter of stem section 2
d_3	[mm]	Diameter of stem section 3
d_4	[mm]	Diameter of 2-flat-end
d_i	[mm]	Ball valve body internal diameter
d_o	[mm]	Ball valve body outer diameter
$d_{i,s}$	[mm]	Body internal diameter for nozzle validation
$d_{i,b}$	[mm]	Nozzle internal diameter
d_{con}	[mm]	Relevant diameter of conical side part
d_S	[mm]	Diameter of the bolt
d_{2RB}	[mm]	Rod end bearing's head diameter
D_1	[mm]	Diameter of RGM vertical shell
D_2	[mm]	Diameter of RGM horizontal shell
D_a	[mm]	Outer diameter of the bellows corrugation

D_i	[mm]	Inner diameter of the bellows corrugation
D_m	[mm]	Average diameter of the bellows corrugations
D_b	[mm]	Diameter of pawl's hole
D_C	[mm]	Diameter of pawl
D_G	[mm]	Diameter of ratchet wheel
D_{Gh}	[mm]	Diameter of wheel's bore hole
D_L	[mm]	Diameter of the lever
D_{STK}	[mm]	Diameter of top section of the stem
e_b	[mm]	Thickness of the board
e	[mm]	Wall thickness of the bellows
e^*	[mm]	Thickness of the bellows corrected for thinning during forming
e_p	[mm]	Shell thickness of a one ply bellows
e_{pbv}	[mm]	Ball valve body shell thickness
e_a	[mm]	Distance between the layers of the corrugation
e_p^*	[mm]	Corrected thickness of a layer
e_c	[mm]	Required body shell thickness - design condition
e_{test}	[mm]	Required shell thickness - test conditions
e_s	[mm]	Ball valve body shell thickness
e_b	[mm]	Nozzle shell thickness
e_{cKmin}	[mm]	Minimal shell thickness conical side part
e_{ac}	[mm]	Minimal wall thickness conical side part
e_{con}	[mm]	Required conical side part shell thickness
e_{cRGM}	[mm]	Required shell thickness of RGM vertical shell, design condition
$e_{RGM\ test}$	[mm]	Required shell thickness of RGM vertical shell, test

		condition
E_b	[MPa]	Modulus of elasticity of the bellows material
E	[MPa]	Modulus of elasticity
f_4/s_4	[-]	Ratio of stem section 4
$F_{Axial\ red}$	[N]	Axial force on rod end bearing
F_{Allow}	[N]	Maximal allowable hand force on the lever according to API 6D and PED
F_{Cmax}	[N]	Force appeared on bold joint from pressing
F_G	[N]	Tangential force on ratchet wheel
F_L	[N]	Force required on the lever to overcome the maximal allowable stem torque
F_P	[N]	Tangential force on pawl' tooth transferred from the lever
$F_{P\ reb}$	[N]	Race material compressive strengths
F_S	[N]	Shearing force on the key
F_{smax}	[N]	Force appeared on bold joint from shearing
F_{tread}	[N]	Rod end bearing's head strength insert construction
F_1	[N]	Force appeared from internal pressure on contact media surface of the ball
F_2	[N]	Force appeared from the internal pressure on the seat
f_b	[mm]	Deflection of the bellows
f_S	[-]	Safety factor for stem according to API 6D
f	[MPa]	Allowable tensile stress - design condition
f_{test}	[MPa]	Allowable tensile stress - test conditions
G	[mm]	Thread dimensions

G_{reb}	[mm]	Thread dimensions of rod end bearing
h	[mm]	Wall thickness of the single-layer of the bellows
h_r	[mm]	Height from middle of a ball to the tread end
h_p	[mm]	Height of the pawls tooth
h_G	[mm]	Height of the ratchet wheel tooth
h_{SK}	[mm]	Height of the key in pressing section of stem
h_{KRW}	[mm]	Height of the key in pressing section of ratchet wheel
h_1	[mm]	Height of rod end bearing to middle point of ball
H_1	[mm]	Height of the RGM vertical shell
H_2	[mm]	Height from weld seam of vertical shell to middle point of horizontal shell
I	[mm^4]	Moment of inertia
j	[°]	Angle of conical side part
k_c	[-]	Weld joint efficiency factor
l	[mm]	Length of U-shaped bellows
l_3	[mm]	Length of the rod end bearings tread
l_4	[mm]	Length of the rod end bearing
l_7	[mm]	Length of the rod end bearing from beginning of tread to middle point of ball
l_{S0}	[mm]	Effective length body
l_{b0}	[mm]	Effective length nozzle
l_{VS0}	[mm]	Effective length of RGM vertical body
l_{Hb0}	[mm]	Effective length of RGM horizontal body
l_{L1}	[mm]	Length from rod end bearing to the point of applied force

l_{L2}	[mm]	Length of lever from pawl to rod end bearing
l_{1S}	[mm]	Length of the key's hub on stem
l_{2RG}	[mm]	Length of the key's hub on ratchet wheel
L_{GK}	[mm]	Length of the key's pass
L_t	[mm]	Length of the bellows boards
L_p	[mm]	Length of the pawl
L	[mm]	Horizontal length of the ratchet RGM body
LS	[mm]	Length from middle line of RGM vertical body to welding point of rod and bearing
M_ϕ	[N·m]	Bending moment in ϕ direction
M_θ	[N·m]	Bending moment in θ direction
M_{stem}	[N·m]	Torque/Moment appeared on the top section of the stem due to bending of the stem
M_{seat}	[N·m]	Torque/Moment appeared on the top section of the stem due to influence the internal pressure on the seat
M_{total}	[N·m]	Total Torque/Moment appeared on the top section of the stem
M_L	[N·m]	Moment on the lever
M_p	[N·m]	Moment on the tip of pawl's tooth:
$M_{MASTexisting\ stem}$	[N·m]	Maximum allowable stem torque (MAST), existing
$M_{MATratchet\ wheel}$	[N·m]	Maximum allowable torque of ratchet wheel
$M_{MAT\ pawl}$	[N·m]	Maximum allowable torque of pawl
$M_{MAT\ lever}$	[N·m]	Maximum allowable torque of lever
$M_{MAT\ key}$	[N·m]	Maximum allowable torque of key
m	[-]	Auxiliary function m

m_G	[-]	Module m_G of the ratchet wheel
m_W	[-]	Throat of welding seam
N_ϕ	[N]	Normal force in the ϕ direction
N_θ	[N]	Normal force in the θ direction
n_G	[-]	Number of ratchet wheel teeth
n_p	[-]	Number of the layers of the bellows
n_k	[-]	Number of keys
n_S	[-]	Number of bolt joints
p	[MPa]	Internal pressure
Δq	[mm]	Total equivalent axial displacement per corrugation of the bellows
$R_{p0,2}$	[MPa]	0,2 % - yield strength
$R_{p0,2/T}$	[MPa]	0,2 % - yield strength at temperature °C
$R_{p1,0}$	[MPa]	1,0 % - yield strength
$R_{p1,0/T}$	[MPa]	1,0 % - yield strength at temperature °C
R	[mm]	Radius of the contact seat to the ball
$R_{bearing}$	[mm]	Radius of the stem bearing
R_h	[mm]	Radius of pawl's tooth
R_{tread}	[mm]	Radius of rod end bearing’s tread
r_1	[mm]	Bevel of internal diameter of rod end bearings ball
r	[mm]	Radius of conical side part
S	[-]	Safety factor (design conditions)
S_{test}	[-]	Safety factor (test conditions)
S_t	[-]	Safety factor of stem components
S_{min}	[-]	Minimal safety factor of ball valve parts
S_G	[-]	Safety factor for ratchet wheel

S_{xS}	[-]	Safety factor for key
s_4	[mm]	Width across of 2-flat-end
T	[°C]	Temperature
t	[mm]	Width of the board
t_1	[mm]	Thickness of the RGM vertical shell
t_2	[mm]	Thickness of the RGM horizontal shell
t_3	[mm]	Thickness of the RGM vertical body cover
t_{1K}	[mm]	Key thickness for hub on stem
t_{2K}	[mm]	Key thickness for hub on ratchet wheel
t_{RG}	[mm]	Hub depth on ratchet wheel
t_S	[mm]	Hub depth of stem
t_{1P}	[mm]	Width of the pawl (upper)
t_{2P}	[mm]	Width of the pawl (down)
t_{LP}	[mm]	Width of the lever's end for bolt joint
W_L	[mm^3]	Axial moment of resistance
W_p	[mm^3]	Polar moment of resistance
W_G	[mm^3]	Polar moment of resistance of ratchet wheel tooth
$W_{t,i}$	[mm^3]	Polar section modulus
w	[mm]	Height of the corrugations
x	[-]	Distance variable
X	[-]	X-direction
Y	[-]	Y-direction
Z	[-]	Z-direction
z	[-]	Number of ratchet wheel teeth

Greek symbols

α	[°]	Bending angle
α_r	[°]	Angle of rotation of rod end bearing's ball
α_L	[°]	Angle of pawl connection to lever
α_{reb}	[°]	Rod end bearing maximal possible angle of tilt
β	[-]	Auxiliary function β
ε	[-]	Stiffness of material
λ	[-]	Auxiliary function
κ	[-]	Safety factor
ν	[-]	Poisson's ratio of bellows material
μ	[-]	Auxiliary function
$\mu_{StemBearing}$	[-]	Friction on the contact of stem and bearing
$\mu_{Seat/Ball}$	[-]	Friction on the contact seat to ball
π	[-]	π number
σ_{eq}	[MPa]	Equivalent stresses (von Mises)
$\sigma_{m\ stem}$	[MPa]	Allowable design stress of stem
σ_{SK}	[MPa]	Pressing stress on stem hub from key
σ_{RGK}	[MPa]	Pressing stress on ratchet wheel hub from key
σ_{bL}	[MPa]	Maximal bending stress on lever tip
σ_{bLK}	[MPa]	Maximal bending stress on key
σ_m	[MPa]	Membrane stress
σ_b	[MPa]	Bending stress
σ_{nl}	[MPa]	Peak stress
$\sigma_{\phi max}$	[MPa]	Maximum stress in ϕ direction
$\sigma_{\theta max}$	[MPa]	Maximum stress in θ direction

$\sigma_{\phi,m}$	[MPa]	Normal membrane stress in ϕ direction
$\sigma_{\phi,b}$	[MPa]	Normal bending stress in ϕ direction
$\sigma_{\theta,m}$	[MPa]	Normal membrane stress in θ direction
$\sigma_{\theta,b}$	[MPa]	Normal bending stress in θ direction
$\sigma_{\theta,t}$	[MPa]	Stresses of the board in the circumferential direction
$\sigma_{\theta,E}$	[MPa]	Stresses of the outer bellows corrugation in the circumferential direction
$\sigma_{\theta,I}$	[MPa]	Stresses of the inner bellows corrugation in the circumferential direction
σ_v	[MPa]	Uniaxial stress
σ_{SK}	[MPa]	Allowable average primary pure shear stress for keys
σ_{SC}	[MPa]	Allowable maximum primary shear stress for circular solids
σ_p	[MPa]	Maximal stress on pawl
σ_G	[MPa]	Maximal stresses on ratchet tooth
σ_{vS}	[MPa]	Maximal stress on key
τ_{qL}	[MPa]	Maximal shear stress on key
$\tau_{t,i}$	[MPa]	Allowable maximum primary shear stress for circular solids
φ	[°]	Deflection by the angle φ
ϕ	[°]	Angle of investigated corrugation of toroidal shell
ω	[-]	Coefficient the ratchet wheel to the module
θ	[-]	θ-characterizes the ratio of the width of direction
Ψ	[-]	Auxiliary function

Ψ'	[-]	Derivation of the auxiliary function

Abstract

The aim of this doctor thesis is experimentally, analytically and with the help of the FE analysis improve the work ability of the ratchet gear close/open mechanism for a utility model of ball valve. To achieve all these tasks, the literature is analysed for different constructions of the valves/ball valves, with designs that compared to the utility model, the fully welded valve with a ratchet gear mechanism. This subject was analysed in the 2nd and 3rd chapter of this thesis.

The main task is to simplify calculation analysis of the thin toroidal shell (a main ball valve seal element - bellows) and develop a new analysis method for reduction of computational efforts and more accurate analytical analysis, which is dependent on Clark's theory of thin toroidal shells.

As follows, a laboratory set up built to improve all the abilities of investigated design of utility model ball valve with ratchet gear mechanism. However, it was analysed equivalent stresses in the structure of multi-ply circular bellows with U-shaped convolution cross section.

The experiments carried out in two steps. First part of the experiment was to check the work ability of a fully welded ball valve with the ratchet gear mechanism. For that, a section of the laboratory set up built with a ball valve of nominal diameter 100 mm. Instead of a lever for closing/opening was installed a ratchet gear mechanism, which was directly connected to stem of the ball valve. In operation, the stem rotated, which lead to closing or opening the cross section of the ball valve.

The second part of the experiments (laboratory set up) was to analyse the stresses under internal pressure and bending in the weakest areas of the investigated multi-ply stainless steel bellows corrugations with the help of strain gages. For this purpose, a second section of the laboratory setup was built.

Consequently, the experiments results validated by Finite Element (FE) analysis and analytical analysation. The analytical analysis of single- and multi-ply bellows has been obtained by standards ISO EN 13445 Part 3 [21], EMJA [60], and a new calculation method.

Hence, in frame of this doctor thesis, new calculation method developed for analysis of critical points of single- and multi-ply stainless steel bellows, which dependent on Clack's theory of the thin toroidal shells.

The FE analysis of ratchet gear mechanism for investigated fully welded ball valve carried out in two steps. First, the ratchet gear mechanism was analysed. It was investigated which

equivalent stresses appeared in the components of the system in different load cases such as internal pressure and high temperature (also bending of bellows). FE analysis helped to find and detailed analysed the critical areas of ratchet gear mechanism, which leaded to feature optimization of the system.

In the second part of the FE analyses, three different geometries of single-, two- and three-ply stainless steel bellows with U-shaped convolution cross section were analysed. These FE analyses indicate which geometry of the bellows most fitted to different case of loads, such as internal pressure, high temperature, and bending. The fatigue life of investigated metal bellows defined with help of Ansys® Workbench software package.

In addition, it considered the thickness of single-, two- and three-ply stainless steel bellows, as well as number of corrugations, dimensions and the length.

In conclusion, the results of laboratory experiments, FE analysis and new mathematical calculation method validated. In addition, it explanted the advantages and disadvantages of the new ratchet gear mechanism for ball valves application.

1. Introduction

It is a fact, that pipelines are found everywhere where people work and live, providing water or other liquids, heat, and gases either to householders or to industries like chemical plants. Hence, pipelines provide important utilities to our daily lives.

However, pipelines cannot operate without fittings and valves. Fittings and valves are responsible for closing, opening and regulating of amount or volume of media in the cross-section of the pipelines. They also control and redistribute media to other pipelines. Therefore, there is no pipeline without any fitting or valve.

Hence, in modern power, food, nuclear, chemical, and petrochemical industries a huge amount of fittings and valves, which are performing a large range of functions, for instance, regulation of flow rate; instantaneous closing of the cross-section in case of an emergency. Consequently, the valves and fittings are designed for different operation temperatures, pressure ranges, and chemical solutions.

Nevertheless, fitting and valves designed for the chemical industry have a deficiency of specific abilities, for instance, high or cryogenic temperatures, and aggressive chemical solutions. In these cases, the problem of polymer seats, obturators, and elastomer seal elements appear which are mostly used in the construction of any fitting and valve. The problem of polymer and elastomer seal elements in the construction of fittings is not solved yet, due to the physical properties of polymers and elastomers. Hence, this doctor thesis presented a sealing solution for three different types of designs of valves. Namely, an external metallic element, the multi-ply metal bellows, instead of polymer and elastomer seal elements. The metal bellows provide workability with high and cryogenic temperatures and aggressive media resistance.

However, finite element analysis (FE) of multi-ply thin toroidal shells (metal bellows) has not been studied in a profound way. In this case, the FE analysis of multi-layer thin toroidal shells (bellows) is complex and time-consuming. Hence, research on the topic of FE analysis of the multi-layer thin toroidal shells (bellows) for the valve industry is proposed [5].

In this doctor thesis, a new design of a ball valve for high and cryogenic temperature, aggressive media resistance, and better seal performance is presented. The main advantage of the ball valve is that it does not contain any not metal sealing elements between media and environment.

To prove the workability and reliability of the new ball valve design, a laboratory set up of the ball valve with ratchet gear has been built in the department of Chemical Process Engineering

of the University of Stuttgart [6].

In addition, in the frame of this work, we created a new methodology of calculation of the single- and multi-ply bellows for ratchet gear, which is dependent on Clark's work: "On the theory of thin toroidal shells" [25].

The new methodology provided the structure analysis of single- and multi-ply metal bellows. Therefore, it was possible to determine the critical areas of single- and multi-ply bellows cross-section, which was analysed.

The new calculation method can find implementation in any bellows applications, for example, pipelines, nuclear industry, chemical devises.

Finally, it was designed a product line of the ball valves with ratchet gear and two-ply bellows of nominal diameters 100 mm, 150 mm, 200 mm and 300 mm. The advantage of these ball valves is that they withstand a large range of thermal loads, up to 500 °C, and cryogenic temperatures below –70 °C. In addition, the operation of the ball valve is possible in a wide range of aggressive media. The disadvantage is that the operating pressure of these ball valves is from 0,3 to 2 MPa according to standards EN ISO 1333 [63] and specification for pipeline valves API 6D [51]. The design of presented ball valves can also operate as on/off valves as well as throttling control valves.

1.1 Motivation

Due to the development of economies of the third countries, the infrastructure of pipelines and valves for chemical industries, transportation of oil, natural gas, and heat, is growing. Hence, to improve the properties and quality of supply, new designs of the valves often come to the market.

However, for each application, it is necessary to design a different type of valve or fitting due to specific designs, as well as utilize of polymer and elastomer seal elements such as gaskets, seal rings, and O-rings. Therefore, for each media, temperature ratio, and pressure class it is necessary to choose a different design of the valve, which increase the cost of a single unit application.

Hence, the global valve market is in search of a design, which can cover many application cases, such as high and cryogenic temperatures, implementation with a wide spectrum of different liquids, and addition, cover different pressure classes. However, at a certain time that is not

possible due to the polymer-based seal elements, as well as construction disadvantages of the existing fittings and valve designs.

The main aspect to start this work was that during the practical experience on the chemical plant "Nikochem Group" [105] in Volgograd, Russia, it has been noticed that many valves required replacement due to loss of technical performance after several months in operation. The polymer or elastomer seal elements could not resist aggressive media, which after some time were either harmed or completely vanished. The valves themselves were workable, but the leakages in flanges, stems and obturators appeared. Therefore, the valves could not perform their applications anymore. The reparation required a high cost, consequently, replacement of the valve was a cheaper and faster solution.

To solve this problem, it was necessary to create a design of a valve, which does not include non-metallic (polymer) seal elements and has the possibility to operate in a wide spectrum of media and temperature ratios.

Hence, the study and analysis of the global valve market and the disadvantages of existing types of the fittings helped to create new valve designs [2], [3], [4], which cover high- and cryogenic temperature ratios, in the same time these valves have corrosion resistance to the wide spectrum of media [1], due to the implementation of non-metal (polymer) components in the design. In addition, it covers the pressure ratio up to 20 atm. (2 MPa according to specification for pipeline and piping valves API 6D Class 150 [51], or 20 bar according to DIN EN ISO 1333 [63]).

1.2 Goals and objectives

To achieve the goal of creating a new valve design of multitasking fitting, three different designs of fully welded valves were created [2], [3], [4]. As a based design, it was designed a fully welded knife valve with a metal crimped diaphragm as a seal element [1], [2]. The disadvantages of this design are the low-pressure rate, up to 0,6 MPa. Therefore, the design was improved, the metal crimped diaphragm replaced with a metal bellows [1], [3]. New design is able to operate in higher-pressure ratio, up to 2 MPa (according to specification for pipeline valves API 6D [51], or DIN EN ISO 1333 [63]). However, due to its specific design [3] the utility model knife valve is not practical, and requires high cost in the production. Therefore, third utility model design [4], [5], [6] of a ball valve with ratchet gear mechanism (RFM) based on the standard ball valve, which is cheaper and easier in the production and applying, than previous two utility model valve designs [2], [3].

The main goal of this work is to analyse the design of the utility model of the ball valve with ratchet gear [4], i. e. analysis the issue of operation properties of the investigated utility model, such as minimal and maximal temperature and pressure ratio, as well as workability with different types of media.

In addition, the seal element of the ratchet gear mechanism is a multi-ply metal bellows, therefore, the goal was to analyse the maximal operation properties of the multi-ply metal bellows with Finite Element Analysis (FEA), with standards ISO EN or EIGA [21], [44] and new calculation methodology, based on Clark's theory of thin toroidal shells [25]. That component afterward influenced the design of the ratchet gear mechanism, which adjusted to the existing designs of investigated ball valves. Hence, the design of the ball valve with the ratchet gear mechanism is dependent on the properties of investigated multi-ply metal bellows.

1.3 Scope of work

Hence, this study is examined the design of the utility model of the ball valve with the ratchet gear mechanism [4], as well as single- and multi-ply metal bellows, which is the main seal element of the design.

To prove the performance of the design of the ratchet gear mechanism, it provided analytical analysis in chapters 3 and 4, the laboratory experiments in chapter 5, as well as FE analysis in chapter 6. The laboratory experiments and FE analysis of the ratchet gear mechanism proved the issued operation properties of the design [4]. Hence, it discussed in detail the principles of the operation condition of the design, such as mechanical properties of single- and multi-ply bellows as an example.

The single- and multi-ply metal bellows were in detail analysed according to operation loads in chapters 2, 3, 4, 5 and 6. Hence, the safety and performance of the ball valve with the ratchet gear mechanism are directly tied to bellows operation loadings conditions, such as operating temperature and pressure.

Possible operation cases of the metal bellows, which are used in the investigated design discussed in chapter 2. The metal bellows are used to accumulate temperature expansions, operate under internal pressure, and it is bending to a certain angle. The maximal value of the loads, which are applied, depended on the geometrical dimensions of the metal bellows.

Dimensions of single- and multi-ply metal bellows are performed and analytically analysed in

chapter 3. The analytical analysis depended on the calculation method for metal bellows by Anderson [12], Andreeva [78] and standard EN ISO 13445 Part 3 [21]. The internal pressure and bending load cases of the bellows is difficult to analyse by given analysis methods due to the combination of angular rotation and lateral deflection of the bellows for bending load case and fixed support due to welded installation of the bellows on the ratchet gear mechanism.

Hence, the analysis of these load cases required a new analytical calculation method for the metal bellows [5]. Therefore, it was created a new calculation method dependent on Clark's theory of thin elastic toroidal shells [25]. This analysis method has been adjusted to geometrical properties, dimensions, installation, and load cases of investigated single- and multi-ply metal bellows. The new analysis method helps to reduce the calculation time of the circular bellows with a U-shaped convolution cross-section.

The experimental analysis (presented in chapter 5) proved issued maximal internal pressure, as well as bending load case for investigated two-ply metal bellows. For experimental analysis were used metal bellows, which were produced by Witzenmann Ltd. [93]. The laboratory experiments of the investigated two-ply metal bellows of Witzenmann Ltd. [93] have been separately provided for each load case, respectively for internal pressure and investigated bending cases. The laboratory result of maximal equivalent stresses were obtained with the strain gauges (SG), M model of HBM Ltd [90] for internal pressure and investigated bending cases. Thermal analysis was avoided due to the difficulties of laboratory experiments.

Finite element analysis was carried out for thermal, internal pressure, and bending cases for the bellows and investigated loads for constructive parts of RGM using the dimensions developed in chapter 3. The validation of investigated single- and multi-ply metal bellows is necessary to improve their reliability. Hence, FE analysis results of the internal pressure and bending have been validated to experimental results (presented in chapter 5), as well as to the analytical analysis (presented in chapter 3) and new calculation method (presented in chapter 4) respectively.

In the scope of results obtained from the analytical analysis, FEA and laboratory experiments, important conclusions were achieved and performed in chapter 7. In addition, the maximal number of cycles of investigated single- and multi-ply metal bellows have been determined respectively for maximal possible loads. Finally, the potentially extend of the work is explained in chapter 7.

2. Introduction in valves design aspects

Historically, valves and fittings have undergone tremendous changes. Starting from the first valve to modern electromagnetic or pneumatic devices. Therefore, the functional performance of the valves also has changed at the peak of chemical industry revolution. The valves and fittings had been manufactured for pumping highly concentrated chemical medium under high pressure, which could disable these devices. At that time, special coatings of the internal surfaces of the stop valves appeared, which had direct contact to the media. In addition, many different kinds of sealing are developed, for different purposes. However, the main issue that remained unresolved for a long time was these sealing elements or O-rings, which were the primarily failure in the design of the valves. It entailed a costly repairs or complete replacement of the devices. Similarly, polymer sealing or O-rings are poorly susceptible to high temperatures (up to 200 °C), which is ineffective in chemical plants, where the temperature of the processes and medium reaches 500 °C.

Furthermore, development of the chemical industry and nuclear power plants, where temperatures reach values of 500 °C and higher, inculcated the fact that the design of old-type valve devices with polymer seats and sealing elements became ineffective and a co-ordinate change in the design is required. Therefore, new devices appeared with the development of the industry, which include sealing elements such as a bellows (corrugated thin toroidal shell), metal seats and carbon sealing elements. Accordingly, it led to an increase of the temperature spectrum of the valves, reliability and service life of the valves.

In modern chemical, oil and gas industries a great number of valves are used, which are an essential part of the rectification columns, absorbers, heat exchangers, reactors, pipelines. Hence, the valves divided based on performance, and specific variations, for instance: a regulation valve, which regulates the medium current; safety devices, used in case of increasing of the pressure discharge.

2.1 Global industrial valve market

The global industrial valve market size estimate at 78 billion Euro (81,5 USD billion) in 2019 [101] (see Figure 2.1). Because of growing automation, which increased industrialization and expansion of existing equipment, the global industrial valve market projected to rise in demand.

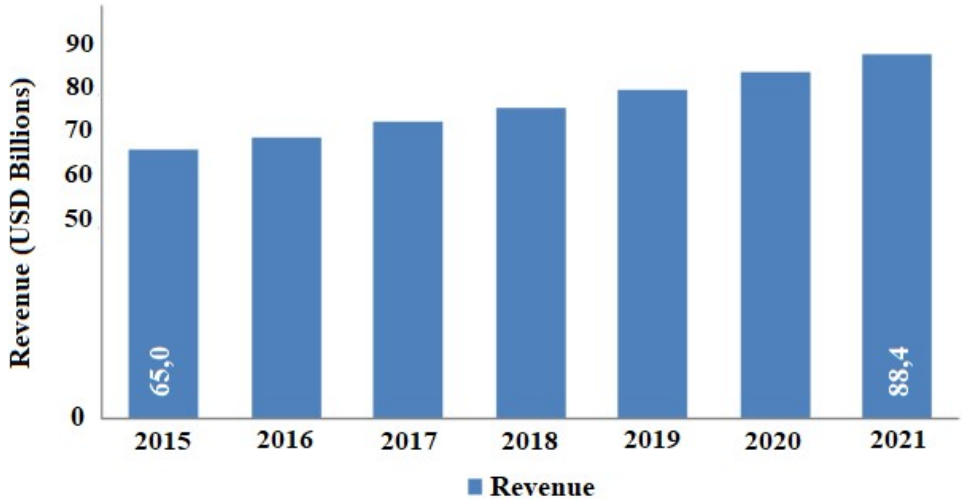

Figure 2.1: Anniversary revenue of global industrial valve market [101]

The regions that analysed for the global industrial valves market included North America, Europe, South America, Asia-Pacific, and the Middle East and Africa. The Asia-Pacific region became the largest market for industrial valves demand, with the market value of USD 38.65 billion in 2019 [101].

Factors such as urbanization and industrialization in the developing countries such as India and Thailand are promoting the growth of the global industrial valve market. North America, Middle East, and Africa had significant market share in the global industrial valves market due to the oil and gas production. Nevertheless, growing exploration activities of the oil and gas sector in Nord Amerika, for example, are having a positive impact on the market growth in these regions [103].

Hence, the global industrial valve market will show the growth in next decades due to increasing demand in existing sectors, as well as due to opening of new industries, such as renewable energy and hydrogen supply chain. These sectors mostly have influence on the European, Asia-Pacific, and Nord America valve market.

Due to new industrial sectors, the demand on the global valve market is growing for ball valves with smart control systems, which expected to incise significant importance of these fittings. That expect to influence of further development of ball valves manufacture [103].

The global market always in search for new designs of valves, which can increase the range of the functionality. Better material properties of the steel, such as X80 and P355LN2 [108], increase the technical properties, which influence on the design aspects of the valves, for example, decreasing of the wall thickness, less corrosion effects. [38]. However, the volatility

of the material prices and erratic supply in the global industrial valve market is directly influence on it growth [103].

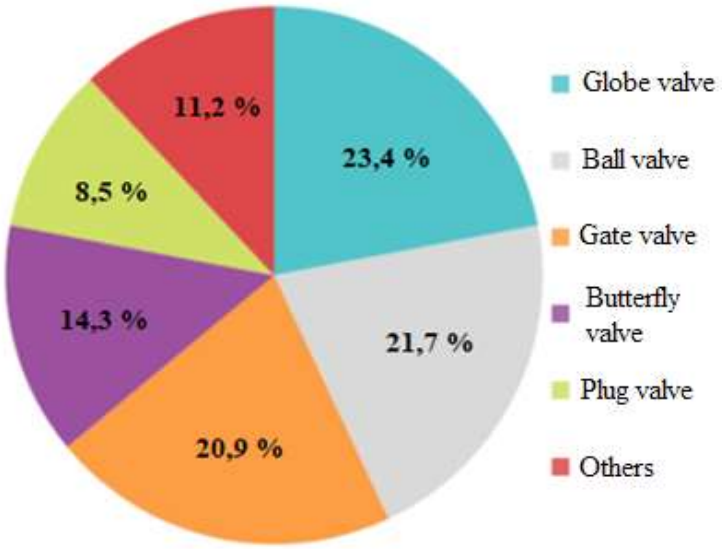

Figure 2.2: Industrial valve market, Revenue shear %, by type, Global, 2018 [102]

The global industrial valve market segment divided into ball, gate, knife, wedge, diaphragm, control and butterfly valves [104] (see Figure 2.2). Ball valves used for media control and in case of tight shut-off. The ball valves have accounted for 21,7 % of the revenue share in 2019 [102]. Innovations in the ball valves design, for example, fully welded ball valve, allowed greater seal performance. Another example of innovation is segmented ball valve, which allowed control over flow rates, also it enhance the efficiency of the control equipment.

The global valve market includes oil and gas industry, pharmaceutical, water supply, chemical, and power [102]. The oil and gas industry have accounted for circa 25 % of the overall revenue share in 2019. That influenced by the increased reserves in natural gas exploration that helped to increase the market demand of the ball valves. The increasing of pharmaceutical and chemical industries has also influenced in growing demand of industrial ball valves [103].

2.2 Utility models of the new valve designs

Most types of the industrial valves have polymer sealing system or some non-metal components, for example, gaskets, seats, which seal work medium. Therefore, often these components of industrial valves lead to leakages of the devices. The solution could be in complex designs of the existing fittings, such as adding amount of seal components to prolong production live of the industrial valves.

Hence, the analysis of disadvantages of the industrial valves provided designs of new valves with the ratchet gear mechanism (utility models [2], [3], [4]).

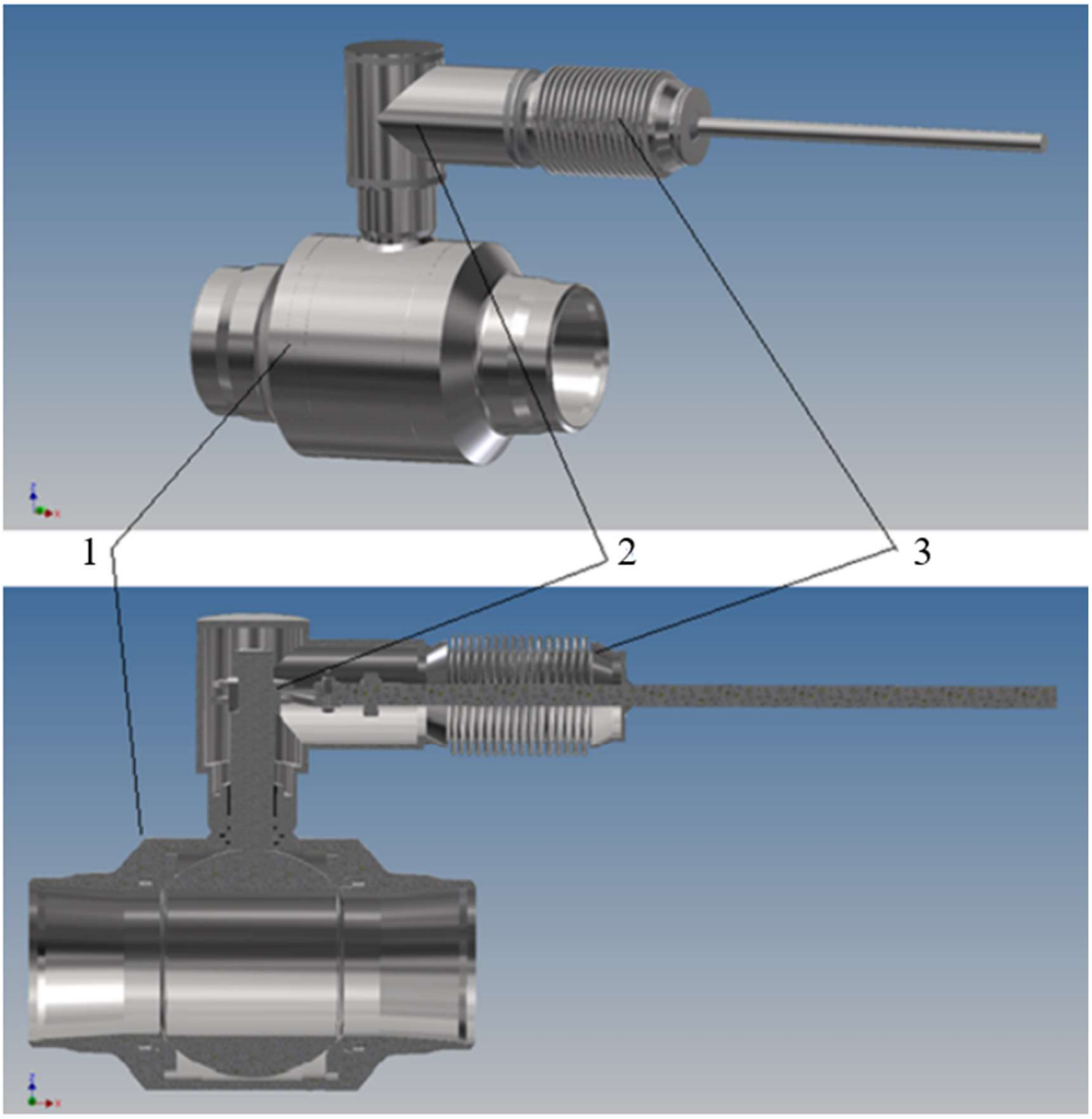

Figure 2.3: Sample design of the utility model № 139949 ball valve with a ratchet gear and two-ply metal bellows 27.03.2014 [4]:

1. Basis ball valve DN 100 mm, design of the Boehmer Ltd [88];
2. Ratchet gear mechanism with ratchet gears and pawls;
3. Two-ply metal bellows Witzenmann Hydra BE 356230-bb 68 [93]

As it was noticed, to increase a seal performance of the industrial valves, utility models were received at the Volgograd Technical University and tested at the University of Stuttgart, such as utility model № 107836 “Valve” 29.03.2011 [2]; utility model № 123877 “Valve” with ratchet gear 10.01.2013 [3]; utility model № 139949 “Ball valve with a ratchet gear mechanism” 03.27.2014 [4].

The ball valves distinguish by their simplicity of construction and durability. The polymer seats, gaskets and elastomer O-rings, which are mostly used in their designs, are not very effective. That leads to leakages, thus costly repairs or replacement. Temperature range of these applications is from –60 until +250 °C (see Figure 2.3). However, these types of valves are quite effective in the case of high-pressure up to 42 MPa, according to 420 bar DIN 1333 [63] or Class 2500 API 6D [51]), which is an advantage of ball valves.

Hence, in the design of the utility model № 139949 'ball valve with the ratchet gear mechanism' published on March 27th, 2014 [4] does not contain any elastomer or polymer-sealing elements. Moreover, in the design of the ball valve, the gate ball with the stem rotates by the movement of the ratchet (wheels) gear mechanism (Figure 2.3). A metal bellows provides the sealing of this design.

The basis of the ball valve design for utility model № 139949 "Ball valve with ratchet gear" 27.03.2014 [4], considered a design of a ball valve of company "Boehmer Ltd.", Germany [88]. A basis ball valve design was considered to have a nominal diameter of 100, 150, 200, 300 mm, according to 20 bar DIN 1333 and ANSI Class 150 PN 16 [50].

Hence, in this doctor thesis will be described the ball valve design with the ratchet gear mechanism, which is designed for the case of high temperatures or special media (for instance, for hydrogen gas, where the atoms or molecules are the smallest, therefore usual elastomer and polymer sealing are not effective).

The main difference of the utility model ball valve is that the ratchet gear is sealed with a bellows (thin toroidal shell) instead of an elastomer and polymer sealing (Figure 2.3). The bellows connected to the body of the gearbox by welding, as well as gearbox body connected to ball valve housing by welding, which ensures complete sealing of the device. Therefore, all main parts of the ball valve connected by welding, which ensured a long service life of the ball valve.

In the new design, sealing made of elastomer or other polymer materials were not used. Hence, main advantages of the investigated ball valve are:

- resistance of the high temperature;
- operation with corrosive mediums (gases and liquids), such as hydrogen, oxides;
- increasing the service life;
- simplification and minimization of the diagnostic process.

Thereby, the ball valve due to its unique design reduce the costs of production and exploitation.

The disadvantages include the inseparability of the design and the complexity of the ball valve. Detailed description of the dimensions of design of the ball valve with ratchet gear [4] (see Figure 2.3) in chapter 3.

2.2.1 Function of ball valve design with ratchet gear mechanism

The ball valve has a function of fully opening/closing the medium flow through the cross section of a pipeline. In many cases, it is sufficient if the ball valve is technically fully sealed (very small amount of medium allowed to leak trough the seats or stem sealing). However, there are also cases, where a very small amount of the leakage is not allowed and the valve must be fully sealed. That is the case, for example, of natural gas, hydrogen or very toxic chemicals. For this purposes, the new utility models of the valves contain welded connecting parts, which reduce the possibility of leakages.

2.2.2 Bellows in valve's design

Metal bellows manufactured from thin-walled pipes, for example, by hydraulic reshaping [8]. Moreover, depending on the task of requirement, the metal bellows are designed as single- or multiple-ply. Single-ply metal bellows feature low spring rates and used particularly for vacuum applications. Multi-ply bellows are sutified pressure resistant and at the same time very flexible. They used, for instance, as valve stem seal components for operating pressures up to 1000 bar [8].

Single- and multi-ply metal bellows in this design of the ball valve with ratchet gear mechanism [4] is a seal element, which is made of metal (stainless steel in this case) [8]. Furthermore, bellows provide two functions: first, it is to seal the ratchet gearbox mechanism; second, it is to transfer movements, in this case a spring effect, from lever to the ratchet gear (for the manual control) [10]. Hence, in this doctor thesis the significant part of the research focused on the bellows as a sealing element of the ball valve with ratchet gear [1], [5], [6].

2.2.2.1 Advantages and disadvantages of bellows

The bellows used in pipelines [9], fittings [11], chemical equipment [17], machinery [15], for example, as a sealant component of moving parts.

Advantages of the bellows include resistance to high temperatures; bending 10 - 15 °, depended on the geometry; multi-ply effect [14]; good pressure resistance.

Disadvantages of the bellows include instability, expensive in production, difficulties of calculation the loads influence due to complex geometry.

2.2.2.2 Internal pressure load in the valve with a bellows

Krovvidi [59] presented the FE analysis of formed bellows for the case of internal pressure in a valve for the nuclear industry (Figure 2.4 a.), which involves high temperatures, operating pressures and toxic media.

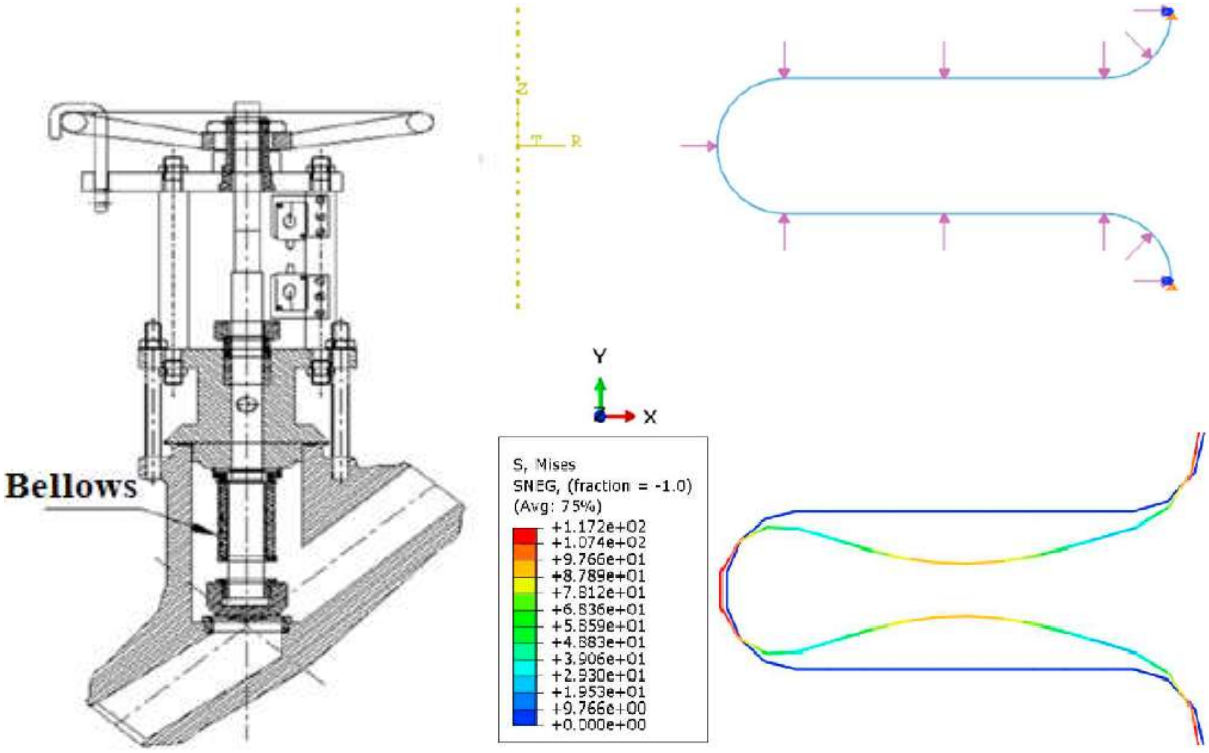

a. b.

Figure 2.4: Finite element analysis of bellows in valve for nuclear applications with ABAQUS® software:

a. Cross section of valve with a bellows [59] for nuclear applications;

b. FE analysis of a bellows corrugation using ABAQUS® software [59].

The finite element analysis was carried out on a bellows corrugation using ABAQUS 6.14 FE software package, Figure 2.4 b. In addition, the FE analysis of a bellows corrugation was compared to ASME code section III [53], RCC-MR section I [61] and EJMA standard [44].

Hence, for FE analysis of the isotropic kinematic and hardening model used ABAQUS software package, which gave results that are more exact in comparison with ASME code section III or RCC-MR section I. Finally, the investigated bellows was design based on EJMA application [60].

In conclusion, the authors explained how results are matched using different types of analysis of single-ply metal bellows corrugation for nuclear application. The ASME code section III, as well as RCC-MR section I contain an inherent factor of safety [61], which prevents exact analysis of a bellows corrugation.

In addition, Krovvidi presented the FE analysis of the geometry of bellows corrugations, the authors described the FE analysis of compression of bellows from the movement of valve's stem, which is not considered in this doctor thesis.

2.2.2.3 Bending of the bellows

Zhu [7] explained the fatigue life of the single- and multi-ply metal bellows under bending moment in aggressive media. However, it considered the investigation of the sections of the bellows, with the help of finite elements analysis (FEA). It helped to analyse the weakest areas of the standard metal bellows design, which concluded to increase the thickness of the bellows at the spots with high peak stresses. These spots were fully analysed by FE analysis, which was a starting point of this research, analysing the single-, two-, and three-ply metal bellows with the considered shell thickness to find a better solution for a new design. In addition, the experimental investigations were made of the most loaded spots of the bellows by the strain gages. The strain gauges were installed on the areas which have maximum stresses in investigated design. This gave the possibility to compare the experimental data to FE analysis. The compared result presented on Figure 2.5 b. [7].

The equivalent stresses from bending load case of the bellows depended on the angle of bending and could be fatal in few cycles. Therefore, it is important to create a design of the single- or multi-ply metal bellows, which can resist the required number of the bending cycles. This task is difficult, because the investigated design of the bellows operates under two different load cases. Therefore, the equilibrium of these two load cases required to be considered [5], [6].

Zhu [7] described which kind of materials is necessary to select metal bellows to meet a required resistance of corrosion in case of certain types of media.

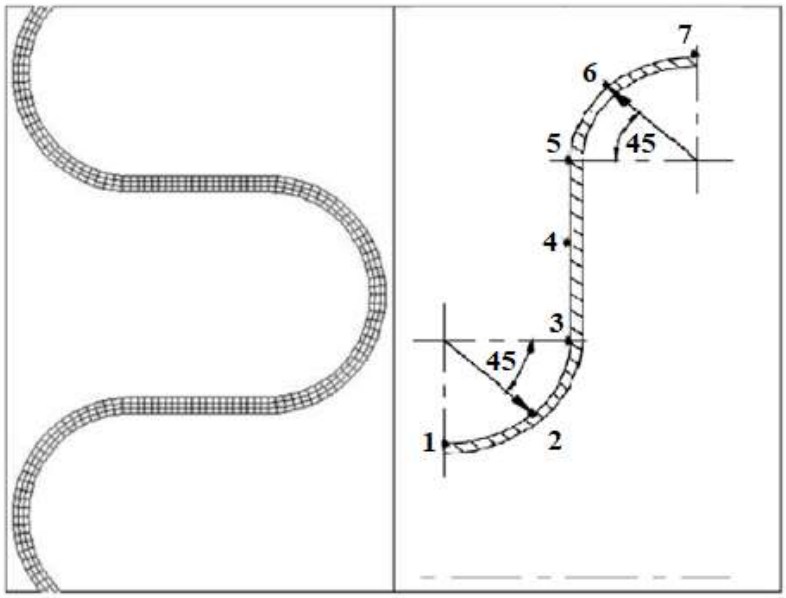

a.

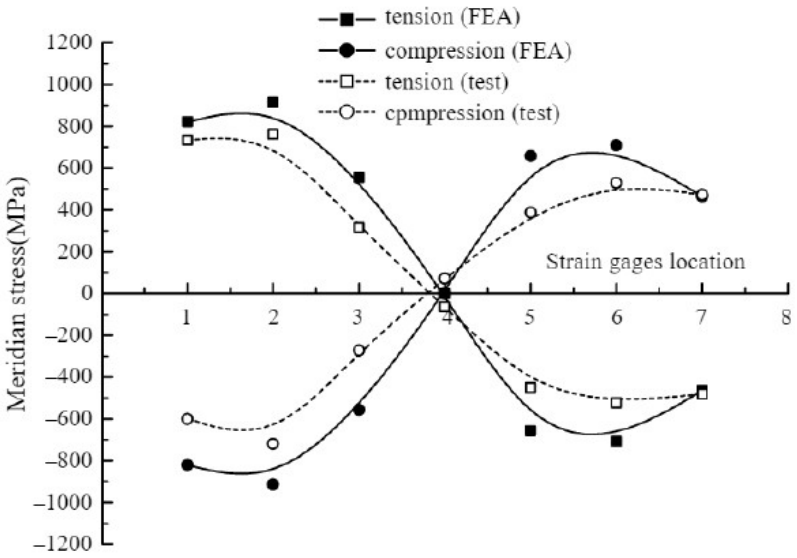

b.

Figure 2.5: Bellows cross section analysis:

a. FE analysis and analytical model of the bellows [7];

b. Stress distribution on outside shell surface of the bellows cross section (experiments and FEA results)

The focus of Zhu [7] was on the crack of the bellows after a few cycles, due to corrosive mediums and bending. That was another point to issue the influence of the medium on the investigated type of the metal bellows.

2.2.2.4 Design of control ball valve with a bellows seal component

A ball valve has a function of closing/opening of flow cross section, and it has a function of regulating the flowing media, so that is only a certain percentage of possible media could pass through the pipeline cross section. Hence, it is sufficient for the ball valve to be technically fully sealed (leak rate of A, or 0 according to ISO 20486 Part 1 Non-destructive testing - leak testing [169]).

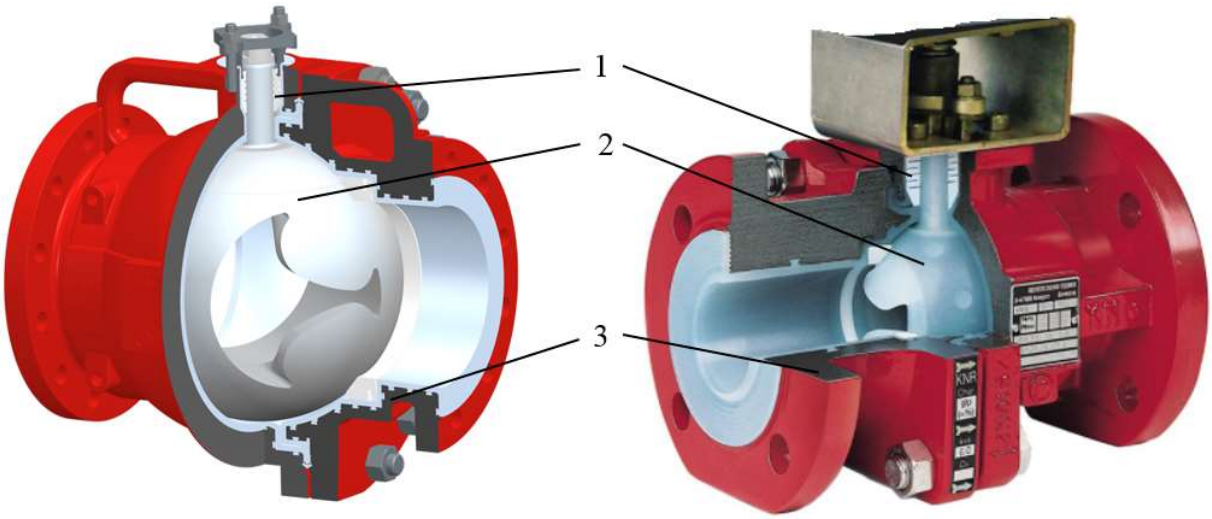

Figure 2.6: Design of control ball valve with a bellows seal component [99]:

1. Bellows;
2. Valve's ball (plug);
3. Housing.

However, there are also cases, which permit small leakages. Nevertheless, the ball valve has to be fully sealed. This is cases for natural gas, hydrogen or very toxic chemicals as an example.

For such cases fully sealed valve are used, see Figure 2.6 [99]. In presented control ball valve design, the bellows (1) operate under internal pressure load, which appears with increasing internal pressure in cavity of the ball valve housing (3). The bellows protect from aggressive media the sealings in stem area of the ball valve, as well it provides additional sealing effect. The valve's ball (2) has function of closing/opening and controlling the media flow of flow section of the ball valve.The ball rotates to the 90 ° of it's Z-axis, which bellows (1) must compensate and remain fully sealed [99].

2.2.2.5 Hydrogen design

Hydrogen is becoming more popular as an energy supply for industry and households.

However, the transportation of hydrogen is one of the most important topics to be solve, because current pipeline and valve technologies are not a guaranteed solution. However, there are some pipelines, which used for transport of hydrogen in Europe, USA, Asia-Pacific regions. These are mostly old natural gas pipelines. Nonetheless, no one could give a guarantee of the protection from hydrogen corrosion, which could lead to leakages of the pipes, valves and pipeline constituent elements. In addition, hydrogen is the smallest element that exists, which makes possibility of leakages of the sealing elements of the valves, such as gaskets and O-Rings. The utility model [4] the ball valve with ratchet gear is possible solution for hydrogen valves presented in this doctor thesis.

2.2.2.5.1 Advantages and disadvantages of hydrogen design

Hydrogen might become one of the most useful fuels in near future. As mentioned above, there are some difficulties to transport it due to corrosion or leakages. Corrosion occur on the surface of fittings and pipeline due to high-temperatures and high-pressure transportation of hydrogen, leakages occur due to the size of hydrogen. Nevertheless, hydrogen could be transported with room temperature and pressure up to 80 bar (8 MPa), without any corrosion of the material of the valves and pipeline.

The typical hydrogen ball valves represented a fully welded body design [50] (see Figure 2.7) with thick wall thickness and many sealing components on the stem area to abuse leakages of hydrogen. Additional safety provided by the double piston design in the upper seat ring, which constitutes a second barrier. Therefore, it leads to high cost of these fittings. In addition, the disadvantage is that the transportation of hydrogen with solid particles could harm the soft sealing system of the seats and stem area, which no longer guarantee hydrogen leak-tightness of the ball valve [50].

Hence, the new utility model of the ball valve [4], which presented in this doctor thesis, should aim to satisfy the given parameters of hydrogen transportation. Advantage of the utility model is the reliability of the constructed ball valve theoretically increased, because neither polymer nor metal sealing (packing) used to seal the stem. Secondly, the mass of the designed ball valve reduced, due to using neither flanges nor bolt connections. Thirdly, the ratchet gearbox connected to the valve body by welding, which also sealed by the bellows.

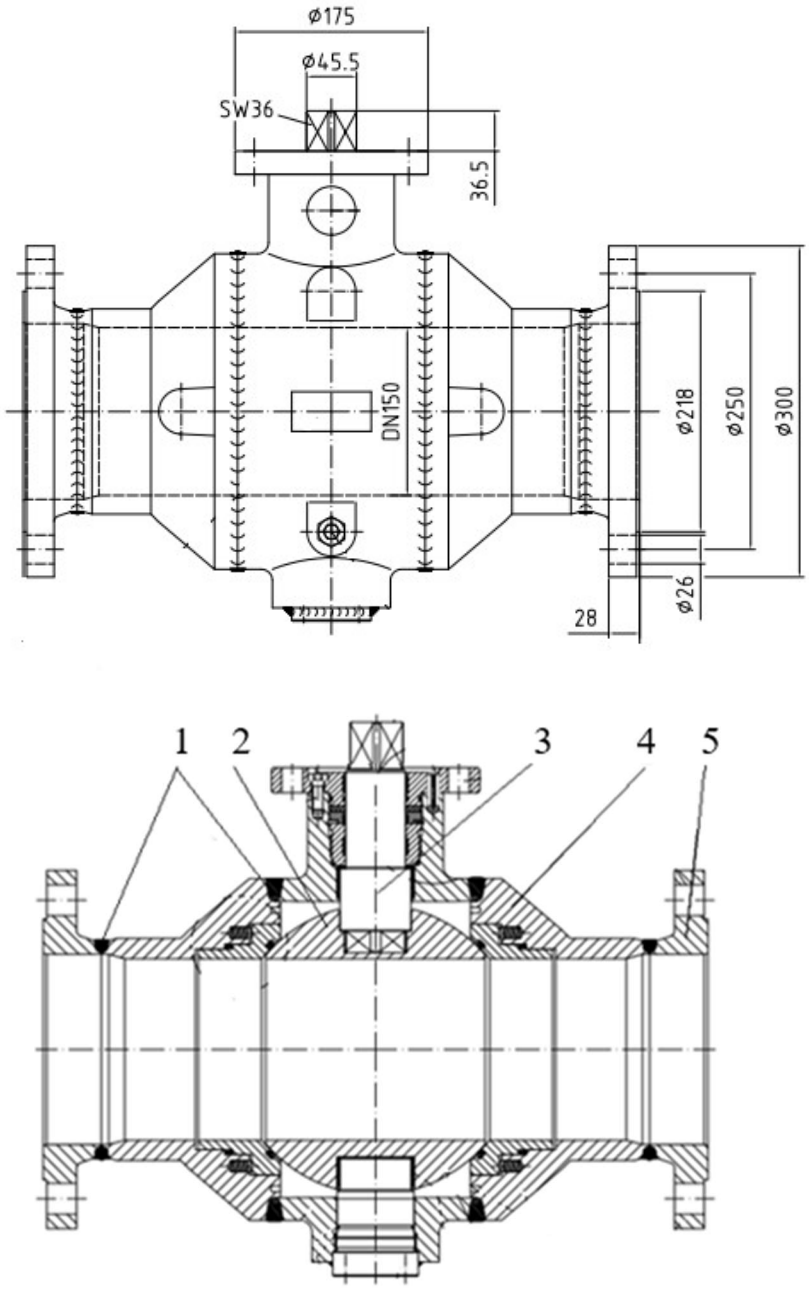

Figure 2.7: Typical design of hydrogen ball valve DN 150 of Boehmer Ltd [50]:
1. welding seams; 2. gate ball; 3. stem; 4. ball valve housing; 5. flange;

Disadvantage of the investigated utility model [4] is that RGM connected by the welding to the housing of the ball valve [88], which leads to unseparated construction of the ball valve. That changes the cost of reparation, which are increased or impossible.

2.2.2.5.2 Weld seams in case of hydrogen

In this case, the investigated ball valve has mostly welding connections (weld seams), to avoid

any kind of sealing between components of the ball valve; for instance, a weld seam between the body of the ball valve and ratchet gear mechanism. For this purpose, it is important to investigate the welding connections in the case of hydrogen transportation.

The behaviour of high-strength, high frequency inductively welded steels with regard to their resistance to hydrogen-influenced corrosion assessed in this sub-capital. For this purpose, Slow-Strain-Rate-Tests (SSRT) [40] in the weld seam area were carried out under labor conditions, for instance, under 8 MPa of pressurized hydrogen and 8 MPa of nitrogen, as reference medium. The suitability of the material assessed based on toughness values, maximum stresses and assessment of the fracture surfaces [39].

The investigations carried out on the base material and the weld connections of investigated ratchet mechanism of the ball valve [4]. The welding connection produced using the process of metal inert gas welding, as in the case of multi-ply metal bellows welding seams [8], as well as all other components of the investigated ball valves. In addition, it is important to notice how the weld fracture mechanisms work with hydrogen gas [40].

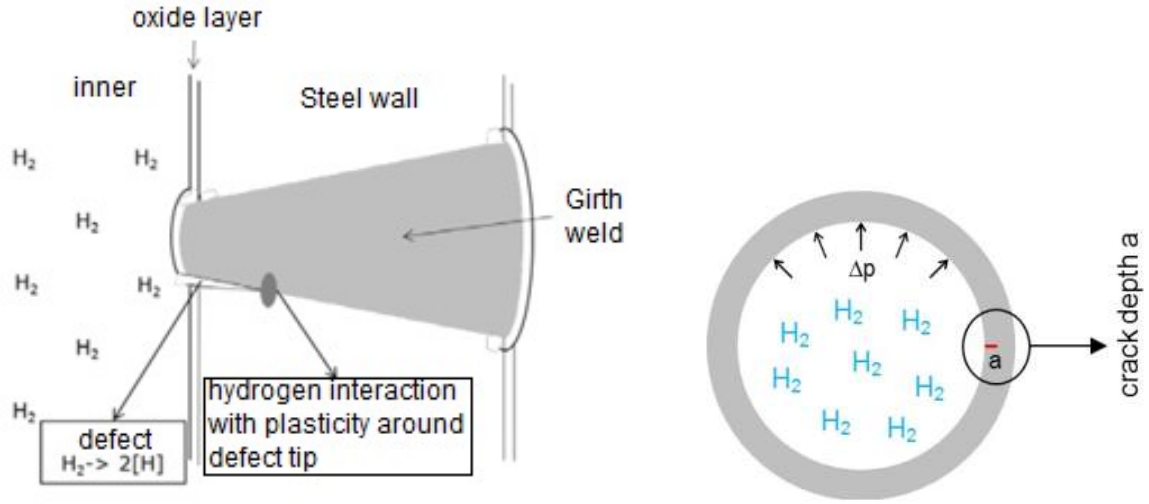

Figure 2.8: Hydrogen-enhanced fatigue crack growth [45]

Welding defects can grow faster in hydrogen gas under fatigue due to pressure cycles, than in nitrogen or natural gas. Hydrogen molecules dissociate on newly created steel surfaces and are absorbed in the weld seam [45]. Hydrogen atoms interact with the steel around the plastic zone of a growing crack-like defect, which increases crack growth (Figure 2.8).

In order to observe the position of the fracture in relation to the weld seam, the samples examined after the test. All tested samples are broken into cross sections [40]. However, a clear notch effect found in all cases. In the case of full-wall samples tested in hydrogen gas and in

nitrogen [41]. The stress-strain curves of the solid wall samples (see Figure 2.9) present a significantly changed fracture behaviour due to the notch effect.

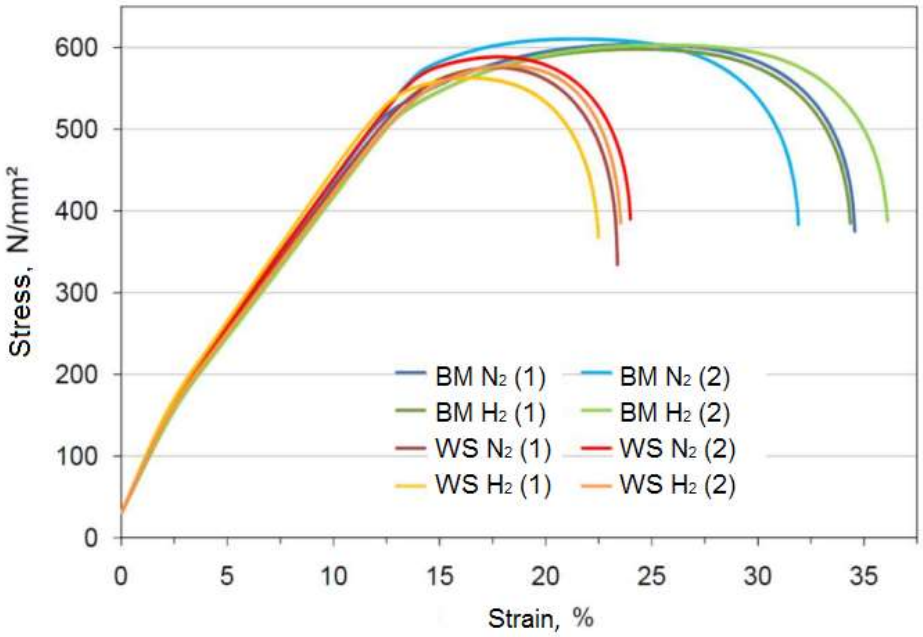

Figure 2.9: SSRT tests of the samples in the weld seam area (WS) and in the base material (BM) in nitrogen N_2 and in hydrogen H_2 enviroment [39]

Hence, a significant influence of the hydrogen on the course of the train curves could not be determined [43]. Due to the changed sample geometry, fracture constriction and plastic elongation could not be determined as characteristic values of ductility.

It noticed that the results presented are exemplary examinations of a single circular seam from a laboratory weld. Since the resistance to hydrogen-influenced corrosion may depend on the material used and the welding process used to create the circular seam, future tests on further circular seams for investigated bellows should be carried out in individual cases [38].

The utility model [4] of the ball valve with the ratchet gear and bellows has many welding connections, all unmovable components connected by welding. Hence, in the case of hydrogen transportation, the hydrogen does not influence the welding seams in the investigated pressure range and temperature. Furthermore, in the design of utility model [4] avoided the leakages, also, due to the welding connections of the unmovable components.

Therefore, the design of the fully welded ball valve with ratchet gear mechanism [4] could be used in further hydrogen pipelines as seal and control fittings.

2.2.2.6 High temperature design

To resist high temperature most of designs of ball valves have ceramic-based (Figure 2.10). This type of ceramic ball valve due to design suitable for media at high temperature up to 950 ºC [98]. On the Figure 2.10, it is a defined clearance between the ceramic ball (1) and the fixed upstream and downstream seats (3). The valve housing (4) and stem (5) are made of stainless steel. The stem packing (6) is made of graphite for temperature resisting.

Nevertheless, the presented ceramic design of the ball valve is expensive and required high tolerances and quality performance in manufacturing that leads to additional costs.

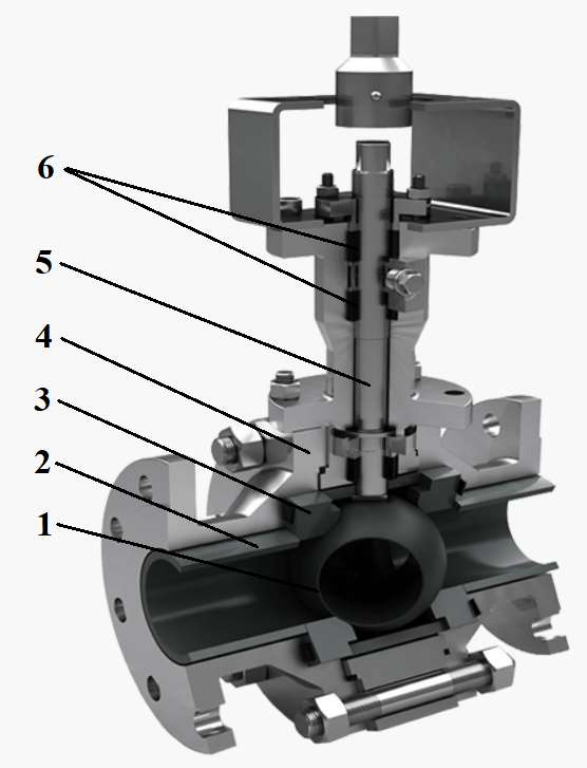

Figure 2.10: High temperature ceramic floating ball valve Samson Group [98]:
1. ceramic ball; 2. ceramic inner pipe; 3. ceramic seats; 4. metal housing; 5. metal stem; 6. graphite packing of the stem

The utility model of the ball valve [4] could be used in the case of high temperatures up to 500 °C. In this case, of high temperature, most of the valves with polymer and elastomer packings lose their performance. The valve components such as seats, gaskets, O-rings, cannot resist high temperature (above 300 °C) due to their physical properties.

Hence, to resist leakages and failure of the investigated valves [2], [3], [4] in the case of high temperature, the bellows used as a seal component, which is highly resistant to expansion in length, in the case of high temperatures. However, for better seal performance, the graphite

packing used in the design of utility model [4] ball valve with ratchet gear mechanism.

2.2.2.7 Cryogenic temperature design of a ball valve

The utility model of ball valve with ratchet gear mechanism [4] for cryogenic purposes can be designed in accordance to industrial standards such as DIN ISO EN 28921 Part 1 [114], BS6364 [113], MSS SP-134 [115]. Besides, the cryogenic ball valve with ratchet gear mechanism can be manufactured depending on service condition, material properties, temperature and pressure range, environment and technical requirements.

The utility model of ball valve with ratchet gear is suitable for corrosive and non-corrosive media and gases without mechanical additional parts. The utility model approved for high and cryogenic temperatures, for media in groups 1 and 2 according to pressure equipment directive (PED) 2014/68/EU [106].

Figure 2.11: Cryogenic ball valve design by Red Point Ltd [111]:
1. stainless steel seats; 2. stainless steel housing; 3. stainless steel ball; 4. stainless steel packing of the stem; 5. stainless steel stem; 6. graphite upper packing of the stem; 7. lever.

Mostly in cryogenic valve applications used liquefied gases, such as liquid hydrogen, nitrogen

and helium. For example, liquid hydrogen used for transportation properties, due to it less volume in liquid substance. For valves applications considered temperatures below –20 °C as low temperature operation case and less than –73 °C as cryogenic operation, which offered an extensive range of specific valves. One of it presented on Figure 2.11.

Cryogenic ball valve produced, for example, by Habonium Ltd. “Industrial valves & actuators” [112] or by Red Point [111] is isolating valve designed to fully open/close the work media. The working temperature ratio from −196 to +70 °C.

2.3 Material properties for constructive parts of investigated ball valve with RGM

Hence, the designed parts of the ball valve with ratchet gear mechanism [4] for cryogenic and high temperature specifications of the used fluids/gases, i. e. the maximal or minimal temperature, which applied to the surface of the considered parts, with temperature range from –273 °C to +500 °C according to DIN EN ISO 13445 Part 2 [116], DIN EN 10028 Part 7 [138], DIN EN 10222 Part 5 [139], DIN EN 10272 [140], DIN EN 10216 Part 5 [141] and AD 2000 [142] Datasheet W2 and W10, as well as for aggressive media chosen the stainless steel 1.4571 [68], [116], [117]. The composition materials of stainless steel 1.4571 are Chrome 18 %, Nickel 10 %, Titan 1 % (Cr18Ni10Ti) [68], [116], [117].

If necessary, for costs reduction of the investigated ball valve with RGM [4], the constructive parts, such as body, seats, ratchet gears body, lever, rod and bearing, stem packing and cover, for temperatures ranges from –50 °C to +350 °C could be manufactured from pressure vessel steel P355NL2 [107], [108], [116] with accordance to DIN EN 10216 Part 3 [148], DIN EN 10028 Part 3 [117] and ASTM A350 LF2 according to ASME-BPVC Section-II Part A [143].

Another parts, such as ratchet wheel for temperatures ranges from –20 °C to +300 °C manufactured from steel 1.1191 (C45E) according to DIN EN 10083-2 [145] and A194 Gr.2 according to ASME-BPVC Section II Part A [143]. The pawls for temperatures range from –20 °C to +300 °C manufactured from steel 1.0037 according to EN 10025 Part 2 [146] and ASTM A283/A283M according to ASME-BPVC Section II Part A [143].

However, the design parts such as ball, stem and single- and multi-ply metal bellows with U-shaped convolution cross section will be manufactured from austenitic stainless steel 1.4571 [68], [116], [117], 1.4006 [116], [147] and 1.4462 [116], [132], [149], due to it physical

properties. Mechanical properties of austenite stainless steel 1.4571 according to DIN EN 10216 Part 5 [141] presented in Table 2.1.

Hence, for application in cryogenic (below –73 ºC) and high (above +280 ºC) temperature ranges, the designed parts of the ball valve and RGM, including ratchet gear housing, made of austenitic stainless steels 1.4571 [68], [116], [117], [149], 1.4006 [116], [147] or 1.4462 [116], [149].

Table 2.1: Mechanical properties of austenite stainless steel 1.4571 according to DIN EN 10216 Part 5 [141], and DIN EN 10088 Part 2 [149]

Yield stress *R*p0,2 min., MPa	Tensile strength *R*m, MPa	Elon-gation *A* min., %	Yield stress *R*p0,2 min. in MPa at high Temperatures:										
			50 °C	100 °C	150 °C	200 °C	250 °C	300 °C	350 °C	400 °C	450 °C	500 °C	550 °C
240	540 till 690	40	207	185	177	167	157	145	140	135	131	129	127

A high proportion of chromium in the steel significantly increase the thermal stability and corrosion resistance. However, the suitability of the stainless steel for welded joints reduced. Nickel increases the yield strength and the impact resistance of the stainless steel. Titanium has an anti-oxidizing effect [18], [116].

The materials of design parts of ball valve design with ratchet gear [4] considered in chapter 3, which are depending on the temperature specification, i. e. the maximal or minimal temperature, which applied to the investigated design.

Table 2.2: Physical properties of austenite stainless steel 1.4571 [68]

Density at 20 °C	Elasticity kN/mm^2 at							Thermal conductivity at 20 °C	Heat capacity at 20 °C
kg/dm³	20 °C	100 °C	200 °C	300 °C	400 °C	450 °C	500 °C	W/m K	J/kg K
7,7	215	212	205	200	190	184	179	30	460

Mechanical and physical properties of stainless steels, which presented in Tables 2.2 - 2.4, are necessary for analytical and FE analysis for more accurate calculations and analysation of investigated constructive parts of the investigated ball valves with RGM [6] in high temperature ranges.

For high temperatures (above +280 °C) and high pressure (1,6 - 2 MPa) design applications, some design parts of ball valve with RGM are manufactured from stainless steel 1.4006 [147].

It is a martensitic stainless steel, which presents satisfied mechanical properties. As a result of its nominal chromium content, 1.4006 displays moderate corrosion resistance to slightly aggressive, non-chloride containing environments, detergents and organic acids. This stainless steel is also resistant to oxidizing atmospheres up to temperatures of about 600 °C [155].

Table 2.3: Mechanical properties of austenite stainless steel 1.4006 according to DIN EN 10088 Part 3 [147]

Yield stress *R*p0,2 min., MPa	Tensile strength *R*m, MPa	Elon-gation *A* min., %	Yield stress *R*p0,2 min. in MPa at high Temperatures:										
			50 °C	100 °C	150 °C	200 °C	250 °C	300 °C	350 °C	400 °C	450 °C	500 °C	550 °C
450	650 till 850	15	437	420	410	400	385	365	355	305	280	255	230

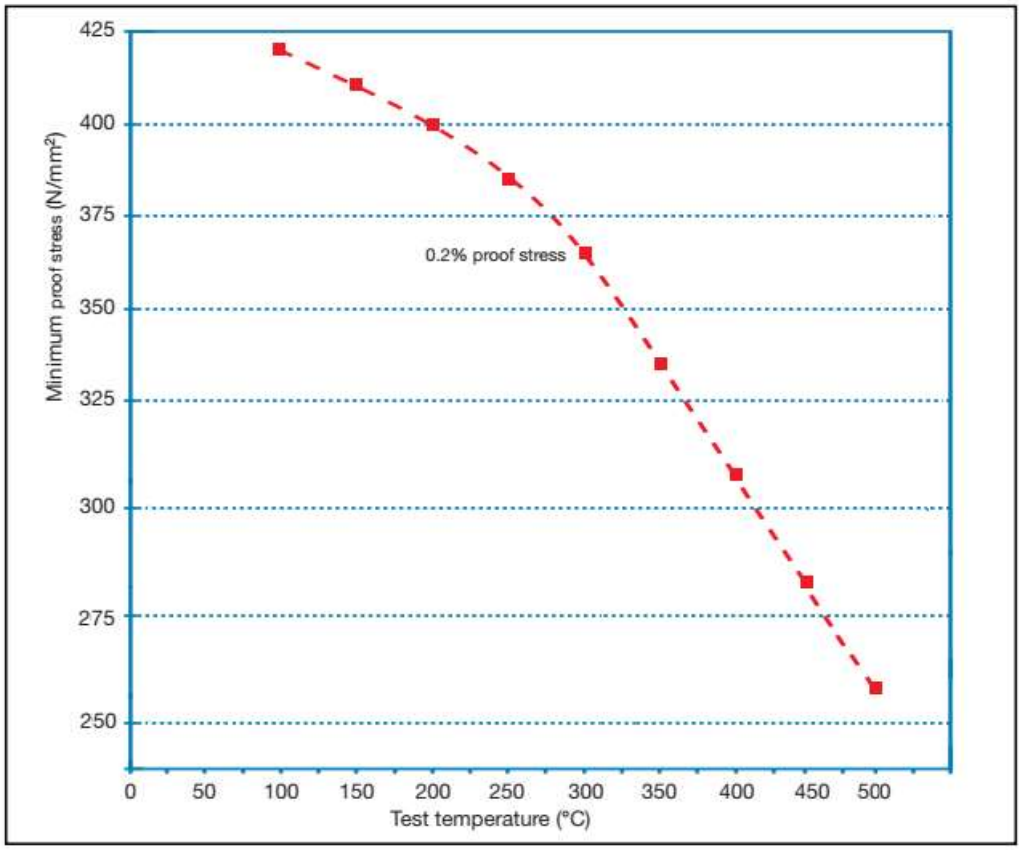

Figure 2.12: Mechanical properties of stainless steel 1.4006 in case of high temperature up to 500 °C

Moreover, design of bellows for high temperature (above +280 °C) and high pressure (1,6 – 2 MPa) applications, could be manufactured from duplex stainless steels, such as 1.4462 [116], [149], which contain varying proportions of ferrite and austenite in the microstructure and the ferritic phase is highly alloyed. Therefore, due to it excellent mechanical and physical properties

this stainless steel is perfectly suitable for high temperature applications [156].

Table 2.4: Physical properties of austenite stainless steel 1.4006 [68]

Density at 20 °C	Elasticity kN/mm² at							Thermal conductivity at 20 °C	Heat capacity at 20 °C
kg/dm³	20 °C	100 °C	200 °C	300 °C	400 °C	450 °C	500 °C	W/m K	J/kg K
7,7	215	212	205	200	190	184	179	30	460

Nevertheless, due to high cost of 1.4462 [149] for further analytical and FE analysis above +280 °C will be used stainless steels 1.4006 [147]. In addition, the considered austenitic steels 1.4006, 1.4462 and 1.4571 are commonly specified for cryogenic service according to EN ISO 10088-2 (3) [147], [149], and to EN ISO 13445-2 [116].

Therefore, they are purified of metalloid impurities and, lightly alloyed with beneficial grain boundary surfactants (C and Si), also their solution strengthened with interstitial nitrogen. The considered alloys have significant concentrations of Cr, which increase the nitrogen solubility with concentrations of 0.2 - 0.4 % mass without embrittling grain boundaries [157].

2.4 Conclusion

Analysis of global industrial valve market presented important advantages aspects of utility model ball valve with ratchet gear mechanism [4], such as workability in wide temperature range, resistance to many chemical solutions. Presented design of the ball valve could be a solution for low-pressure industrial applications on the market.

Presented utility models [2], [3], [4] are created on behave of analysation designs of industrial valves, for instance ball valves [85], butterfly valves [87], wedge gate valves [84], knife valves [83], diaphragm valves [86]. The designs of existing types of industrial valves were analysed and the main problems determined, such as seal elements, which are varied and chosen according to working media (fluids or gases), internal pressure and temperature. Therefore, it makes production of ball valve more expensive due to different designs for each kind of operation case.

The presented utility models [2], [3], [4] do not have a non-metallic seal element (seats, gaskets or O-rings), therefore, the designs of new industrial valves can cover wide range of required properties. That makes the designs unique for many applications, which leads to decry costs of

production.

The ball valve design with ratchet gear mechanism [4] is one type of industrial valves, which can be increasingly used for various applications in industry. The ball valve as a standard design is cheap in production, also has high reliability, therefore, this design has been selected for a basement of the utility model [4].

Further analysation of ball valves for high or cryogenic temperature applications provided consolidation of responsibility and reliability of utility model ball valve with ratchet gear mechanism [4] for temperature range from – 271 °C till 500 °C. Hence, as it mentioned, it is unique design for many industrial applications.

Contemporaneously, along with each constructive element of the utility model ball valve with ratchet gear mechanism [4], the bellows will be the main analysis element, considered in this research work.

Hence, a stainless steel multi-ply bellows is a main seal component of the utility model ball valve with ratchet gear [4]. It compensates three loads, such as temperature expansion, internal pressure and bending. Therefore, it was important to study different installation cases of investigated bellows.

Nevertheless, the bellows is the most unstable component of the utility model ball valve with ratchet gear mechanism [4], therefore, it required a more detailed and accurate analysis of this constructive element of the design. In addition, its unique installation case on the ratchet gear mechanism had to be detailed analyzed by analytical and finite element analyses to consider the workability and reliability of the whole design.

The difficult analysis model of the bellows provides an idea to develop a new analytical analysis model for the bellows with a U-shaped convolution cross-section for gentle and prompt analysis. For this purpose, it would consider Clark's theory [25] (on the theory of thin elastic toroidal shells) and developed for the bellows with U-shaped convolution cross-section analysis.

Finally, after design consideration of investigated ball valve with ratchet gear mechanism and bellows, it was necessary to decide on dimensions and develop different sizes and pressure ranges for industry applications.

3. Ball valve - sizing and interpretation for FE analysis

In this chapter considered the designs of ratchet gear mechanism constructive elements for ball valves [4] with nominal diameter of 100 mm, 150 mm, 200 mm, and 300 mm.

As standard dimensions of the ball valve were determined, the next step was to consider dimensions of the RGM. Hence, the definition of dimensions of construction elements of RGM required analysation of required stem torque [62]. For this purpose, the analysation of the seats, closure (ball) and stem (Figure 3.1) was achieved with analytical and FE analysation methods. The required stem torque (or breakaway torque) and these three constituent elements of ball valve design with the defined boundary conditions, such as internal pressure, were most important to further design constituent elements dimensions of RGM, due to main influence of torque on the top section of the stem.

The investigated constituent elements of ball valve with RGM presented on Figure 3.1.

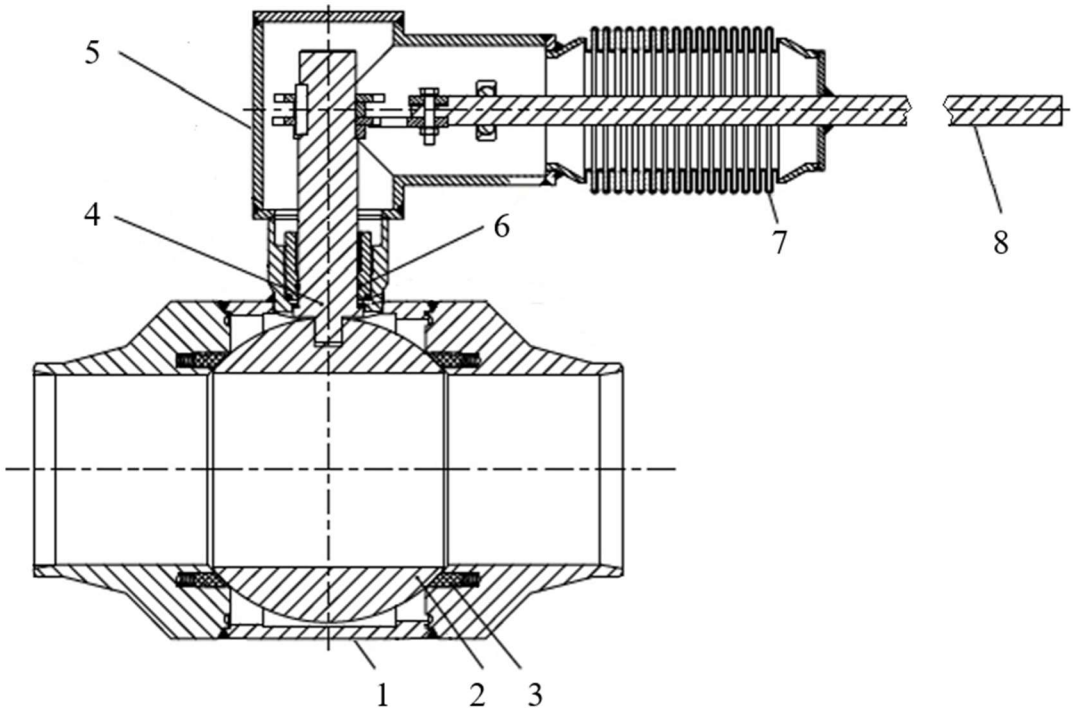

Figure 3.1: Sketch of investigated ball valve [4] of nominal diameter 100 mm with RGM constituent elements (Technical drawings and parts list - Appendix C):
1. valve body; 2. ball; 3. seat; 4. stem; 5. gear body with ratchet wheels, pawls and rod end bearing; 6. packing; 7. bellows with circular U-shaped convolution cross section; 8. lever.

The operation loads for designed ball valves with RGM consider: maximal internal pressure - 2 MPa; maximal bending of bellows - 10 °; temperature influence: minimal –271 °C and maximal +500 °C. These operation loads detailed analysed for each designed element, as well

as for the RGM design.

The validation of investigated ball valve [4] and construction parts considered according to ISO 9000 [150].

3.1 Stem torque analysation for investigated ball valve with RGM

The initial phase of ball valve design is the appeared maximal torque (breakaway torque plus safety factor) on the stem. The design of all parts of the ball valve depended to that torque, which appears due to influence of internal pressure on the contact area of seats to ball and on the surface of the ball in closed position. The analytical scheme presented on Figure 3.2.

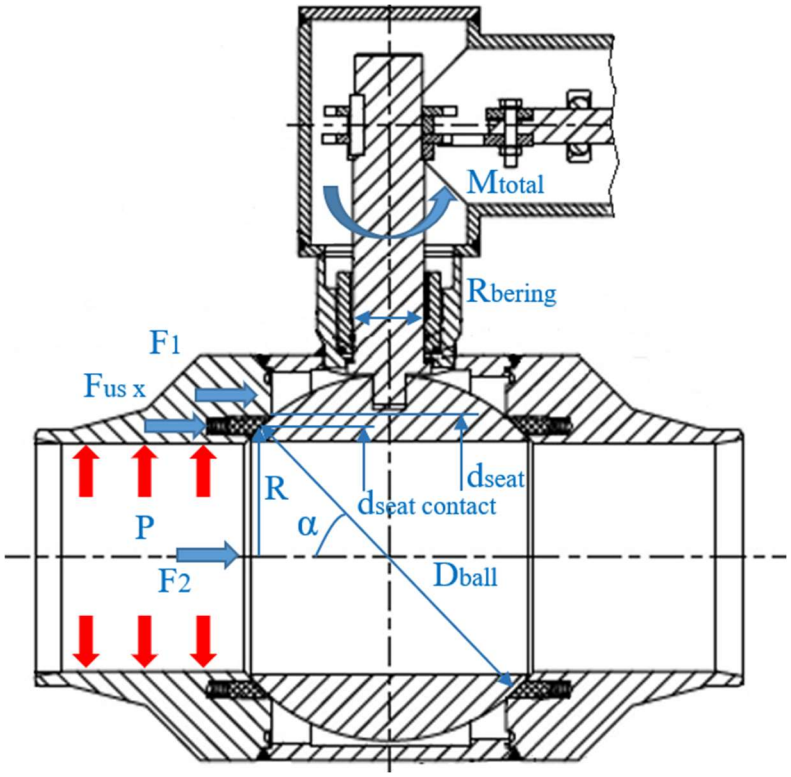

Figure 3.2: Analytical scheme of the stem torque (full open position of the ball)

Hence, the design of ratchet gear mechanism with bellows required to consider the breakaway torque (maximal stem torque) [62]. To receive the value of the torque, which appeared on the connection point of the stem to ratchet gear wheels, has used analytical, FE analysis and experimental laboratory setup (see chapter 5). In addition, the required stem torque has proved with FE analysis (see chapter 6) of investigated RGM with defined boundary conditions and its dimensions. Hence, the required torque value, which appeared on the stem in the investigated ball valve design of utility model 139949: ball valve with ratchet gear mechanism [4], is main factor, which is influencing to dimensions of all construction elements of defined RGM design. In this doctor thesis, design of the investigated fully welded ball valve [4] is not significant;

notwithstanding the ratchet gear mechanism, which is detailed analysed in this chapter.

Namely, there are various numbers of the torque calculations methods, for example, calculation method, which described K. Sotoodeh in "The importance of maximum allowable stem torque in valves" [62]. It is important to notice that value of the torque depends on the type of seats, ball and support bearings.

For analysis of the torque without influence of pressure, i. e. required moment on the stem to overcome the force that appeared on the contact surface of ball from spring's force, which pressure the seats to ball to make ball valve fully seal in low pressure range, it is necessary to consider the seat contact angle:

$$\alpha_{seat} = \sin^{-1}(d_{seat\ contact}/D_{ball}) \tag{3.1}$$

Next step is to consider the seat preload force appeared on the seat contact surface to ball:

$$F_{us} = \pi \cdot d_{seat\ contact} \cdot b_{seat\ u} \cdot c_{spf} \tag{3.2}$$

The seat preload force in X-direction considered as follows:

$$F_{usx} = F_{us} \cdot \cos \alpha_{seat} \tag{3.3}$$

Hence, friction torque from seat preload force equal:

$$M_{us} = F_{uvx} \cdot \mu_{seat/ball} \cdot \frac{R}{\cos \alpha_{seat}} \tag{3.4}$$

To approach the analytical analysation of required torque to rotate the ball, due to influence of internal pressure, it is necessary to find force F_1, which considered as influence of internal pressure (on media attached surface of the ball) in closed position:

$$F_1 = {d_{seat}}^2 \cdot \frac{\pi}{4} \cdot P \tag{3.5}$$

In case of closed position of the ball appeared the maximal torque of investigated ball valve design, due to maximal area on which has influence the internal pressure *P*.

Another force F_2 appeared from influence of internal pressure on the contact area of seat to ball:

$$F_2 = A_{seat\ area} \cdot P \tag{3.6}$$

where,

$$A_{seat\ area} = \frac{\pi}{4} \cdot \left({d_{seat}}^2 - {d_{seat\ contact}}^2\right) \tag{3.7}$$

The force F_1 influence on the torque, which appeared on the stem:

$$M_{stem} = \frac{F_1}{2} \cdot \mu_{stem-bearing} \cdot R_{bearing} \tag{3.8}$$

The force F_2 leads to the torque M_{seat}, which appeared from influence of internal pressure on contact area of seat to the ball:

$$M_{seat} = R \cdot F_2 \cdot \mu_{seat-ball} \tag{3.9}$$

where, $\mu_{seat-bal}$ is friction constant, which depended on the seat and ball materials, also on the flow media; R is radius from middle axis of the ball valve to contact point of seat to ball:

$$R = \sqrt{\left(\frac{D_{ball}}{2}\right)^2 - \left(\frac{d_{seat\ contact}}{2}\right)^2} \tag{3.10}$$

However, the maximal friction constant on the contact area of seat to ball appeared during dry contact condition, i.e. in this case the reduction of friction due to influence of flow media does not considered. Therefore, the friction constant $\mu_{seat/ball}$ supposed as maximal possible friction on the contact area of the seat to ball, which depended on their material properties.

The total stem torque (breakaway torque) is equal:

$$M_{total} = M_{stem} + M_{seat} + M_{us} \tag{3.11}$$

Hence, the RGM must surmount the total stem torque M_{total} [N·m] to achieve the rotation of the gate ball to closed/opened position. The results of total stem torque analytical analysation presented in Table 3.1, and depended on considered internal pressure and diameter of the ball valve.

Moreover, the required stem torque M_{total} [N·m] (see Figure 3.2) for the nominal diameter of 100 mm equals to 26,64 N·m. For safety reasons, the safety factor *S* equals to 1,5, according to pressure equipment directive PED [106] and specification for pipeline and piping valves API 6D [51]. Therefore the torque for investigated ball valve with ratchet gear mechanism is equal to $M_{total} \cdot S_t$ [N·m], for instance, for ball valve with DN 100 mm and nominal pressure of 2 MPa the $M_{total} \cdot S$ is equal to 39,97 N·m [5].

To validate analytical results of required stem torque [62] was used FE analysis (Figure 3.3), therefore the optimisation tool and user defined parameters, helped to scope dimensions of RGM for investigated ball valves with nominal diameters of 100 mm, 150 mm, 200 mm and 300 mm (see Table 3.1, FEA).

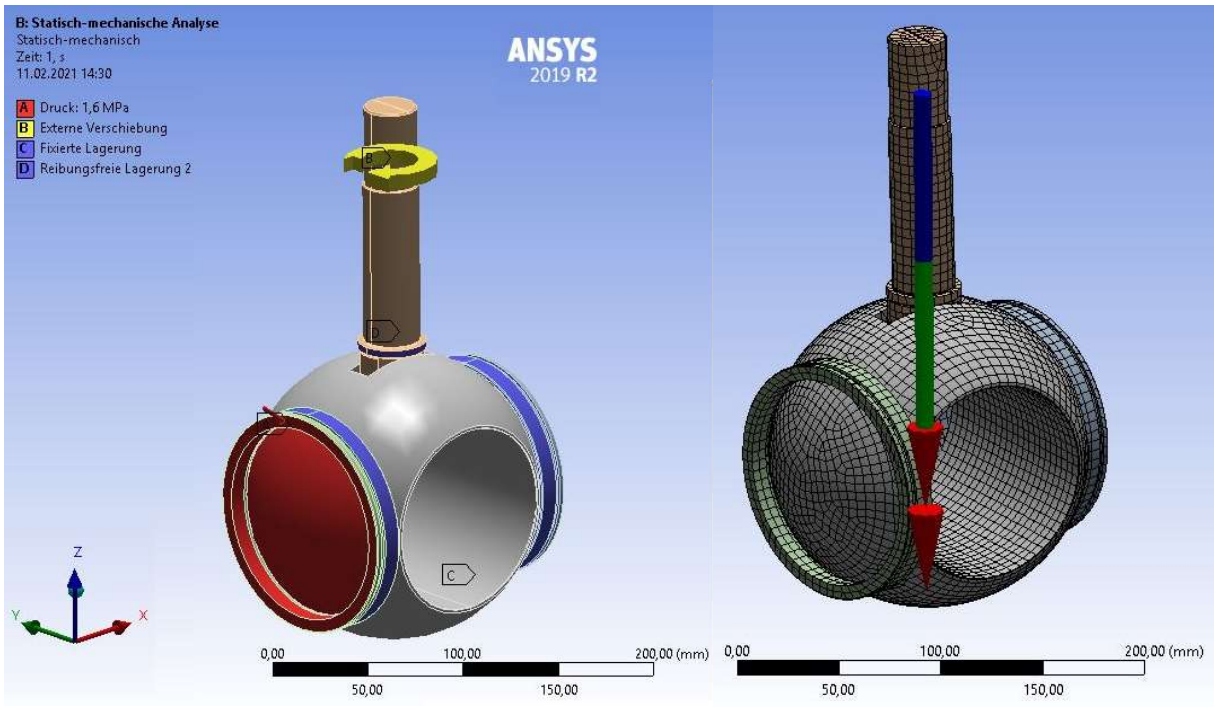

a. b.

Figure 3.3: Required torque on the stem of investigated ball valve DN 100 PN 20, Class 150:

a. C, D: user defined support; A: internal pressure; B: angle of deflection from 0 to 90°;

b. Results of torque simulation (the required stem torque equals to 26,53 N·m for investigated stainless steel seats).

Table 3.1: Analytical (AA) and finite element (FEA) analyses of required torque (breakaway torque) in N·m of investigated ball valves [4] with nominal diameters of 100 mm, 150 mm, 200 mm and 300 mm

	M_{total}, N·m							
Torque	DN 100, N·m		DN 150, N·m		DN 200, N·m		DN 300, N·m	
PN, MPa	AA	FEA	AA	FEA	AA	FEA	AA	FEA
0,3	8,12	8,04	20,25	20,21	33,31	33,37	99,13	99,26
0,6	11,39	11,25	29,71	29,63	48,19	48,16	155,06	155,37
1	15,75	15,58	42,32	42,27	68,04	67,98	229,62	229,87
1,6	22,29	22,17	61,23	61,19	97,82	97,78	341,46	340,24
2	26,64	26,53	73,85	73,82	117,66	117,73	416,03	414,91

Whereas, for further analytical and FE analyses, the friction on the contact between seat and ball is admitted as 0,11 [175] for the friction case of stainless steel to stainless steel [68]. The friction coefficient considered for clean and dry features, due to approached maximal torque in this contact condition. The friction coefficient between the main shaft section of the stem and stem bearing assumed as 0,1 [135], graphite to stainless steel 1.4006 [147].

The FE analysis presented the torque appeared on the top section of the stem, more precisely, on the key that connected to ratchet wheels (Figure 3.3). Another words, it was determinated required torque on the top section of the stem, which must fulfill the ratchet gear mechanism to move the gate ball to open or closed position.

Therefore, required torque without safety factor S for different nominal diameters of the investigated ball valves designs presented in Tables 3.1. The presented results of required torque received for loading case of internal pressure till 2 MPa according to ISO EN 1333 [63] and specification for pipeline and piping valves API 6D [51]. The safety factor S_t for required torque shall be more or equal to 1,5, according to API 6D [51] and PED [106]. Due to weakest component the ratchet wheel of RGM, the existing torque, the maximal allowable existing stem torque, according to Attachment B, section B.1.2, is equal to 39,97 N·m for investigated ball valve DN 100 with RGM [4].

Namely, FE analysis have proved the required torque of the analytical calculations. This is main point to start the further design of the ratchet gear mechanism, such as lever and bellows for the investigated utility model of the ball valve with RGM [4].

3.2 Analytical and FE analyses of ratchet wheels, pawls and lever

To approach required stem torque [62] for investigated ball valves was created the ratchet gear mechanism [5] (see Figure 3.4), which consist four main constructive parts, namely ratchet wheel 1, which firmly fixed on the stem and turns about its axis. The ratchet wheel 1 has a coupling with pawl 2. The pawls 2 hinged together by turning bolting pair on the lever 3, which turns about fixed axis of rod end bearing 4. The rod and bearing fixed welded to housing of the RGM.

The force F_L applied on the one end of the lever, which could be applied by hand or any automatic mechanism, such as pneumatic or electric motor. On another end of the lever 3 the force F_L transferred to the pawl 2 with force F_P. The force F_P must be enough to rotate the ratchet wheel, which firmly connected on the stem by the key. The maximal force F_L according to specification for pipeline and piping valves API 6D [51] required at the end of lever (wrench) to apply the breakaway torque shall not exceed 360 N.

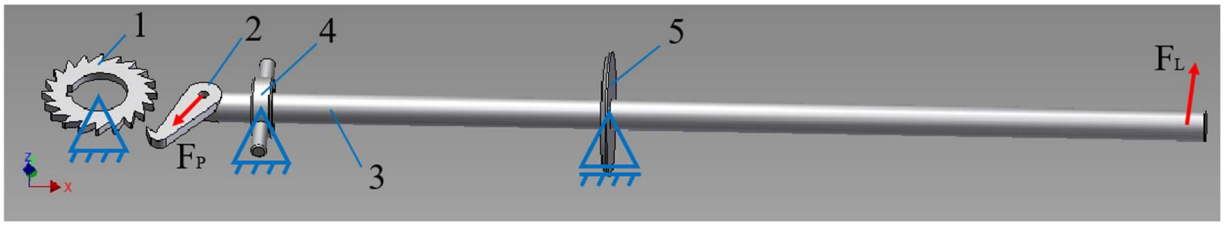

Figure 3.4: Ratchet gear mechanism, analysation model:

1. ratchet wheel; 2. pawl; 3. lever; 4. rod end bearing; 5. cover of bellows.

The force F_P calculated depending on the interrelation from end of the lever until rod end bearing and from rod end bearing to connection point of pawl to tooth of ratchet wheel. The interrelation of dimensions influencing F_P presented in Table 3.2.

Table 3.2: Interrelation of dimensions influencing force F_P:

DN 100		DN 150		DN 200		DN 300	
F_L, N	F_P, N	F_L, N	F_P, N	F_L, N	F_P, N	F_L, N	F_P, N
27,91	444,07	51,58	820,51	61,64	980,54	118,87	1891,03

The bellows in the design of RGM is main sealed element, and it functioned as a spring to fix lever 3 at centre position, when none of pawls contact the ratchet wheels. To provide full sealing of the RGM, the bellows sealed by the cover 5, which firmly, by welding, fixed on the lever 3.

In this subchapter will be analysed the main construction elements of RGM. Whereas, it will be analytically and FE analysed and defined dimensions of the constructive parts for the further design of the investigated ball valve with RGM [4].

3.2.1 Analytical and FE analysis of RGM: ratchet wheel, pawl, lever

The investigated ratchet wheel mechanism (see Figure 3.4) with constituted elements: ratchet wheel, pawl, lever and rod end bearing, was analytically analysed and validated (see Attachment B, sections B.2.2-B.2.4). In addition, the analytical results were compared to FE analysis.

The dimensions of the ratchet wheels and pawls have influence to the entire constituent parts of investigated ratchet gear mechanism. Hence, the definition of these constituent elements was primary for the design of ball valve with RGM (Figure 3.5).

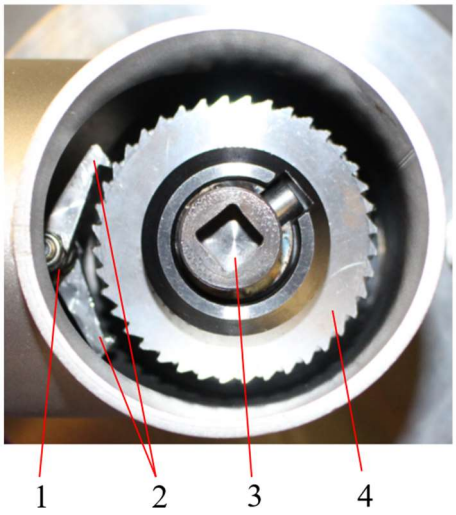

Figure 3.5: Installed pawls hinged together by turning bolting pair on the lever and firmly installed ratchet wheels on the stem by the key:
1. Lever; 2. Pawls; 3. Stem; 4. Ratchet wheel.

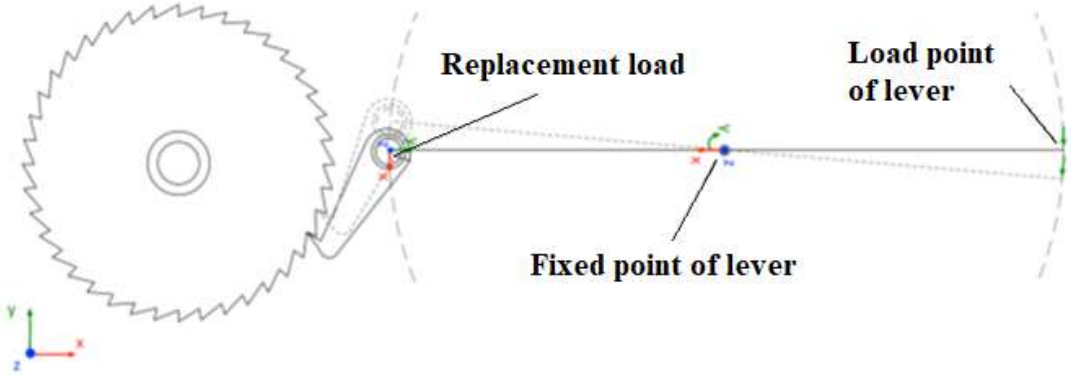

Figure 3.6: Analytical model of investigated ratchet gear mechanism

Whereas, for analysation the force balance of RGM and equivalent stresses of the constituent parts of RGM, it has created the analytical model (Figure 3.6). With the help of analytical model and its validation with FE analysis (for detailed FE analysis see chapter 6) were considered dimensions of the RGM constituent elements for investigated nominal diameters of ball valves [4].

For the definition of the investigated RGM model assumed that the ratchet wheel is centred rigid, thus, a clamping was applied (see Figure 3.7, point A). For simplification, a central clamping was determined in comparison with to FE analysis model (see chapter 6) and rigid area was not a radial. For a realistic behaviour of the ratchet wheel, a model with an articulated centre and a forced surface load would assumed. However, the maximum possible load has considered for the ratchet wheel and pawl. Thus, the maximum unfavourable load case would

considered. Therefore, in the analytical analysation of the real model, a fixed bearing of the ratchet wheels is used.

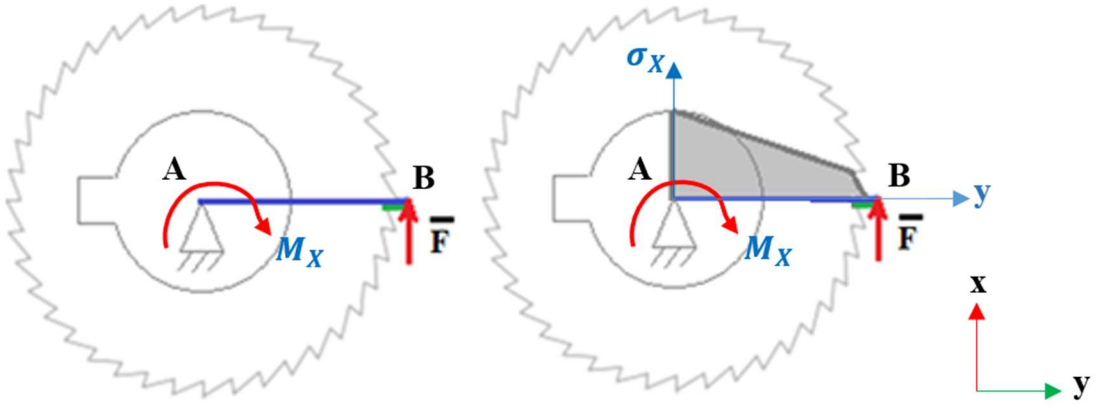

a. b.

Figure 3.7: Analytical model and stress curve of investigated ratchet wheels:
a. analytical model; b. stress curve of investigated ratchet wheels

Hence, to solve the analytical model which presented on Figure 3.6, two approaches followed to develop an analytical solution for the RGM. In the first approach, a mechanical replacement model has defined for the ratchet wheel (see Figure 3.7). The second approach was the analysis of equivalent stresses, which appeared in ratchet wheels according to validation methodology of the standard EN ISO 3990 [77].

The following equation used to determine an approximate stress on coupled tooth of the ratchet wheel:

$$\sigma_x = \frac{F_x}{A} + \frac{M_x}{W} \tag{3.9}$$

Accordingly, the investigated area of the respective acting force was determined as area of the contact of the pawl with the tooth of the ratchet wheel at point B. Hence, it was determined an approximate stress curve (Figure 3.7), where B point of Y-coordinate system assumed as the tip of the investigated tooth of the ratchet wheel. The length of to the middle point of investigated ratchet wheel in this case was 25 mm, according to considered dimensions of ratchet wheel for ball valve with nominal diameter of 100 mm. The following hatched area chosen as the acting area. For the stress curve, the equation (3.9) was determined as a function of X-coordinate system.

The ratchet wheel validated by this approach. The analytical model depended on the standard EN ISO 3990 Part 3 [77]. However, the stresses in the contact area of the investigated coupled

tooth of the ratchet wheel from stem torque analysed with followed equations:

$$\sigma_{FO} = \frac{F}{b \cdot m_n} \cdot Y_{Fa} \cdot Y_{Sa} \cdot Y_{\varepsilon} \cdot Y_{\beta} \tag{3.10}$$

By simplifying the assumption of the correction factors (Y_{Fa}, Y_{Sa}, Y_{ε}, Y_{β}) which presumably equal to 1. Therefore, following equation used to calculate the stress at the tip of investigated ratchet wheel tooth:

$$\sigma_{FO} = \frac{F}{b \cdot m} \tag{3.11}$$

where, $m = \frac{Diameter\ of\ the\ ratchet\ wheel}{Teeth\ amount\ of\ ratch\quad whee}$

According to EN ISO 3990 [77], the calculated stress must be compared with the maximum tangent stress at ratchet wheel tooth tip. The maximum tensile stresses of the ratchet wheel were analysed according to EN ISO 3990 [77] at the tip of the tooth flank, on which the force acts from the coupling with the pawl. The FE analysis of the ratchet gear mechanism confirmed the local maximum equivalent stresses (see Chapter 6.1). Since the results were validated (see Attachment B, section B.2.2), the stress results of analytical analysis have been compared to FE analysis (see Table 3.3).

Table 3.3: Analytical and FE analysis of equivalent stresses σ_{eq} of ratchet wheel, pawls and lever

DN, mm	Equivalent stresses σ_{eq}, MPa					
	Ratchet wheel		Pawl		Lever	
	Analytical analysis	FE analysis	Analytical analysis	FE analysis	Analytical analysis	FE analysis
100	158,53	152,19	131,58	124,87	131,07	124,12
150	170,39	167,72	136,75	132,91	140,15	133,94
200	157,98	155,36	120,07	117,29	85,75	82,19
300	142,77	139,18	140,08	136,02	113,61	106,78

The design dimensions of ratchet wheels and pawls for RGM determined in Table 3.4 and Table 3.3 respectively. The results of analytical validation and FE analysis of equivalent stresses σ_{eq} of ratchet wheel, pawls and lever presented in Table 3.3.

The analytical validation and FE analysis of equivalent stresses of ratchet wheel, pawls and lever approached with stainless steel 1.4006 with yield strain stress at 500 °C is 255 MPa according to EN 10088 Part 3 [149]. The maximal equivalent stress of analysed designs of investigated ball valve with RGM [4] DN 100 PN 20 Class 150 is 158,53 MPa at ratchet wheel, which is satisfied for this design, with safety factor of 1,8.

3.2.2 Ratchet wheel

Hence, after definition and validation of the analytical model of RGM and maximal allowable stem torque, it required to define dimensions of ratchet wheel for investigated ratchet gear mechanism. The ratchet wheels had defined with standard EN ISO DIN 867 [118] for maximal required stem torque of according nominal diameters of investigated ball valve with RGM [4]. For ratchet gear wheels used stainless steel 1.4006 [147].

The ratchet wheels in the design of RGM must achieve the maximal required stem torque [62]. Therefore, dimensions of the ratchet wheels defined depending on maximal required stem torque, which was considered in Table 3.1, multiplied by safety factor 1,5. Therefore, for each considered nominal diameter of investigated ball valve [4], the dimensions of ratchet wheels defined according to analysation of standard EN ISO DIN 867 [118] and validated with FE analysis.

Table 3.4: Ratchet wheel dimensions for investigated ball valve designs [4]

DN, mm	Max. required torque M_{Total}, N·m	Ratchet wheel diameter D_G, mm	Number of ratchet wheel teeth n_G
100	26,64	60 mm	40
150	73,85	90 mm	50
200	117,66	120 mm	60
300	416,03	220 mm	88

The suitable dimensions of the ratchet wheels considered as standard constituent elements and ordered for experiments from Maedler Ltd. [119] (see chapter 5). The defined dimensions of ratchet wheel presented in Table 3.4.

3.2.3 Pawls

As the dimensions of the ratchet wheels were defined for different nominal diameter of investigated ball valves with RGM [4], dependent on maximal required stem torque, the next step required the definition of the pawl's dimensions (Table 3.5). For pawls used stainless steel 1.4006 [147].

Table 3.5: Pawl dimensions for investigated ball valve with RGM designs [4]

DN, mm	L, mm	Db, mm	Dc, mm	Ab, °	At, °	Rh, mm
100	49,5	5	18	10	15	4
150	49,5	5	18	10	15	6
200	75	8	26	12	20	7
300	100	12	38	15	25	9

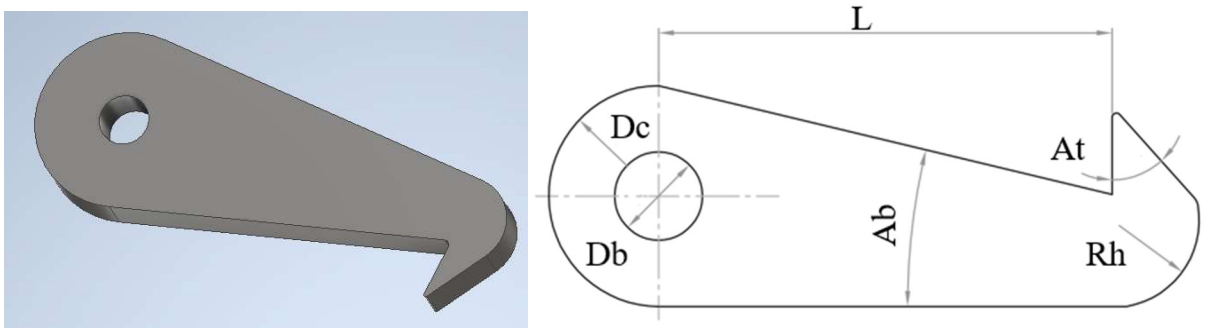

Figure 3.8: CAD sketch and dimensions of the pawl

3.2.4 The lever

The pawls hinged together by turning bolting pair on the lever (Figure 3.9). The lever moved axial either by the engine or per hand force. The defined dimensions of the lever analytically validated in Attachment B, section B.2.4. Forces equilibrium for lever defined by following equation:

$$F_L \cdot l_{L1} = F_p \cdot sin\alpha \cdot l_{L2} \tag{3.12}$$

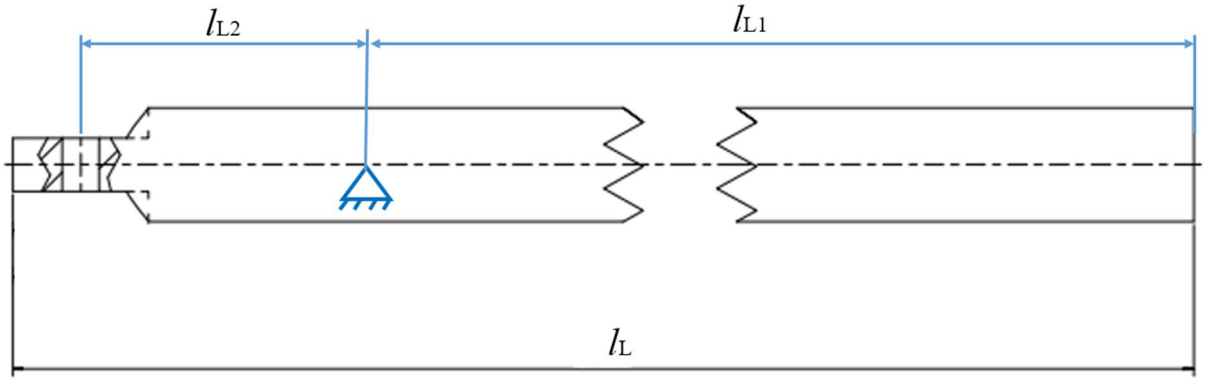

Figure 3.9: Sketch and dimensions of investigated lever

The lever diameter considered as 10 mm for DN 100 mm and as 12 mm for 150 mm and 14 mm for DN 200 mm and as 16 mm for 300 mm. The length of the lever is 500 mm for all investigated nominal diameters of ball valves [4]. The lever made of stainless steel 1.4006 [147]

for high and cryogenic temperatures as well.

3.2.5 Rod end bearing

For firmly fixation of the lever, and to insure it function as the rocker lever, the dimensions of rod end bearing (Figure 3.11) defined according to the standard EN ISO 12240 Part 4 [137].

The rod end bearing firmly connected by welding to the RGM housing from both sides to remain the rocker lever in the middle axis of the bellows. The materials for rod end bearing used as stainless steel 1.4571 [68], [116]. The defined dimensions of the rod end bearing as a standard construction element considered in Table 3.6.

Table 3.6: Dimensions of rod end bearing according to EN ISO 12240 Part 4 [137]

	d, mm	d_2, mm	G	h_1, mm	α_{red}, °	C_1, mm	B, mm	d_k, mm	l_3, mm	l_4, mm	l_7, mm
DN 100	10	29	M10x1,5	48	19,73	7	9	16	26	62,5	15
DN 150	12	34	M12x1,75	54	14,63	8	10	18	28	71	15
DN 200	14	40	M14x2	63	11,32	10	12	22	34	83	20
DN 300	16	46	M16x2	69	15,12	12	14	25	35	92	23

Therefore, presented dimensions of the rod end bearing in Table 3.6 considered according to EN ISO 12240 Part 4 [137] (Figure 3.10), consist: α_{red} - max. angle of rotation of rod end bearing's ball; B - thickness of the rod end bearing's ball; C_1 - thickness of the rod end bearing's head; d - diameter of a hole in the ball; d_k - diameter of the ball; d_2 - head diameter of rod end bearing; G - thread diameter; h_1 - height from middle of a ball to the tread end; l_3 - length of the tread; l_4 - length of the rod end bearing; l_7 - length/radius of the rod end bearing's head.

The angle of tilt in a rod end controlled by the outside diameter of the ball and head. The maximum degree of tilt is obtained, when the ball contacts the edge of the head or bearing in which it is mounted. Maximum angle of rod end bearing tilt is assumed by following equation α_{reb}:

$$\alpha_{reb} = sin^{-1}\left(\frac{B}{d}\right) - sin^{-1}\left(\frac{C_1}{d}\right) \tag{3.13}$$

The maximum static radial load allowable for a rod end bearing depends on three factors: pressure strength; strength of rod end bearing head; and strength of threaded section rod end bearing. The maximum static radial load of investigated rod and bearing is determined by taking the lowest of the three following values:

a.) Pressure strengths $F_{Preb\,max}$:

$$F_{Preb\,max} = d_K \cdot C_1 \cdot R_{p0,2/T} \tag{3.14}$$

b.) Rod end bearing head strength $F_{reb\,max}$:

$$F_{reb\,max} = (d_2 \cdot (d_K + 0{,}176 \cdot C_1)) \cdot C_1 \cdot R_{p0,2/T} \tag{3.15}$$

c.) Strength $F_{thread\,max}$ of threaded section rod end bearing:

$$F_{thread\,max} = (R_{threa}^2 \cdot 0{,}78) \cdot R_{p0,2/T} \tag{3.16}$$

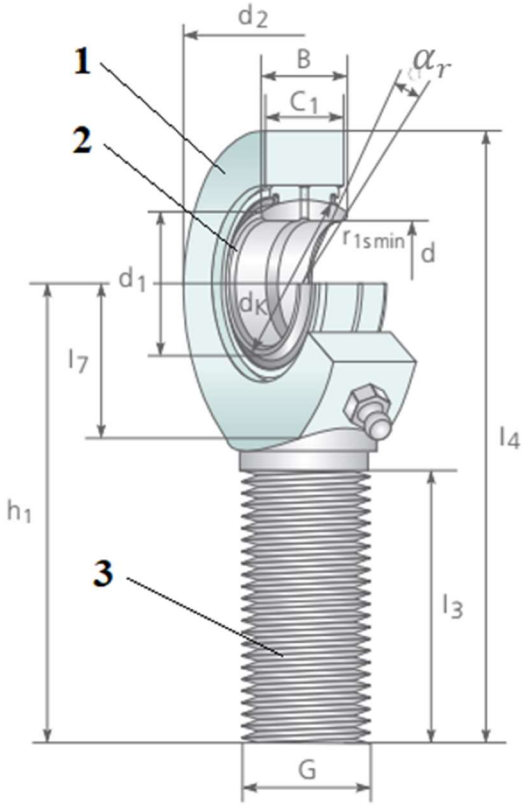

Figure 3.10: Rod end bearing Ø15 mm for investigated ball valve of nominal diameter 100 mm: 1. thread; 2. rod end bearing's ball; 3. rod end bearing's head.

The maximum available axial load for a rod end bearing is determined by following equation, which does not take into consideration bending of the thread. The axial strength of rod end bearing is $F_{Axial\,reb\,max}$:

$$F_{Axial\,reb\,max} = 0{,}78 \cdot ((d_K + 0{,}176 \cdot C_1)^2 - d_K^2) \cdot R_{p0,2/T} \tag{3.17}$$

3.2.6 Gearbox housing

The RGM housing (Figure 3.11) designed to withstand the maximal internal pressure and

temperature influence. Thereby, the RGM housing (Figure 3.12) designed to fix bellows and rod end bearing on it. For gearbox housing used steel P355NL1/ASTM350 LF2 [132] and for high and cryogenic temperatures stainless steel 1.4571 [68].

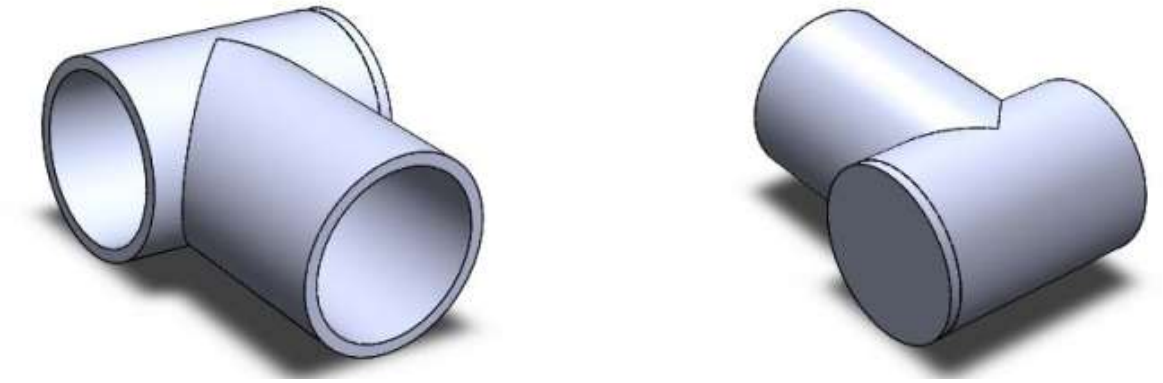

Figure 3.11: Design of RGM housing for investigated ball valve with nominal diameter of 100 mm

The analytical analysation of RGM housing achieved with standard EN ISO DIN 13445 Part 3 [116]. It defined dimensions of the shell thickness as well as analysation of the welding connections of the RGM housing. Therefore, to insure defined dimensions of the RGM housing, in such complex load case, analytical results validated with FE analysis (Figure 3.12).

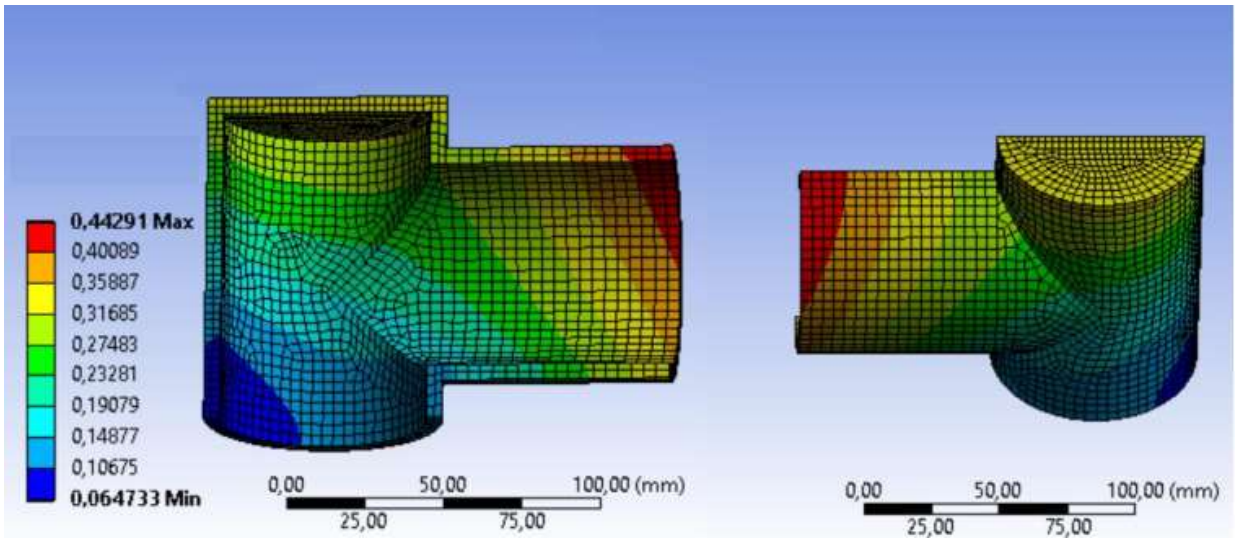

Figure 3.12: Ratchet gear mechanism housing FE deformation analysis (the scale shows deformations of the structure of the RGM housing in mm)

The FE analysis of equivalent stresses presented on Figure 3.13. The internal pressure, for this analysation case, was considered as 1,6 MPa, which leaded to maximal equivalent stresses of ~206 MPa. These stresses occurred in the lower area of the main housing part (red circle). However, since these are the fixed nodes, no further attention required to this high stress.

Rather, it is an inaccuracy accepted for the fix support.

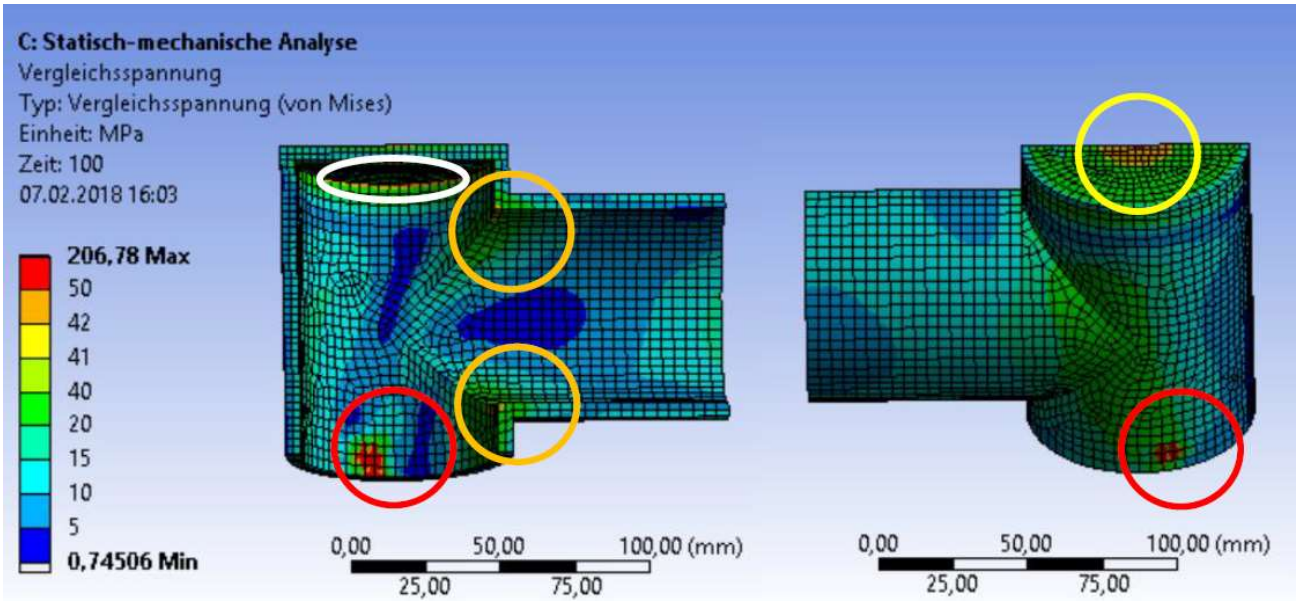

Figure 3.13: Ratchet gear mechanism housing FE equivalent stress analysis

Further increased stresses occur in the area of the edges of the branch (orange circles), in the area of the centre of the cover (yellow circle) and at the inner edge of the transition between main housing part and cover (white circle). Since the transition is in the immediate area of the defined contact surface, between the cover and the main pipe, deviations and inaccuracies can occur in the analysis. This is due to the fact, that in reality the connection created via an all-round weld seam, which was not used in this construction element analysis.

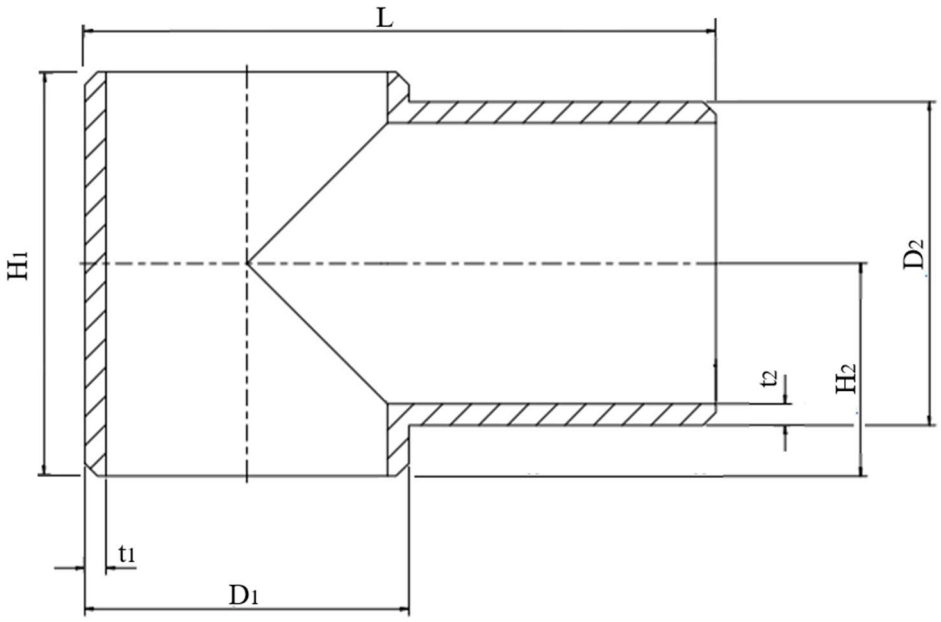

Figure 3.14: Dimensions of analytical and FE analysation of RGM body

In the following, the increased stress areas of the edges (orange circles), at the transition between the main housing part and the cover (white circle) and in the middle of the cover (yellow circle) are considered.

The FE analysis with multitask load case had been consumed for nominal diameter of 100 mm. Though, with the parameter tool of the Ansys® Workbench it expanded to 300 mm of nominal diameter of the investigated ball valve with RGM (Figure 3.14).

The results of FE analysis of parameter tool of Ansys® Workbench presented in Table 3.7. Where, it consumed the main parameters of the RGM housing, consequently: D_1 - diameter of ratchet wheel shell; D_2 - diameter of lever shell; H_1 - high of the ratchet wheel shell; H_2 - high of connection of lever shell to ratchet wheel shell; L - length of the ratchet gear box body; L_S - dimension from the middle of ratchet wheel shell to the rod end bearing; t_1 - thickness of the ratchet wheel shell; t_2 - thickness of the lever shell; t_3 - thickness of the cover of the ratchet wheel shell.

Table 3.7: Dimensions of the ratchet gear box in [mm]

Dimensions of the ratchet gear box, mm				
	DN 100	DN 150	DN 200	DN 300
D_1	76	100	175	256
D_2	76	76	76	76
H_1	122	122	122	122
H_2	60	60	60	60
L	148	172	207	298
LS	78	102	177	258
t_1	5	5	5	6
t_2	5	5	5	6
t_3	7	7	7	8

3.3 Dimensions of the bellows

The most critical and complex part of the RGM is bellows. It required detailed analytical and FE analysation due to it complex geometry, and load case.

The dimensions of bellows are depended on the length of the lever, angle of the lever axial movement, and on the internal pressure of the investigated ball valve with RGM [4].

The milestone of this design is that bellows loaded with two different load cases, the internal pressure and bending.

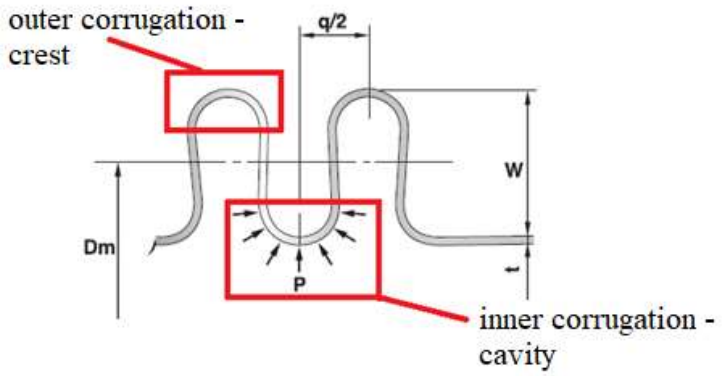

Figure 3.15: Influence of internal pressure to bellows corrugation cross section

The internal pressure (Figure 3.15) influence on shell thickness of the bellows, which defined by following equation (safety factor Sκ is 1,5):

$$e_a = \frac{D_m \cdot P_{max}}{2 \cdot f \cdot z} \cdot 1{,}5 \tag{3.18}$$

Therefore, in the case of increasing of the internal pressure, the thickness of the bellows shell must also increase.

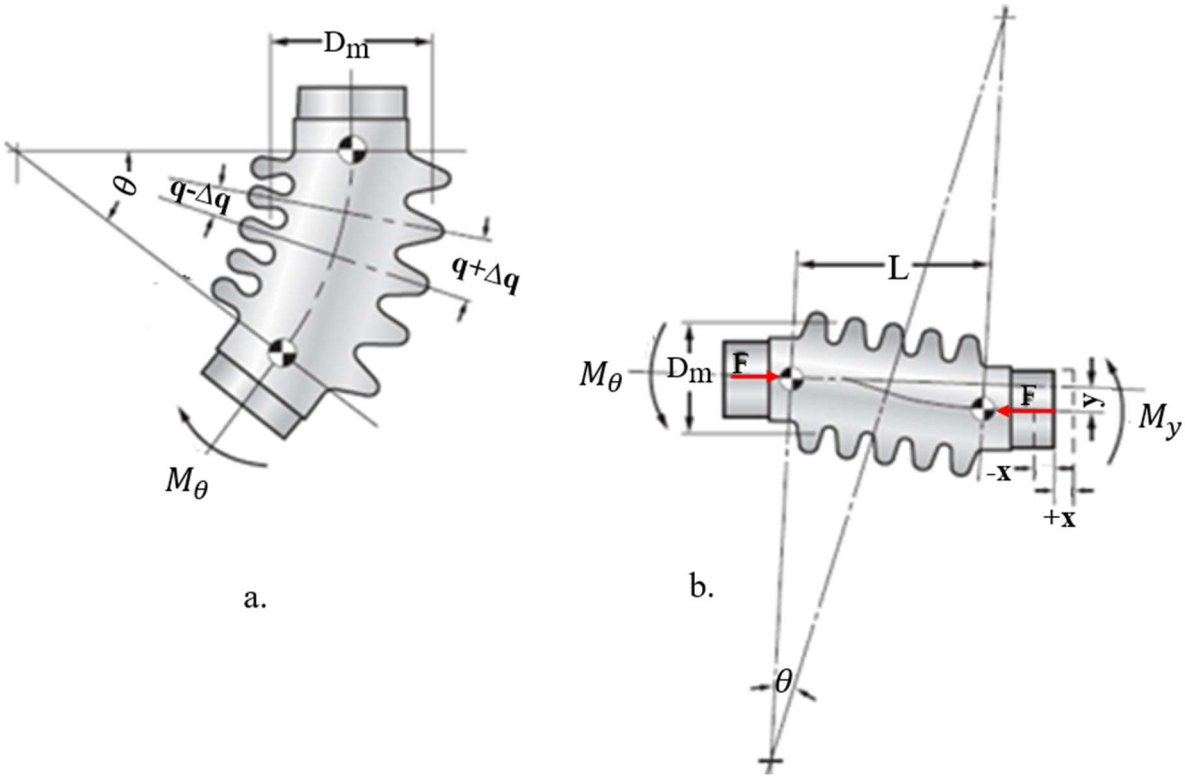

Figure 3.16: Bending cases of metal bellows according to standard EN ISO 13445 Part 3 [21]:

a. bellows subjected to an angular rotation θ;

b. bellows subjected to lateral deflection y.

In the same moment, the bending angle of the metal bellows influence on the thickness of the shell in opposite way. As deflection of the bellows increases, the thickness of the bellows shells should decry, so that the maximal allowed tensile stresses in the bellows corrugations are not exceeded (see Figure 3.16).

In order to determine the membrane and bending stresses obtained by lateral deflection and angular rotation in the meridian direction, which presented the investigated bending case, the auxiliary equations defined as (EN ISO 13445 Part 3 [21]):

$$\Delta q_\theta = \frac{D_m}{2N} \cdot \theta \tag{3.19 a}$$

$$\Delta q_y = \frac{3D_m}{N \cdot (N \cdot q + x)} \cdot y \tag{3.19 b}$$

Hence, the metal bellows design consists the equilibrium between two different loads (internal pressure and complex bending), number of corrugations and length. Moreover, the metal bellows design consists two plies (see Figure 3.17), which has affirmative further in the case of bending, and internal pressure.

In the case of the complex bending of two-ply (multi-ply) metal bellows has an advance that each ply functions as individual ply. Hence, the tensile stresses from the bending reduces up to two times (N times, depended on the number of plies). On another hand, the tensile stresses of the multi-ply metal bellows in the case of loading with internal pressure are increasing, proportional to each added individual ply.

Figure 3.17: Inventor CAD drawing of unreinforced bellows with circular U-shaped convolution cross section

Therefore, it is a difficult task to solve this problem of designing the multi-ply bellows for

investigated ratchet gear mechanism. For this case, the FE analysis applied to accomplish the design of the multi-ply bellows for ball valve with RGM of different nominal diameter of 100 mm, 150 mm, 200 mm and 300 mm.

In addition, to improve the task of the multi-ply metal bellows design to the investigated utility model [4] was implemented new methodology of calculation of thin toroidal shells depended on Clark's theory [25] (on the theory of thin elastic toroidal shells). Moreover, the results were compared to the experiments results, analytical analysis with standards EN ISO 13445 Part 3 [21] and EJMA [60], FE analysis.

As it mentioned above, the two-ply metal bellows design for the utility model ball valve with RGM [4] was defined depended on the difficult load case. To insure the capability of this multi-ply bellows design was implemented FE analysis, scheduled with maximal loads, including high temperature and buckling simulation. After the final design of the bellows for ball valve with RGM of nominal diameter of 100 mm (see Figure 3.17) was proved, it was expanded with the help of parameter tool of the Ansys® Workbench to respective RGM dimensions.

3.3.1 Analytical analysation of influence of internal pressure and investigated bending loads on single- and multi-ply metal bellows

The analytical analysis of internal pressure for single- and multi-ply metal bellows was managed with the help of ISO EN 13445 Part 3, new method of calculation of thin toroidal shell (bellows) based on Clark's theory [25].

The single- and multi-ply metal bellows was detailed analysed with FE software package Ansys® Workbench (see chapter 6), to prove and expand analytical results. In addition, it is considered the full FE analysis of investigated single- and multi-ply metal bellows design, to study weak areas and points, for instability and peak stresses.

For better analysation and understanding the behaviour under loads of the single- and multi-ply metal bellows, it was analysed a literature of the bellows designs and cases in which the single- and multi-ply metal bellows applied. In addition, the experimental, analytical and FE analysation of the single- and multi-ply metal bellows achieved with one-, two- and three-ply metal bellows produced by the company Witzenmann Ltd [93].

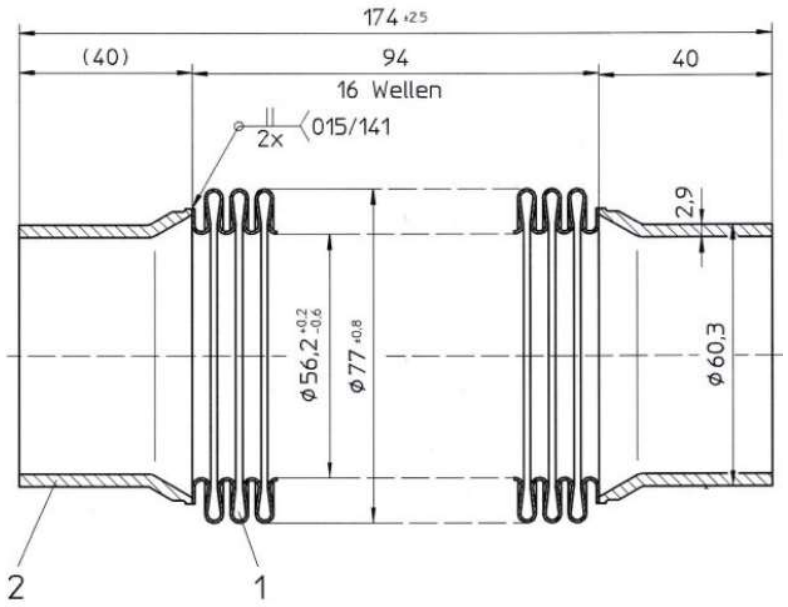

Figure 3.18: Technical sketch of investigated two-ply metal bellows manufactured by Witzenmann Ltd [93] Type Hydra BE 356230-bb 68:

1. bellows corrugations; 2. board.

3.3.1.1 Design of the investigated two-ply metal bellows

The metal bellows is a thin-walled cylindrical (toroidal) shell, which surface area features a corrugated structure, which is perpendicular to the cylinder axis. Hence, this corrugated structure affects to high flexibility during axial, lateral deflection and/or angular rotation. At the same time, the metal bellows has good operation pressure-resistant, tight, temperature-, corrosion- and torsion-resistant [8]. The technical drawing of a two-ply metal bellows presented on Figure 3.18 and in Attachment C.

In addition, the metal bellows is a thin toroidal shell for a combination of properties such as, for example:

- the pressure and temperature resistance;
- sealants for valve stem;
- tight spring elements in sliding ring seals.

The design of the bellows (Figure 3.18) consists two boards (left and right), over which the bellows corrugations are connected to the other construction components. The 16 corrugations of the bellows are crucial for the functionality in the chosen design [10] for the ball valve with RGM [4] (see Figure 3.1).

3.3.1.2 Multi-ply metal bellows

A stainless steel multi-ply metal bellows with a nominal diameter of 56,2 mm could consist up to eight plies. The thicknesses of each bellows ply often is so small that it is necessary enlargement with a magnifying glass or a microscope, to be able to recognize the plies of the bellows clearly. The cross section of the investigated two-ply metal bellows presented on Figure 3.19.

In this case, a section of the two-ply metal bellows corrugation was enlarged with an electronic microscope, then photographed (the enlargement is marked of red frame). It is circumstantially to realize that the two-ply metal bellows corrugations are not made of a continuous ply, but rather consists two plies with approximately same ply thickness. The number of plies has a great influence on the stresses in the multi-ply metal bellows, in the case of applying external loads. This detailed discussed in the next subchapter.

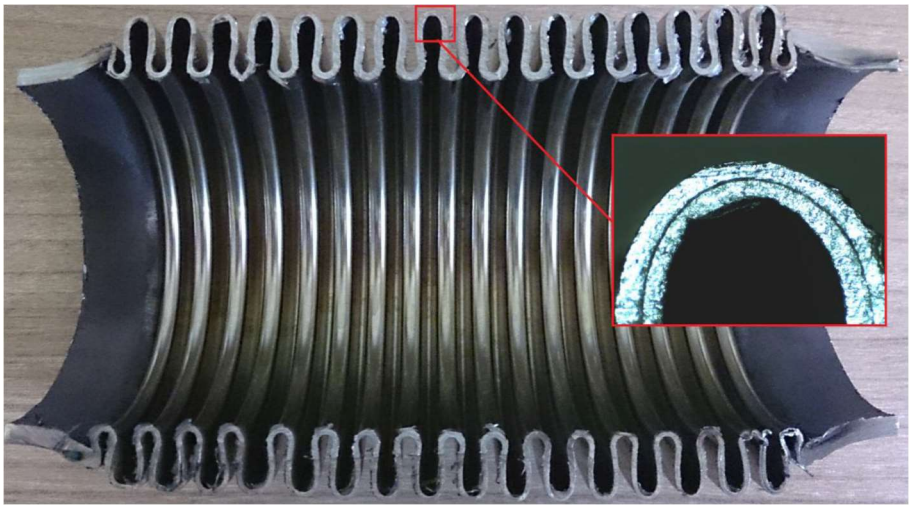

Figure 3.19: Cross section of two-ply stainless steel bellows manufactured by Witzenmann Ltd., type Hydra BE 356230-bb 68 [93]

3.3.1.3 Multi-ply effect of metal bellows

In order of representation the multitask principle of the multi-ply stainless steel bellows, first it will be considered two idealized models Figure 3.20. Hence, a single-ply design, with shell thickness of e_p, compared to a two-ply design, where each of the two plies has a shell thickness of $e_p/2$. The total shell thickness is the same in both cases. Therefore, if in the context of this doctor thesis was mentioned three-ply or (n)-ply metal bellows, each ply of the investigated bellows has a shell thickness of $e_p/(n)$.

The study model (Figure 3.20) compared a single-ply beam to the two-ply beam. Where, one side of the beam firmly fixed, at the same time the other side is loaded by a force F_1 and F_2 (Figure 3.20 [19]). That leaded to the deflection f, which is in both cases equal, and the bending stresses σ_{b1} and σ_{b2} accordingly.

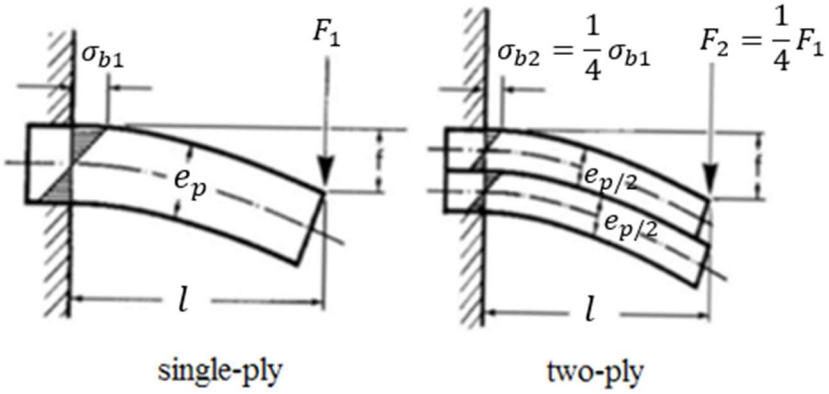

Figure 3.20: Influence of the number of plies in the case of bending [19]

In the ideal case of bending (two-ply beam), the each of ply can be considered separately, and has deflection f, which for both plies is equal. Consequently, the neutral line separates the plies, which in this case the bending stress σ_{b2} equal to $\sigma_{b1}/2$.

Henceforward, in the case of bending of the bellows around a determined deflection f, the stresses are reducing in geometrical progression with increasing number of the plies. Another positive effect of the multi-ply metal bellows is that the force F_2, which bend the two-ply beam to the deflection distance f reduced by 75% compared to F_1. This case explained by following equations 3.20-3.23:

$$\sigma_{b2} = \frac{1}{2}\sigma_{b1} \tag{3.20}$$

$$\frac{M_{b2}}{W_{b2}} = \frac{1}{2} \cdot \frac{M_{b1}}{M_{b2}} \tag{3.21}$$

$$\frac{F_2 \cdot l}{I} \cdot e_p = \frac{1}{2} \cdot \frac{F_1 \cdot l}{I} \cdot \frac{e_p}{2} \tag{3.22}$$

$$=> \qquad F_2 = \frac{1}{4}F_1 \tag{3.23}$$

Nevertheless, in the case of applied operating pressure on single- and multi-ply beam, the behaving of the number of the plies is opposite, compare to bending scenario. Which considered that the stresses are significantly higher for two-ply beam (Figure 3.21 b.), than for single-ply beam (Figure 3.21 a.).

Contrariwise, the model of single-ply bellows (Figure 3.21 a.) with beam thickness e_p compared to the model of two-ply bellows with beam thickness $e_p/2$ (Figure 3.21 b.). In both models, the loaded area in the case of operating pressure p_i equalled to $l \cdot e$. In the idealized case of the two-ply beam model (Figure 3.21 b.), it assumed that the plies do not have contact in the middle point and acting separately.

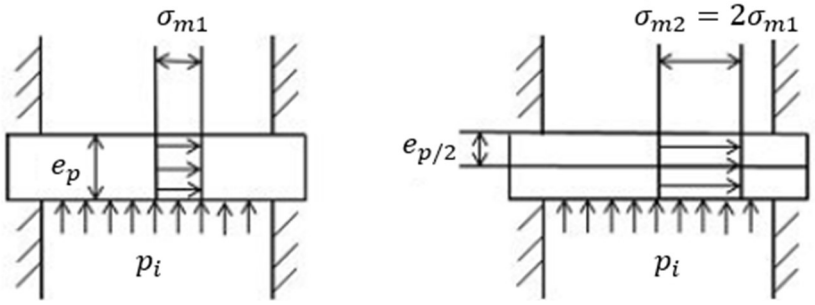

a. b.

Figure 3.21: Influence of the plies number in the case of applied operating pressure [76]

The stress-absorbing cross section in the single-ply model equals to $l \cdot e_p$ and for two-ply model is $l \cdot e_p/2$. Accordingly, it was deduced that the membrane stress for two-ply beam σ_{m2} was twice large than for single-ply beam σ_{m1}. This state proved by following equations [19]:

$$\sigma_{m2} = \frac{F_p}{A_2} \tag{3.24}$$

$$\sigma_{m1} = \frac{F_p}{A_2} \tag{3.25}$$

$$\sigma_{m2} = \frac{p_i \cdot l \cdot t \cdot 2}{l \cdot e_p} \tag{3.26}$$

$$\sigma_{m1} = \frac{p_i \cdot l \cdot t}{l \cdot e_p} \tag{3.27}$$

$$=> \qquad \sigma_{m2} = 2 \cdot \sigma_{m1} \tag{3.28}$$

Hence, in the case of increasing the number of plies of bellows the stresses, in the case of the operating pressure, increase proportionally. That state is valid, if the number of plies increases, at the same time the shell thickness of the bellows remained constant.

In the idealized model (see Figure 3.21) not considered the influence of the friction between the separate plies of the beams. Moreover, the geometrical conditions for combined case of operating pressure, bending and temperature influence for single- and multi-ply bellows

described in this doctor thesis. In addition, some cases of production-related influencing factors are not determined.

3.3.2 Analytical analysis of the single- and multi-ply metal bellows

Conventionally, the bellows are designed using EN ISO standard, EJMA and ASME code. In the case of this doctor thesis, the bellows designed using EN ISO 13445 Part 3 [21] or of EJMA 2019 [60]. However, there are many numbers of different designing/analysation methods for bellows. Any production company of the bellows required their own design analysis or experiment models, which considered of standardization institutes (as TueV in Germany, for example).

Hence, in frame of this work, for calculation, analysis and more accurate result for investigated bellows designs, it was developed a new calculation method/analysis of the single- and multi-ply bellows, which is depended on the Clark's theory of thin toroidal shells [25]. The results of new analytical method validated to the standard EN ISO 13445 Part 3, EJMA, FE analysis and experiments results of the investigated single- and multi-ply bellows.

3.3.2.1 Analytical analysis of internal pressure load case for single-, two- and three-ply stainless steel bellows

The internal pressure applied on the single-, two- and three-ply stainless steel bellows, which generate the stresses in the meridian, circumferential and radial directions in the corrugations of bellows structure.

Since the internal pressure appears in case of opening/closing the gate ball and leakages of the stem, this is not main load, which constantly appeared on the bellows in RGM [5]. The internal pressure appears as peak load occasionally or not at all.

Nevertheless, during the analysation the amount of tension/compression in the radial direction was relatively smaller than in other two directions, only the tension/compression in the circumferential and meridian directions considered (analogue to experiments, see chapter 5).

Moreover, the tension/compression of the bellows boards in circumferential and membrane direction is considered. The membrane stresses generated by operating pressure determined circumferentially as presented in following modified equation of the standard ISO EN 13445 Part 3 [21]:

$$\sigma_{\theta,t}(P) = \frac{1}{2} \cdot \frac{D_i}{e_b} . p \tag{3.29}$$

The following equations considered the stresses in outer bellows corrugations $\sigma_{\theta,\,E}$ and in the inner bellows corrugations $\sigma_{\theta,\,I}$:

$$\sigma_{\theta,E} = \frac{1}{2} \cdot \frac{q \cdot D_m + L_t \cdot (D_i + e)}{A + e^* \cdot L_t} \cdot \mathrm{P} \tag{3.30}$$

$$\sigma_{\theta,I} = \frac{1}{2} \cdot \frac{q \cdot D_m}{A} \cdot \mathrm{P} \tag{3.31}$$

To avoid the failure of the material, the following conditions must be considered:

$$\sigma_{\theta,E} \leq f \tag{3.32}$$

$$\sigma_{\theta,I} \leq f \tag{3.33}$$

where, f - nominal stress at the operating temperature.

For further analytical and FE analysis assumed, that the outer and internal bellows corrugations referred of following areas, as presented on Figure 3.15. Where, the “crest” represented the outer bellows corrugation. Where else, a cavity represented the internal bellows corrugation. The assumption task was to compare the appeared stresses on the cavity to crest, for future FE analysis, calculation and experiments.

It is important to notice, that during the experiment analysis the (tensile /extension) stresses measured on the surface of the crest of the outer bellows surface (see Figure 3.15). However, in the investigated support and loading case of the single-, two- and three-ply bellows the highest stresses appeared on the cavity of the bellows surface. Due to size of strain gauges, which used in experiments (see chapter 5), the measurement of cavity was impossible. Therefore, in analytical model and FE analysis (chapter 6), both investigated areas were considered, analysed and validated.

The equation (3.27) determined a centreline average stresses of the inner bellows corrugations (cavity) in the circumferential direction. Nevertheless, with the auxiliary variables, which were determined in advance, and generated by the operating pressure, the membrane stresses $\sigma_{m,m}(P)$ and bending stresses $\sigma_{m,b}(P)$ considered in the meridian direction as:

$$\sigma_{m,m}(P) = \frac{w \cdot}{2 \cdot e^*} \tag{3.34}$$

$$\sigma_{m,b}(p) = C_p \cdot P \cdot \frac{1}{2 \cdot n_p} \cdot \left(\frac{w}{e_p^*}\right)^2 \tag{3.35}$$

where, C_p is an empirical constant with the coefficients C_1 and C_2.

The coefficients C_1 and C_2 determined as:

$$C_1 = \frac{q}{2 \cdot w} \tag{3.36}$$

$$C_2 = \frac{q}{2{,}2 \cdot \sqrt{D_m \cdot e_p^*}} \tag{3.37}$$

In addition, the results of the membrane stresses $\sigma_{m,m}(P)$ and bending stresses $\sigma_{m,b}(P)$ considered as positive. It determined that in investigated analytical model of the single-, two- and three-ply bellows the stresses in the inner corrugation in outer surface considered as tensile stresses. In conclusion, the tensile stresses have more negative effect on the material, in case of the strength test, as for example compressive stresses.

Hence, for strength test verification, a worst-case scenario (maximal possible stresses) for investigated single-, two- and three-ply bellows was performed. In comparison, the tension in the meridian direction was significantly greater, than, for example, in the circumferential and radial directions. Therefore, the following analysis considered the tension in the meridian direction, which is composed of meridian and bending stresses. For safe design, the following conditions approached:

$$\sigma_{m,m}(P) \leq f \tag{3.38}$$

$$\sigma_{m,m}(P) + \sigma_{m,b}(P) \leq K_f \cdot f \tag{3.39}$$

where, K_f is a coefficient, which equals to 3,0 due hardening, in other cases it equals to 1,5. Here, f stands for quotient of $R_{p0.2}/S$, where $R_{p0.2}$ is the yield strength at 0,2 % of tension, S is safety coefficient in the value of 1,5.

The results of the operating pressure analysis were considered with the EN ISO 1333 [63] pressure classes 0,3; 0,6; 1; 1,6 MPa, and to specification for pipeline and piping valves API 6D [51] Class 150 (2 MPa).

The results of analytical analysis of internal pressure for single-, two- and three-ply stainless steel bellows presented on Figure 2.22.

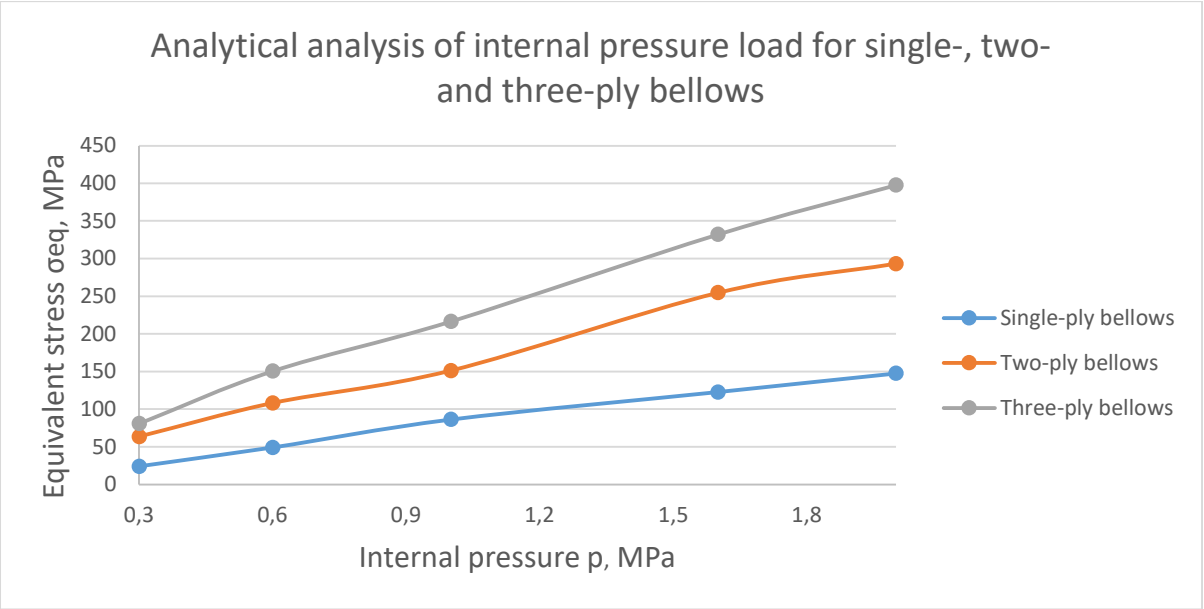

Figure 3.22: Analytical analysis of internal pressure load for single-, two- and three-ply bellows with pressure classes 0,3, 0,6, 1, 1,6, 2 MPa according to EN ISO 1333 [63] and to specification for pipeline and piping valves API 6D [51] Class 150

3.3.2.2 Validity and condition of the standard ISO EN 13445 Part 3

In order to design and analyse the stresses of the investigated bellows designs, it was applied the standard ISO EN 13445 Part 3 [21]. Hence, the investigated single- and multi-ply bellows designed unreinforced and with circular U-shaped convolution cross section (Figure 3.23).

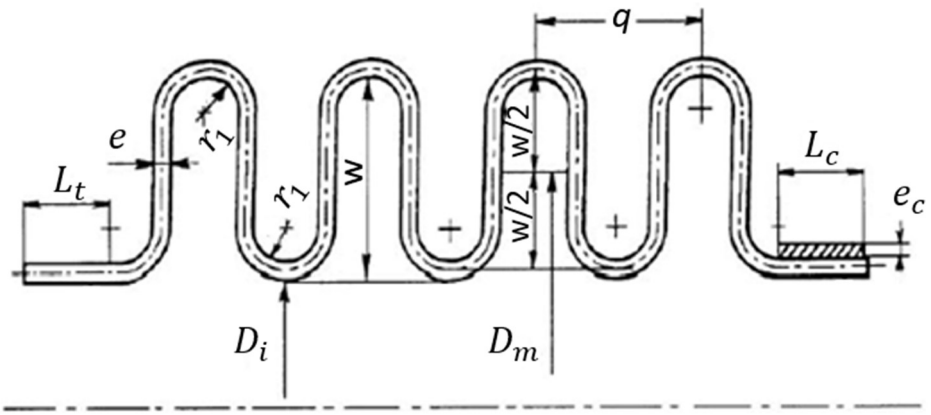

Figure 3.23: Dimensions of investigated single- and multi-ply bellows [21]

The analysis method assumed that the number of plies of the bellows was not more than five ($n_p \leq 5$). In production, the number of bellows plies can consist up to 10 and more. In this work was analysed single-, two- and three-ply stainless steel bellows, which fulfill the requirement of standard ISO EN 13445 Part 3 [21]. In addition, the maximal operating temperature T °C

was applied as [18]:

$$T \leq 500\,℃ \quad for\ stainless\ steel\ 1.4571\ and\ 1.4006 \tag{3.40}$$

For further analysis, are defined the following auxiliary equations:

$$e = e_p \cdot n_p \tag{3.41}$$

$$\mathrm{q} = 4 \cdot r_i + 2 \cdot e \tag{3.42}$$

$$w = \frac{D_a - D_i}{2} + e \tag{3.43}$$

$$D_m = D_i + w + e \tag{3.44}$$

$$e_p^* = e_p \cdot \sqrt{\frac{D_i}{D_m}} \tag{3.45}$$

$$e^* = n_p \cdot e_p^* \tag{3.46}$$

$$A = \left(\left(\frac{\pi - 2}{2}\right) \cdot q + 2 \cdot w\right) \cdot e^* \tag{3.47}$$

Where, the auxiliary equations, considered the stress analysis for investigated designs of the single-, two- and three-ply stainless steel bellows. These auxiliary equations are relevant to the designs of the single-, two- and three-ply stainless steel bellows.

3.3.2.3 Analytical analysis of investigated bending case for single-, two- and three-ply stainless steel bellows

The bending of the bellows proceeds during closing/opening of the ball gate. Therefore, it is load mostly appears during operation of RGM, which detailed analysed and considered in this subchapter.

The bending of the single- and multi-ply bellows as it concluded in chapter 5 has an unusual performance for analytical analysis. The bending case of single-, two- and three-ply bellows is combination of an angular rotation and lateral deflection. In standard EN ISO 13445 Part 3 [21] it is analysed either angular rotation or lateral deflection of bellows. Therefore, during the experiments (see chapter 5), it is determined the analytical bending model, which is concluded of these both bending cases at same time.

The single-, two- and three-ply bellows loaded with internal pressure and bended to an angle of 10 °. The investigated bendig case of the bellows for design of ball valve wth RGM is unique. Therefore, it requires additional analysation due to its nature. The bending case according to EN ISO 13445-3 is an angular rotation and lateral deflection (see Figure 3.16 a. and b.). It means that two cases of bending according to standard EN ISO 13445-3 [21] appeared in this bellows installation.

To analyse the stresses, which have appeared during investigated bending of the bellows, it assumed that an angular rotation of the bellows is an angle θ, which accordinally causes bending stress $\sigma_{m,m}(\Delta q)$ and $\sigma_{m,b}(\Delta q)$, and also the lateral deflection in X and Y directions, as it presented on Figure 3.16 a. and b.

The equations for angular rotation determined as $\sigma_{m,m}(\Delta q)$ for membrane and $\sigma_{m,b}(\Delta q)$ for bending stresses obtained by angular rotation in the meridian direction. The auxiliary equations for the rotation angle defined as:

$$\theta = \pi \cdot \frac{\phi}{180°} \tag{3.48}$$

where, an angle ϕ considered as radian number; an angle θ determinate degree of bending of the bellows, which define the equivalent axial displacement Δq:

$$\Delta q = \frac{D_m}{2 \cdot N} \cdot \theta \tag{3.49}$$

Therefore, as a result of the equivalent axial displacement Δq, membrane and bending stresses in the meridian direction are calculated using the following equations:

$$\sigma_{m,m}(\Delta q) = \frac{E_b \cdot \left(e_p^*\right)^2}{2 \cdot w^2 \cdot C_f} \cdot \Delta q \tag{3.50}$$

$$\sigma_{m,b}(\Delta q) = \frac{E_b \cdot \left(e_p^*\right)^2}{2 \cdot w^2 \cdot C_f} \cdot \Delta q \tag{3.51}$$

where, C_f and C_d are two empirical constants, which considered either graphically or by equations like C_p from C_1 and C_2.

The strength condition for angular rotation is equal as for internal pressure:

$$\sigma_{m,m}(\Delta q) \leq f \tag{3.52}$$

$$\sigma_{m,m}(\Delta q) + \sigma_{m,b}(\Delta q) \leq K_f \cdot f \tag{3.53}$$

When the end of bellows is subjected to lateral deflection (Figure 3.16 b.) the maximum equivalent axial displacement per convolution determined according to following equation:

$$\Delta q_y = \frac{3D_m}{N \cdot (N \cdot q + x)} \cdot y \tag{3.54}$$

For the analytical analysis of angle ϕ, it assumed five values of bending of the investigated single-, two- and three-ply bellows, namely 2 °, 4 °, 6 °, 8 °, 10 °. These investigated bending cases compared to experimental and FE analysis results, which gives better explanation of bellows behaviour in loaded case. The results of investigated bending case with angular rotation and lateral deflection according to standard EN ISO 13445-3 [21] (see Figure 3.16) are presented in Table 3.8 and on Figure 3.24.

Table 3.8: Analytical analysis of investigated bending case for single-, two- and three-ply stainless steel bellows

Analytical analysis of investigated bending case for single, two and three-ply bellows			
	Single-ply bellows	Two-ply bellows	Three-ply bellows
Degree, °	σeq, MPa	σeq, MPa	σeq, MPa
2	84,38	36,11	22,57
4	168,70	96,25	45,11
6	252,90	144,27	67,61
8	336,94	192,22	90,04
10	420,77	240,03	112,37

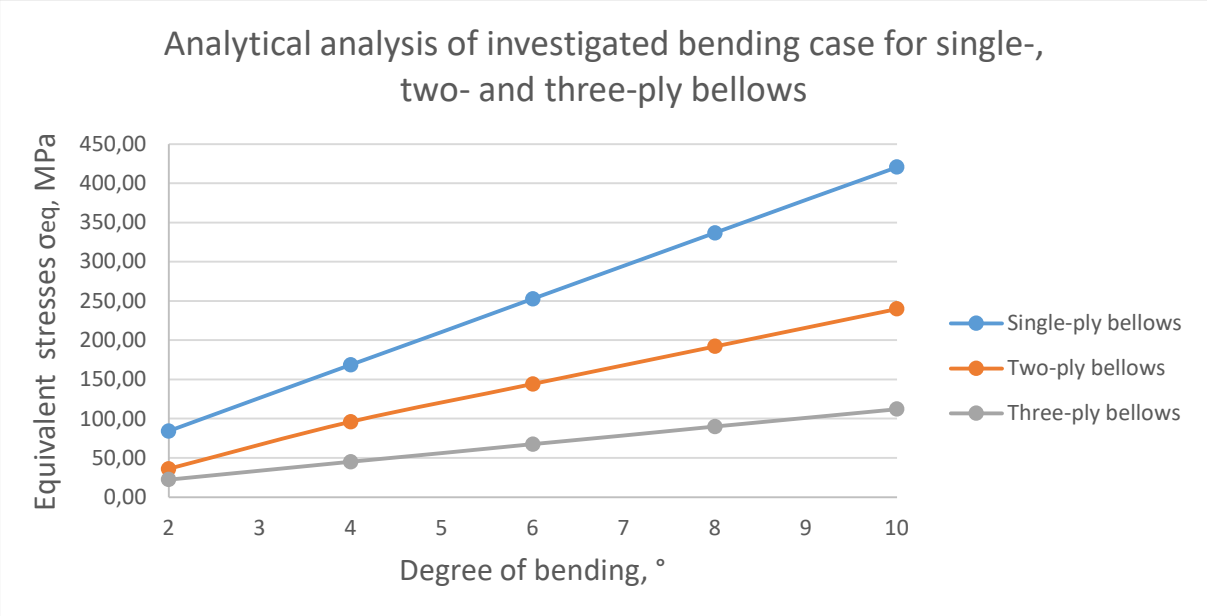

Figure 3.24: Analytical analysis of investigated bending case for single-, two- and three-ply stainless steel bellows

The approximation of equivalent stresses for investigated angular rotation and lateral deflection of bellows bending case means the total amount of equivalent stresses from impact of each bending case due to this specific bellows installation on RGM.

The impact of each bending case (angular rotation and lateral deflection) for this bellows installation was obtained during the laboratory experiments with investigated ball valve design with RGM. Therefore, it equals to 78 % of angular rotation and 22 % of lateral deflection amount of equivalent stresses for investigated bending case.

Hence, when internal pressure and investigated bending load cases appear at the same time, also with additional designed temperature influence, it will be worst-case scenario during exploitation of investigated bellows. This load case will be detailed analysed with help of FEA in chapter 6.

3.3.3 Analytical analysis of maximal load case for investigated bellows

Analytical analysis of maximal load case for investigated bellows consume investigation of three load cases. First case, when bellows is loaded with internal pressure (static case). Second case, the bellows bend to an θ angle. Third case, the bellows loaded with internal pressure and bend to the investigated angle θ. Third case scenario determined in standard EN ISO 13345-3 [21] by equation:

$$\sigma_{eq} = 0{,}7\left(\sigma_{m,m}(P) + \sigma_{m,b}(P)\right) + (\sigma_{m,m}(\Delta q) + \sigma_{m,b}(\Delta q)) \tag{3.55}$$

Hence, during the analytical analysis of maximal load cases for investigated bellows geometry, it obtained results that presented on Figure 3.25. The single, two- and three-ply bellows loaded with operating internal pressure and bending to an angle of 10 °, accordingly equations (3.29-3.54). The total equivalent stresses in this maximal load case determined by equation (3.55). The equivalent stresses of bellows board are considered as small compare to equivalent stresses of bellows corrugation. Therefore, the equivalent stresses of bellows board will not be analysed in this chapter. The result of FE analysis discussed in chapter 6.

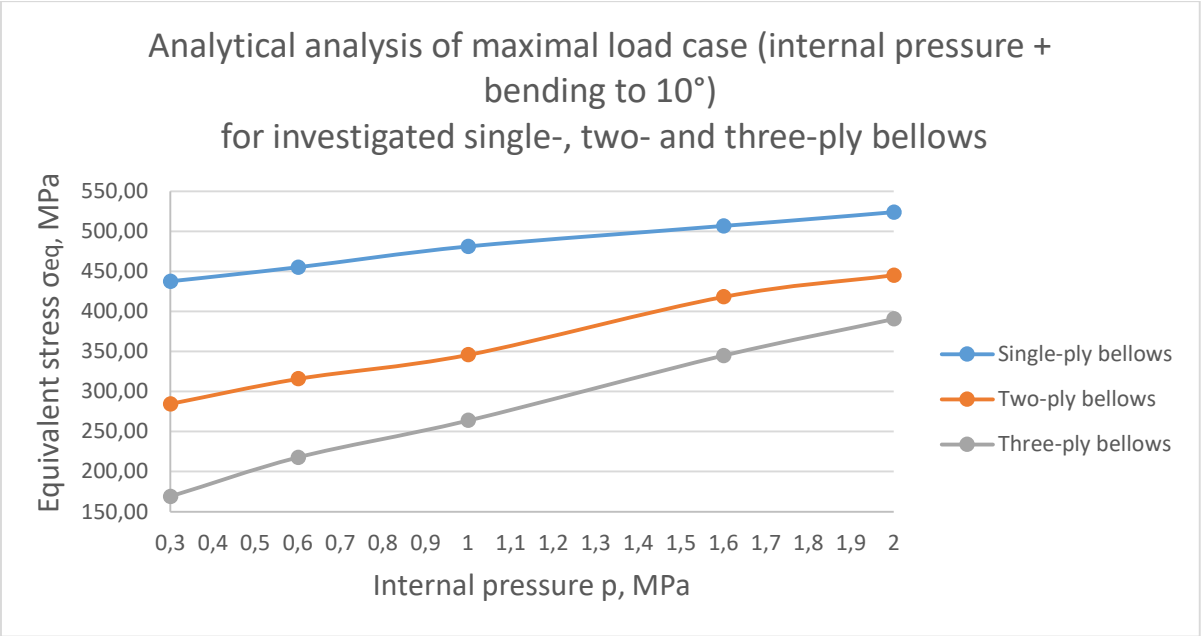

Figure 3.25: Equivalent stresses of the investigated single- and multi-ply stainless steel bellows

It is important to notice for the results presented on Figure 3.25, that the dimensions of the investigated bellows geometries were equivalent, but number of the plies was different, i. e. thickness of the single-, two- and three-ply stainless steel bellows was same and equalled to 0,8 mm. Hence, it can be noticed that membrane and bending stresses increase linearly with increasing of internal pressure. However, in any load case, bending stresses are much greater than the membrane stresses due to bellows geometry.

Worth to notice that analytical analysis of internal pressure classes is according to standards EN DIN 1333 [63] and API 6D [51]. In addition, the bending angle θ of bellows in this case was assumed as maximal and it is equal to 10 ° (see Table 3.8).

As it is mentioned before, single-, two- and three-ply stainless steel bellows have total shell thickness of 0,8 mm. However, the membrane and bending stresses constantly increase with increasing value of investigated internal pressure for two- and three-ply bellows against single-ply bellows. It concluded that the thinner the total ply thickness of investigated bellows is, the larger membrane and bending stresses occur in the geometry of the bellows.

Nevertheless, the analytical analysis of investigated bending cases of bellows to certain angle θ (as presented in Table 3.8) deduced that equivalent stresses σ_{eq} for two- and three-ply against single-ply bellows decrease their value, if the total thickness of single-, two- and three-ply bellows remain constant and equal to 0,8 mm, as described in this work. It concludes, that each ply of bellows in bending case of bellows works separately from another ply (just for multi-ply bellows), but the friction between the plies would be constant and equal to 0.

Consequently, investigated bellows, which are mainly loaded with operating internal pressure, require to be designed with largest ply thickness. On the other hand, investigated bellows, which are primarily subject to bending, required as small as possible thickness of each ply, to reduce the total equivalent stresses. Therefore, for designs of the bellows which subjected to internal pressure and bending, it is necessary to consider the equilibrium between total bellows corrugation thickness and number of plies to reduce equivalent stresses. That is one of main goals of this work for design of investigated ball valve with RGM [4], [5], [6].

3.3.4 Determination of the fatigue life of the investigated bellows

The fatigue life is main index of reliability of investigated bellows. It is representing which loads could be fatal for the structure of investigated bellows and how many cycles (opening/closing cycles of the gate ball), it can achieve under these loads. That is most important value for the design of investigated ratchet gear mechanism (RGM) [4], which has function of ball valve actuator.

The equations of the fatigue life for investigated stainless steel bellows applied as follows (where σ_{eq} in MPa):

$$\text{If } \frac{E_0}{E_b}\,\sigma_{eq} \geq 1080 \text{ MPa:} \tag{3.56}$$

$$N_{alw} = \left[\frac{9283{,}3}{\frac{E_0}{E_b}\sigma_{eq} - 372{,}3}\right]^{3{,}4} \tag{3.57}$$

$$\text{If } \frac{E_0}{E_b}\,\sigma_{eq} < 1080 \text{ MPa:}$$

$$N_{alw} = \left[\frac{10259{,}4}{\frac{E_0}{E_b}\sigma_{eq} - 297{,}9}\right]^{3{,}4} \tag{3.58}$$

The curve and the equation applied to EN ISO 13445 Part 3 [21]: $370 \leq N_{alw} \leq 10^6$.
The elasticity module of the stainless steel E_b variates with the temperature, the Table 3.9 describes the relationship between elasticity module and temperature of the material.
Results of calculation method of the standard EN ISO 13445 Part 3 [21] were coincided to the stress state in the bellows corrugation on the inner ply, where the maximum stresses accrued.

The number of oscillatory cycles as a function of temperature and internal pressure p calculated by the equations (3.56-3.58).

Table 3.9: Elasticity of the stainless steel 1.4571 [68], [116] in the case of different temperatures

Temperature T, ° C	20 °C	100 °C	200 °C	300 °C	400 °C	500 °C
Elastic module E_b, MPa	$2\ 10^5$	$1{,}94\ 10^5$	$1{,}86\ 10^5$	$1{,}79\ 10^5$	$1{,}72\ 10^5$	$1{,}65\ 10^5$

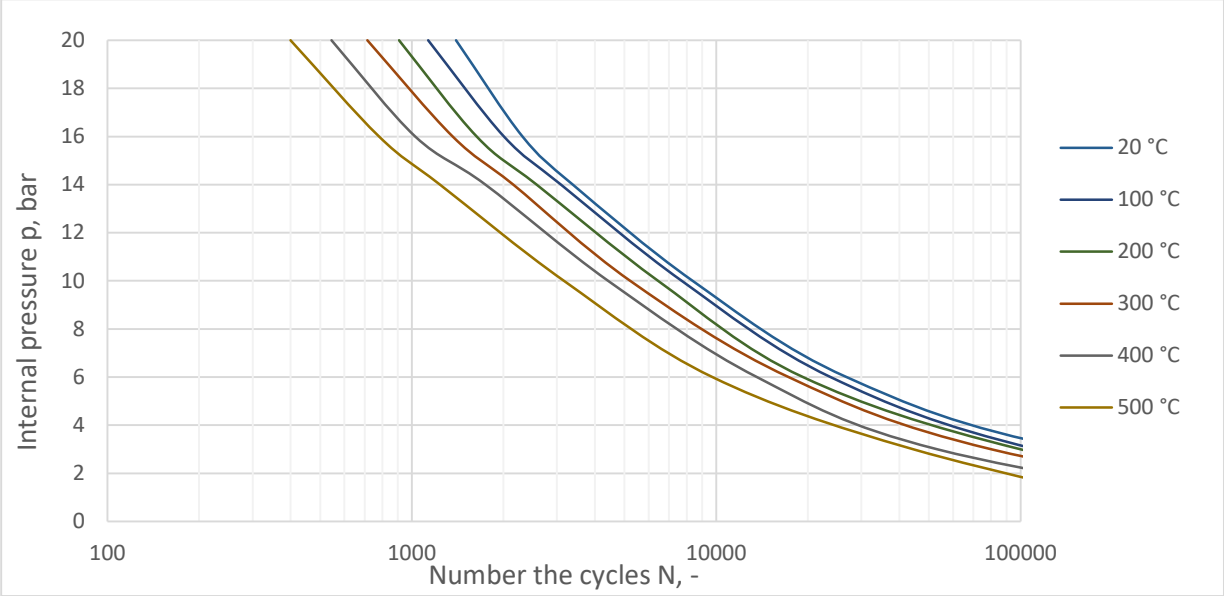

Figure 3.26: Fatigue life curves of the bellows in the case of different internal pressure and design temperatures [74] for investigated two-ply bellows with a U-shaped convolution cross-section from stainless steel 1.4006 [116], [147]

The diagram on Figure 3.26 presents how the fatigue life is changing with increasing of internal pressure and the temperature. It represents that the higher the internal pressure and the temperature, the shorter fatigue life range for investigated RGM design.

For example, at internal pressure of 8 bar and temperature of 20 °C the two-ply bellows with a U-shaped convolution cross-section has around 15.000 fatigue cycles; at 20 bar and temperature 500 °C the two-ply bellows has 399 cycles, which is satisfied according to EN ISO 13445-3 [21], $370 \leq N_{alw} \leq 399$.

3.4 Conclusion of analytical study of investigated ball valve parts

The analytical study of the construction parts of the utility models [2], [3], [4] provided the understanding of the function and reliability of the design elements, which were detailed

analysed by FEA afterwards. The FEA provided examination of the critical areas of the design elements and more accurate results due to fine mesh, and possibilities to simulate real element geometry.

Hence, maximal operation loads, such as internal pressure, temperature, influence dimensions of constructive elements of the ball valve design. The most sensible element of investigated ball valve design with RGM is bellows, which was detailed analysed for all cases of investigated loads and for worst-case scenario.

Therefore, the maximal loads influence on dimensions of all parts of the ball valve with RGM design with nominal diameter of 100 mm, 150 mm, 200 mm and 300 mm, instead of bellows, which has constant dimensions for all investigated diameters of ball valve design.

The dimensions of the constructive elements of ball valve with RGM determined according to EN ISO 13445-3 [21], EN 1333 [63], EN 1983 [108] and specification for pipeline and piping valves API 6D [51].

Furthermore, there were detailed analysed and determined dimensions for single- and multi-ply bellows of different operating pressure cases according to EN ISO 13445-3 [21]. The bending of bellows to an angle of 2 °, 4 °, 6 °, 8 °, 10 °, and at temperature of 20 °C, 100 °C, 200 °C, 300 °C, 400 °C, 500 °C, considered that investigated two-ply stainless steel bellows approached to the investigated ball valve design with ratchet gear mechanism. The main aim of the analytical analysis is to compare different designs of the bellows. Moreover, analytical study is less time consuming than FE analysis and experiments. After, there were considered the final design dimensions of investigated bellows, next step was to analyse the investigated bellows by FE analysis and experiments.

After all, the experimental model (chapter 5) presented the workability of RGM with bellows. Finally, experimental results of the investigated bellows design were compared to analytical (chapter 3.3) and FE (chapter 6) models.

The maximal load case of the single-, two- and three-ply stainless steel U-shaped bellows presented on diagram Figure 3.25. The equivalent stresses were analysed by maximal bending angle of 10 °, temperature range up to 500 °C and for different value of internal pressure up till 2 MPa according to standards EN ISO 1333 [63], EN ISO 13445-3 [21]. The equivalent stresses of investigated single- and multi-ply bellows calculated by the equation 3.55. For the additional analysis of the fatigue life depended on the temperature presented on the diagram Figure 3.26.

4. Analytical analysis of single- and multi-ply bellows based on the theory of thin elastic toroidal shells

The analysis of single- and multi-ply thin toroidal shell is a difficult task, due to complex load case and geometry, which considered investigated single- and multi-ply bellows. The idea of analysis of single- and multi-ply thin toroidal shell came in focus due to many different bellows analysis methods [12], [8], [25], [78], [21]. Most of them consider empiric coefficients for calculation and failure of the structure. For instance, some of them required to be determined from diagrams, such as described in standard EN ISO 13445-3 [21], as well as Anderson [12] bellows analysis or Andreeva [78]. Hence, beam analysis theory of thin toroidal shells (bellows), as presented in chapter 3 according to EN ISO 13445-3 for bending case, does not compared auspiciously to experimental results [12], due to bellows unique installation case on RGM [4].

For this purpose, to reveal a new solution of analysis single- and multi-ply thin toroidal shells (bellows), it was created a new method of U-shaped bellows analysis depended on fundament of Clark's theory: "On the Theory of Thin Elastic Toroidal Shells" [25].

The Clark's theory used an asymptotic integration method for the solution of governing differential equations of bending of a thin toroidal shell subject to axisymmetric loading [25]. The new method applied to the stress analysis of bellows subjected to axial load and internal (lateral) pressure. Numerical results of single-, two- and three-, four- and five-ply thin toroidal shell model evaluated using a new code programmed with MatLab® software package (see Attachment A).

Clark's theory involved a thin toroidal shell of positive curvature (Figure 4.1 a.). The analysed model of the bellows had a different shape compare to Clarks model, therefore the model of thin toroidal shell was adjusted to the geometry of circular bellows with U-shaped convolution cross section (see Figure 4.1 b.).

Hence, in investigated bellows the structural elements between points A, B, C, D [52] involved a toroidal shell of positive curvature (A-B), a cylindrical shell (B-C) and a toroidal shell of negative curvature (C-D) (Figure 4.1 c.).

The motivation to apply Clark's theory for analysis of a thin toroidal shell (bellows) resulted from the fact that this calculation method is allowed calculation of stresses at any point of investigated circular bellows with U-shaped convolution cross section geometry, depending on

the angle of positive or negative curvature, likewise in cylindrical shell section of bellows corrugation [173].

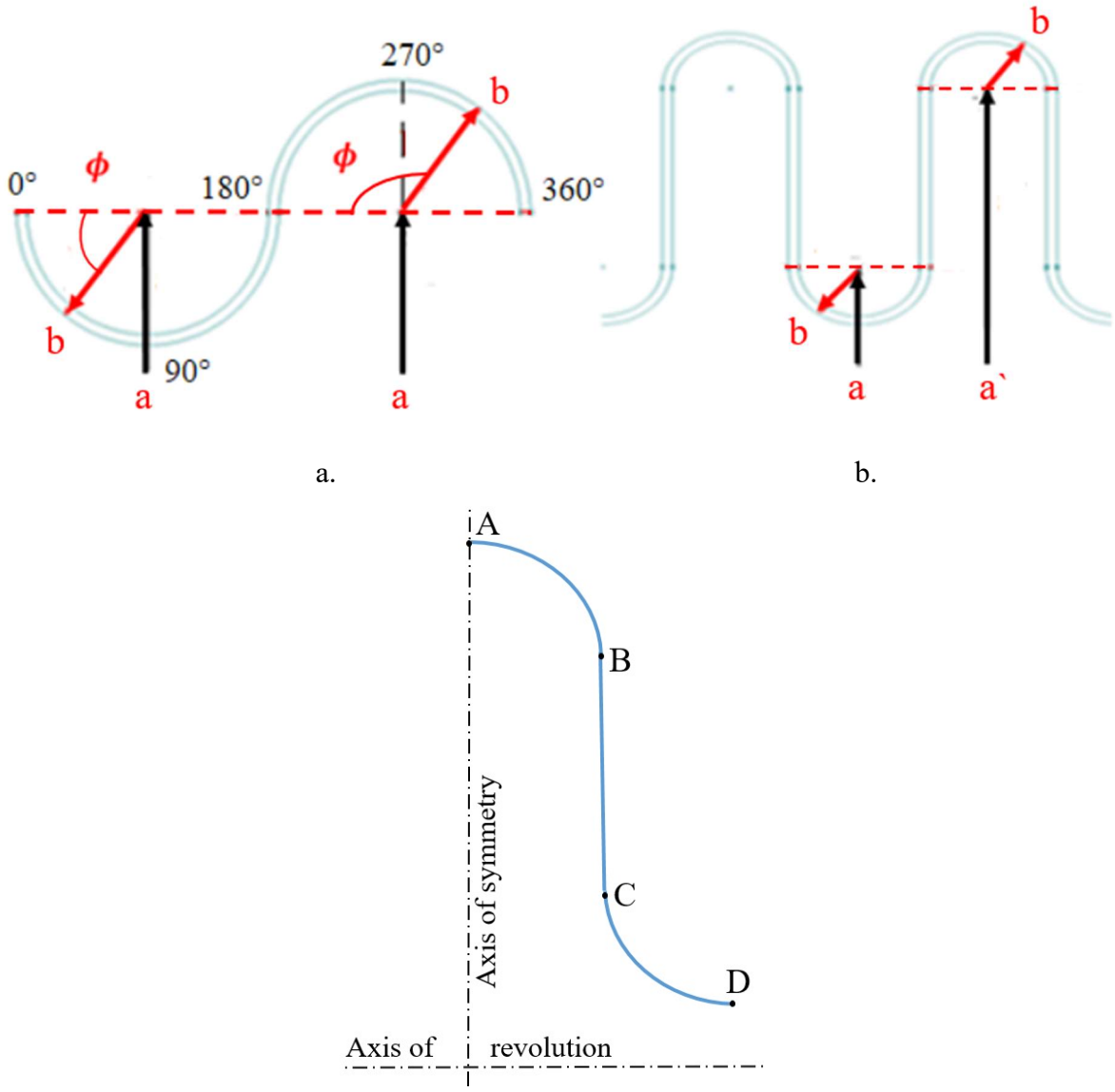

a. b.

c.

Figure 4.1: a. Principle sketch of Clark's theory for analysis of a thin toroidal shell [25];
b. modification of Clark's theory for bellows corrugations [26];
c. junctions of a circular bellows with U-shaped convolution cross section [6].

Investigated thin toroidal shell (bellows) can be detailed analysed in the critical points of its cross section. Afterwards, this model of investigated thin toroidal shell will be transferred to the circular bellows with U-shaped convolution cross section (as it presented on Figure 4.1 a. and b.) and it determined the maximal equivalent stresses at critical point D 270 ° (cavity) and at point A 90 ° (crest [crown] of circular bellows with U-shaped convolution cross section as it

presented on Figure 4.1 c.). Dimensions *a*, *b* and *a´* on Figure 4.1 a. and b. present the radiuses of investigated toroidal sphere; the angle ϕ (in °, see Figure 4.1 a.) belong to the angle of investigated corrugation of the toroidal shell. The letters A, B, C and D on Figure 4.1 c. present investigate section with maximum concentration of stresses for this geometry.

4.1 Theory of shells of revolution

To begin with analysis of modifyed Clark's theory of thin toroidal shell for circular bellows with U-shaped convolution cross section, it is necessary to consider a bending element of loaded shell of revolution in the $\{\phi, \theta\}$ coordinate system, which presented on Figure 4.2.

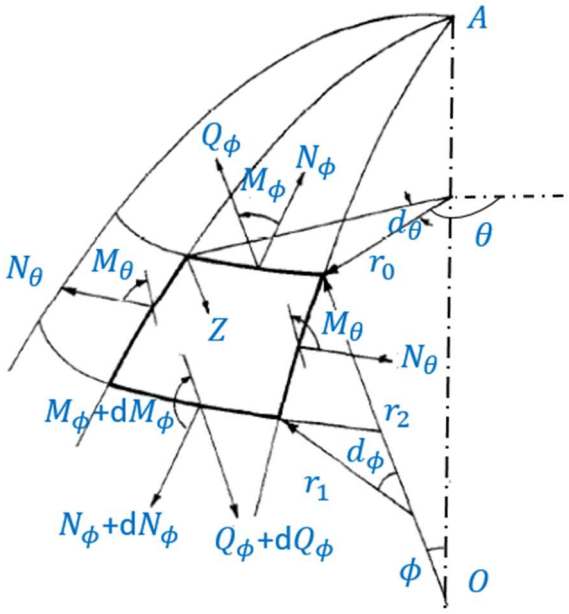

Figure 4.2: Resultant forces and moments in general shell of revolution [58]

In a circular bellows with U-shaped convolution cross section, the basic structure elements present a toroidal shell of positive curvature, a side wall and toroidal shell of negative curvature continuing with next U-shaped toroidal section with side wall of bellows [26].

The normal forces $N_\phi, N_\theta,$ shear force Q_ϕ and bending moments M_ϕ, M_θ occurred in meridional (ϕ) and circumferential (θ) directions [173]. Likewise, the angle ϕ identifies the position of the point along the meridian of the investigated corrugation, while the angle θ is the circumferential angle measured from an arbitrary vertical plane to investigated point of U-shaped bellows corrugation. The meridional angle ϕ considered as a positive, if measured in anticlockwise direction from the axis of revolution for positive and negative curvature [170].

The bending element of an asymmetrically-loaded shell of revolution is in equilibrium under the loads acting over its surface. The forces N_ϕ, N_θ, Q_ϕ and moments M_ϕ, M_θ acting along the element. N_ϕ, N_θ are forces per unit length of the element edges, acting in direction of the tangent to the U-shaped shell meridian in investigated point. M_ϕ, M_θ are bending moments per unit length of the element edges. Q_ϕ is a shear force considered in the meridional section. In horizontal section is none of shear force due to axisymmetry of investigated bending element [174].

4.2 Theoretical analysis of circular bellows with U-shaped convolution cross section

The geometry of investigated bellows is different from Clark's description of a thin toroidal shell (see Figure 4.1 a.). Therefore, to solve the equation optimally, Clark's calculation method was modified for this specific case [23]. The geometry of U-shaped bellows and geometrical (model) parameters, which are required for the analysis, are presented on Figure 4.1 b.

Corresponding to Figure 4.3 a., at the angle ϕ from 0 ° to 180 °, the half circle is considered as positive curvature, the tangent to meridian rotated in anticlockwise direction [58]. While the angle ϕ from 0 ° to 180 °, the half circle determined as negative curvature (Figure 4.3 c.). Between the positive and negative curvatures located a cylindrical shell (Figure 4.3 b.). The equivalent stresses, which appeared in this cross section, are smaller compare to positive and negative curvatures. Resultant forces and moments in shell of revolution for different shell elements presented on Figure 4.3 d.

For the thin toroidal shell of positive curvature, the value of the internal pressure considered as *pi*. At the same time, the value of internal pressure for negative curvature replaced by *–pi*, and the radius *b* considered as negative.

Hence, to determine the point of the investigated bellows geometry, the cylindrical coordinates *r, ϕ, x* represented the middle line by the following parametric equation:

$$r = a + b \cdot sin\phi \tag{4.1}$$

$$x = -b \cdot \cos\phi \tag{4.2}$$

where, *b* is radius of the circular cross section; *a* is the distance of the centre of the cross section from the investigated axis of revolution.

For the circular bellows with U-shaped convolution cross section and uniform thickness the

theory of thin toroidal shells of revolution based on force and moment equilibrium, which used in a Bessel differential equation [23] presented in the following form [26]:

$$\frac{d^2U}{d\phi^2} + f_1 \cdot (\phi, \lambda)\frac{dU}{d\phi} + [i \cdot \mu \cdot f_2(\phi, \lambda) + f_3(\phi, \lambda)] \cdot U = f_4(\phi, \lambda, \mu) \qquad (4.3)$$

where, i is the imaginary number. For further explanations, it referred to corresponding mathematical analysis by E. Reissner [57] and Clark [25].

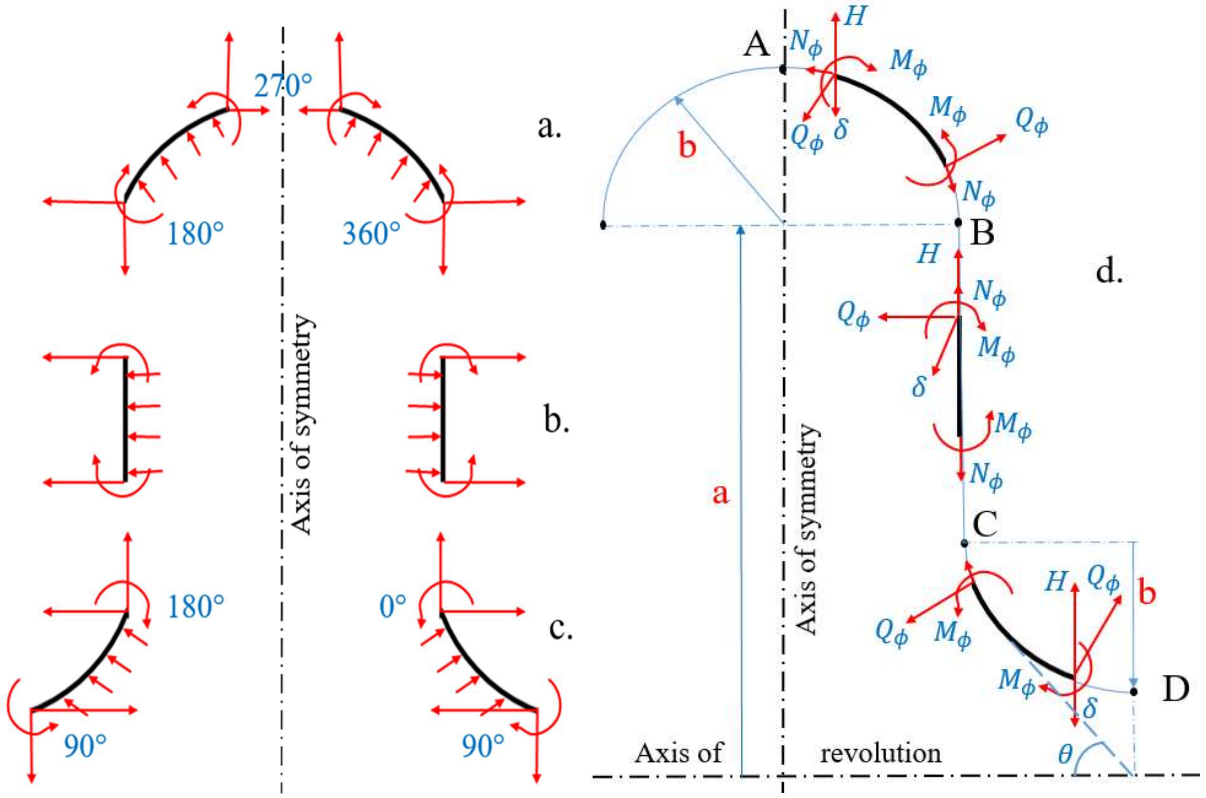

Figure 4.3: Analytical model of the circular bellows with convolution cross section [58]:
a. positive direction of stress resultants and stress couples for a shell of revolution;
b. cylindrical shell;
c. negative direction of stress resultants and stress couples for a shell of revolution;
d. resultant forces and moments (see Figure 4.2), direction of rotations in composite shells of revolution [58].

According to theory of thin elastic toroidal shells, the governing differential equation for circular bellows with U-shaped convolution cross section can be written in presented form [25]:

$$W'' - \left[i\mu\frac{\sin\phi}{1 + \lambda \cdot \sin\phi}\right] \cdot W = f(x) \cdot \frac{\mu}{\sqrt{1 + \lambda \cdot \sin\phi}} \qquad (4.4)$$

where:

$$f(x) = \Omega \cdot \cos\phi - \left(\frac{i}{\mu}\right) \cdot [(1 + \lambda \cdot \sin\phi) \cdot P_H' + (1 + \upsilon) \cdot \lambda \cdot \cos\phi \cdot P_H] \tag{4.5}$$

The equation (4.4) can also be approximated by:

$$W'' - i\mu W = \mu f(x) \tag{4.6}$$

According to equation (4.3) it possible to introduce the function U as:

$$U = \beta + i\kappa\psi \tag{4.7}$$

where,

$$\kappa = \sqrt{(1 + (\upsilon\lambda/\mu)^2} + i \cdot \left(\frac{\upsilon\lambda}{\mu}\right) \tag{4.8}$$

Therefore W can be rewritten in the form:

$$W = (1 + \lambda \cdot \sin\phi)^{1/2} \cdot (\beta + i\psi) \tag{4.9}$$

Or now it is possible to define the functions β, Ψ from equation (4.9) as:

$$\beta = (1 + \lambda \cdot \sin\phi)^{\left(-\frac{1}{2}\right)} \cdot W_r \tag{4.10}$$

$$\psi = (1 + \lambda \cdot \sin\phi)^{\left(-\frac{1}{2}\right)} \cdot W_i \tag{4.11}$$

where, functions β, Ψ and their derivatives are part of the solution of differential equation 4.4, where, index *r* stands for real part, the index *i* for imaginary part.

The equations (4.4-4.11) base the membrane solution of shell problems [25] for investigated case of circular bellows with U-shaped convolution cross section geometry.

To solve these equations (4.3-4.11), it is nessesary to define auxiliary functions:

$$\lambda = \frac{b}{a} \tag{4.12}$$

$$m = \sqrt{12 \cdot (1 - \nu^2)} \tag{4.13}$$

$$\mu = \frac{m \cdot b^2}{a \cdot h} \tag{4.14}$$

$$P_H = \frac{m \cdot (a + b \cdot \sin\phi) \cdot b \cdot (p \cdot \sin\phi)}{E \cdot h^2} \tag{4.15, a}$$

$$P_V = \frac{m \cdot (a + b \cdot \sin\phi) \cdot b \cdot (p \cdot \cos\phi)}{E \cdot h^2} \tag{4.16, b}$$

$$\Omega = -\int P_V d\phi = \frac{m \cdot a \cdot b \cdot p}{E \cdot h^2} \cdot \left[\sin\phi + \lambda \cdot \sin\phi^2 + \frac{\lambda}{4} \cdot cos2\phi\right] \cdot \begin{matrix}\phi_2 \\ \phi_1\end{matrix} \qquad (4.17)$$

where, μ stands for the Poisson ratio, and h for the shell thickness of a single-ply of the bellows. Some of these auxiliary functions depend on the angle ϕ, such as the pressure P_H and Ω.

Considering the equilibrium of investigated element (see Figure 4.2) and determine of strain-displacement relations and Hooke's law, the equation (4.21-4.24) used to consider normal forces and bending moments for circular bellows with U-shaped convolution cross section in terms of displacement, according to [57] and [25]:

$$N_\phi = \frac{E \cdot h^2}{m \cdot a} \cdot \left(\frac{\psi \cdot \cos\phi + \Omega \cdot \sin\phi}{1 + \lambda \cdot \sin\phi}\right) \qquad (4.18)$$

$$Q_\phi = \frac{E \cdot h^2}{m \cdot a}\left(\frac{-\psi \cdot \sin\phi + \Omega \cdot \cos\phi}{1 + \lambda \cdot \sin\phi}\right) \qquad (4.19)$$

$$N_\theta = \frac{E \cdot h^2}{m \cdot b} \cdot (\psi' + P_H) \qquad (4.20)$$

$$M_\phi = \frac{E \cdot h^3}{m^2 \cdot b} \cdot \left(\beta' + \frac{\nu \cdot \lambda \cdot \cos\phi \cdot \beta}{1 + \lambda \cdot \sin\phi}\right) \qquad (4.21)$$

$$M_\theta = \frac{E \cdot h^3}{m^2 \cdot b}\left(\nu \cdot \beta' + \frac{\lambda \cdot \cos\phi \cdot \beta}{1 + \lambda \cdot \sin\phi}\right) \qquad (4.22)$$

The normal forces and bending moments in ϕ and θ directions resulted in the stresses in the respective directions:

$$\sigma_{\phi,m} = \frac{N_\phi}{h} \qquad (4.23)$$

$$\sigma_{\theta,m} = \frac{N_\theta}{h} \qquad (4.24)$$

$$\sigma_{\phi,b} = \frac{6 \cdot M_\phi}{h^2} \qquad (4.25)$$

$$\sigma_{\theta,b} = \frac{6 \cdot M_\theta}{h^2} \qquad (4.26)$$

where, the indexes *m* and *b* stand for membrane and bending stresses. The maximum value of stresses determined as:

$$\sigma_{\phi max} = \left|\sigma_{\phi,m}\right| + \left|\sigma_{\phi,b}\right| \qquad (4.27)$$

$$\sigma_{\theta max} = |\sigma_{\theta,m}| + |\sigma_{\theta,b}| \tag{4.28}$$

Hence, the maximum principal stresses $\sigma_{\phi max}$ and $\sigma_{\theta max}$, which occurred in the investigated bellows corrugations, will be determined as the maximum equivalent stresses (σ_{eq}) according to equation [166]:

$$\sigma_{eq} = \sqrt{\frac{1}{2} \cdot \left[\left(\sigma_{\phi max} - \sigma_{\theta max} \right)^2 + (\sigma_{\phi max})^2 + (\sigma_{\theta max})^2 \right]} \tag{4.29}$$

Finally, equation (4.25) provided the possibility to analyse the maximum equivalent stresses in any considered point of investigated bellows corrugations.

4.3 Asymptotic integration of the non-homogeneous equation for investigated circular bellows U-shaped convolution cross section

According to nonlinear interlaminar stress analysis by multi-layer shell elements [23] the function *x* is a complex number of the form:

$$x = Re(x) + i \cdot Im(x) \tag{4.30}$$

where, *Re (x)* and *Im (x)* are the real and imaginary parts of *x*.

For analysis and comparison of the results, in case of internal pressure, the stresses in the bellows corrugations will be analysed from 0 ° to 180 ° of the crest (point A, where obtained measurements during the experiments), and from 180 ° to 360 ° of the cavity (the critical point D of bellows corrugation, or the point where occurred the maximum equivalent stresses).

Therefore, for analysis of the considered investigated points of X coordinate, which was used to determine the values of $h_{1,r}(x), h_{1,i}(x)$ and their derivations $h'_{1,r}(x)$, $h'_{1,i}(x)$ will be considered as:

$$Im(x) = \begin{cases} 0 - \ point\ of\ maximal\ equivalent\ stresses, \phi = 90\ ° \\ 2 - \ analysed\ point\ of\ experiments, \phi = 270\ ° \end{cases} \tag{4.31}$$

The corresponding imaginary part of *x* calculated as follows [23]:

$$Im(x) = \mu^{\frac{1}{3}} \cdot \phi \tag{4.32}$$

Therefor the equation (4.4) may be written in form:

$$W_p(\phi) = \mu^{1/3} \cdot f(x) \cdot (1 + \lambda \cdot \sin \phi)^{\frac{1}{2}} \cdot T(x) \tag{4.33}$$

Where the funktion T(x) to be considered as differentional equation:

$$\frac{d^2T}{dx^2} - ixT = 1 \tag{4.34}$$

The equation above (4.34) has asymptotic behaviour, which can be expressed obviously as:

$$T(x) = -\frac{2}{3}(ix)^{\frac{1}{2}} \cdot S_{0,1/3}\left[\frac{2}{3}(ix)^{\frac{3}{2}}\right] \tag{4.35}$$

where $S_{0,1/3}$ is a Lommel function [176].

Hence, equation (4.34) can be considered as a function of $T(x)$. That definition presents the real and imaginary part of $T(x)$ and their derivatives [25]. The functions $T_r(x)$, $T_i(x)$, $T_r{}'(x)$, $T_i{}'(x)$ devited with the values of the functions T_r and T_i and of their derivatives $T_r{}'$, $T_i{}'$ according to modified Hankel's functions of order one-third and their derivatives [27] and the Bessel tabulated functions [176] $h_{1,r}(x)$ or $h_{1,i}(x)$.

For solution of asymptotic integration of non-homogeneous equation for circular bellows with U-shaped convolution cross section subject to internal pressure (see [25], p. 165-177), equations (4.10-4.11) for functions β, Ψ and their derivations β', Ψ' can be written in form:

$$\beta = \mu^{\frac{1}{3}} \cdot T_r(x) \cdot \cos\phi \cdot \Omega \tag{4.36}$$

$$\psi = \mu^{\frac{1}{3}} \cdot T_i(x) \cdot \cos\phi \cdot \Omega \tag{4.37}$$

$$\beta' = [\mu^{\frac{2}{3}} \cdot T_r{}'(x) \cdot \cos^2\phi - \mu^{\frac{1}{3}} \cdot T_r(x) \cdot \sin\phi] \cdot \Omega \tag{4.38}$$

$$\psi' = [\mu^{\frac{2}{3}} \cdot T_i{}'(x) \cdot \cos^2\phi - \mu^{\frac{1}{3}} \cdot T_i(x) \cdot \sin\phi] \cdot \Omega \tag{4.39}$$

Replace the defined functions β, ψ and their derivations β', ψ' from equations (4.36-4.39) into (4.18-4.22) we obtain the following equations:

$$N_\phi = \frac{E \cdot h^2}{m \cdot a} \cdot \left(\frac{\mu^{\frac{1}{3}} \cdot T_i(x) \cdot \cos\phi \cdot \cos\phi + \sin\phi}{1 + \lambda \cdot \sin\phi}\right) \cdot \Omega \tag{4.40}$$

$$Q = \frac{E \cdot h^2}{m \cdot a}\left(\frac{-(\mu^{\frac{1}{3}} \cdot T_i(x) \cdot \cos\phi \cdot \sin\phi) + \cos\phi}{1 + \lambda \cdot \sin\phi}\right) \cdot \Omega \tag{4.41}$$

$$N_\theta = \frac{E \cdot h^2}{m \cdot b} \cdot \left([\mu^{\frac{2}{3}} \cdot T_i{}'(x) \cdot \cos^2\phi - \mu^{\frac{1}{3}} \cdot T_i(x) \cdot \sin\phi] \cdot \Omega + P_H + P_V\right) \tag{4.42}$$

$$M_{\phi} = \frac{E \cdot h^3}{m^2 \cdot b} \cdot \left([\mu^{\frac{2}{3}} \cdot T_r{}'(x) \cdot \cos^2 \phi - \mu^{\frac{1}{3}} \cdot T_r(x) \cdot \sin \phi] \cdot \Omega + \frac{\nu \cdot \lambda \cdot \cos\phi \cdot \beta}{1 + \lambda \cdot \sin\phi} \right) \quad (4.43)$$

$$M_{\theta} = \frac{E \cdot h^3}{m^2 \cdot b} \left(\nu \cdot [\mu^{\frac{2}{3}} \cdot T_r{}'(x) \cdot \cos^2 \phi - \mu^{\frac{1}{3}} \cdot T_r(x) \cdot \sin \phi] \cdot \Omega + \frac{\lambda \cdot \cos\phi \cdot \beta}{1 + \lambda \cdot \sin\phi} \right) \quad (4.44)$$

Solving equations (4.40-4.44) and substituting into defined equations (4.23-4.29), it is possible to calculate the equivalent stresses for circular bellows with U-shaped convolution cross section and uniform thickness at any defined point.

4.4 MatLab code for mathematical analysis of investigated bellows corrugations

The code programmed with MatLab® software package solve the defined equations and consider the equivalent stresses of investigated sections of the circular bellows with U-shaped convolution cross section. The code evaluated the internal stress resultants and deformations. The considered sections, as it presented on Figure 4.3, the negative direction of stress resultants and stress couples for a shell of revolution from 0 ° to 180 ° of the cavity section, with maximal tensile stress at point D, the critical point of bellows cross section, or the point where occurred the maximum equivalent stresses. The positive direction of stress resultants and stress couples for a shell of revolution from 180 ° to 360 ° on the crest section, which considered the point A, where obtained measurement results during the experiments. In addition, it considered the side wall (shell) section of the circular bellows with U-shaped convolution cross section.

The code statement considered the parameters of geometry of investigated circular bellows with U-shaped convolution cross section, as well as material properties, load case, and input of definition presented the real and imaginary part of $T(x)$ and their derivatives [25].

For example, below it presented the part of the MatLab® code (algorithm) for the equivalent stress analysis of negative curvature from 0° till 180 ° of investigated circular bellows with U-shaped convolution cross section geometry, which loaded with internal pressure of 1,6 MPa:

```
%single-ply bellows
format compact;
%for values of x(T) the following asymptotic expansion of functions
%T_r(x), T_dr(x), T_i(x), T_di(x) are tabulated according to Clark's numerical
%integrations for investigated bellows with U-shaped convolution cross section:
xT =0:0.05:5;
Tr=[-1.288, -1.287, -1.283, -1.277, -1.268, -1.257, -1.244, -1.228, ...
    -1.21, -1.19, -1.168, -1.144, -1.118, -1.09, -1.061, -1.03, -0.998, ...
    -0.965, -0.931, -0.896, -0.86, 0.823, -0.786, -0.749, -0.711, -0.673, ...
    -0.636, -0.599, -0.562, -0.525, -0.489, -0.454, -0.419, -0.385, -0.352, ...
    -0.32, -0.29, -0.261, -0.232, -0.204, -0.178, -0.153, -0.130, ...
```

```
    -0.108, -0.088, -0.069, -0.051, -0.035, -0.02, -0.006, 0.006, 0.017, ...
    0.027, 0.036, 0.044, 0.05, 0.056, 0.061, 0.065, 0.068, 0.07, 0.071, ...
    0.072, 0.073, 0.073, 0.072, 0.071, 0.069, 0.067, 0.065, 0.063, 0.06, 0.058,
...
    0.056, 0.053, 0.05, 0.047, 0.044, 0.041, 0.038, 0.035, 0.032, 0.029, ...
    0.027, 0.024, 0.022, 0.02, 0.018, 0.016, 0.014, 0.012, 0.011, 0.009, ...
    0.008, 0.007, 0.006, 0.005, 0.004, 0.003, 0.003, 0.002]; %Tr
Tdr=[0, 0.05, 0.1, 0.149, 0.197, 0.245, 0.292, 0.337, 0.38, 0.422, ...
    0.462, 0.5, 0.535, 0.568, 0.599, 0.627, 0.652, 0.675, 0.695, 0.712, ...
    0.726, 0.737, 0.745, 0.75, 0.753, 0.753, 0.75, 0.745, 0.737, 0.727, 0.715, ...
    0.7, 0.683, 0.664, 0.644, 0.623, 0.601, 0.578, 0.554, 0.529, 0.503, ...
    0.476, 0.449, 0.421, 0.394, 0.336, 0.339, 0.312, 0.286, 0.26, 0.235, ...
    0.211, 0.188, 0.165, 0.144, 0.123, 0.104, 0.086, 0.069, 0.053, 0.038, ...
    0.024, 0.011, 0, -0.01, -0.019, -0.027, -0.034, -0.04, -0.045, -0.05, ...
    -0.053, -0.056, -0.058, -0.059, -0.059, -0.059, -0.059, -0.058, -0.057, ...
    -0.056, -0.054, -0.052, -0.05, -0.048, -0.046, -0.043, -0.04, -0.038, ...
    -0.035, -0.032, -0.03, -0.027, -0.025, -0.022, -0.02, -0.018, -0.016, ...
    -0.014, -0.012, -0.01]; %Tdr
Ti=[0, 0.047, 0.094, 0.14, 0.186, 0.231, 0.276, 0.32, 0.362, 0.403, ...
    0.443, 0.482, 0.519, 0.554, 0.588, 0.619, 0.649, 0.677, 0.702, 0.726, ...
    0.747, 0.767, 0.784, 0.799, 0.812, 0.822, 0.830, 0.836, 0.841, 0.844, ...
    0.846, 0.845, 0.842, 0.837, 0.831, 0.823, 0.814, 0.804, 0.793, 0.78, ...
    0.766, 0.751, 0.736, 0.72, 0.703, 0.686, 0.669, 0.651, 0.633, 0.615, ...
    0.597, 0.579, 0.561, 0.543, 0.525, 0.508, 0.491, 0.475, 0.459, 0.443, ...
    0.428, 0.413, 0.399, 0.386, 0.373, 0.36, 0.348, 0.337, 0.327, 0.317, 0.307,
...
    0.298, 0.29, 0.282, 0.275, 0.268, 0.261, 0.255, 0.25, 0.246, 0.242, ...
    0.238, 0.234, 0.23, 0.226, 0.223, 0.22, 0.218, 0.215, 0.213, 0.21, 0.208, ...
    0.206, 0.205, 0.203, 0.201, 0.2, 0.198, 0.197, 0.195, 0.194]; %Ti
Tdi=[0.939, 0.937, 0.932, 0.924, 0.913, 0.899, 0.882, 0.862, 0.839, ...
    0.813, 0.785, 0.755, 0.723, 0.688, 0.652, 0.614, 0.574, 0.534, ...
    0.493, 0.45, 0.407, 0.364, 0.321, 0.278, 0.235, 0.193, 0.151, ...
    0.11, 0.07, 0.031, -0.007, -0.043, -0.078, -0.111, -0.142, -0.171, ...
    -0.198, -0.222, -0.244, -0.264, -0.282, -0.298, -0.313, -0.326, ...
    -0.337, -0.346, -0.353, -0.358, -0.361, -0.362, -0.362, -0.361, ...
    -0.358, -0.354, -0.349, -0.342, -0.335, -0.327, -0.318, -0.308, ...
    -0.298, -0.287, -0.276, -0.264, -0.253, -0.241, -0.23, -0.218, -0.206, ...
    -0.195, -0.184, -0.173, -0.163, -0.152, -0.142, -0.132, -0.123, -0.114, ...
    -0.106, -0.098, -0.09, -0.083, -0.077, -0.071, -0.066, -0.061, -0.057, ...
    -0.053, -0.049, -0.046, -0.043, -0.04, -0.038, -0.036, -0.034, -0.033, ...
    -0.031, -0.03, -0.029, -0.029, -0.028]; %Tdi
%Geometry properties of investigated bellows with U-shaped convolution
%cross section:
R_1 = 1.41212 * 10^(-3); %defined dimension of negative corrugation
R_c1 = 28.5 * 10^(-3); % defined dimension of negative corrugation
h = 0.8 * 10^(-3); % thickness of the shell
E = 2*10^11; %elastic modulus of the investigated material
v = 0.3; % v: Poisson number
nl = 1; %number of bellows plies
p = -1.6 * 10^6; % Pa, Internal pressure:
% thin toroidal shell of negative curvature from 0° till 180°:
x1 = 0:1:180;
n = length(x1);
for i = 1:1:n
y(i) = pi / 180 * x1(i)
% Equation for analysation lambda, m, omega, my, fx:
lambda = R_1 / R_c1;
m = sqrt(12 * (1 - v^2));
%Equation of omega with integration limits from 0 to pi:
```

```
omega = ((m * R_1 * R_c1 * p) / (E * h.^2)) *(nl *(((lambda * x1(i)) / 2 +
cos(y(i)) + lambda * cos(y(i)) * sin(y(i)) + 0.25 * lambda * cos(y(i)) *
sin(y(i)))));
my = m * (R_1)^2 / (R_c1 * h);
fx = my^(1/3) * y(i);
P_H = (m * (R_1 * sin(y(i)) + R_c1) * R_1 * p * sin(y(i))) / (E * h.^2);
P_V = (m * (R_1 * sin(y(i)) + R_c1) * R_1 * (p * cos(y(i)))) / (E * h.^2);
% for negative curve according to Clark considered T_r(-x) = T_r(x), T_dr(-x) = -
T_dr(x), T_i(-x) = -T_i(x), T_di(-x) = T_di(x)
%Interpolation in 2-Dimension
 T_r=interp1(xT,Tr,fx,'spline')
 T_dr=interp1(xT,Tdr,fx,'spline')
 T_i=interp1(xT,Ti,fx,'spline')
 T_di=interp1(xT, Tdi, fx,'spline')
% stress resultants, stress couples and the rotation in the no dimensional form N,
Q, M:
% stress resultant in meridional direction:
N_phi = (E * h.^2 / (m * R_c1)) * ( my.^(1/3) * (-T_i) * (cos(y(i))).^2 +
sin(y(i))) / (1 + lambda * sin(y(i))) * omega;
% transverse shear stress resultant:
Q = (E * h.^2 / (m * R_c1)) * ((- my.^(1/3) * (-T_i) * sin(y(i)) * cos(y(i))) +
cos(y(i))) / (1 + lambda * sin(y(i))) * omega;
% stress resultant tangential to parallel circle:
N_teta = ((E * h.^2) / (m * R_c1)) * ((my.^(2/3) * (T_di) * (cos(y(i))).^2 -
my.^(1/3) * (-T_i) * sin(y(i))) * omega + P_H + P_V);
% stress couple in meridional direction:
M_phi = (E * h.^3 / (m.^2 * R_1)) * ( my.^(2/3) * (T_dr) * (cos(y(i))).^2 -
my.^(1/3) * (-T_r) *sin(y(i))) * omega + (v * lambda * my.^(1/3) * (-T_r)
*(cos(y(i))).^2 * omega) / (1 + lambda * sin(y(i)));
% stress couple in direction tangential to parallel circle:
M_teta = (E * h.^3 / (m.^2 * R_1)) * (v * (my.^(2/3) *  (cos(y(i))).^2 - my.^(1/3)
* (-T_r) *sin(y(i)))) * omega + (lambda * my.^(1/3) * (-T_r) *(cos(y(i))).^2 *
omega) / (1 + lambda * sin(y(i)));
% Stress resultants and deformations at investigated point on the bellows
corrugation (crest, side shell, or cavity:
% h: Wall thickness, p: Internal pressure:
sigma_tetaD = N_teta / h;
sigma_phiD = N_phi / h;
sigma_tetaB = 6 * M_teta / h.^2;
sigma_phiB = 6 * M_phi / h.^2;
sigma_tau = Q / h;
%membrane and bending stresses at investigated point on the bellows corrugation:
sigma_phi = abs(sigma_phiD) + abs(sigma_phiB);
sigma_teta = abs(sigma_tetaD) + abs(sigma_tetaB);
% Shape change energy hypothesis (two-dimensional):
sigma_GEH(i) = sqrt(0.5 * ( (sigma_phi - sigma_teta).^2 + (sigma_phi).^2 +
(sigma_teta).^2) + 3*sigma_tau.^2)%sigma_GEH
%results negative curvature:
end
plot(x1,sigma_GEH,'r--o')
xlabel('degree of revolution, °')
ylabel('Equivalent stress, sigma eq MPa')
title('Internal pressure analysis')
legend('sigma eq')
grid
```

The full version of the code presented in Attachment A.

The results of equivalent stresses for negative curvature of investigated circular bellows with

U-shaped convolution cross section geometry presented on Figure 4.4.

As presented on Figure 4.4, the maximal value of equivalent stresses located between 80 ° and 90 ° at the inner cavity of negative curvature with maximal value of 122,2 MPa (point D). From 90 ° till 100 ° the results are unstable and showed some error. Therefore, these results would not be considered.

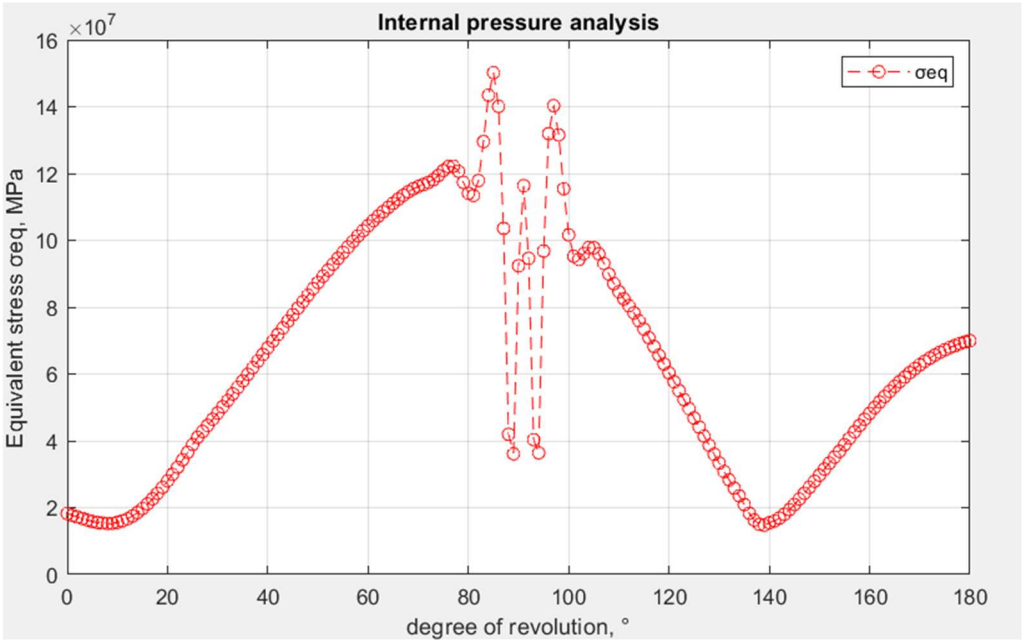

Figure 4.4: Results of equivalent stresses of negative curvature for investigated circular bellows with U-shaped convolution cross section geometry for outer side of cavity

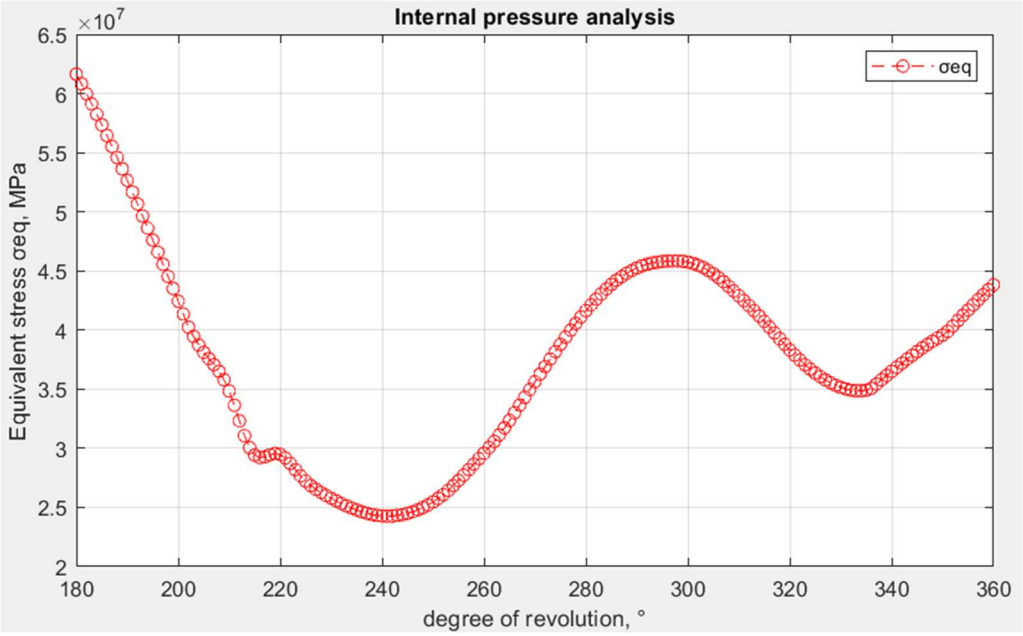

Figure 4.5: The results of equivalent stresses for positive curvature for investigated circular bellows with U-shaped convolution cross section geometry for outer side of cavity

For positive curvature (crest section) of investigated circular bellows with U-shaped convolution cross section the maximal value of equivalent stresses 68,72 MPa at 180 ° (at B point), where positive curvature connected to the side wall of the bellows cross section. Second peak of the equivalent stresses 43,25 MPa located between 270 ° and 290 ° at the crest section of bellows corrugation (at point A).

On Figure 4.6 presented the results of equivalent stresses for positive, negative curvatures and side wall (blue color) of investigated circular bellows with U-shaped convolution cross section. The peaks of the equivalent stresses located in the investigated points of cavity, crest and side wall, namely at investigated points A (270 °, 43,25 MPa), B (180 °, 60,94 MPa), C (180 °, 68,72 MPa) and D (90 °, 122,2 MPa), see Figure 4.3.

The result presented for cavity, side wall and crest sections of investigated circular bellows with U-shaped convolution cross section, namely with middle radius of corrugation 1,41212 mm presented on Figure 4.6.

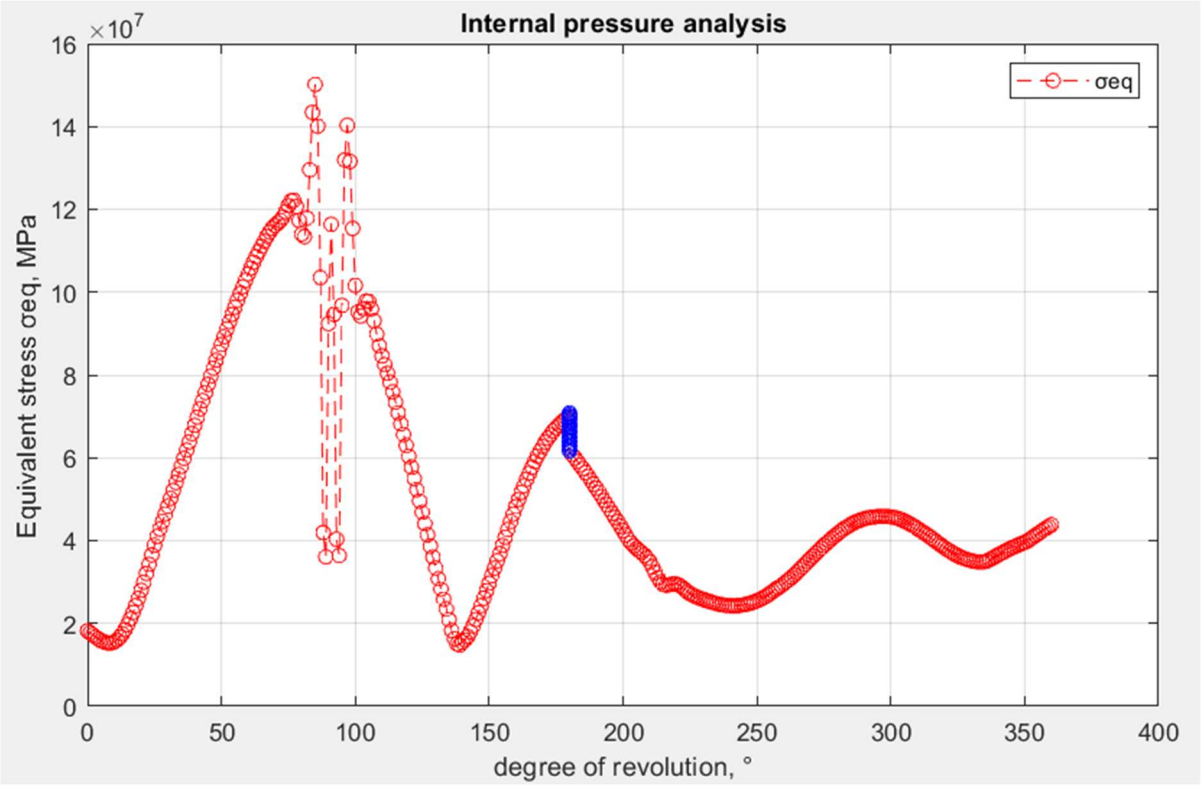

Figure 4.6: The results of equivalent stresses for cavity, crest and side shell (wall) with radius 1,41212 mm for investigated circular bellows with U-shaped convolution cross section geometry (full geometry of one bellows corrugation according to bellows calculation model on Figure 4.1)

Hence, as it was already described, the maximal equivalent stresses in middle radius of curvature of investigated circular bellows with U-shaped convolution cross section located in

negative curvature and have peaks at 80 ° and at 90 °. However, between 90 ° and 100 ° is a mathematic error due to geometry parameters, derivation and integration constants. The maximal equivalent stresses also located in crest section of investigated circular bellows with U-shaped convolution cross section with the maximal value of 68,72 MPa at 180 ° (at B point), and in crest section of bellows corrugation (at point A) with the maximal value of equivalent stresses 43,25 MPa located between 270 ° and 290 ° (see Figure 4.1).

The results obtained from mathematical analysis are coincide to FEA results at the investigated points of bellows geometry. Likewise, the maximal value of equivalent stresses from analysis with EN ISO 13445-3 [21], as well coincide (with small divergence) to maximal value obtained from presented mathematical investigation.

FEA results of negative, positive curvatures and side (shell) wall of investigated circular bellows with U-shaped convolution cross section presented on Figure 4.7. On the Figure presented samples of equivalent stresses in investigated points A, B, C and D at (bellows) radius 1,41212 mm of negative, positive corrugations and side wall (figure in red rectangle).

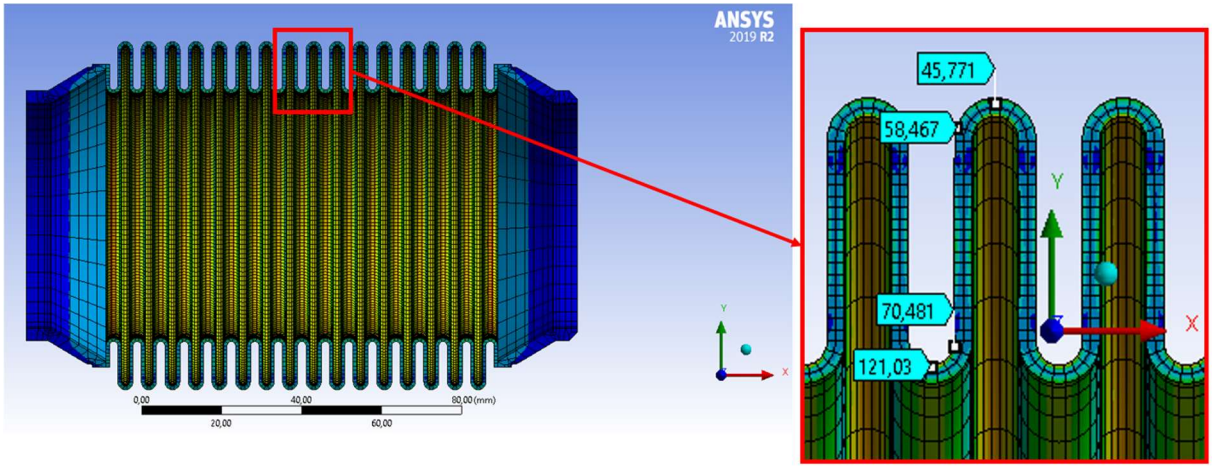

Figure 4.7: FE analysis results of equivalent stresses for investigated circular bellows with U-shaped convolution cross section geometry. For red rectangle presented the point D in cavity, internal side points B and C, and point A at crest of investigated circular bellows with U-shaped convolution cross section with middle radius of 1,41212 mm at corrugation.

4.5 Discussions and results of analytical analysis

The presented MatLab® code was used to evaluate equivalent stress resultants at investigated circular bellows with U-shaped convolution cross section geometry. The stress analysis was carried out for five investigated bellows geometries such as single-, two-, three-, four- and five-

plies implementations, to evolve and verify different geometrical parameters. These results were thereafter used for the evaluation of membrane and bending stresses in meridional as well as circumferential directions of investigated bellows.

The magnitude of $\sigma_{Q\phi}$ is smaller compared to the remaining stresses in all investigated cases. This is as expected, the value of $\sigma_{Q\phi}$ is small at the junction of the toroidal shell of negative and positive curvature, as well as side (wall) shell (see Figure 4.3).

The investigated MatLab® code correspond the maximum values of meridional bending stress $\sigma_{\phi b}$ and their locations on the meridian for different numbers of plies. In most cases, the location of maximum $\sigma_{\phi b}$ is at the cavity section, at vertical plane of symmetry of the toroidal shell of positive curvature. The maximum $\sigma_{\phi b}$ occurred within the two toroidal shells. The stress $\sigma_{\phi b}$ is the greatest of investigated stresses, which defined the geometry of investigated bellows under internal pressure loading.

The magnitude of the circumferential membrane stress $\sigma_{\theta b}$ is large compared to $\sigma_{\theta m}$ in all of the cases. The maximum values of $\sigma_{\theta m}$ and their locations is on the same point of meridian for various cases. The distribution of $\sigma_{\theta b}$ is similar to that of $\sigma_{\phi b}$, but the magnitude is always lower than $\sigma_{\phi b}$. The maximum values of $\sigma_{\theta b}$ and their locations on the meridian of investigated cross section geometry are analysed for various cases. From the investigated MatLab® code it was observed the maximum ratio of bending stresses $\sigma_{\theta b}$ at the vertical plane of symmetry of the toroidal shell of positive curvature.

The maximum values of $\sigma_{\phi m}, \sigma_{\phi b}, \sigma_{\theta m}, \sigma_{\theta b}$ for different geometries and internal pressure cases of bellows were investigated in cross section location at segments A, B, C, D (see Figure 4.3).

Hence, after analysis of membrane and bending stresses in meridional as well as in circumferential directions the equivalent stresses were determined according to equation (4.29).

The Table 4.1 present the maximum value of equivalent stresses of negative curvature (at cavity section from 0 ° till 180 °), positive curvature (at crest section from 180 ° till 360 °) and side wall (shell) section of the single- and multi-ply circular bellows with U-shaped convolution cross section in the case of internal pressure of 1,6 MPa and 2 MPa.

Results of maximal value of equivalent stresses for positive, negative curvatures and side wall (shell) of investigated circular bellows with U-shaped convolution cross section presented on Figure 4.8. However, on the diagram is shown maximal value of equivalent stresses, which

located at outer side of cavity section at point D, see Figures 4.1 and 4.7.

Table 4.1: Maximal values of equivalent stresses of the bellows corrugation at 90° and 270° in the case of internal pressure of 1,6 MPa and 2 MPa.

Number of plies, N	P = 1,6 MPa			P = 2 MPa		
	90 °, point D	180 °, points B and C	270 °, point A	90 °, point D	180 °, points B and C	270 °, point A
1	122,80	68,72	43,25	153,50	85,91	54,10
2	245,60	137,40	85,82	307,01	171,80	107,30
3	368,40	206,20	128,40	460,50	257,70	160,50
4	490,60	274,90	171,00	612,40	343,60	213,70
5	612,50	343,60	213,50	765,70	429,50	266,90

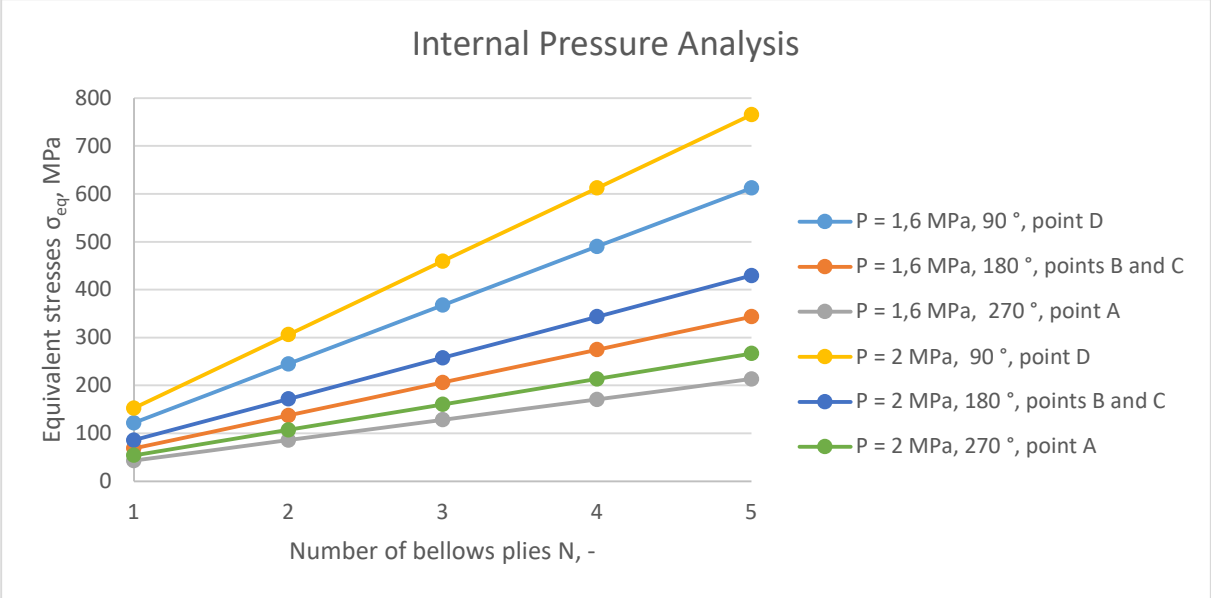

Figure 4.8: Results of maximal equivalent stresses σ_{eq} for investigated circular bellows with U-shaped convolution cross section geometry with developed MatLab® code (see Attachment A)

4.6 Conclusion

The new mathematical analysis provides the analytical investigation of single- and multi-ply circular bellows with U-shaped convolution cross section, the computation of equivalent stresses of its corrugations, such as cavity, crest and side shell (wall) sections (see Figure 4.1), for this investigated internal pressure load case of 1,6 MPa and 2 MPa [6].

Hence, during the mathematical analysis of single- and multi-ply circular bellows with U-shaped convolution cross section it was concluded that the maximum equivalent stresses appeared in the case of internal pressure in cavity section, accordingly at 90 ° in point D, in crest section accordingly at 270 ° in point A, and in side (shell) wall section at 180 °, points B

and C, which presented on Figure 4.1, c. These points of investigated single- and multi-ply circular bellows with U-shaped convolution cross section, are weak areas which were closely analysed via developed mathematical method.

The developed algorithm and code of mathematical method was programmed on MatLab® software package, where input parameters are geometrical and material properties of single- or multi-ply circular bellows with U-shaped convolution cross section, and boundary conditions of the investigated (internal pressure) load case.

The developed algorithm and code relevant for detailed mathematical analysis of bellows which considered for the ball valve [4] with ratchet gear mechanism. Nevertheless, the mathematical model can be used for analyses of the U-shaped metal bellows installed in the pipelines, or for any kind of industrial applications.

Finally, presented mathematical method of analytical analysis of single- and multi-ply circular bellows with U-shaped convolution cross section requires improvement for further investigation of bending load case and temperature influence, which has potential to extend the work [5].

5. Experiments investigation

5.1 Experimental study of performance of the investigated ball valve with RGM and two-ply bellows

Study of workability of the ball valve with RGM [4] design and its components required experimental analysis, which had carried out and proved the results obtained from the finite element (FEA) and analytical analysis. The analytical analysis carried out according to EN 13445 Part 3 [21], ASME code [53] and EMJA [60] design of the bellows. In addition, according to accumulated information it has been developed the computational application code in MatLab® for analysis of bellows structure dependent on the Clark's theory of the thin toroidal shells [25].

The laboratory installation built in the laboratory of the University of Stuttgart at the department of chemical process engineering. The laboratory set up (see Figure 5.1) consist two parts:

1. The two-ply circular bellows with U-shaped convolution cross section [14] for analysing critical load cases using the strain gages [90];
2. The ball valve (nominal diameter of 100 mm) with a ratchet gear mechanism and two-ply bellows.

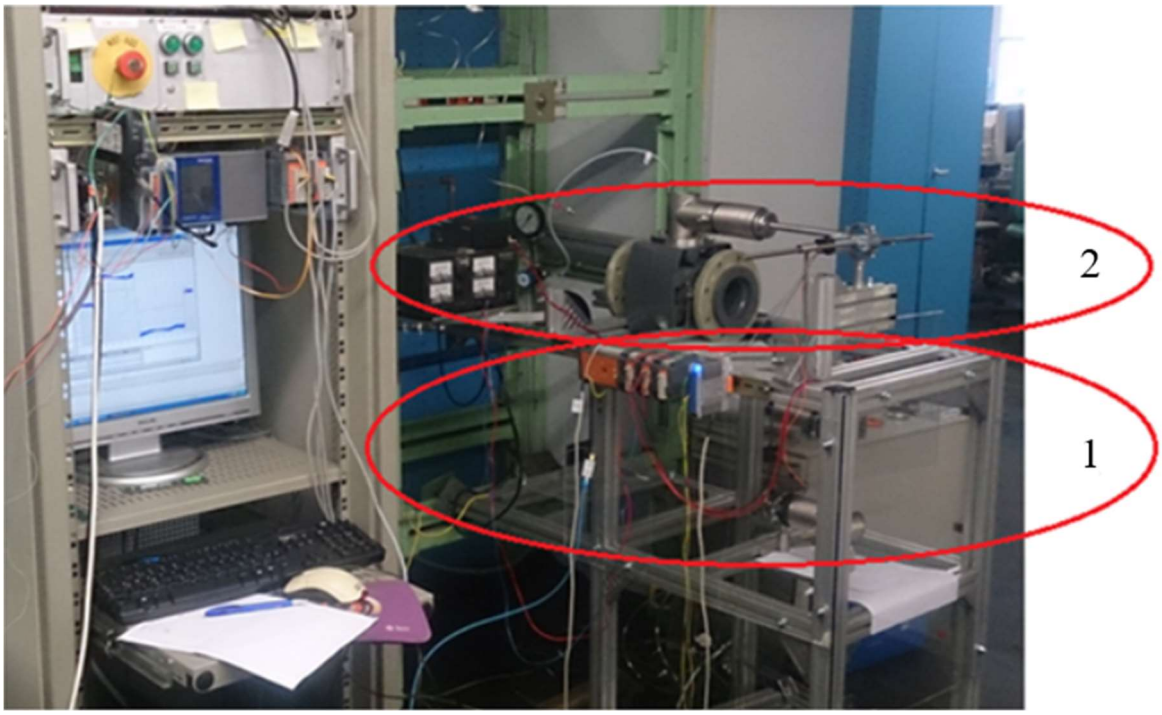

Figure 5.1: Laboratory installation for the experiments of investigated utility model № 139949 ball valve with RGM [4].

In order to collect experimental data, it has built laboratory installation Figure 5.1, which consist two parts. First part of the laboratory installation (Figure 5.2) constructed to study strength limits of the two-ply bellows at defined critical points of bellows cross section (for cases of internal pressure and bending).

In order to determine appeared critical stresses in the structure of bellows the experiment setup with the following components has constructed (see Figure 5.2):

1. Witzenmann Hydra (Figure 5.2, (4)) BE 356230-bb 68 bellows [93];
2. Strain gauges (HBM Ltd.) [91];
3. Gantner Instruments (Figure 5.2, (1) and (2)) [92];
4. Bosch profile (Figure 5.2, (3)) with the Plexiglas for safety reasons.

Consequently, for operation of this part of the laboratory installation, it was programmed the code on Gantner Instruments software package, which used for measuring the strains respectively stresses in the structure of investigated two-ply bellows corrugations on the critical points. This program had received measurement data from strain gauges (see Figure 5.4 and 5.5) through the Gantner Instruments (see Figure 5.2, (1) and (2)). Furthermore, it analysed the differences between the initial resistance and current resistance at a measurement point [91].

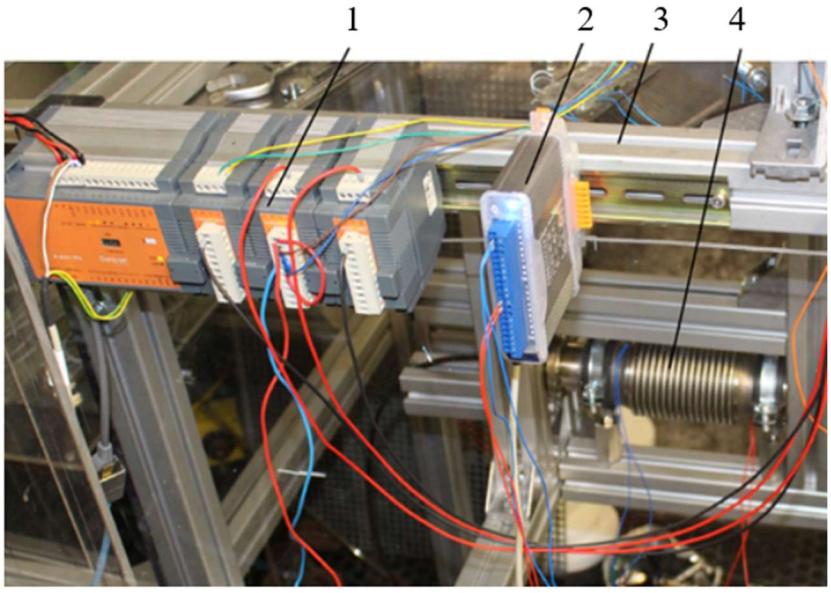

Figure 5.2: Part of the laboratory installation for studying the strain respectively stresses, which appear in the structure of investigated two-ply bellows in the case of internal pressure and bending:
1. Gantner Instruments;
2. Gantner Instruments strain gages sensor;
3. Bosch construction modules;
4. two-ply bellows

Hence, another part of the laboratory installation (presented on Figure 5.3) based on the ball valve (1) (nominal diameter 100 mm) with RGM and two-ply bellows (3). The two-ply bellows used as a seal component of ratchet gear mechanism (2).

In this experimental laboratory installation, a lever (4) due welding connection attached to the two-ply bellows (3). The movement of the threaded rod (6), which attached to the engine (5), deflected the lever (4) to adjusted angle. The deflection of the lever caused a lateral and angular moment of the two-ply bellows. The pawls, which connected on the end of the lever due bold connection in ratchet gear housing (2), due to axial deflection of the lever, rotated the ratchet gear wheels of the ratchet gear mechanism. Consequently, the ratchet gear wheels connected by keys to the stem. Therefore, during rotation of the ratchet gear wheels, the stem rotates the ball (obturator) of the ball valve (1). The work principle of the ball valve with ratchet gear mechanism and two-ply bellows detailed described in chapter 6.

In addition, two-ply bellows had to be able to withstand deflection and the internal pressure loads. Full automatization of this part of the laboratory installation achieved with a help of Gantner Instrument modules [92].

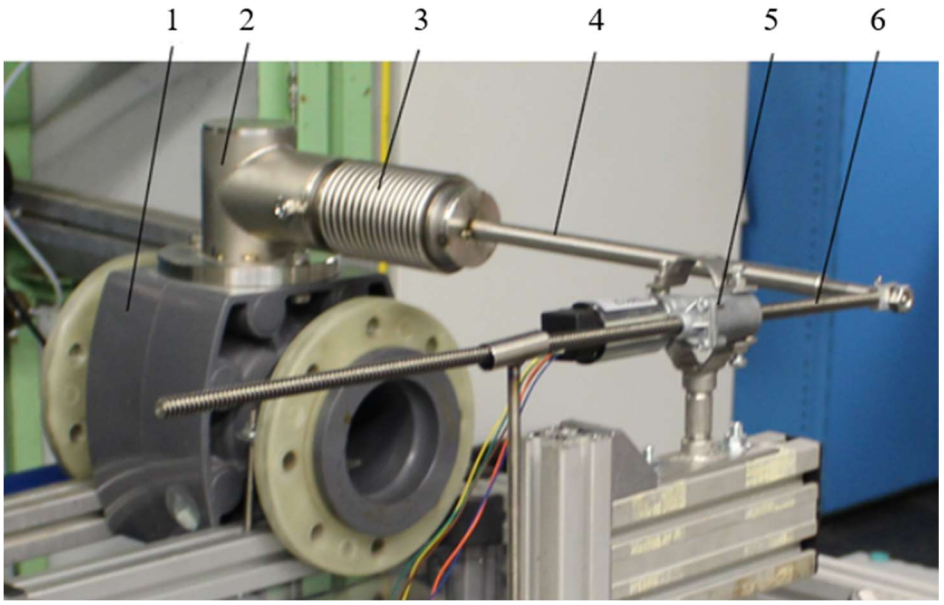

Figure 5.3: Second part of laboratory installation:

1. ball valve with nominal diameter of 100 mm;
2. ratchet gear housing;
3. two-ply bellows;
4. lever;
5. electrical engine;
6. threated rod.

5.2 Experimental analysis of stresses in investigated two-ply bellows with strain gauges

For experimental analysis of the critical stresses on the surface of investigated two-ply circular bellows with U-shaped convolution cross section were used the strain gauges (SG), M model of HBM Ltd [90] (see Figure 5.4).

Hence, the strain gauges (see Figure 5.5) consist two rectangular measuring grids. The grids consist certain number of meandering grids, which located parallel to each other. One of these grids located in vertical direction, another aligned horizontally on the outer surface of investigated two-ply bellows corrugation. Accordingly, the grids measure changing of resistant in meridian and in angular directions. Both measuring grids had two connections to Gantner Instruments® modules, which transform changes of resistance in the grids of SG with the help of programmed code into stresses.

The strain gauges attached on the surface of the top crest (crown) section of the investigated two-ply bellows corrugation using special glue (see Figure 5.4). The red and blue cables soldered on the special wires of the strain gauges. The connections checked using a multimeter with a voltage difference. The voltage difference measured between the soldered connections before and after soldering. Therefore, the measured difference before soldering must be equal to the voltage difference between the ends of the two same-coloured cables after soldering (see Figure 5.4).

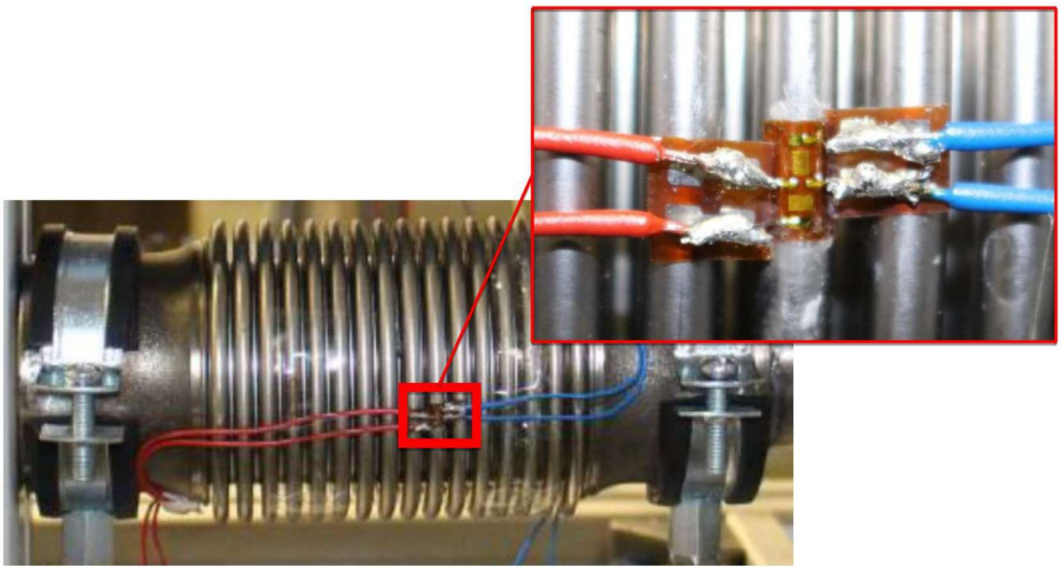

Figure 5.4: Strain gages attached on the surface of the top crest (crown) section of a corrugation of investigated two-ply bellows

Consequently, during the experiments the upper measuring grid measured the elongation in the vertical direction (see Figure 5.5), which had sent the signal to the Gantner Instruments® via the blue cables. The below measuring grid analysed the stretching in the horizontal direction, which had sent the signal to the Gantner Instruments® via red cables.

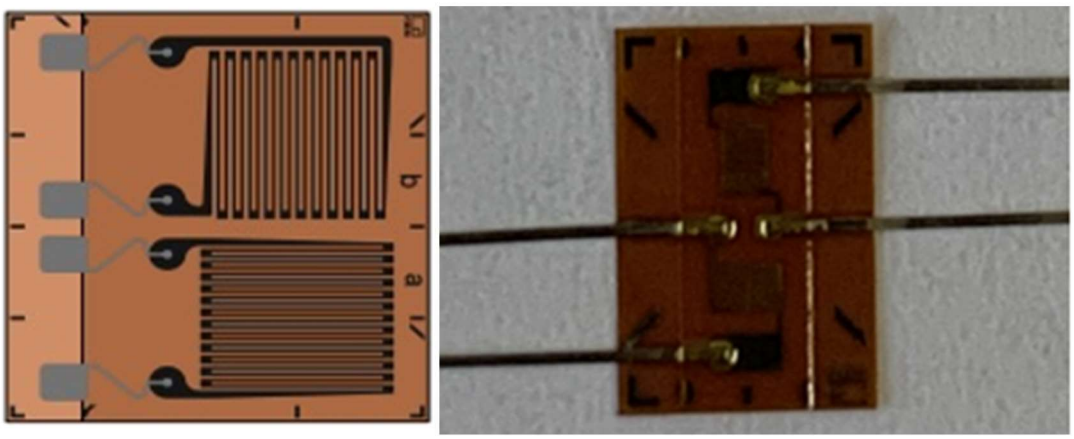

Figure 5.5: Strain gauges M series of HBM Ltd. in installed position [90]

For the test evaluation, the experimentally accessible measuring point for the strain gauges on the surface of the crest (crown) of the investigated two-ply bellows corrugation is not equal to the critical section, which located in the cavity of bellows corrugation. The stresses at the measuring point is correspondingly smaller, than the maximum equivalent stresses at the critical point in the cavity.

Furthermore, it considered that a bending stress had become in triaxle stress state. However, used M model of strain gauges could be strained in X and Y-directions, but not in the Z-direction. Therefore, it had led to a small mistake, which considered in FE and analytical analyses. Since, the strain in Z-direction comparatively is very small, it was neglected. For the strains in X- and Y-directions Hooke's law was applied. This has the form [94] for a biaxial state (accordingly strain in “Z”=0):

$$\varepsilon_x = \frac{1}{E} \cdot \left(\sigma_x - \mu \cdot \sigma_y\right) \tag{5.1}$$

$$\varepsilon_y = \frac{1}{E} \cdot \left(\sigma_y - \mu \cdot \sigma_x\right) \tag{5.2}$$

By reshaping and inserting equations (5.1) and (5.2), results of the stresses in X- and Y-directions are determined as:

$$\sigma_x = \frac{E}{1-\mu^2} \cdot \left(\varepsilon_x - \mu \cdot \varepsilon_y\right) \tag{5.3}$$

$$\sigma_y = \frac{E}{1-\mu^2} \cdot \left(\varepsilon_y - \mu \cdot \varepsilon_x\right) \tag{5.4}$$

Hence, according to theory of equivalent tensile stress (ETS), the comparison stresses ETS in the biaxial stress state considered as:

$$\sigma_{ETS} = \frac{1}{\sqrt{2}} \cdot \sqrt{(\sigma_1 - \sigma_2)^2 + (\sigma_2 - \sigma_3)^2 + (\sigma_3 - \sigma_1)^2} \tag{5.5}$$

where, $\sigma_1 = \sigma_x$ and $\sigma_2 = \sigma_y$. The stress $\sigma_3 = 0$, according to stress in Z-direction equal to 0.

5.2.1 Experiments of internal pressure of investigated two-ply bellows

The laboratory setup was prepared systematically as follows, for experimental analysis of equivalent stresses in the structure of investigated two-ply bellows due to influence of internal pressure:

1. The strain gauges (4) were prepared as described in the subchapter 5.2 (see Figure 5.4 and 5.5).

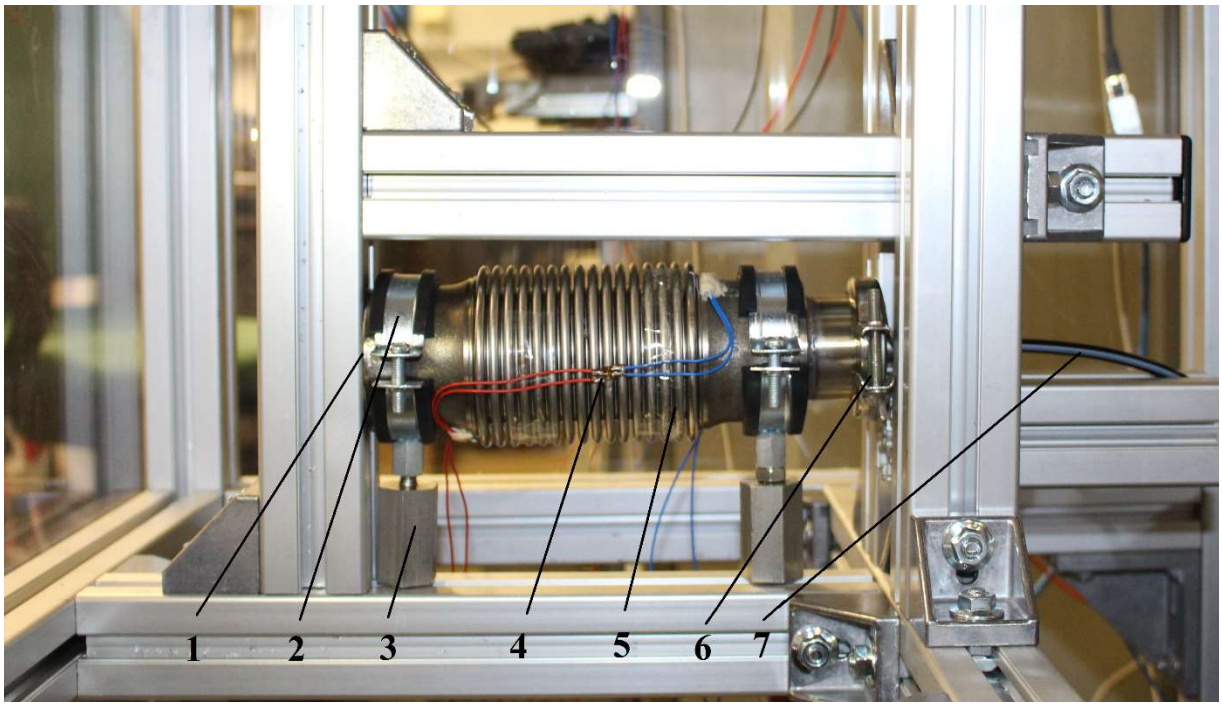

Figure 5.6: Internal pressure experiments of the investigated two-ply bellows, laboratory installation

2. For the sealing of the investigated two-ply bellows was used a blind flange (1) from the left side (see Figure 5.6). From the right side of the investigated two-ply bellows was used a flange (6) with the thread connection. The inlet of this flange connected to a hosepipe (7), which

accordingly connected to a nitrogen (N_2) container, with nominal pressure of 30 MPa. The nitrogen container through a control valve, which installed on the hosepipe, provided required pressure to the investigated two-ply bellows (5). The operating pressure in the investigated two-ply bellows was regulated using an analogue manometer.

3. For the internal pressure experiments, the investigated two-ply bellows was firmly fixed on the boards of two-ply bellows from both sides via clamps (2), which were adjusted on the bolt support (3). This firmly fixed support helped to avoid additional bending stresses in lateral Y- and axial X-directions. In addition, the bolt supports (3) were connected to the Bosch profile of the laboratory installation with the screws, which made construction solid.

After, firmly fixation and adjusting of the investigated two-ply bellows, next step was to connect SG to the Gantner Instrument® strain gauges station via blue and red wires. The Gantner Instrument® strain gauges station has two channels for two resistant signals from the strain gauges grid. Therefore, the measurements of σ_x and σ_y were completed in the same time during the internal pressure experiment.

To analyse the signals, the Gantner Instruments® strain gauge station connected to a Gantner Instruments® main station, which was synchronised with a PC. Consequently, the algorithm depended on the equations 5.1-5.4 was coded in the Gantner Instruments® software package on PC, which is transferring the signal of changing resistant of the strain gauges from *Ohm* into stresses in *MPa*. These results of the tensile stresses have been overwritten in the Excel Table two times per second during the experiments.

The transferred signals of the stresses (see graph on Figure 5.7) were analytically analysed by the equation 5.5 and presented on the graph of Figure 5.7. As assumed, in the equation 5.5, σ_3 is equal to 0, while the strain in the Z-direction was not measured.

As described above, each internal pressure experiment of investigated bellows was approximately 1 hour long (Figure 5.7). At first step, the internal pressure in the investigated bellows was slowly adjusted to 1,6 MPa using the valve and manometer, which were mounted on the hosepipe (see Figure 5.5). The adjustment of the internal pressure in the investigated bellows was approximately 5 minutes. After stabilisation of the internal pressure, the experiment started. The internal pressure was measured for 50 - 55 minutes. In case of a sudden increase of the pressure to 1,6 MPa, the investigated bellows could lose stability due to improper installation; therefore, to avoid this the pressure was slowly increased step by steps, as it shown on graph (see Figure 5.7). Accordingly, on this graph, the stresses Sigma 1 (σ_1) are equal to

stresses measured in the X-direction and stresses Sigma 2 (σ_2) are equal to the stresses in the Y-direction.

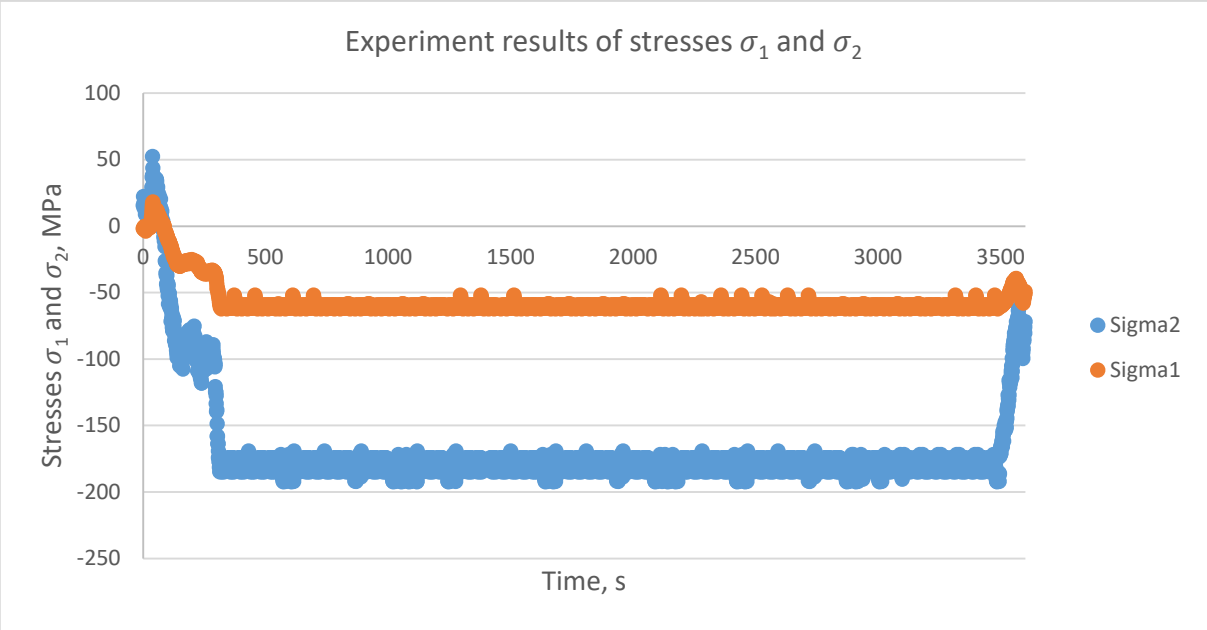

Figure 5.7: Experiment results of stresses obtained from strain gauges in load case of internal pressure (1,6 MPa), 1-hour measurement

The equivalent stresses from σ_1 and σ_2 were computed by equation (5.5) to σ_{eq} (see Figure 5.8). The analysed equivalent stresses σ_{eq} present total stresses (meridian + bending stresses), which appeared on the surface of investigated crest (crown) section of the two-ply circular bellows with U-shaped convolution cross section. The equivalent stress σ_{eq} must not be more than the yield point of the material. It is important to notice that, if stresses will be over the yield point, then the experiment must be stopped [91]. Otherwise, the results will be wrong due to high strains.

The analysed results of the internal pressure experiments presented on Figure 5.9. On the graph presented the results of the maximum equivalent stresses, which appeared on the crest (crown) of the outer surface of the bellows corrugation. The corrugation for experimental measurement was considered in the middle (8th corrugation) of the investigated bellows design [19], while on the middle (8th corrugation) appeared maximal equivalent stresses due to geometrical properties of the investigated bellows.

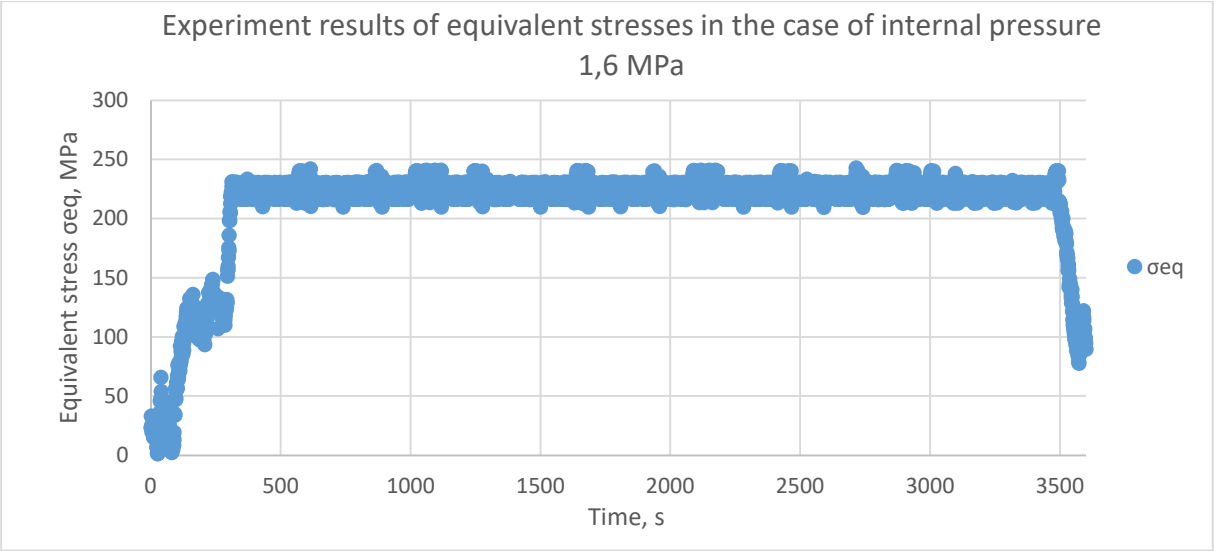

Figure 5.8: Experiment results of equivalent stresses σ_{eq} in the case of internal pressure of 1,6 MPa, 1-hour measurement

In total, 30 suitable measurements of 1,6 MPa accordingly to EN ISO 1333 [63] and specification for pipeline and piping valves API 6D [51], completed for analysing the internal pressure experiment data of equivalent stresses σ_{eq}. The internal pressure in the internal section of the investigated bellows was adjusted to 1,6 MPa, and measured continuously for 50 - 55 minutes. The internal pressure experimental data of the measurements presented on the Figure 5.11. The results have 7 % difference in the case of 30 measurements.

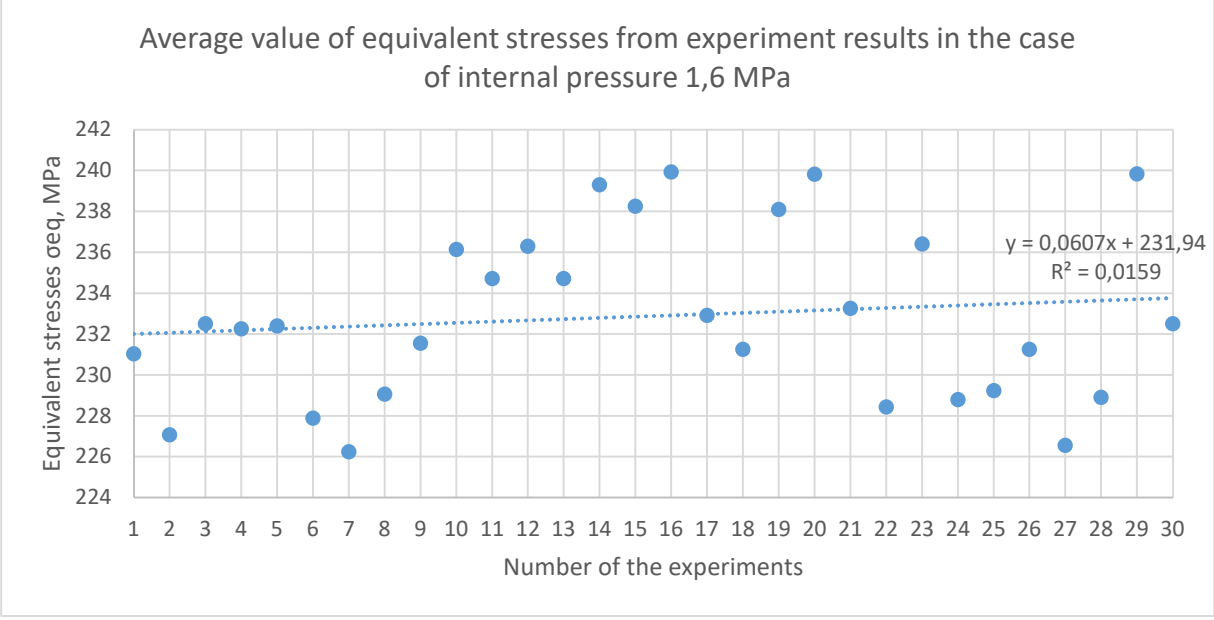

Figure 5.9: Average value of equivalent stresses from experiment results in the case of internal pressure 1,6 MPa

The trend line of the graph (see Figure 5.9) of the experimental data present the correlation between the numerous of equivalent stresses [69]. The correlation described on the Gausses theory [70] of normal distribution. As it is noticeable that the results of the internal pressure experiments are not the same, nevertheless, they are located in the same area of the equivalent stresses in MPa. The "Trend line" on the Excel diagram (Figure 5.11) describes the correlation between results. From the equation $y = 0{,}0607 \cdot x + 231{,}94$ it is concluded that the average equivalent stress is 232,85 MPa at internal pressure of 1,6 MPa.

A normal distribution or probability distribution for the experiments of the internal pressure and bending of the two-ply bellows is determinate by the function of probability density, which is coincides with the Gaussian function [71]:

$$f(x) = \frac{1}{\sigma\sqrt{2\pi}} \cdot e^{-\frac{1}{2}(\frac{x-\mu}{\sigma})^2} \tag{5.6}$$

where μ is the mean value, the median and distribution parameter; σ is standard deviation, variance of the distribution.

Normal distribution of function $f(x)$ is symmetry to the X-axis, however its deviation is equal to σ. It is mportant to notice, more accurate the measurements that denser the results of individual measurement located near the average value. The standard normal distribution, when the $\mu = 0$, and $\sigma = 1$ [72].

In the case of carried experimental data the $\sigma = 0{,}98$, which can be concluded as acceptable experimental results.

5.2.2 Experiments of bending of the two-ply circular bellows with U-shaped convolution cross section

The experiments of complex bending of the investigated two-ply bellows were carried out with the analogue to the internal pressure experiment with strain gauges.

To begin the bending experiments of the investigated bellows, the experiment chamber has redesigned (as present on Figure 5.10). Hence, one side of the board of investigated two-ply bellows was firmly fixed (1) to the plate (3) via claims and bolt connection. The plate (3) has holes for fixing a rod (2) to a certain angel from -10 ° to 0 ° and to 10 ° (a step of 2 °). During the complex bending experiments the rod (2) was moved to considered angle (namely to required hole on the plate) to simulate the deflection of the investigated bellows. For analysis

of obtained data, the strain gauges used in the same location on the outer crest (crown) surface of the investigated bellows, as it was explained in the case of the internal pressure experiments (subchapter 5.2.1).

The experiment of complex bending started from zero degrees or unloaded position of the investigated two-ply bellows (hole with 0 °). First, investigated bellows was deflected to two degrees (2 °) in the chosen direction, namely to the direction of closing position of the ball in the cross section of the investigated ball valve.

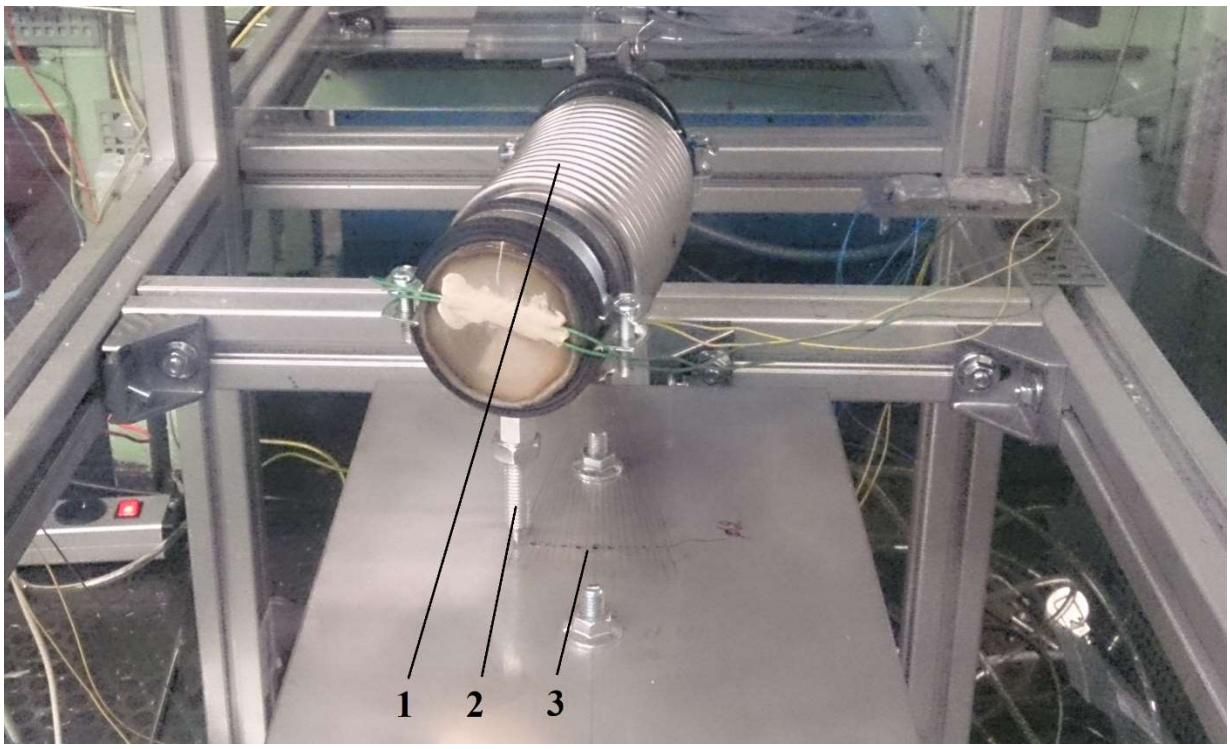

Figure 5.10: Complex bending experimental installation:

1. investigated two-ply bellows;
2. fixing rod;
3. steel plate.

Consequently, to insure stabilized measurements of the strain gauges, applied a waiting time of twenty seconds to measure the correct value of the bending stress. Furthermore, the analogue procedure applied for 4 °, 6 °, 8 ° and 10 ° in the direction of bending of the investigated bellows. At the angle of 10 °, the investigated bellows achieved the last point of complex bending experiments, according to maximal deflection angle from real model of RGM (see Figure 5.11). Subsequently, after reaching the bending angle of 10 ° the investigated bellows was bent in the opposite direction angle by angle with a step of 2 °, until it had achieved the unloaded position of 0 ° position on the plate (3).

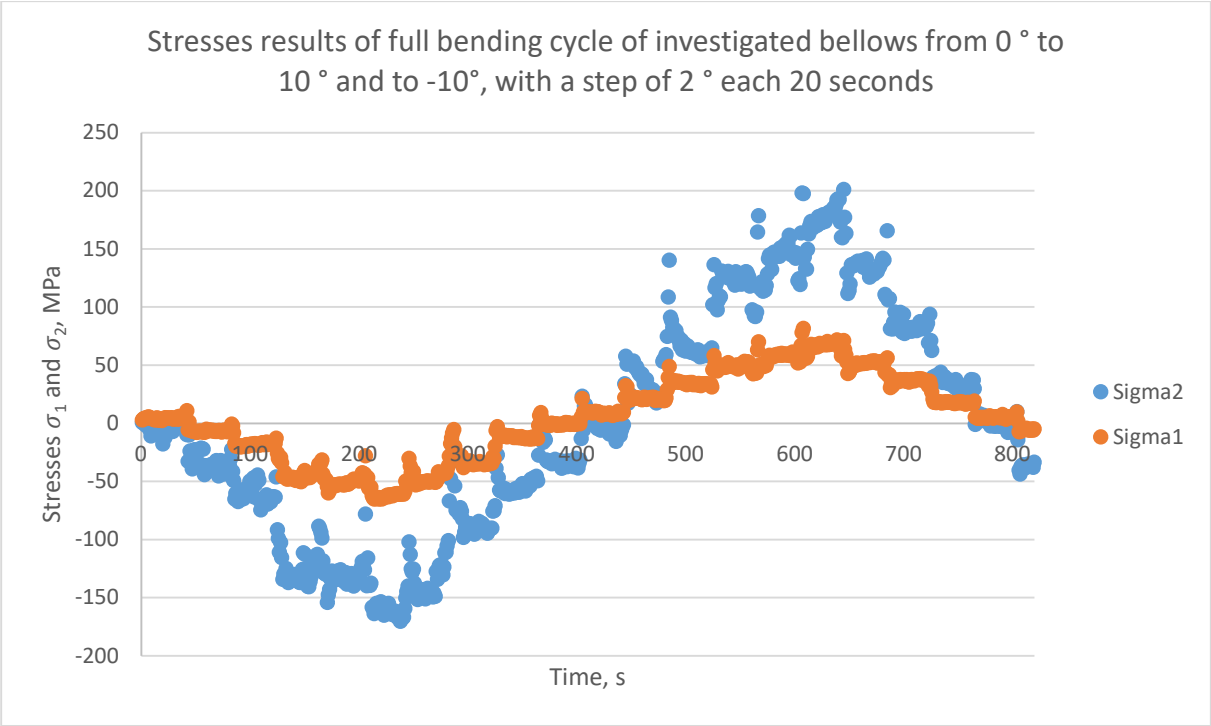

Figure 5.11: Stresses results of full bending cycle of investigated bellows from 0 ° to 10 ° and to -10 °, with a step of 2 ° each 20 seconds

Once, the investigated bellows was in the unloaded position of 0 ° (see Figure 5.11) the experiment continued in the opposite direction, direction of opening the ball in the cross section of the ball valve.

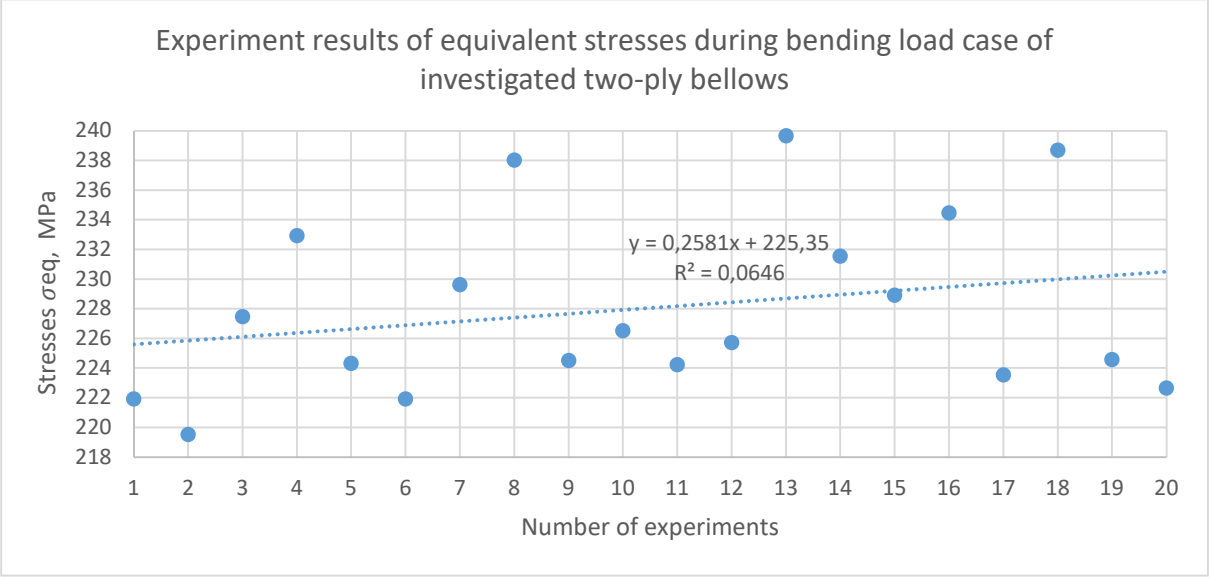

Figure 5.12: Experiment results of equivalent stresses during bending load case of investigated two-ply bellows

The experiments of the bending in another direction achieved using the previous methodology,

i.e. to complete one full cycle of the bending test, the investigated bellows was bent to -10 ° with step of 2 ° each 20 seconds, then back to unloaded position of 0 °. The obtained experiments results averaged arithmetically and associated to the equivalent stresses (see chapter 5.2.1).

The “Trend line” on the diagram (Figure 5.14) describes the correlation between results of the bending to 10 °. The equation $y = 0{,}2581 \cdot x + 225{,}35$ concluded that the average equivalent stress on the outer ply of the 8th two-ply bellows corrugation in the case of bending to the angle of 10 ° equals to 227,29 MPa.

In the case of bending experiments, the deviation of the results is equal to $\sigma = 0{,}99$. Hence, depending on the Gaussian theory [70] of normal distribution it is excellent coincident of the experiment results.

5.3 Functional examination of the ratchet gear mechanism

This part of the experiment analysis performed the workability and reliability of the RGM with the investigated two-ply circular bellows with U-shaped convolution cross section. For that purpose, the second part of the experimental setup was built (see Figure 5.13), which consists: two-ply bellows (1); the ratchet gear mechanism with housing (2); the investigated ball valve with a nominal diameter of 100 mm (3); a lever (4); an electric engine (5); a threaded rod (6); the Gantner Instruments strain gauge module with the Gantner Instruments main station (7).

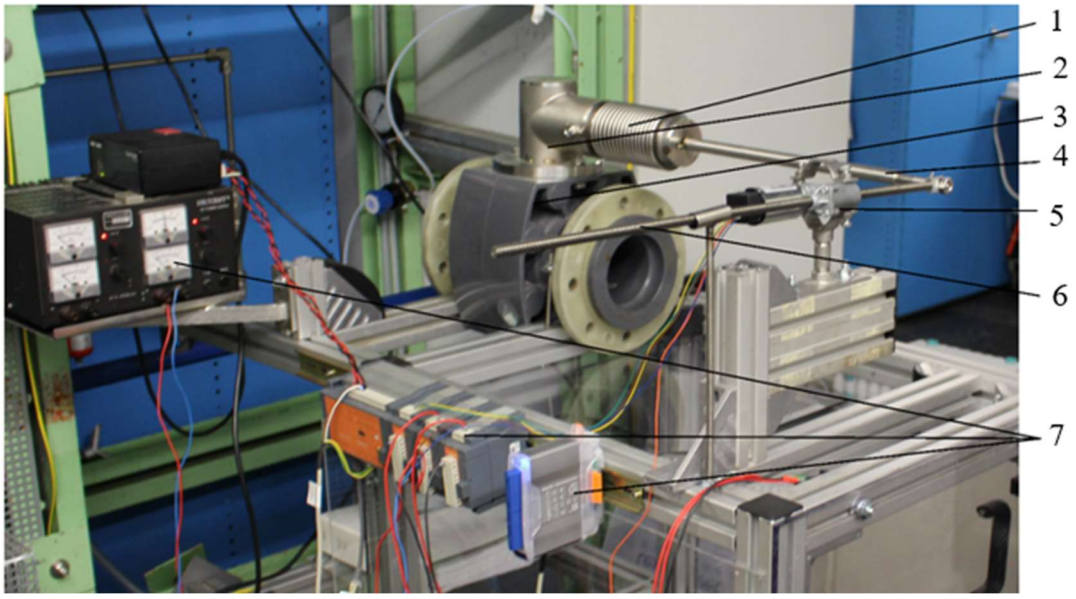

Figure 5.13: The laboratory installation with the investigated ball valve with RGM and two-ply bellows:

1. two-ply bellows;
2. the ratchet gear mechanism with housing;
3. the investigated ball valve with a nominal diameter of 100 mm;
4. lever;
5. electric engine;
6. threaded rod;
7. the Gantner Instruments strain gauge module with the Gantner Instruments main station

For this experiment, the stainless steel two-ply bellows manufactured by the Witzenmann Ltd company, model Hydra BE 356230-bb 68 [93] was used.

The main definition of this part of the experiments was to prove the workability of the brand-new ratchet gear mechanism (RGM) for the ball valve without operational loads, such internal pressure and temperature influence.

The test performed in two parts. In the first part of the experiment (see Figure 5.14 a. and b.), the lever, with a two-ply bellows, moved in the direction of opening the cross section of the ball valve (to the left). The steps of experiments were as follows: (see Figure 5.13) the engine (5) rotated the threaded rod (6), which moved the lever (4) and the two-ply bellows to the angle of 10 °. That led one of the pawls (see Figure 5.15 (2)), which are connected on the other side of the lever (4) in the ratchet gear mechanism housing (3), to be coupled with the ratchet gearwheel, which are coupled to a stem of the ball valve (see Figure 5.15 (1)). Consequently, with the axial movement, the pawls rotated the ratchet gear wheel, which concordantly rotated the stem of the ball valve (2). The stem accordingly rotated the gate ball of the ball valve (2) to the closed position of the cross section. After this, the threaded rod (6) was released, and the engine (5) returned the lever (4) and the two-ply bellows (1) to the unloaded position (0 ° position) by running in the reverse direction. This one full circle, in the case of this laboratory ball valve installation, rotated the gate ball to 15 °, which required six complete cycles to achieve the closed/opened position of the cross section of the ball valve [4].

In the second part, to return the gate ball of the ball valve to an opened position, the lever with the two-ply bellows was bent in the opposite direction (to the right), to an angle of 10 ° (Figure 5.14 c.). The process of opening the gate ball of the ball valve achieved as analogue to the closing case.

For automatization of these steps, a program was created with the help of Gantner Instruments® software package measure station. The programmed algorithm fully automated the process of closing and opening gate ball of the ball valve by repeating the cycles that were described above

(see Figure 5.14 a., b., c.).

During these tests, it achieved 10.000 full cycles in both directions, which considered as an excellent result since the task of this experiment was to maintain functionality of the new ratchet gear mechanism with two-ply bellows for a ball valve.

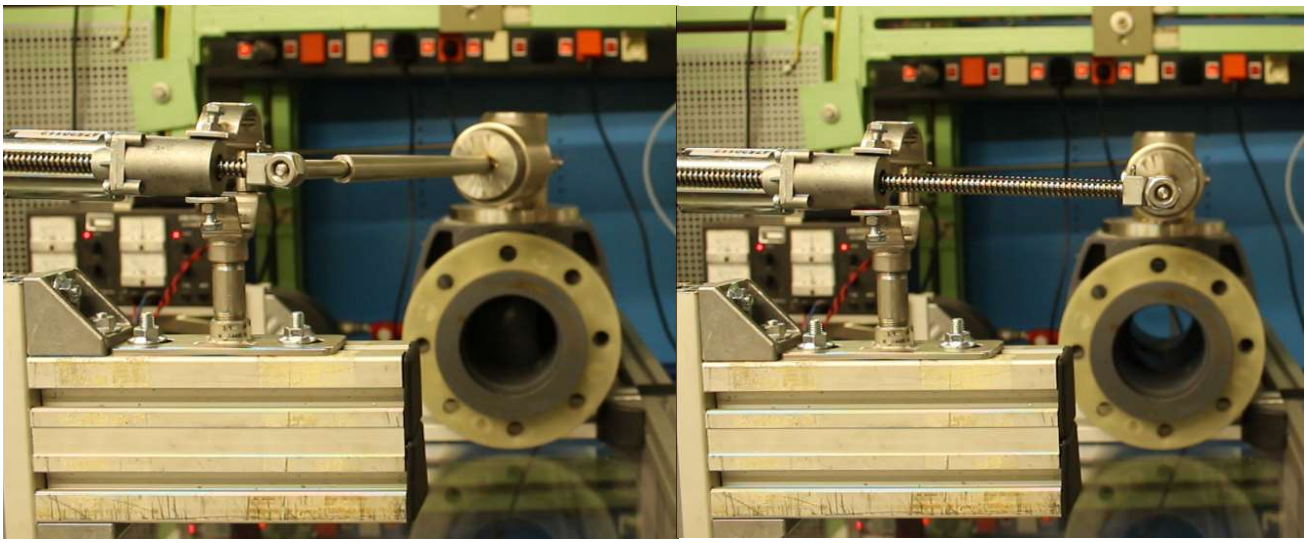

a. b.

c.

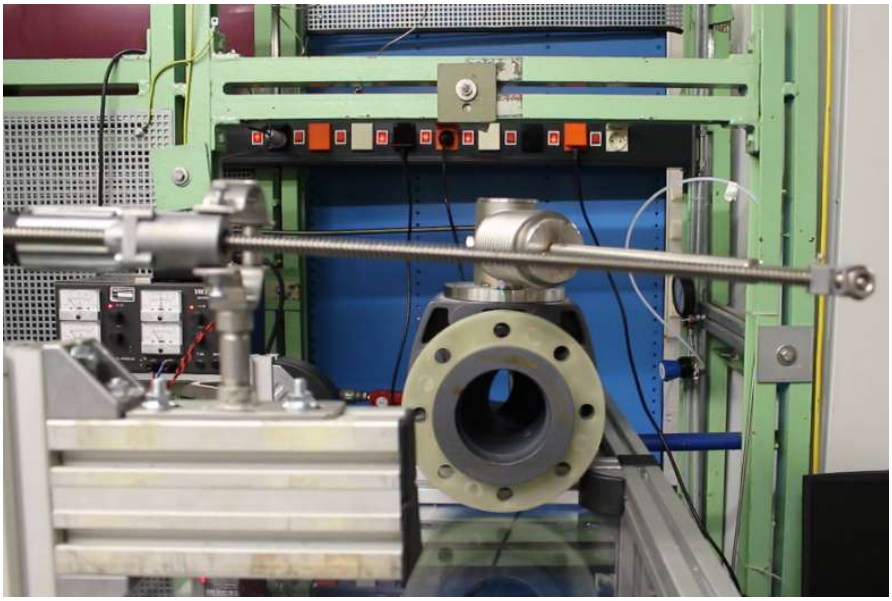

Figure 5.14: Functionality of new design of the ball valve with RGM [4], experiment:

a. process of closing the cross section of the ball valve;

b. middle point 0 ° (unload position of the two-ply bellows);

c. process of opening the cross section of the ball valve

The new ratchet gear mechanism with bellows (see Figure 5.15) used as a mechanical device that allowed continuous rotary motion of the stem (2) in direction of closing/opening gate ball in the cross section of the ball valve. For this purpose, two ratchet gear wheels (1) and two

pawls (3) implemented in the RGM design.

Consequently, if one of the ratchet pawls (3) coupled with accordantly gear wheel (1), the second pawl (3) is uncoupled with another ratchet gear wheel (1). In this case, the ratchet gear wheel (1) rotated the stem (2) to considered direction. The stem (2) rotated the gate ball of the ball valve respectively in the direction. If the upper gear wheel (1) coupled with the upper pawl (3), as presented on Figure 5.17, the ball rotated in the direction of closing of the cross section of the ball valve, i. e. the rotation to opposite direction provided by coupling the down pawl (3) with down ratchet wheel (2).

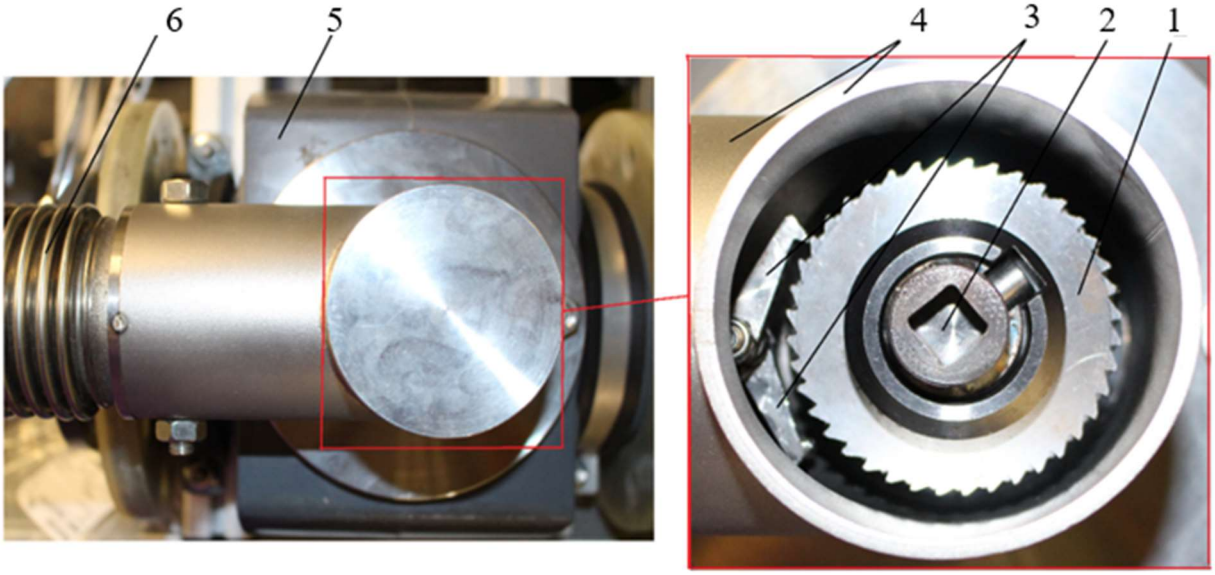

Figure 5.15: Ratchet gear mechanism with two-ply bellows:
1. ratchet gearwheel; 2. stem; 3. pawls; 4. ratchet gearbox shell; 5. ball valve; 6. investigated two-ply bellows.

5.4 Conclusion of the experimental analysis

In the first part of experimental analysis, there were considered the equivalent stresses that occurred on the surface of critical areas of investigated two-ply circular bellows with U-shaped convolution cross section. Namely, crest area of investigated two-ply bellows corrugation. Nevertheless, it was impossible to measure the equivalent stresses on the cavity (outer surface) of the bellows corrugation due to size of considered strain gauges and design dimensions.

Hence, according to experimental process, it was obtained results of equivalent stresses from strain gauges on second investigated critical area, namely the area on outer crest surface of 8th two-ply bellows corrugation (see Figure 5.6). The strain gauges measured the changes of

electric resistants during investigation of internal pressure and bending accordingly, which were convert in equivalent stresses [91]. Two load cases were analysed separately to insure the accurate equivalent stresses from each loading case. Total equivalent stresses were computed analytically by equation 5.5 [8].

The derived experimental results present that investigated design of two-ply bellows with U-shaped convolution cross section withstand against the named loads. The equivalent stresses do not exceed the yield point of the stainless steels 1.4571 [68], [116], [117], [149], 1.4006 [116], [147] and 1.4462 [116], [149], at room temperature. In addition, the obtained experimental results were compared and validated to FE and analytical analyses.

The second part of investigated laboratory installation (see Figure 5.10) presented that bending of single- and multi-ply bellows, is between a lateral deflection and angular rotation (see Figure 3.17 a. and b.), in ratio of 22 % of lateral deflection and 78 % of angular rotation according to standard EN ISO 13445-3 (pp. 331-332) [21].

Consequently, it was considered that analytical analysis model presented in standard EN ISO 13445-3 [21], by Anderson [12] or Andreeva [78] could not correct determinate and validate, investigated bending case of single- and multi-ply bellows with U-shaped convolution cross section due to specific (unique) installation case on ball valve with RGM [4].

Hence, the laboratory experiments helped to analyse and study the behavior of investigated multi-ply bellows under internal pressure and bending case for ball valve with the ratchet gear mechanism [4]. That considered the future analysis process of validation investigated loading cases.

In the third part of the laboratory experiments (see Figure 5.13-15), it was analysed the functionality of the ratchet gear mechanism [4]. The main definition of this part of the experiments was to prove the workability and reliability of brand-new ratchet gear mechanism (RGM) with investigated two-ply circular bellows with U-shaped convolution cross section for ball valve without operation loads, such internal pressure and temperature influence. In this case was simulated the workability of RGM, i. e. how RGM operate in unloaded condition. The reliability of RGM was also proved, i. e. it was analysed how many cycles of closing/opening of ball valve can achieve presented design. Hence, the RGM with investigated two-ply circular bellows with U-shaped convolution cross achieved 10.000 full cycles of closing/opening of ball valve in both directions, which considered as excellent result for this design.

6. FE analysis of the ratchet gear mechanism

Hence, for purpose of detailed and more precise analysis of investigated internal pressure, temperature influence and bending cases of the ball valve with ratchet gear mechanism and single- and multi-ply bellows with U-shaped convolution cross-section was used Finite Element analysis (FEA). The FEA of 3D model of ball valve with RGM analysed in two parts.

In first part it was considered the FE analysis of the ratchet gear mechanism with considered weakest areas of investigated design, which are ratchet wheels, pawls and two-ply circular bellows with U-shaped convolution cross section.

The main tasks of first part of FE analysis are:

- to consider the workability of new design of the ratchet gear;

- to consider dimensions of the RGM, investigated two-ply bellows and ball valve;

- to determine the weak elements and spots of the design;

- to validate and to compare the data, which derived from analytical, mathematical and experiments analyses to FEA.

The main goal of second part of the FE analysis is to analyse single-, two-, and three-ply bellows expansion joint, i. e. to consider how different number of plies of bellows influence to equivalent stresses in the case of internal pressure and periodic bending [5]. In addition, it was analysed different contact condition between layers of investigated bellows (such as friction and bonded, due to different manufacture processes [8]).

Consequently, during the experiments it was considered that bending case of investigated two-ply bellows consist from lateral deflection and angular rotation according to standard EN ISO 13445-3 (pp. 331-332) [21]. The unusual bending case accrued in the experimental installation due to the welded connection of investigated two-ply bellows to RGM housing and rotation of the lever around Z-axis to 10 ° from unloaded position. The lever is also firmly fixed on the rod end bearing at Z-axis of its rotation (see Figure 3.1). This fixed support of investigated two-ply bellows made this case unique, which difficult to be analysed analytically. Therefore, it was necessary to consider the detailed FE analysis of investigated two-ply bellows.

Hence, in this chapter will be discussed the FE analysis of the ratchet gear mechanism with single-, two- and three-ply bellows, which considered as a main seal element for investigated

design of ball valve with RGM [4]. For this analysis used a FE software package Ansys® Workbench. The CAD model of the RGM, single-, two- and three-ply bellows designed in Ansys® CAD Geometry Designer and Autodesk Inventor® software packages.

6.1 FE analysis of the ratchet gear mechanism

As it noticed in chapter 5, the ratchet gear mechanism with bellows is loaded of internal pressure, periodic bending and temperature. These loads could appear in the system at same time or they could appear separately. Hence, it required analysis of investigated bellows designs under separate load cases as well as under all mentioned loads at the same time. When maximum internal pressure (2 MPa), periodic bending (10 °) and maximum temperature (+500 ° C) perform at the same time, then this load case will be called a worst-case scenario for investigated design.

6.1.1 CAD model of the ratchet gear mechanism

For FE analysis of the RGM considered the CAD model in the Geometry Designer of Ansys® software package, which consisted following parts: 1. bellows; 2. ratchet wheel; 3. pawl; 4. a bolt connection; 5. ratchet gear housing; 6. lever, 7. rod end bearing; 8. housing cover; 9. bellows cover (as presented on Figure 6.1).

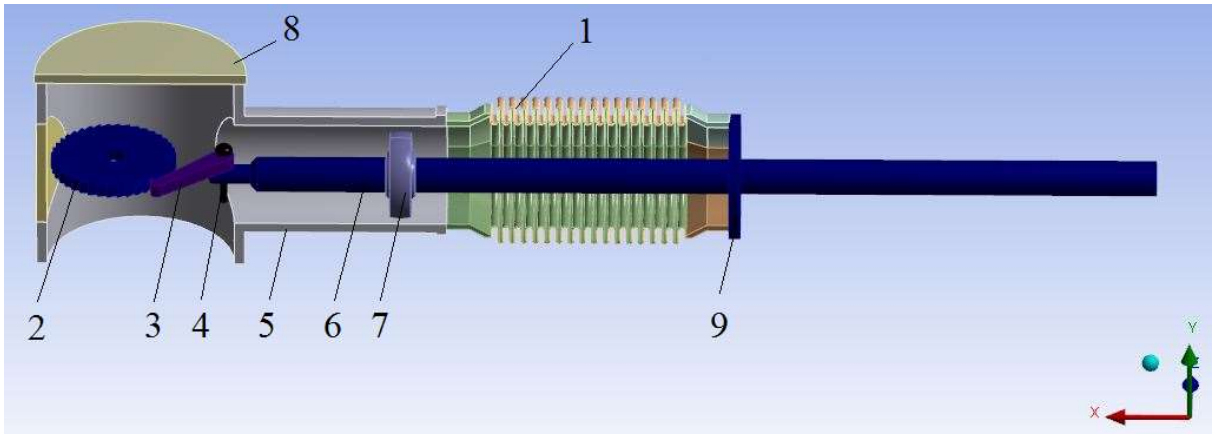

Figure 6.1: CAD model of the RGM in global coordinate system, with following components [75]: 1. two-ply bellows; 2. ratchet wheel; 3. pawl; 4. a bolt connection; 5. ratchet gear housing; 6. lever; 7. rod end bearing; 8. housing cover; 9. bellows cover.

Presented CAD model in this example considered for the investigated ball valve with RGM of nominal diameter 100 mm [75]. Dimensions of the design parts of RGM presented in chapter 3 and CAD drawings in Appendix D.1.

The bellows 1, RGM housing 5, RGM cover 8, bellows cover 9 and rod end bearing 7 considered from stainless steel 1.4006 [149], 1.4462 [149] and 1.4571 [68]. For ratchet gear wheels 2, pawls 3 and lever 6 made of stainless steel 1.4462 [149].

6.1.2 Mesh of the RGM with bellows

To begin FE analysis, it is necessary to consider the mesh of RGM with bellows, using the mesh tools of Ansys® Workbench. The mesh must be fine enough to avoid numerical errors and stresses concentration that appeared during FE analysis. The example of mesh presented on Figure 6.2, the number of elements is 80.977; the number of notes is 354.801 [75]. Used element types of mesh are Solid 186 and Contact element 174. The Solid 186 is a higher order 3D 20 nodes element, which exhibits quadratic displacement behaviour. The Contact 174 is used to represent contact between 3D solid 186 elements and its deformable surface [73]. The contacts between all components determine as bonded with the augmented Lagrange method. It is used by default for three-dimensional self-contact with node-to-surface discretization for pressure-overclosure relationship, due to weld connection between pressure influenced parts [6].

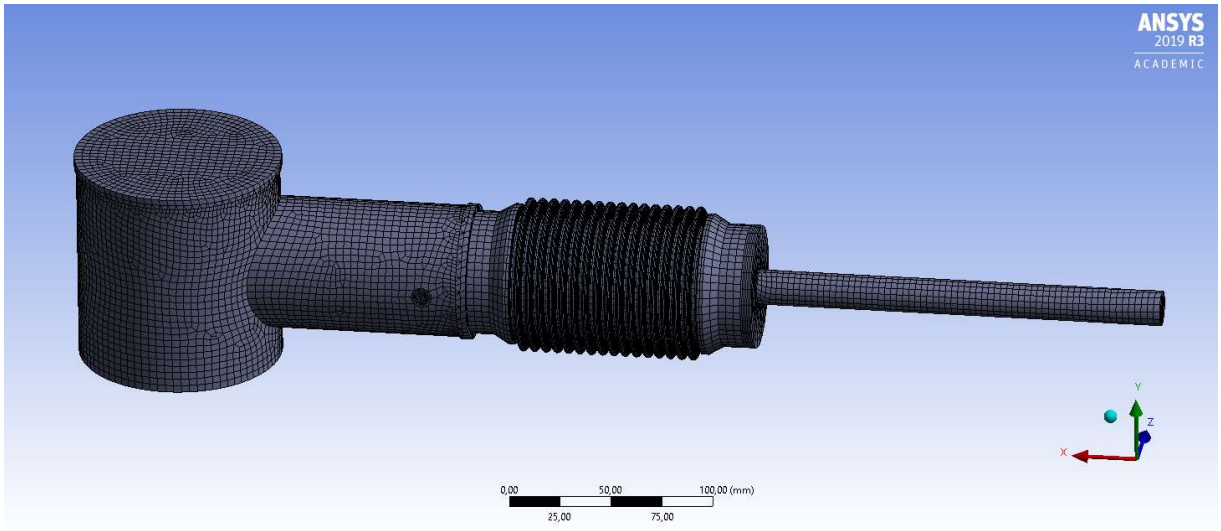

Figure 6.2: The mesh of the ratchet gear system with bellows FE analysis

Hence, the boundary conditions for FE analysis are determined as for experiments and analytical analyses. The internal pressure was considered as 0,3 MPa, 0,6 MPa, 1 MPa, 1,6 MPa, 2 MPa according to standards EN ISO 13445-3 [21], EN ISO 1333 [63] and specification

for pipeline and piping valves API 6D [51], the bending angle of lever, consequently, bending of bellows was determined as 2 °, 4 °, 6 °, 8 °, 10 °. In addition, the RGM housing has a virtual fixed support (a welding connection) to a body of the ball valve; the lever was bent with the remote displacement to 10 ° from the unloaded position.

6.1.3 Boundary condition

The RGM with bellows operate under internal pressure, bending and temperature expansion. It was important to analyse each investigated load separately, and maximal load case, worst-case scenario, as it mentioned in chapter 3. For this purpose, loads are set on the investigated model as presented on Figures 6.3 - 6.4.

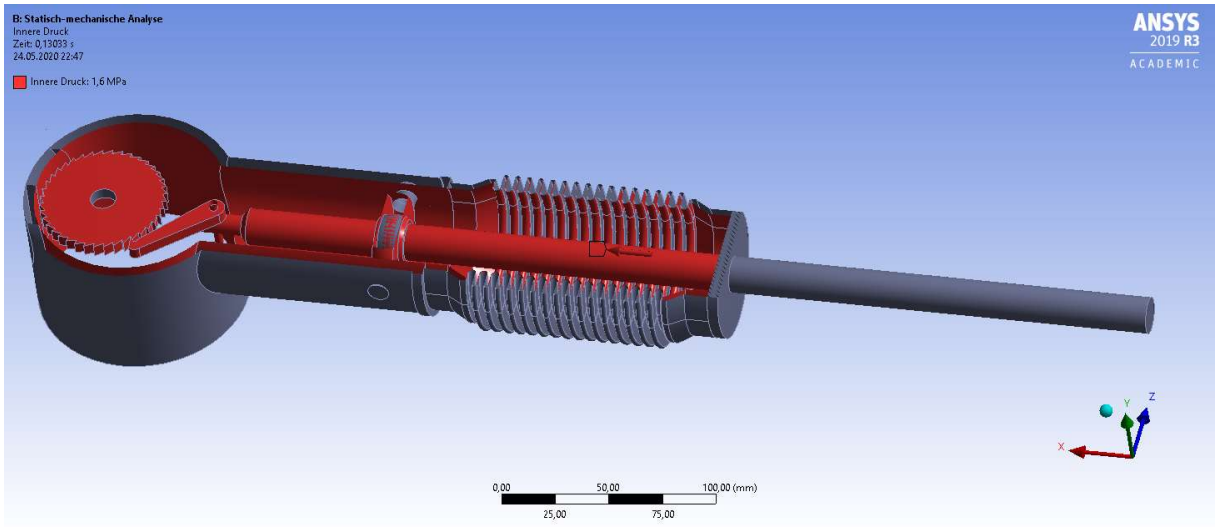

Figure 6.3: Static pressure was analysed according to the ISO EN 1333 [63] and to specification for pipeline and piping valves API 6D [51] and set as 0,3 MPa, 0,6 MPa, 1 MPa, 1,6 MPa, 2 MPa.

With the craft module application of Ansys® Workbench was simulated the bending of the lever with the single- and multi-ply bellows to analysed angles of 2 °, 4 °, 6 °, 8 ° and 10 °.

The temperature influence simulated with the temperature module of the Ansys® Workbench software package. The temperature influence of operating media for FE analysis considered at 20 °C, 100 °C, 200 °C, 300 °C, 400 °C and 500 °C. In the FE analysis considered the temperature heat transfer of the operating media (heat oil, as example for high temperature FE analysis) on internal surface of RGM with bellows as thermal convection [171] with heat transfer coefficient 400 W/(m^2·K) [172].

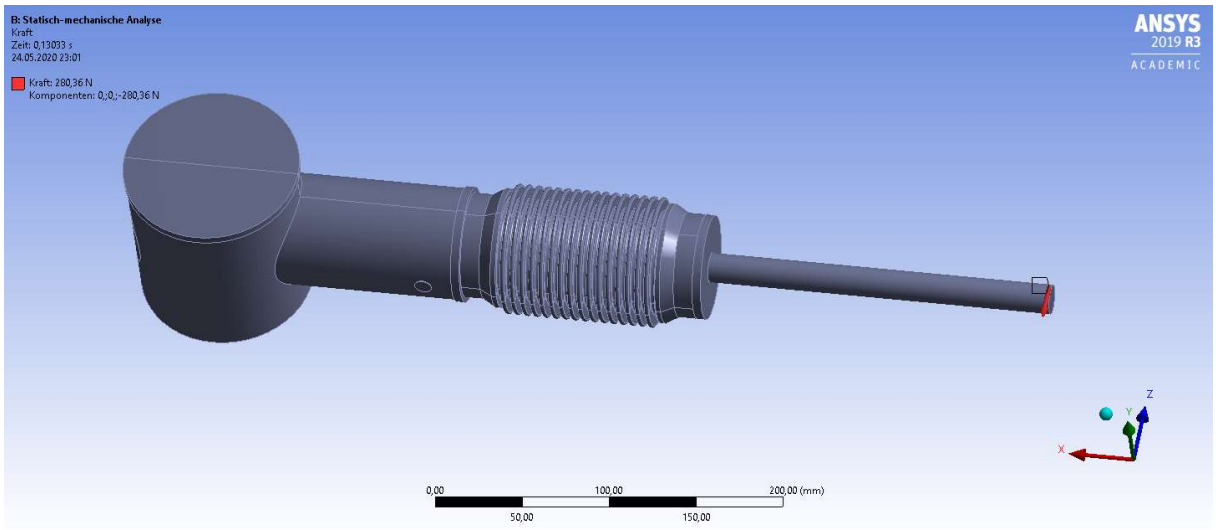

Figure 6.4: FE analysis of bending case of lever, consequently, single- and multi-ply bellows

The outer surface of RGM with bellows considered as thermal convection of the air with heat transfer coefficient – 10 W/m^2·K [172]. The thermal conductivity of the RGM with bellows considered for stainless steel with thermal conductivity coefficient 15 W/m·K [172].

6.1.4 FE analysis of the ratchet gear mechanism with single- and multi-ply bellows

In presented FE analysis of RGM, the aim is validation of investigated bellows under applied loads such as bending, internal pressure and temperature expansion. Moreover, it is necessary to consider an exact behaviour model of RGM components for FE analysis. The results of FEA compared to the laboratory experiments and analytical analyses. In addition, it is important to validate FE analysis results of critical areas of bellows corrugations to determined new mathematical analysation methodology (see chapter 4).

The visualisation of some FE analysis results of investigated ratchet gear mechanism with bellows presented on the Figures 6.5 - 6.7.

Hence, one of goal of FEA was to analyse bellows for the case of maximal allowable bending to angle of 10 ° from unloaded position. That also consider displacement model of lever, rod end bearing, pawls and ratchet wheel. Therefore, one end of lever connected to an electrical actuator or it moved axial per hand. As it was described in chapter 3.2.4 the lever fixed on the rod end bearing, which considered as an axis of rotation. The mechanical model of lever arm and forces, which are appearing on both sides of the lever, described in chapter 3.2.4. The maximal displacement, for example, in this case is 57,8 mm on one end of the lever, where applied axial forces from an electrical actuator or per hand (see Figure 6.5). The displacement

on the applied force end of the lever measured during the experiments for nominal diameter of 100 mm, which equal 58 mm. Likewise, analytically the mechanical model of RGM for bending was analysed for nominal diameter of 100 mm, 150 mm, 200 mm and 300 mm (see chapter 3).

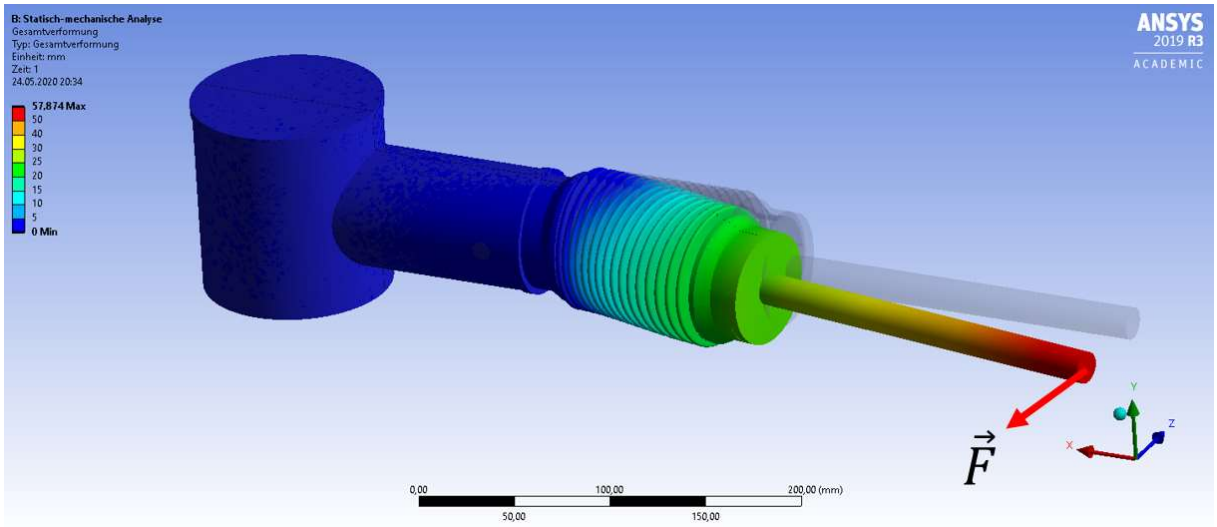

a.

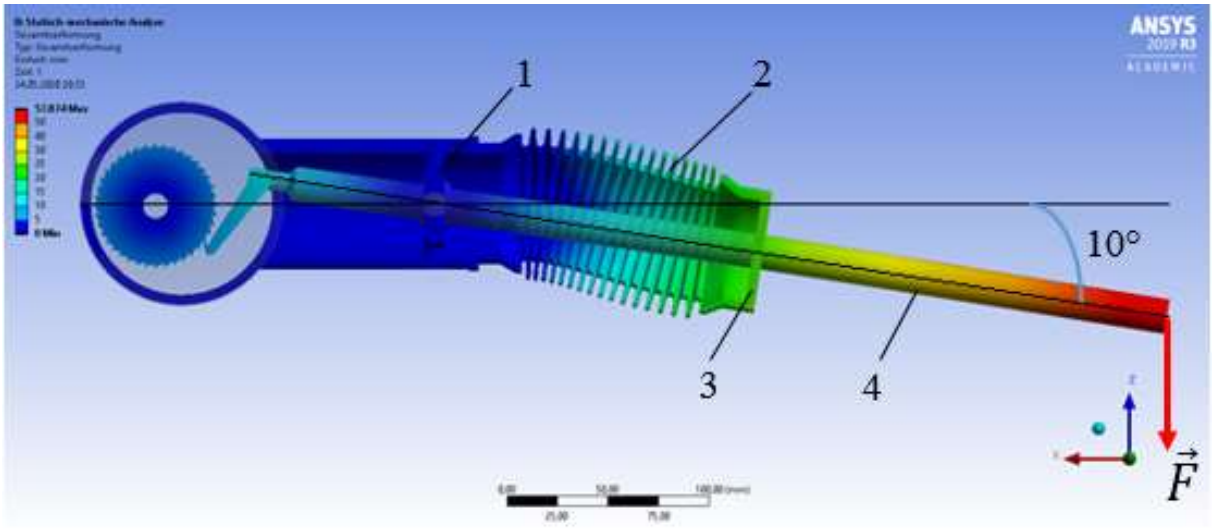

b.

Figure 6.5: RGM FE analysis of bending of the lever (4) to 10 °, from influence of force $\vec{F}$: a. isometric diagram of RGM FE simulation of bending lever (4) to 10 °, from influence of force $\vec{F}$; b. the lever (4) bended to 10 °, which bended the bellows (2) to 10 ° as well, as it possible to see from bending diagram on XZ-Plane cross section. Due to fixation of lever (4) by welding on rod end bearing (1) and on cover (3) of the bellows (2). The bellows (2) has unique for this design case bending, which consider 78 % of angular rotation and 22 % of lateral deflection according to description in ISO EN 13445-3 [21], as it was discussed in chapter 5.

The RGM FE analysis of lever (4) bending that presented on Figure 6.5, determine the deflection of investigated bellows (2), which considered as 78 % of angular rotation and 22 % of lateral deflection according to description in ISO EN 13445-3 [21]. This bending model is unique and related specific for this design case of ball valve with RGM, due to fixation of the lever (4) by welding on rod end bearing (1) and on cover (3) of the bellows (2). Therefore, it does not describe in EN ISO DIN 13445 Part 3 [21] and in EJMA [63] standards. Hence, it would detailed analysed in chapter 6.2. The lever was deflected with an applied axial craft $\overrightarrow{F_x}$ to an angle of 10 °.

Table 6.1: Analysis of equivalent stresses from investigated maximal loads, the worst-case scenario, for ball valve with RGM DN 100 PN 20 (API 6D Class 150)

	FE analysis of RGM
	Maximal equivalent stresses, σ_{eq} MPa
Two-ply bellows	449,10
Ratchet wheel	152,19
Pawl	124,87
RGM Housling (Branche Area)	31,78
Lever	124,10

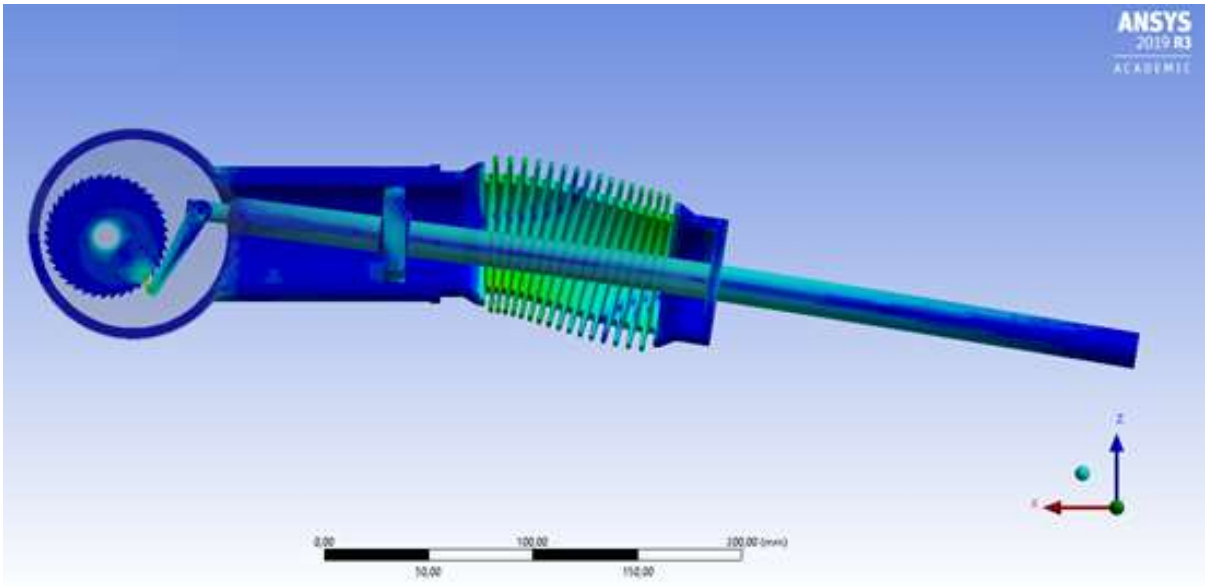

Figure 6.6: FE analysis of equivalent stresses during maximum load case internal pressure is 2 MPa, bending to 10 ° and temperature influence up to 500 °C (worst case scenario for investigated design)

The FE analysis of RGM in worst-case scenario considered the maximal equivalent stresses appeared in the investigated bellows corrugations, and on the coupling of the ratchet wheel and pawl (see Figure 6.6). As an example, the maximal equivalent stresses in worst-case scenario presented in Table 6.1.

The FE analysis of the ratchet gear mechanism, as well as single- and multi-ply bellows were performed for worst-case scenario, the maximum loads case, for each ball valve with RGM with nominal diameter of 100 mm, 150 mm, 200 mm and 300 mm.

The torque on the stem of ball valve with RGM design analysed in chapter 3. In chapter 6 analysed the maximum existing torque, which can achieve the design of ratchet wheels, stem or pawl. The torque of ratchet gear mechanism for ball valve of nominal diameter 100 mm (see Figure 6.7) is equal to 41,27 N·m [75]. The required torque on the stem from chapter 3 M_{Total} [N·m] is equal to 26,64. The safety factor considered as 1,5 according to pressure equipment directive PED [106] and specification for pipeline and piping valves API 6D [51].

The analytical and FE analyses of the maximal allowable stem torque [62] presented in chapter 3.1. The results of analytical torque analysis presented in Table 3.1 and FE analysis in Table 3.2. The components of RGM designed to overcome the maximal required stem torque with safety factor of 1,5, according to pressure equipment directive PED [106] and specification for pipeline and piping valves API 6D [51].

The RGM for ball valve with nominal diameter of 100 mm, 150 mm, 200 mm and 300 mm designed for worst-case scenario, defined maximum applied loads, which appeared in investigated construction. The FE analysis of the ratchet gear mechanism with single- and multi-ply bellows considered areas and critical points of the design, consequently, where the maximum equivalent stresses are appeared. Moreover, the single- and multi-ply bellows due to the unique design and load cases, required detailed analysis, to determine the maximal loads, which it could withstand.

6.2 FE analysis of single- and multi-ply bellows

The single- and multi-ply bellows is the weakest element of the design of RGM, which has a seal, bending and thermal compensation functions. Therefore, it operates under three kind of different loads, such as internal pressure, bending and cryogenic or high temperature. The internal pressure and bending cause strain, which lead to deformation and thus tension. The temperature distribution in the structure of single- and multi-ply bellows involve thermal expansion, which induce additional strain and tension. Moreover, it is determined the influence of the contact condition between plies on investigated stresses for multi-ply bellows. Hence, to analyse complex load case the FE analysis carried out for single-, two- and three-ply stainless steel bellows.

6.2.1 FE analysis of internal pressure

The FE analysis in case of internal pressure of 0,3 MPa, 0,6 MPa, 1 MPa, 1,6 MPa and 2 MPa according to EN ISO 13445-3 [21], EN ISO DIN 1333 [67] and specification for pipeline and piping valves API 6D / EN ISO 14313 [50] is carried out for the single-, two and three-ply bellows (the two-ply bellows was used in laboratory set up, see chapter 5).

The maximum equivalent stresses of the cross section of XY-Plane for single-ply bellows in the circumferential Y-direction of polar coordinate system, occur in the cavity (see Figure 6.7). The maximum equivalent stress of 121,03 MPa is occurred on the cavity outside surface of single-ply bellows corrugation. It is corresponded to the conclusion of analytical analysis according to standard ISO EN 13445-3:2018 [21] and the experiments measurements that in the cavity area (critical point) of the bellows cross section - occurred the critical equivalent stresses, which raised in meridian direction.

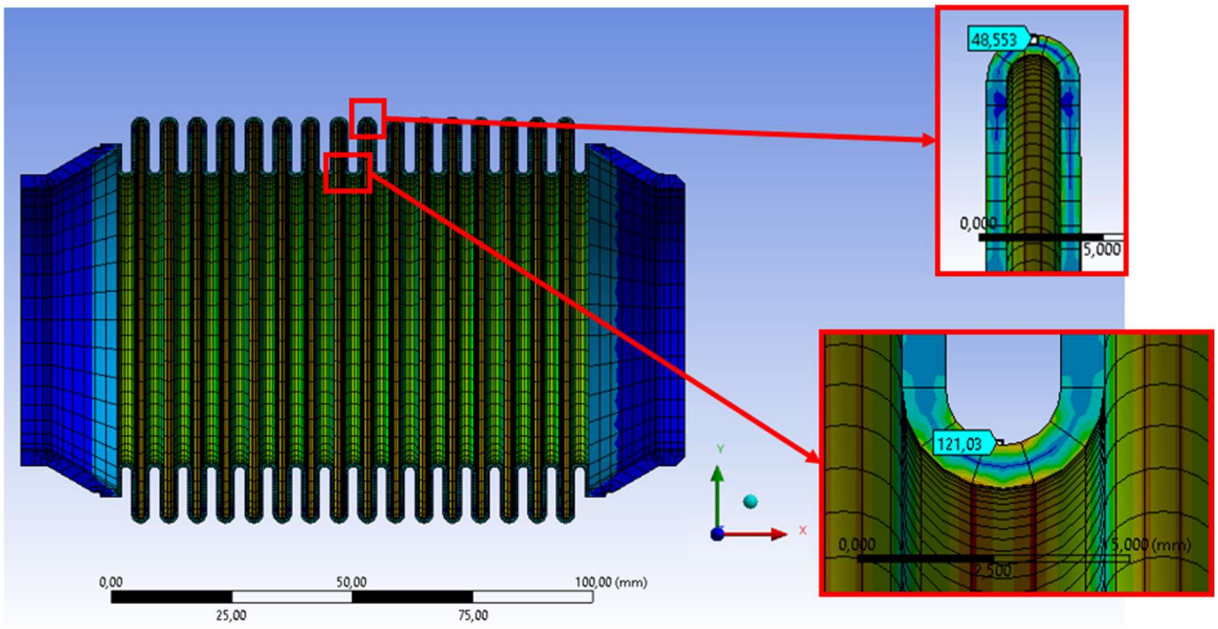

a. b.

Figure 6.7: FE analysis of equivalent stresses of single-ply bellows corrugation:
a. diagram of equivalent stresses of single-ply bellows;
b. maximum equivalent stresses in cavity and crest (critical analysed areas of bellows corrugations cross section, where appeared maximal equivalent stresses)

Therefore, for next analysis assumed that the critical point represents the cavity area of bellows corrugation cross section, where maximal equivalent stresses appeared. The crest area (or

measurement point) of the bellows corrugation cross section represent the area (point) on the surface of bellows corrugation, which was defined during the laboratory experiments, as a second critical point, where was possible to measure stresses with the strain gauges [5].

6.2.2 FE analysis of bellows bending

The bending of single- and multi-ply bellows as it concluded in chapter 5 has an unusual appearance for analytical analysis. The bending of the single- and multi-ply bellows is combination of the angular rotation and lateral deflection according to standard EN ISO 13445-3 [21] (see chapter 3). For FE analysis of bellows considered the real bending case, which validated to experimental model. As it presented on the Figure 6.8., the bending of the bellows has unusual nature. Therefore, this bending case was detailed analysed with FEA.

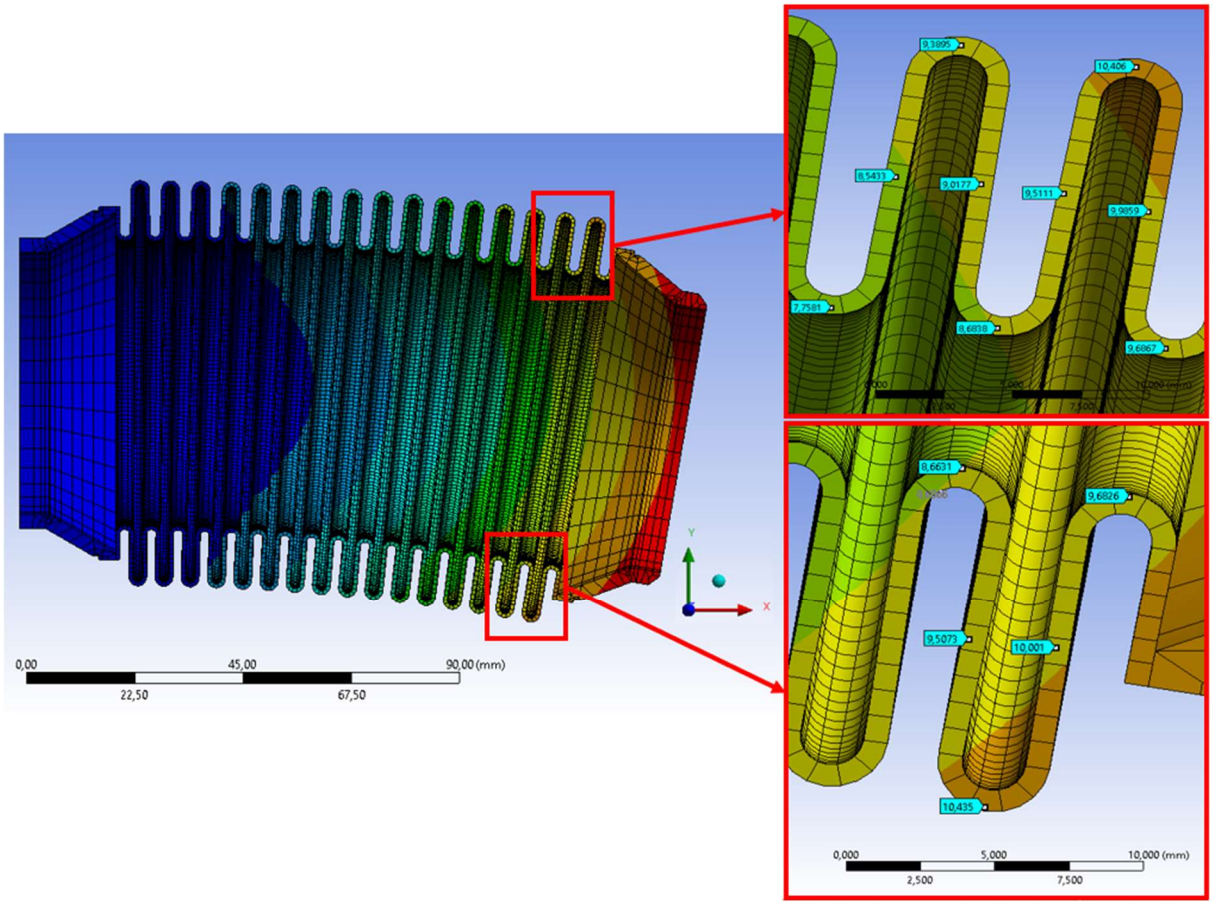

Figure 6.8: Deformation of single-ply bellows bended to 10 °

Consequently, the FE analysis of bending case is carried out for single-, two-, and three-ply bellows with the bending angle of 2 °, 4 °, 6 °, 8 °, 10 °. The FE analysis of multi-ply bellows considered for two different contact condition models: friction and bonded [73]. The precise

FE analysis of friction and bonded contact conditions presented in chapter 6.2.4.3. The deformation of investigated bending case of multi-ply (two-ply) bellows to 10 ° presented on Figure 6.8.

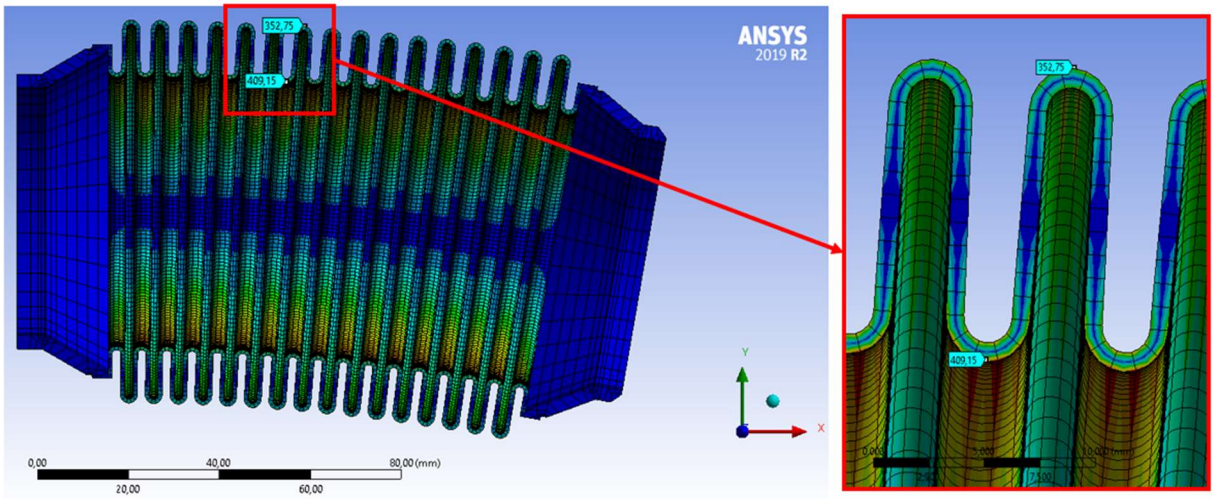

b.

Figure 6.9: FEA model of one-ply bellows for investigated bending case of 10 °:

a. deformation; b. stress

Hence, the maximum equivalent stresses in the cross section of single-ply bellows corrugations present on Figure 6.9. The direction of maximum equivalent stresses considered along the meridian direction on cavity section of the bellows.

For FE analysis with friction contact condition for multi-ply bellows noticed that the maximum equivalent stresses occurred simultaneously in the cavity and crest of each ply of the bellows corrugations. However, the equivalent stresses on each corrugation are different. Therefore, it required to determine the corrugation spots (crest or cavity) with the maximum value of equivalent stresses and accordingly analyse it in details [6].

6.2.3 FE analysis of stresses in the case of temperature influence

The FE analysis of temperature influence considered the multi-ply bellows with friction contact condition. The temperature influence simulated with the temperature module of the Ansys® Workbench software package, as presented in subchapter 6.1.3.

The temperature influence of operating media for FE analysis of investigated bellows considered as 20 °C, 100 °C, 200 °C, 300 °C, 400 °C and 500 °C. In the case of this FE analysis

considered the temperature heat transfer of the operating media on internal surface of bellows as thermal convection with heat transfer coefficient – 400 W/(m^2·K) [172]. The outer surface of bellows considered as thermal convection of the air with heat transfer coefficient – 10 W/(m^2·K).

For example, at 200 °C, it is noteworthy that the two-ply bellows has the largest deformation of 0,47 mm in the radial direction (Y direction), i. e. the two-ply bellows corrugations thermally expands outwards in the radial direction, which leads to increasing the diameter.

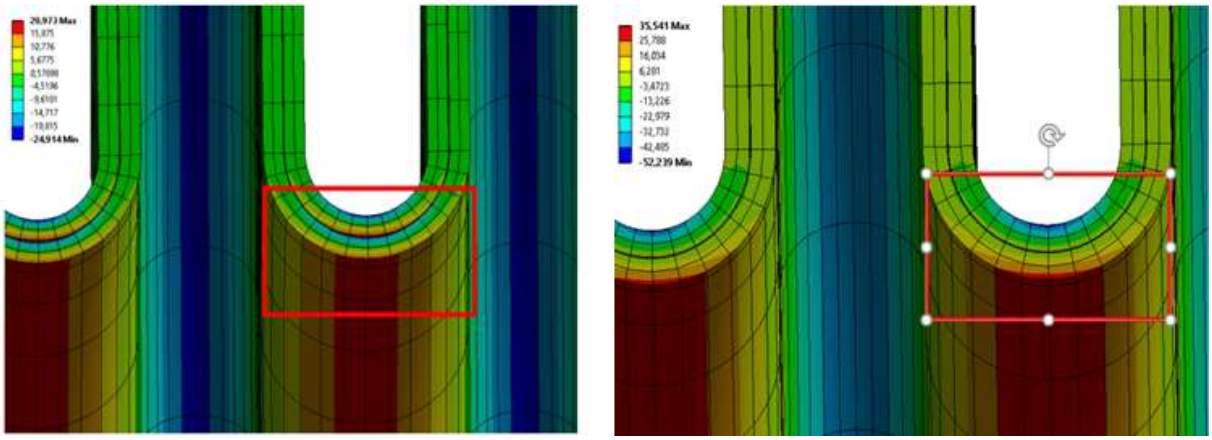

a. b.

Figure 6.10: Equivalent stresses in the two-ply bellows cavity:
a. friction;
b. bonded contact condition [74]

Therefore, a positive strain occurred in the circumferential direction. Hence, the boundary condition of the FE analysis is assumed that the bellows is fixed in the axial direction (X-direction), i. e. the bellows has a fix support of both sides on the boards, accordingly the bellows does not expand in X-direction. That is an assumption, which was different in case of real model. Nevertheless, a single- and multi-ply bellows expansion depended on the thermal expansion of the lever; i. e. expansion of the bellows in X-direction will be same as the expansion for the lever.

In the bellows cavity, inside of the inner ply, for instance (Figure 6.10, a.), occurred a relatively large equivalent stress with a value of 20,97 MPa in the meridian direction (at 200 °C), which is generated by thermal expansion in the axial direction [5].

Hence, due to different contact condition bonded or friction for multi-ply bellows the deformation are similar in the radial direction. Nevertheless, on Figure 6.10 it is obvious that in case of bonded contact condition the equivalent stresses in the multi-ply bellows cavity has

larger value of 35 MPa at 200 °C, as an example, which varies continuously over the total shell thickness [74]. It is also noticeable, that in case of friction contact condition, the equivalent on inside surface of the outer ply has a equivalent stress, while at the same point in case of bonded contact condition, a compression stress occurred [74].

Hence, the multi-ply bellows FE analysed with friction contact conditions, which assumed as real experimental analysation model [6].

6.2.4 FE analysis of linear and non-linear stresses into their components

6.2.4.1 Support section (evaluation path)

The analysis of linear and non-linear stresses carried out across the investigated cross section of bellows shell corrugation thickness along a line called the "support line (path)". The path with length ***e*** is the smallest section between two sides of the investigated bellows shell (see Figure 6.11).

Outside of areas with global imperfections, the support section runs perpendicular to the central shell surface; its length ***e*** equal to the analytically considered investigated shell thickness. For two-ply bellows assumed four critical paths in the middle of outer and inner shell of crest and considered as A_1-A_2, B_1-B_2, and in outer and inner shell of cavity: C_1-C_2, D_1-D_2. For example, the cross section of cavity with path length (thickness ***e***) C_1-C_2 is investigated in this individual case (see Figure 6.11).

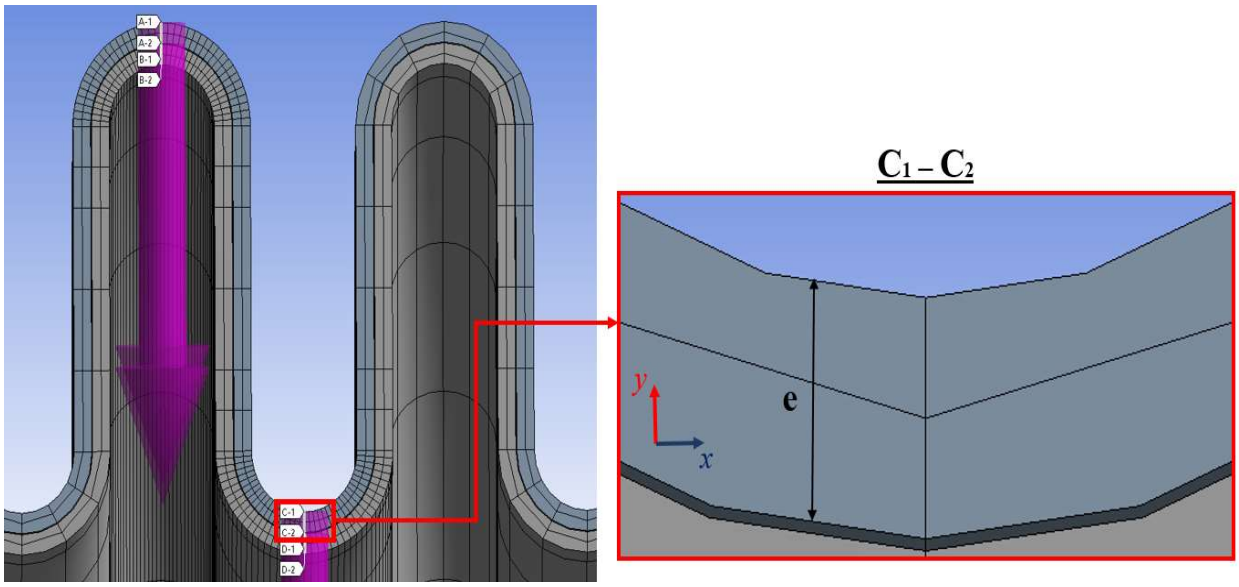

Figure 6.11: Investigated paths (support sections A_1-A_2, B_1-B_2, C_1-C_2, D_1-D_2) of bellows cross section and local axis for analysis the linear and non-linear stresses

6.2.4.2 Membrane stresses

The membrane stress tensor is the tensor that components $\sigma_{ij,m,m}$ are constant along the supporting path and equal to the mean value of the individual stresses σ_{ij} along the evaluation path (see Figure 6.13):

$$\left(\sigma_{ij}\right)_m = \frac{1}{e}\int_{-\frac{e}{2}}^{+\frac{e}{2}} \sigma_{ij} \cdot dy \tag{6.1}$$

6.2.4.3 Bending stress

The bending stress is the tensor, the components of which $\sigma_{ij,b}$ change linearly along the evaluation path and is given by the following equation:

$$\left(\sigma_{ij}\right)_b = \frac{12y_1}{e^3}\int_{-\frac{e}{2}}^{+\frac{e}{2}} \sigma_{ij} \cdot y_1 \cdot dy \tag{6.2}$$

For the stress analysis according to EN 13445 Part 3 Appendix C, on each side of the investigated shell geometry, hence at the ends of the support path, the maximum values of $\sigma_{ij,b}$ have same value. In this case applied the following equation:

$$\left(\sigma_{ij}\right)_b = \pm\frac{6}{e^2}\int_{-\frac{e}{2}}^{+\frac{e}{2}} \sigma_{ij} \cdot y_1 \cdot dy \tag{6.3}$$

6.2.4.4 Linearized stresses

The linearized stress tensor has the components $\sigma_{ij,l}$, which considered in following equation:

$$\sigma_{ij,l} = \sigma_{ij,m} + \sigma_{ij,b} \tag{6.4}$$

6.2.4.5 Non-linear stress

The tensor of the non-linear stress has the components $\sigma_{ij,nl}$ which considered in following equation:

$$\sigma_{ij,nl} = \sigma_{ij} - \sigma_{ij,l} = \sigma_{ij} - [\sigma_{ij,m} + \sigma_{ij,b}] \tag{6.5}$$

Hence, Figure 6.12 presents the analysis of linear and non-linear stresses.

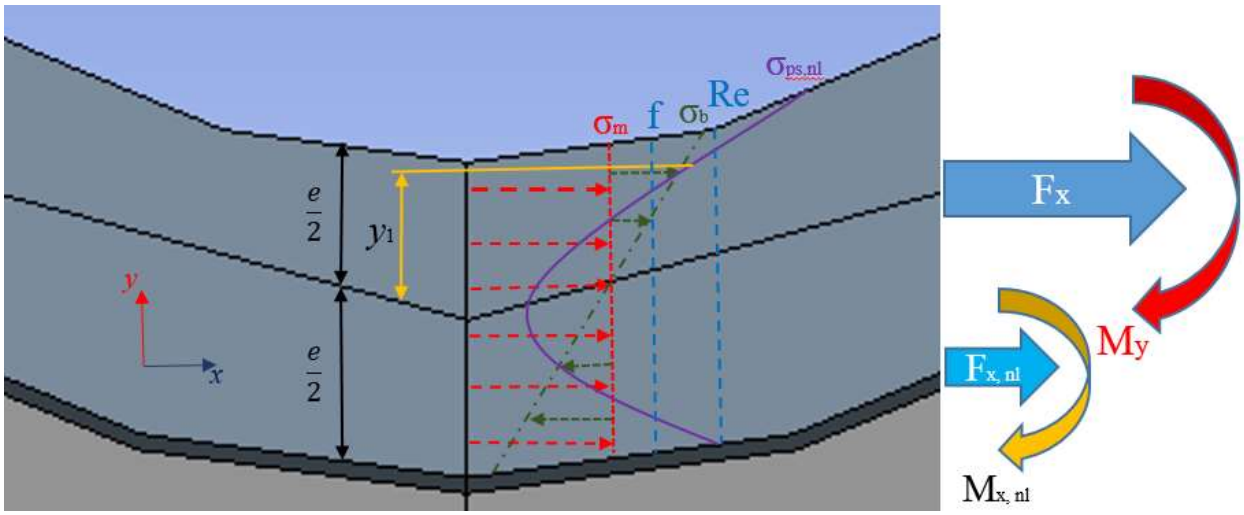

Figure 6.12: Internal pressure load of a cylinder shell in the circumferential and longitudinal direction as well as bending load and temperature influence (in the cross section investigated area by the evaluation path)

6.2.4.6 Definition of maximal equivalent stresses for investigated bellows design (failure against deformation [yield strength])

Strength condition for investigated model of bellows will be approximated to following acceptations of equivalent stresses with safety factor *S* equal to 1,5 (failure against deformation [yield strength])

$$\text{if, } \sigma_{eq} = \sigma_m \leq \mathrm{f} = \frac{\mathrm{Re}}{\mathrm{S}} \tag{6.6}$$

$$\text{if, } \sigma_{eq} = \sigma_m + \sigma_b \leq 1{,}5 \cdot \mathrm{f} = 1{,}5 \cdot \frac{Re}{S} \tag{6.7}$$

$$\text{if, } \sigma_{eq} = \sigma_m + \sigma_b + \sigma_{nl} \leq 3 \cdot f = 3 \cdot \frac{Re}{S} \tag{6.8}$$

Here σ_m stands for membrane stress, σ_b for bending stress and σ_{nl} for peak stress (non-linear stress), these are three components of the stresses, which linearized.

For the nominal analysed stresses *f*, the following equation applies:

$$f = \frac{R_e}{S} \tag{6.9}$$

where, *S* corresponds to the safety factor, which assumed as 1,5 according to PED [106] and specification for pipeline and piping valves API 6D/ EN ISO 14313 [50].

Hence, the limit loads of investigation two-ply bellows were determined under different

temperature ranges of 20 °C, 100 °C, 200 °C, 300 °C, 400 °C, 500 °C and different pressure classes according to EN 13445-3 [21], EN ISO DIN 1333 [67] and specification for pipeline and piping valves API 6D/ EN ISO 14313 [50]. The procedure for determining the elastic limit loads illustrated for two cases:

- determination of the limit number of cycles of investigated two-ply bellows in temperature range of 20 °C, 100 °C, 200 °C, 300 °C, 400 °C, 500 °C and bending of bellows to 10 ° angle;

- determination of the limit number of cycles of investigated two-ply bellows for internal pressure of 0,3 MPa, 0,6 MPa, 1 MPa, 1,6 MPa and 2 MPa. According to considered pressure standards EN 13445-3 [21], EN ISO DIN 1333 [67] and specification for pipeline and piping valves API 6D/ EN ISO 14313 [50] and bending of bellows to 10 ° angle.

6.2.4.7 Material model and maximum equivalent stresses

For investigated model of bellows was considered stainless steel 1.4006 (see sub-chapter 2.2.2.6) with yield strength $R_{0,2T}$ at 500 °C as 255 MPa. Hence, according to equation (6.8) the equivalent stresses with peak stresses (non-linear stress) in investigated paths equal or less then:

$$\sigma = \sigma_m + \sigma_b + \sigma_{nl} \leq 3 \cdot f = 3 \cdot \frac{Re}{1{,}5} = 2 \cdot Re = 2 \cdot 255 \leq 510\ MPa \qquad (6.10)$$

Hence, for cryogen temperatures till –271 °C and high temperatures till +100 °C for investigated bellows designs considered stainless steel 1.4571 [147] (see chapter 2.4.2.6). Whereas, for high temperatures from +100 °C till +500 °C and high pressure 1,6 - 2 MPa considered stainless steel 1.4006 [147]. For FE analysis in worst-case scenario considered stainless steel 1.4006, with maximal allowable equivalent stresses, according to equation (6.9) in investigated paths 510 MPa.

6.2.5 FE analysis of internal pressure, complex bending and temperature influence at same time and maximum value (worst-case scenario)

The loading of the operating pressure of 2 MPa, bending of 10 ° and temperature of 500 °C is the worst-case scenario for investigated single- and multi-ply bellows (the maximal load case). In the normal case, single- and multi-ply bellows is in unload position. If the temperature increases, the single- and multi-ply bellows has a thermal expansion, which arise the stresses. In operation case, the opening/closing of the cross-flow section of the ball valve, the single-

and multi-ply bellows is under bending loads plus thermal expansion loads (for case of high-temperature). In addition, if seal elements of the stem are broken, not implemented according to specific design or there is leakage in stem area, the internal pressure in the RGM housing increase up to operating pressure of the ball valve cross flow section. That leads the single- and multi-ply bellows to operate under the internal pressure load as well. These three loads cause the worst-case scenario, which considered in this chapter.

6.2.6 The FE analysis results of single-, two-, three-ply bellows

Consequently, for the single- and multi-ply bellows considered different stresses, which occurred in the corrugations of the bellows in the case of different loads. Hence, to determine correct geometry, number of plies and corrugations for a design of single- and multi-ply bellows, it is required a FE analysis of the loads for investigated single- and multi-ply bellows.

As it mentioned before, the considered loads for single-, and multi-ply bellows were the internal pressure, bending and temperature influence. These loads required detailed analysis, to determine the fatigue live of the single-, and multi-ply bellows for each load case.

The investigation performed the FE analysis of single- and multi-ply bellows in the loading case of internal pressure, complex bending and temperature influence. The FE results, which obtained by two- and three-ply bellows, have differences at the critical areas of bellows cross section compare to the analytical analyses, according to standards EN ISO 13445 Part 3 [21] and EJMA [60]. Hence, it attributed due to the friction coefficients of the contact condition between the plies of two- and three-ply bellows corrugations, which adjusted in settings of Ansys® Workbench software package. In addition, residue stresses and unperfect geometry, due to manufacture in the structure of the bellows, were nor considered in this FE analysis.

6.2.6.1 FE analysis of internal pressure load case for single- and multi-ply bellows

The results of the internal pressure considered for 0,3 MPa, 0,6 MPa, 1 MPa, 1,6 MPa, 2 MPa and is carried out on the single-, two- and three-ply bellows. The pressure classes taken on behalf of the standards EN 13445-3 [21], EN ISO DIN 1333 [67] and specification for pipeline and piping valves API 6D/ EN ISO 14313 [50]. The FE analysis carried out with temperature range of 20 °C, 100 °C, 200 °C, 300 °C, 400 °C, 500 °C, as described in previous subchapters.

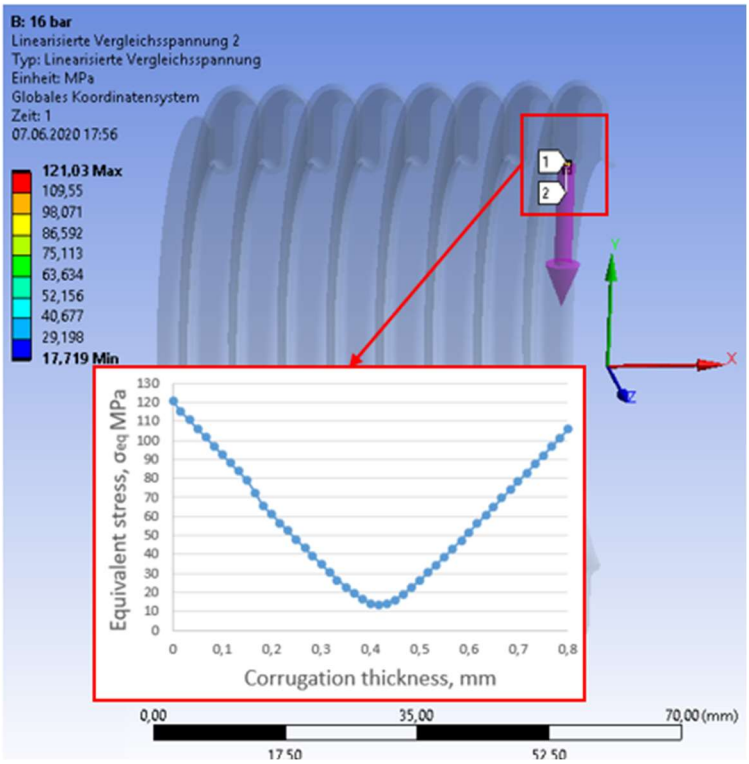

Figure 6.13: Detailed FE analysis of critical area on 8th corrugation of single-ply bellows cross-section at cavity (the point of maximum equivalent stresses on the corrugation surface of the bellows)

The FE analysis results of single-ply bellows at room temperature at 20 °C presented in Table 6.2 and on Figure 6.14.

Table 6.2: FE analysis of stress result of the internal pressure for single-ply bellows according to the standards EN 13445-3 [21] and specification for pipeline and piping valves API 6D [50]

Single-ply bellows						
FE analysis, cavity (critical point[D])						
Pressure, Class	Pressure, MPa	σ_m, MPa	σ_b, MPa	$\sigma_m + \sigma_b$, MPa	σ_{nl}, MPa	σ_{eq}, MPa
PN 2,5	0,3 MPa	3,37	15,88	17,29	5,27	25,48
PN 6	0,6 MPa	2,12	40,45	42,67	8,88	50,97
PN 10	1 MPa	8,51	62,95	71,47	10,69	84,95
PN 16	1,6 MPa	17,91	89,43	98,27	23,71	121,03
PN20	2 MPa	22,47	105,89	115,29	35,17	148,97
FE analysis, crest (measurement point [A])						
Pressure, Class	Pressure, MPa	σ_m, MPa	σ_b, MPa	$\sigma_m + \sigma_b$, MPa	σ_{nl}, MPa	σ_{eq}, MPa
PN 2,5	0,3 MPa	1,06	15,22	15,08	5,44	20,77
PN 6	0,6 MPa	6,74	19,85	38,50	10,55	44,69
PN 10	1 MPa	4,01	51,16	49,64	9,48	60,50
PN 16	1,6 MPa	6,41	81,85	79,42	15,17	94,79
PN20	2 MPa	7,09	101,48	102,89	36,27	138,51

The FE analysis for two-ply bellows is carried out with two different contact conditions. First contact condition is bonded, which determinate model of the two-plies as a single-ply bellows with some approximations [64]. The gap between two-ply in the bellows equal to 0 mm, and the contact condition likely as welded.

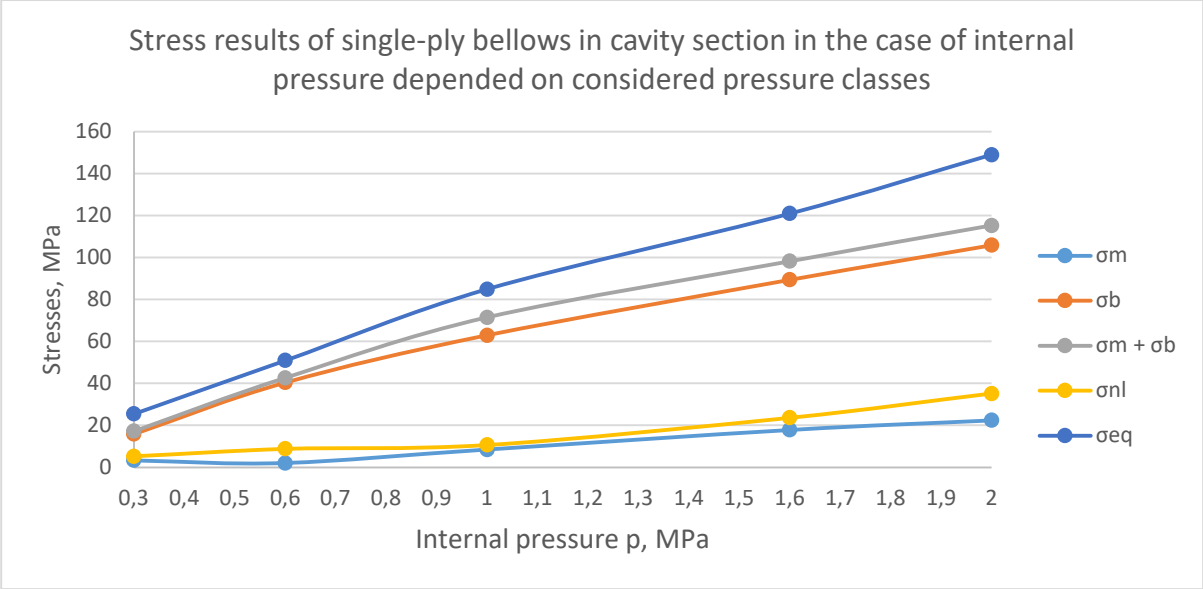

Figure 6.14: FE analysis results of the single-ply bellows in the cavity section in the case of the internal pressure depended on considered pressure classes

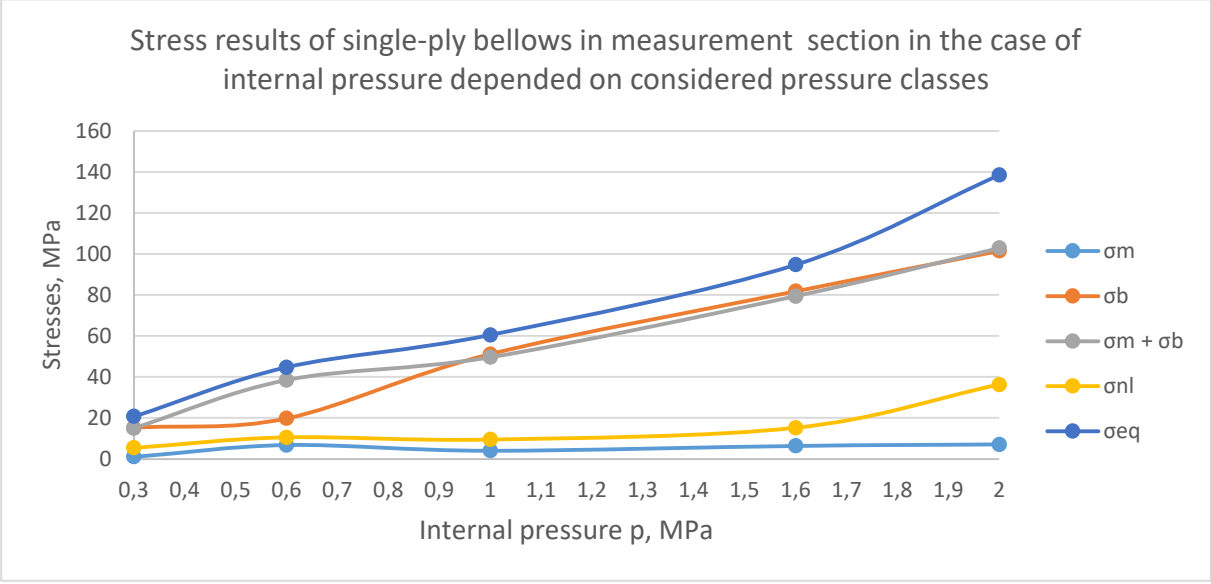

Figure 6.15: FE analysis of stress results of single-ply bellows in measurement point in the case of internal pressure depended on considered pressure class

Therefore, the contact elements of Ansys® Workbench software package (element 145) are firmly connected and not allowed to slice on each other [73]. The similar approximation was

definite by Anderson theory of the analytical analysis of the bellows [12]. The results of the two-ply bellows with bonded contact conditions were precise analysed and it was considered that the results are not acceptable for this analysis case.

The FE analysis of the two-ply bellows with friction contact condition between plies determinate real model of the multi-ply bellows. The friction coefficient between the plies was considered as 0,1 for investigated stainless steels 1.4571 [68], [149], 1.4462 [116], [149] and 1.4006 [147]. The plies in the contact could slide on each other, definition of the contact element 145 of the Ansys® Workbench software package.

Hence, these contact conditions and results are more pertain to the experimental results. The results of the friction contact condition for investigated two-ply bellows presented in Table 6.3 and on Figure 6.16.

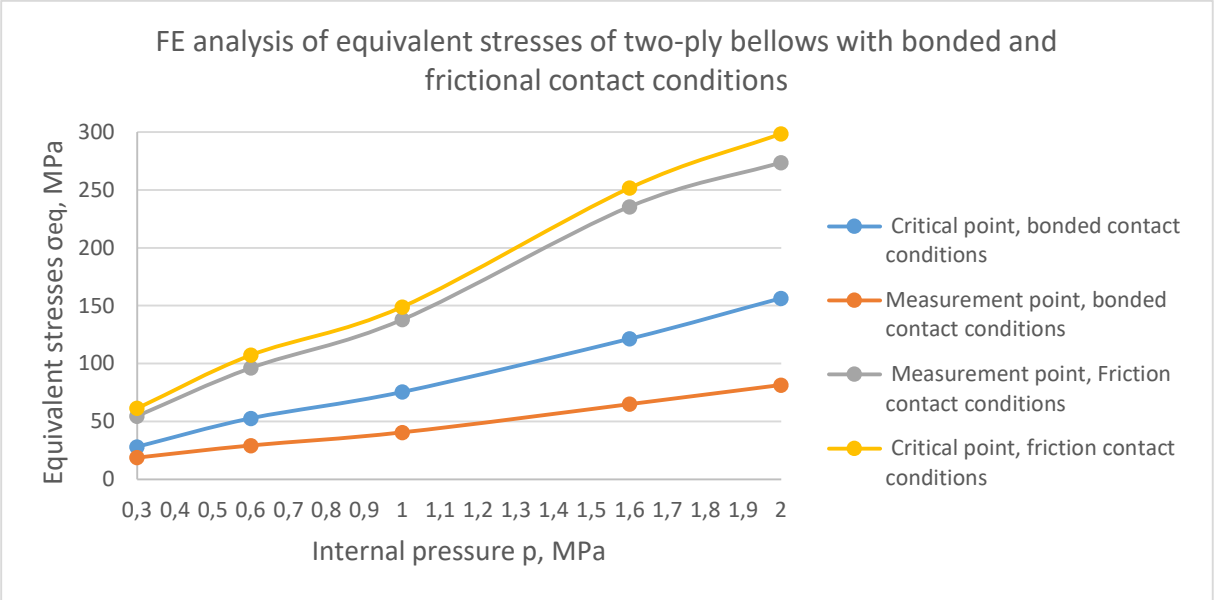

Figure 6.16: FE analysis of equivalent stresses of two-ply bellows with bonded and frictional contact conditions

Consequently, for FE analysis the maximal value of equivalent stress in the crest section for two-ply circular bellows with U-shaped convolution cross section from internal pressure of 1,6 MPa equal to 235,57 MPa (Table 6.3). According to presented mathematical analysis in Chapter 4, the maximal value of equivalent stress equal to 245 MPa for two-ply circular bellows with U-shaped convolution cross section in the case of internal pressure of 1,6 MPa. The value of maximal equivalent stress by the experiments is 232,85 MPa at internal pressure of 1,6 MPa. Finaly, the maximal value of equivalent stress as stated in calculation analysis of ISO EN 13445-3 is 254,75 MPa. Hence, comparing different analyses in conclusion it makes maximal difference about 8 %.

Table 6.3: FE analysis of the two-ply bellows with friction contact conditions

Cavity section (critical point [D]), friction contact conditions						
Pressure, class	Pressure, MPa	σ_m, MPa	σ_b, MPa	$\sigma_m + \sigma_b$, MPa	σ_{nl}, MPa	σ_{eq}, MPa
PN 3	0,3	7,13	41,71	49,39	12,43	61,51
PN 6	0,6	11,52	64,63	75,32	16,11	107,39
PN 10	1,0	15,49	129,94	145,39	21,39	149,03
PN 16	1,6	19,72	211,02	231,52	28,74	251,85
PN20	2,0	23,50	234,97	252,48	45,33	298,68
Crest section (measurement point [A]), friction contact conditions						
Pressure, class	Pressure, MPa	σ_m, MPa	σ_b, MPa	$\sigma_m + \sigma_b$, MPa	σ_{nl}, MPa	σ_{eq}, MPa
PN 3	0,3	6,87	40,30	46,20	9,34	54,80
PN 6	0,6	10,93	73,80	84,10	14,50	96,43
PN 10	1,0	13,01	114,86	127,24	10,98	138,13
PN 16	1,6	16,75	200,47	215,50	22,26	235,57
PN20	2,0	27,91	224,65	252,94	35,20	273,86

6.2.6.2 FE analysis of single- and multi-ply bellows bending case

The FEA of single-ply bellows bending considered the analysis of equivalent stresses for bending angle of 2 °, 4 °, 6 °, 8 °, 10 °. The bending angle considered according to experimental analysis (see chapter 5). The FE analysis results of the bending for single-ply bellows considered in Table 6.4.

Table 6.4: FE analysis of bending load case of single-ply bellows in cavity section (critical point) and crest section (measurement point)

Single-ply bellows					
Cavity section (critical point [D]), FE analysis					
Bending angle, °	σ_m, MPa	σ_b, MPa	$\sigma_m + \sigma_b$, MPa	σ_{nl}, MPa	σ_{eq}, MPa
2	7,19	64,68	71,87	12,96	80,82
4	14,38	139,35	153,73	25,91	159,64
6	21,57	204,03	225,60	38,87	244,47
8	28,75	288,71	317,46	41,83	329,29
10	35,94	343,39	378,33	54,78	409,11
Crest section (measurement point [A]), FE analysis					
2	7,72	61,23	67,47	17,17	74,31
4	15,44	122,47	137,94	34,33	148,63
6	23,16	193,70	210,42	43,50	222,94
8	30,87	234,93	275,89	55,66	297,26
10	38,59	316,17	337,36	65,82	371,57

Consequently, the FE analysis results of the bending case for multi-ply bellows were considered with two contact conditions: bonded and friction, as it mentioned before. The bonded contact condition of the multi-ply bellows determined as the Anderson theory of thin toroidal shell [12], which used in standard ISO EN 13445 Part 3 [21] for analytical analysis of the bellows.

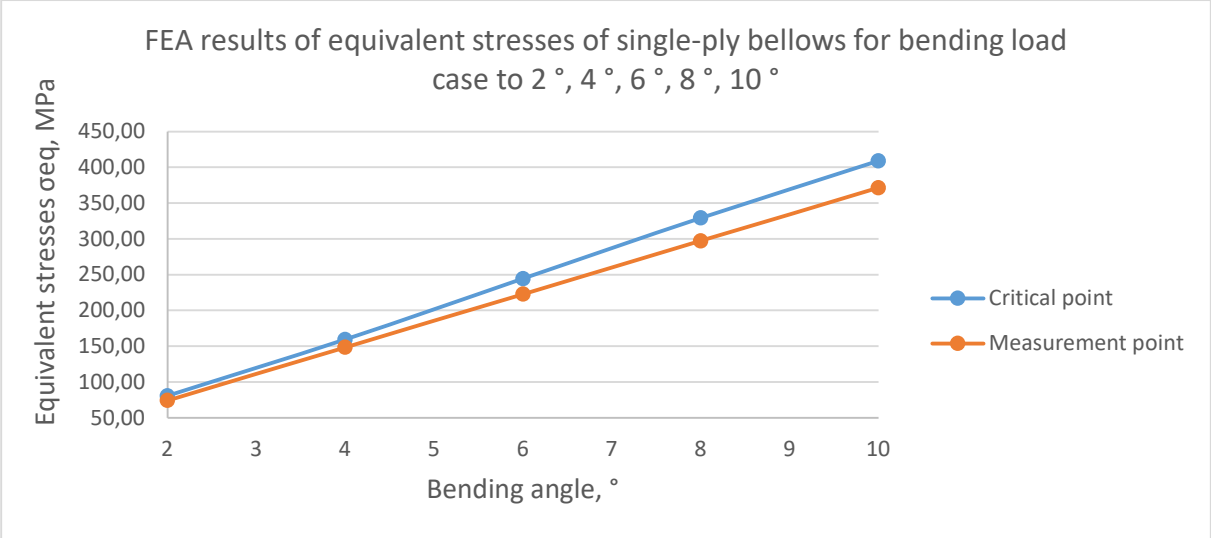

Figure 6.17: FE analysis results of equivalent stresses of single-ply bellows for bending load case to 2 °, 4 °, 6 °, 8 °, 10 °

Table 6.5: FE analysis of bending with two contact conditions: bonded and friction for investigated two-ply bellows at critical point on the cavity section

Two-ply bellows					
Cavity section (critical point [D]), bonded contact condition					
Angle, °	σ_m, MPa	σ_b, MPa	$\sigma_m + \sigma_b$, MPa	σ_{nl}, MPa	σ_{eq}, MPa
2	11,13	59,98	71,01	14,04	77,99
4	18,26	123,95	140,02	28,08	150,98
6	32,38	185,93	215,03	52,11	236,96
8	46,51	267,90	310,04	66,15	325,95
10	60,64	329,88	380,05	80,19	404,94
Cavity section (critical point [D]), friction contact condition					
Bending angle, °	σ_m, MPa	σ_b, MPa	$\sigma_m + \sigma_b$, MPa	σ_{nl}, MPa	σ_{eq}, MPa
2	8,21	24,91	32,88	5,58	34,65
4	17,15	70,05	87,03	11,15	94,79
6	31,24	105,08	130,50	16,70	141,89
8	45,51	140,09	182,79	22,22	190,03
10	53,91	164,94	224,94	27,71	243,07

Hence, it is possible to recognize that the equivalent stresses resulting from FEA are different to analysis according to EN ISO 13445-3 and Anderson theory, due to the nature of the friction

between the plies of the bellows, the specific bending case due to installation on RGM [5], as well as more accurate analysation with exact geometry and fine mesh.

The multi-ply behaviour of bellows according to EN ISO 13445-3 [21] and Anderson theory of thin toroidal shells [12] approximated by the constants such as C_f, C_d, C_p (see chapter 3). That considered the maximum equivalent stress result. However, it does not define at which area or point of the bellows geometry the maximum equivalent stresses appear.

Therefore, FE analysis determinate and particularly considered the areas of maximum equivalent stresses. The FE analysis results of the bending considered in Table 6.5-6.6 for a two-ply bellows, Table 6.7-6.8 for three-ply bellows.

Table 6.6: FE analysis of bending with two contact conditions: bonded and friction, for investigated two-ply bellows at crest section (measurement point)

Two-ply bellows					
Crest section (measurement point [A]), bonded contact condition					
Bending angle, °	σ_m, MPa	σ_b, MPa	$\sigma_m + \sigma_b$, MPa	σ_{nl}, MPa	σ_{eq}, MPa
2	1,84	93,99	94,50	17,96	76,55
4	36,85	187,98	189,00	35,91	153,10
6	55,27	281,97	283,50	53,87	229,65
8	73,70	375,96	378,01	71,83	286,20
10	92,12	469,95	472,51	89,78	352,75
Crest section (measurement point [A]), friction contact condition					
Bending angle, °	σ_m, MPa	σ_b, MPa	$\sigma_m + \sigma_b$, MPa	σ_{nl}, MPa	σ_{eq}, MPa
2	7,40	20,16	27,15	4,89	29,21
4	17,80	54,29	70,78	7,33	75,49
6	24,10	101,72	124,23	11,20	129,80
8	35,50	135,24	168,31	14,60	177,90
10	52,80	160,29	211,89	17,50	225,10

The diagram on the Figure 6.18 and Table 6.6 presented the FE analysis results of the equivalent stresses of the bending of two-ply bellows of 2 °, 4 °, 6 °, 8 °, 10 ° in critical point and in the point, which was analysed during laboratory experiments. The FE analysis performed in two different contact conditions: bonded and friction.

Hence, the difference of the equivalent stresses due to contact conditions in the case of the bending are higher as in case of internal pressure. The bonded contact condition consider that the separated plies of the bellows are firmly connected. Therefore, the plies cannot slide and behave as a single ply. The nots of the contact elements [73] (ELEMENT 145) are continuously bonded. The difference in this case to a single-ply bellows FE analysis that the separate plies

have additional peak stresses in the structure between the separated plies.

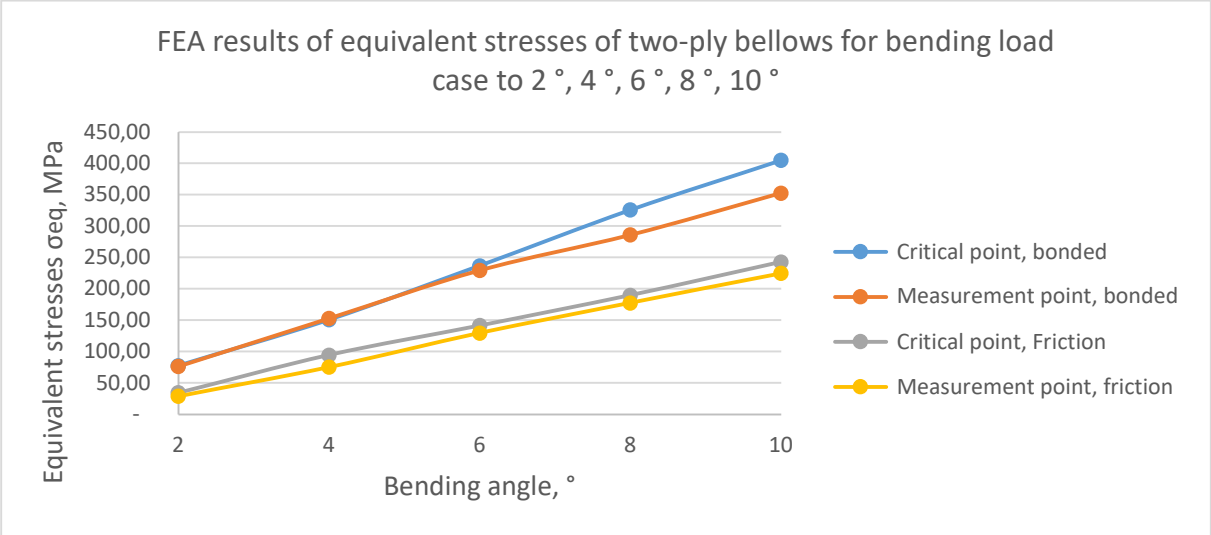

Figure 6.18: FE analysis results of the equivalent stresses of two-ply bellows for bending load case to 2 °, 4 °, 6 °, 8 °, 10 °

The friction contact condition consider that the separated plies of the investigated bellows have friction contact condition between the plies, with the friction coefficient of 0,1 (stainless steel on stainless steel). The equivalent stresses in this case decry, as each ply operates against the bending separately. Hence, the FEA results are comparable to a real experimental model of investigated two-ply bellows, as it proved at the measurement point during the experiments. As it was concluded during the experiments, the average equivalent stress on the outer ply of the 8th two-ply bellows corrugation in the case of bending angle to 10 ° equals to 227,29 MPa. Nevertheless, the FE analysis resulting from the same point (investigated area) considered the equivalent stress equals to 225,1 MPa. That is less than 1 % difference, which considered as very accurate result.

The FE analysis of three-ply bellows carried out as for two-ply bellows. The friction coefficient is considered as 0,1.

Hence, the middle ply of the three-ply bellows had a friction contact condition on outer and internal ply. This case is difficult to analyse analytically. Therefore, the analytical calculation for three-ply bellows approximated according to the theory of Anderson [12] or Andreeva [78], and implemented in standard ISO EN 13445-3 [21], as it presented in chapter 3.

Nevertheless, the maximum equivalent stresses analysed on macro level in three-ply bellows corrugation, but not at the critical areas. The FE analysis presented the critical areas of the bellows corrugations and according its equivalent stresses, which is easy to analyse and

consider the limit loads. The results of the critical areas of investigated three-ply bellows presented in Table 6.7 - 6.8.

Table 6.7: FE analysis of bending load case of three-ply bellows in critical point and measurement point (friction contact condition, real model)

Three-ply bellows					
Cavity section (critical point [D]), friction contact condition					
Bending angle, °	σ_m, MPa	σ_b, MPa	$\sigma_m + \sigma_b$, MPa	σ_{nl}, MPa	σ_{eq}, MPa
2	5,60	17,24	22,84	2,48	23,41
4	8,30	32,49	40,79	4,97	44,16
6	12,90	47,21	60,11	9,39	65,30
8	19,60	67,29	86,89	12,50	91,30
10	28,30	78,94	107,24	19,70	114,30
Crest section (measurement point [A]), friction contact condition					
Bending angle, °	σ_m, MPa	σ_b, MPa	$\sigma_m + \sigma_b$, MPa	σ_{nl}, MPa	σ_{eq}, MPa
2	4,58	15,54	19,75	2,33	20,45
4	9,81	27,90	38,27	4,51	40,81
6	14,26	42,03	55,62	6,67	59,03
8	21,95	56,96	76,80	8,81	81,10
10	28,84	67,62	96,75	10,93	102,96

Table 6.8: FE analysis results of bending load case from 2 ° to 10 ° for three-ply bellows in cavity section (critical point) and crest section (measurement point) at bonded contact condition

Cavity section (critical point [D]), bonded contact condition					
Angle, °	σ_m, MPa	σ_b, MPa	$\sigma_m + \sigma_b$, MPa	σ_{nl}, MPa	σ_{eq}, MPa
2	8,60	45,21	52,89	9,50	54,45
4	12,10	92,34	102,41	13,20	110,81
6	17,70	141,81	157,76	17,60	169,03
8	24,30	192,39	209,52	22,30	221,10
10	32,90	225,96	259,71	27,40	272,96
Crest section (measurement point [A]), bonded contact condition					
Angle, °	σ_m, MPa	σ_b, MPa	$\sigma_m + \sigma_b$, MPa	σ_{nl}, MPa	σ_{eq}, MPa
2	4,10	36,40	39,90	3,70	41,40
4	8,50	68,80	75,20	5,10	78,20
6	11,70	104,10	114,30	8,20	120,50
8	15,30	131,60	149,40	11,20	158,30
10	21,70	173,30	192,70	14,40	208,10

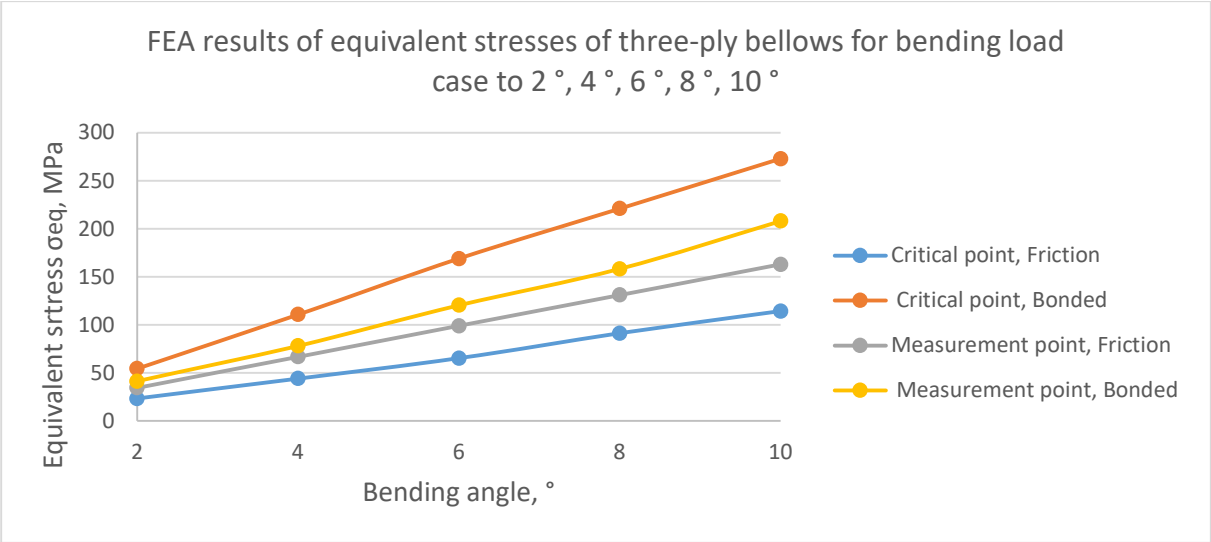

Figure 6.19: FE analysis results of equivalent stresses of three-ply bellows for bending load case to 2 °, 4 °, 6 °, 8 °, 10 °

The equivalent stresses, presented on the Figure 6.19, consider the real model with friction contact condition and analysed model with bonded contact condition. Hence, bonded contact condition (see Table 6.8) approximately considered as the single-ply bellows due to the fixed connection of nodes of implemented contact element 145 [73]. The friction contact condition (see Table 6.7) opposite to bonded considered model, when each ply of multi-ply bellows act separately. Precisely, the additional non-linear stresses appear due to the friction between the plies of multi-ply bellows.

Hence, during the FE analysis of multi-ply bellows bending load case, it considered that higher stresses occur in case of bonded contact condition than in case of friction contact condition. For instance, in the case of identical total ply thickness and bending load case, the three-ply bellows with friction contact condition had lower equivalent stresses than two-ply bellows. However, for internal pressure load case, the impact is opposite.

Hence, for bending load case it considered if the number of plies in multi-ply bellows increase, the smaller equivalent stresses occur. Whereas, for internal pressure load case the impact is opposite. Respectively, if the number of plies of multi-ply bellows increase, the higher equivalent stresses occur.

Consequently, for investigated load cases of the single- and multi-ply bellows the analysis required to achieve the equilibrium of the number of plies and it thickness. In addition, it was important to optimise the number of corrugations for single- and multi-ply bellows, which have impact to bending load case.

6.2.6.3 FE analysis of temperature influence for single- and multi-ply bellows

The FE analysis of the temperature influence for single- and multi-ply bellows is unique in the case of investigated RGM, due to fixed connection of the boards of investigated bellows from one side by welding to housing of the RGM, and from another side by welding to lever. This case of welding connections as well as design of the RGM with the single- and multi-ply bellows considered complex thermal expansion, which analysed by FEA (see Figure 6.20 and Figure 6.21).

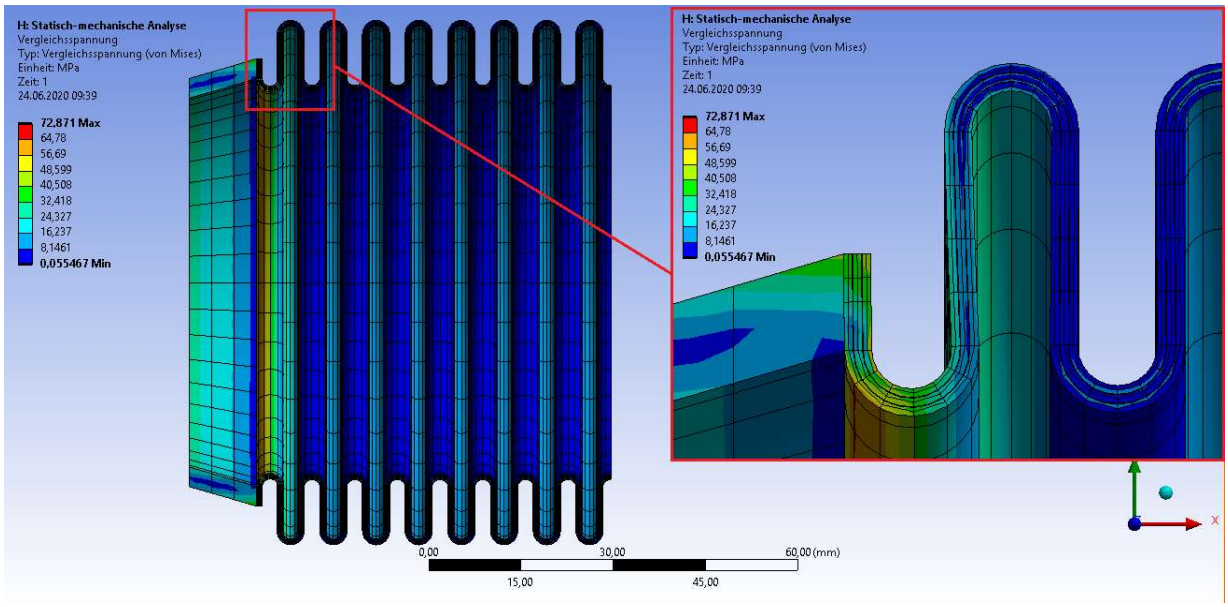

Figure 6.20: FE analysis of thermal expansion at 500 °C for three-ply bellows

The results of the FE thermal analysis presented in the Table 6.9. The FE analysis provides the result with friction contact condition for the multi-ply bellows.

The maximal equivalent stresses occurred in area of contact between corrugations and board of investigated bellows.

Table 6.9: FE analysis of the temperature influence on the structure of the single-, two- and three-ply bellows

FE analysis of temperature influence for single-, two- and three-ply bellows			
Temperature	Single-ply	Two-ply	Three-ply
°C	Equivalent stresses σ_{eq}, MPa		
100	21,54	11,77	10,75
200	49,15	29,40	27,08
300	76,77	44,83	41,21
400	104,38	61,82	56,98
500	132,00	78,85	72,87

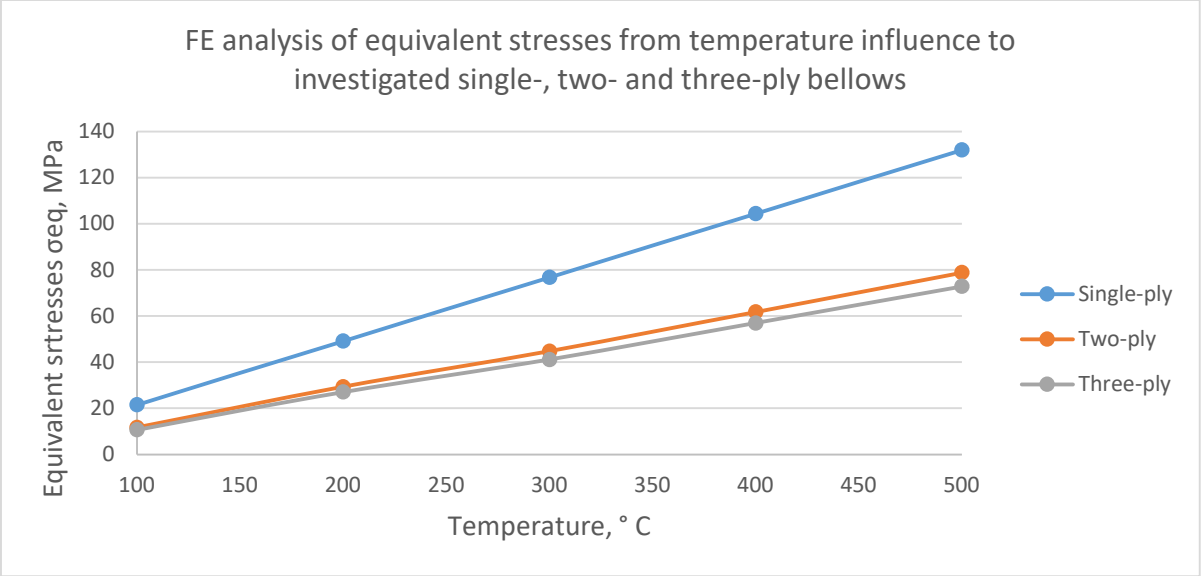

Figure 6.21: FE analysis of equivalent stresses from temperature influence to investigated single-, two- and three-ply bellows

6.2.7 FE analysis of maximum equivalent stresses in the single- and multi-ply bellows (worst-case scenario) depending on the analysed internal pressure classes of investigated ball valves designs

The FE analysis of maximum equivalent stresses, which appeared in the structure of the single- and multi-ply bellows corrugations during analysis of the worst-case scenario presented in Tables 6.10 - 6.12 and on the Figure 6.22.

Table 6.10: FE analysis of maximum equivalent stresses of the single-ply bellows (worst-case scenario) depending on the analysed pressure classes of the ball valves

FE analysis of maximum equivalent stresses in the single-ply bellows (worst-case scenario)				
Pressure, Class	Pressure, MPa	Single-ply		
		σ_{eq} pressure, MPa	σ_{eq} bending, MPa	σ_{eq}, MPa
PN 3	0,3	25,48	420,77	438,60
PN 6	0,6	50,97	420,77	456,44
PN 10	1,0	84,95	420,77	480,23
PN 16	1,6	121,03	420,77	505,49
PN20	2,0	148,97	420,77	525,04

The presented results provide that in the worst-case load scenario the investigated three-ply bellows had fewer equivalent stresses compared to single- and two-ply bellows. It considered that three-ply bellows perfectly fits to design of RGM and for investigated load (operation) case of the bellows.

Table 6.11: FE analysis of maximum equivalent stresses of the two-ply bellows (worst-case scenario) depending on the analysed pressure classes of the ball valves

FE analysis of maximum equivalent stresses in the two-ply bellows (worst-case scenario)				
Pressure, Class	Pressure, MPa	Two-ply		
		σ_{eq} pressure, MPa	σ_{eq} bending, MPa	σ_{eq}, MPa
PN 3	0,3	61,50	240,02	283,07
PN 6	0,6	107,39	240,02	315,2
PN 10	1,0	149,03	240,02	344,34
PN 16	1,6	251,85	240,02	416,32
PN 20	2,0	298,68	240,02	449,10

Table 6.12: FE analysis of maximum equivalent stresses of the three-ply bellows (worst-case scenario) depending on the analysed pressure classes of the ball valves

FE analysis of maximum equivalent stresses in the three-ply bellows (worst-case scenario)				
Pressure, Class	Pressure, MPa	Three-ply		
		σ_{eq} pressure, MPa	σ_{eq} bending, MPa	σ_{eq}, MPa
PN 3	0,3	80,85	112,36	168,96
PN 6	0,6	150,72	112,36	217,87
PN 10	1,0	216,63	112,36	264,00
PN 16	1,6	332,17	112,36	344,88
PN 20	2,0	397,68	112,36	390,74

Nevertheless, due to complex structure of three-ply bellows and highly cost in the production, the two-ply bellows considered as a standard seal element for investigated RGM. The equivalent stresses of single-ply bellows exceed the maximum allowable stresses of 510 MPa according to equation (6.10). Therefore, the single-ply bellows cannot be applied for this ball valve design with RGM [4].

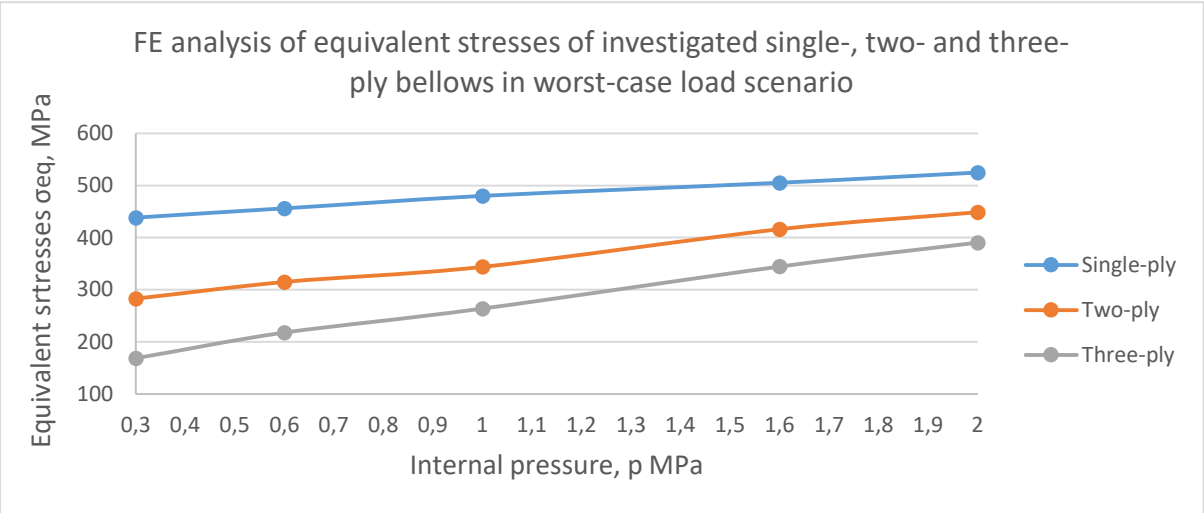

Figure 6.22: FE analysis of equivalent stresses of investigated single-, two- and three-ply bellows in worst-case load scenario

6.2.8 Comparing results of FE analysis, theoretical analysis with MatLab® and analysis of standard EN ISO 13445 Part 3

The single-, two- and three-ply bellows internal pressure FE analysis results were comparing to analysis with standard EN ISO 13445-3 [21] and theoretical analysis with MatLab® [5]. In Tables 6.13-6.15 presented result of different analysation methods.

Table 6.13: Comparing results of single-ply bellows FE analysis to analytical analysis of EN ISO 13445-3 [21] and theoretical analysis with MatLab® [5]

Single-ply bellows				
Internal pressure, *pi*				
Pressure, Class	Pressure, MPa	FE analysis, equivalent stresses σ_{eq}, MPa	Matlab® theoretical analysis, equivalent stresses σ_{eq}, MPa	EN ISO 13445-3, equivalent stresses σ_{eq}, MPa
PN 3	0,3	25,48	23,03	24,14
PN 6	0,6	50,97	46,05	49,29
PN 10	1,0	84,95	76,75	86,41
PN 16	1,6	121,03	122,80	122,79
ANSI 150	2,0	148,97	153,50	147,56

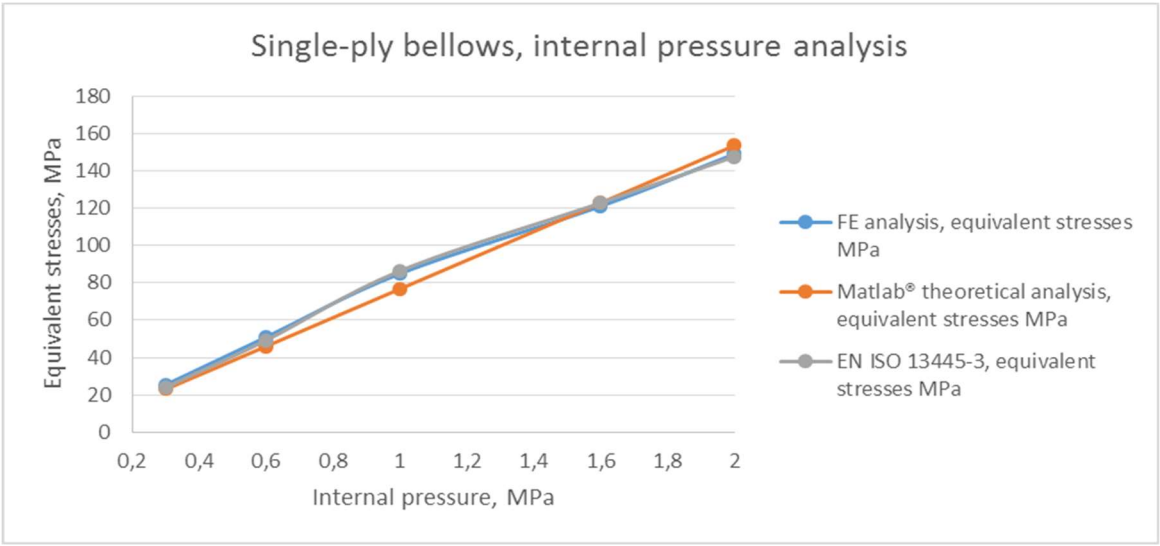

Figure 6.23: Comparing results of single-ply bellows resulting from FE analysis, analytical analysis of EN ISO 13445-3 [21] and theoretical analysis with MatLab®

Hence, on Figures 6.23-6.25 presented the comparing diagrams of internal pressure results of different analysation methods.

Table 6.14: Comparing results of two-ply bellows FE analysis to analytical analysis of EN ISO 13445-3 [21] and theoretical analysis with MatLab®

Two-ply bellows				
Internal pressure, *pi*				
Pressure, Class	Pressure, MPa	FE analysis, equivalent stresses σ_{eq} MPa	Matlab® theoretical analysis, equivalent stresses σ_{eq} MPa	EN ISO 13445-3, equivalent stresses σ_{eq} MPa
PN 3	0,3	61,50	46,05	63,58
PN 6	0,6	107,39	92,10	108,34
PN 10	1	149,03	153,50	151,32
PN 16	1,6	251,85	245,60	254,75
ANSI 150	2	298,68	307,01	293,28

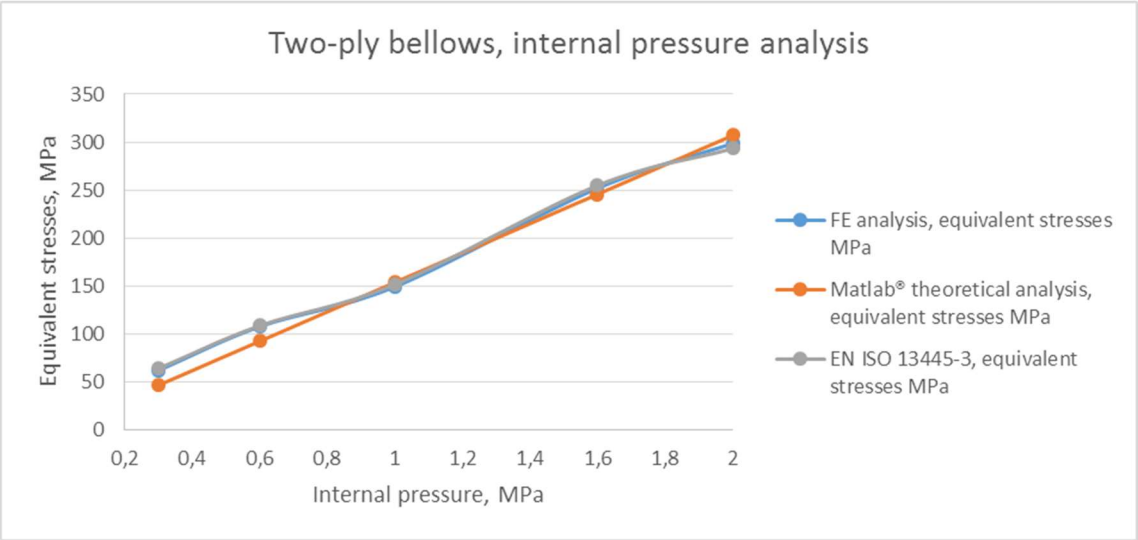

Figure 6.24: Comparing results of two-ply bellows resulting from FE analysis, analytical analysis of EN ISO 13445-3 [21] and theoretical analysis with MatLab®

Table 6.15: Comparing results of three-ply bellows FE analysis to analytical analysis of EN ISO 13445-3 [21] and theoretical analysis with MatLab®

Three-ply bellows				
Internal pressure, *pi*				
Pressure, Class	Pressure, MPa	FE analysis, equivalent stresses σ_{eq} MPa	Matlab theoretical analysis, equivalent stresses σ_{eq} MPa	EN ISO 13445, equivalent stresses σ_{eq} MPa
PN 3	0,3	82,86	69,08	80,85
PN 6	0,6	154,39	138,20	150,72
PN 10	1	219,03	230,30	216,63
PN 16	1,6	321,85	368,40	332,17
ANSI 150	2	398,68	460,50	397,68

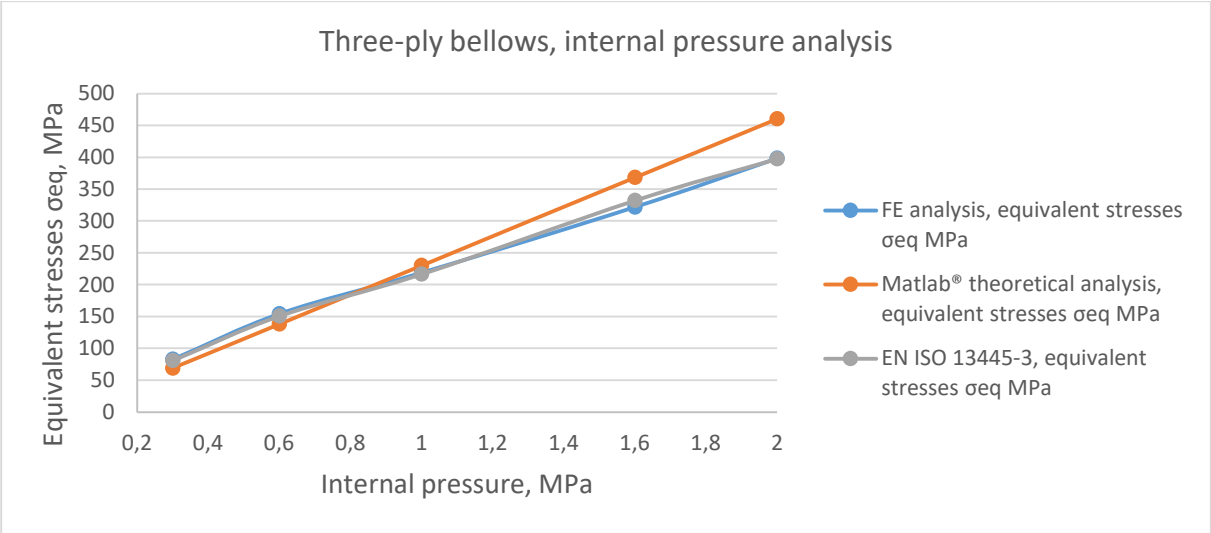

Figure 6.25: Comparing results of three-ply bellows resulting from FE analysis, analytical analysis of EN ISO 13445-3 [21] and theoretical analysis with MatLab®

Therefore, as it noticed from the diagrams (presented on Figures 6.23-6.25), the results for each investigated ply case of the bellows have differences of maximum 3 - 5 %. The results obtained by different analysation methods of investigated bellows designs, resulting from analytical analysis of standard EN 13445-3 [21] and FE analysis, proved the new theoretical analysation method with MatLab® [5] for single- and multi-ply bellows.

Moreover, the presented mathematical model with MatLab® [5] can be expand in further work for bending case of the bellows.

Hence, the presented mathematical analysis with MatLab® for internal pressure load case of bellows is the fast way to analyse, define geometry, dimensions, numbers of plies and corrugations for the single- and multi-ply metal bellows with U-shaped convolution cross section.

6.3 Determination of the limit loads for investigated two-ply bellows design

Consequently, to complete the study of investigated two-ply bellows design in frame of this doctor thesis for ball valve with RGM, it required to determine the limit loads. For this purpose, the investigated stainless steel stress-strain curve could be reduced to two areas, the namely elastic and plastic limit ranges of the material.

6.3.1 Determination of the elastic limit loads for two-ply bellows

The design elements that are subject to uniaxial stresses fail under static load, if the stress in the component reaches the yield point or limit strength. The design elements are usually subject to a multiaxial stress state during operation, e.g. caused by internal (operating) pressure, bending, thermal and compressive loads. However, there is a question, which load or combination of acting loads lead to a failure of design elements [20]. Therefore, to solve these tasks, the maximum distortion criterion theory [166] (von Mises yield criterion) is applied.

Hence, the multiaxial stress state could be converted into an equivalent uniaxial stress state σ_y. The fictitious uniaxial stress σ_y was analysed with the help of the maximum distortion criterion theory [166]. Then it was compared, analogously to the bar analysis, with the material characteristics that were determined in the uniaxial test (R_e , $R_{p0,2}$ and R_m), which is respectively equivalent stress σ_y [20].

The analysis of defined equivalent stress σ_v for investigated cross section critical points (areas) of bellows shell corrugation by FEA considered a line along shell thickness, which called the evaluation path [20]. The principle of this analysis detailed analysed in subchapter 6.2.4.

The path with length $\boldsymbol{e}$ is the smallest section between two sides of the investigated bellows shell (see Figure 6.26). Beyond the areas with global imperfections, the support section runs perpendicular to the central shell surface. For example, the cross section of cavity with path length (thickness $\boldsymbol{e}$) of the inner ply of the bellows investigated in this individual case, as the most critical area of the two-ply bellows with U-shaped convolution cross section.

6.3.2 Determination of the limiting internal pressure for investigated two-ply bellows

Initially, a maximum internal (operating) pressure was estimated as 2 MPa. The maximum equivalent stresses appeared in the internal ply of investigated two-ply bellows corrugations. To linearize the main stresses, the path on the cavity in the inner ply of investigated two-ply bellows corrugation cross section is considered (see Figure 6.26).

Therefore, the stress linearization at investigated critical point and under the following strength conditions, the elastic limit load can be determined as presented in equations (6.6 - 6.8).

Consequently, the stresses in the meridian direction linearized along the path, so that the three stress components were analysed. For instance, for the path in corrugation cross section of two-ply bellows obtained following results:

$$\sigma_m = 102{,}75\ \text{MPa} \leq \frac{R_{p0,2}(T = 500\ °C)}{S} = 170\ \text{MPa}$$

$$\sigma_m + \sigma_b = 195{,}91\ \text{MPa} \leq 1{,}5 * \frac{R_{p0,2}(T = 500\ °C)}{S} = 255\ \text{MPa}$$

$$\sigma_m + \sigma_b + \sigma_{nl} = 371{,}05\ \text{MPa} \leq 3 * \frac{R_{p0,2}(T = 500\ °C)}{S} = 510\ MPa$$

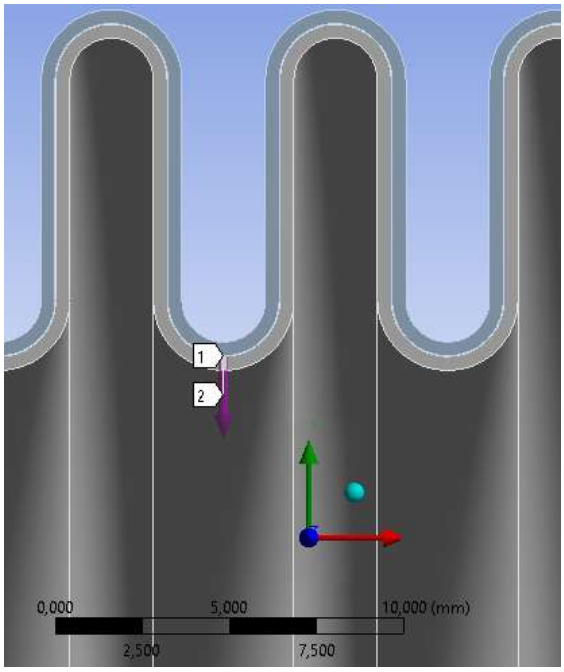

Figure 6.26: FE analysis of investigated path on the corrugation cross section of the inner ply of the two-ply bellows at the cavity section (most critical area)

Table 6.16: Elastic limit of investigated two-ply bellows loaded with internal pressure for stainless steel 1.4006 [147]

T, ° C	$R_{p0,2}$, MPa	Limit Pressure MPa	σ_m, MPa	$R_{p0,2}/S$, MPa	$\sigma_m + \sigma_b$, MPa	1,5· $R_{p0,2}/S$, MPa	$\sigma_m + \sigma_b + \sigma_{nl}$, MPa	3· $R_{p0,2}/S$, MPa
20	450	3,08	77,41	300	291,92	450	449,1	900
100	420	3,04	80,37	280	275,53	420	436,71	840
200	400	3,02	84,29	266,67	264,89	400	422,28	800
300	365	2,97	87,94	243,33	245,07	365	405,14	730
400	305	2,79	93,48	203,33	218,31	305	392,56	610
500	255	2,6	102,75	170	195,91	255	371,05	510

Hence, the FEA result, presented in Table 6.16, considered the second strength condition. It is almost not satisfied to defined safety factor S = 1,5 for 500 °C, instead it is 1.3 (which satisfied for high standards pressure vessels according to PED [106] and industrial valves [107]). Therefore, the pressure limit is 2,6 MPa for two-ply bellows with U-shaped convolution cross section at high temperature T = 500 °C and 3,08 MPa at room temperature T = 20 °C with safety factor S = 1,54, for stainless steel 1.4006 [147].

6.3.3 Determination of the plastic limit loads for investigated two-ply bellows

In case of increasing the load over elastic limit, it proceeds to the plastic deformation or yielding point of the material [168]. Plastic limit load is the load over which the material would lose its load capacity.

The design value RM_d of the strength characteristic of the material (design value of yield stress) will be determined as follows [167]:

$$RM_d = \frac{RM}{\gamma_R} \tag{6.11}$$

where, *RM* - characteristic value of the relevant strength index; γ_R - corresponding particular safety factor.

Hence, in case of determining the characteristic values of the strength characteristics *RM*, the specified minimum values used. For stainless steel 1.4006 [147] it was used γ_R =1,25 [21] for $\frac{R_{p0,2/T}}{R_{m/T}} \leq 0{,}8$.

Consequently, in case of using a bilinear kinematic material model [20], ANSYS® Workbench accepts into consideration of von Mises yield condition [166], therefore the design value of RM_d is further modified as $RM_{d,MISES}$:

$$RM_{d,ETS} = RM_d \cdot \frac{\sqrt{3}}{2} \tag{6.12}$$

The rated value A_d of the load considered by multi-plying the characteristic value *A* by the corresponding partial safety factor γ_A :

$$A_d = A \cdot \gamma_A \tag{6.13}$$

Hence, for internal pressure, bending and thermal influence model, the particular safety factor

γ_A was considered as 1,2.

The determination of the plastic limit load occurred in this way: a load, for example, internal pressure increased until the maximum plastic strain approaches 5%. In this case, the design value of the limit load $A_{d,max}$ is considered, and with the equation (6.13), the limit load A_{max} can be determined.

First, the design values RM_d and $RM_{d,MISES}$ considered as it presented in Table 6.17.

Table 6.17: Strength characteristics and their design values under investigated temperature range from 20 °C until 500 °C

Temperature, ° C	$R_{p1,0,T}$, MPa	RM_d, MPa	$RM_{d,MISES}$, MPa
20	515	412	356,8
100	483	386,4	334,63
200	460	368	318,7
300	415	332	287,52
400	350	280	242,48
500	293	234,4	202,99

For FE analysis assumed the material tangent module is 0,001 Pa. The stress-strain curves at different temperature ranges defined at engineering data of ANSYS® Workbench for stainless steel 1.4006 [149] as presented in Table 6.17.

The temperature for FE elastic-ideal-plastic material model for stainless steel 1.4006 [149] considered at 20 °C, 100 °C, 200 °C, 300 °C, 400 °C, 500 °C, while the internal pressure was oriented so that the maximum plastic strain is about 5 %.

Plastic limit loads for the case of internal pressure and maximum bending angle to 10 ° at investigated temperature range (worst-case scenario), occurred in the cavity of investigated two-ply bellows corrugations (see Figure 6.27).

During the FE analysis the fatigue life of investigated two-ply bellows, the stresses at the potential crack initiation point would established [5].

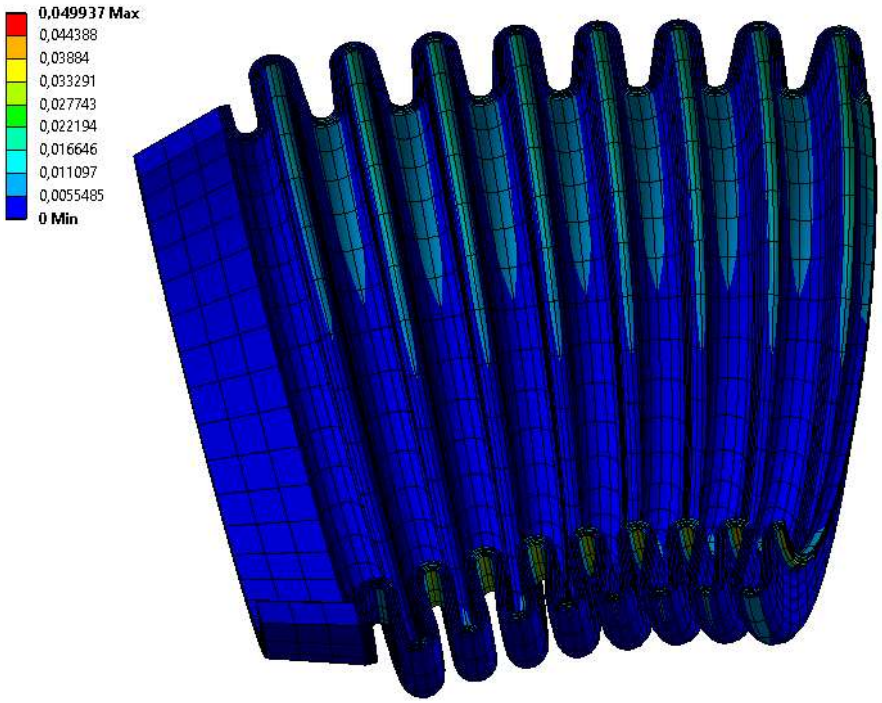

Figure 6.27: Plastic deformation (scale for strains [mm/mm]) of investigated two-ply bellows in the case of internal pressure 1,6 MPa, bending 10 ° and temperature range 200 °C.

Table 6.18: Plastic limit loads of investigated two-ply bellows for the case of load with internal pressure and maximum bending angle to 10 ° at investigated temperature range (worst-case scenario)

Temperature, ° C	$A_{d.max}$, MPa	Plastic strain, %	A_{max}, MPa
20	4,34	5,26	3,78
100	4,04	4,66	3,53
200	4,65	5,34	3,21
300	3,40	4,54	3,00
400	3,20	4,61	3283
500	3,03	4,48	2,67

Nevertheless, maximal plastic deformation occurred not only in the cavity, also in the crest of investigated two-ply bellows corrugation as well as in the middle vertical section.

The fatigue life analytical analysis considered in chapter 3. The fatigue curves and defined parameters such as $\sigma_{m,m}(p)$, $\sigma_{m,b}(p)$, $\sigma_{m,m}(\Delta q)$, and $\sigma_{m,b}(\Delta q)$ were analysed according to standard EN ISO 13445 Part 3 [21].

Consequently, the fatigue curves carried out and considered by FE analysis. Finally, the curves compared in chapter 7.

6.3.4 FE analysis of fatigue life of two-ply bellows in case of bending and temperature influence

As it described in the chapter 6.2.2, for investigated ball valve with ratchet gear mechanism considered two-ply bellows design due to its mechanical stability by high- and cryogenic-temperatures and by bending to an angle of 10 °. The fatigue life of the investigated two-ply bellows in only bending case to 10 ° and temperature range at 20 °C, 100 °C, 200 °C, 300 °C, 400 °C, 500 °C presented on Figure 6.28.

It defined as normal work conditions of the investigated two-ply bellows, when the bellows perform function in the conditions of bending and temperature influence. In this case, the stem of the ball valve is fully sealed and the internal pressure in the ball valve cross section does not influence to the chamber of the RGM. The diagram on Figure 6.28 presents the number of the cycles, which can achieve investigated bellows, depended to the angle of deflection and the temperature range at 20 °C, 100 °C, 200 °C, 300 °C, 400 °C, 500 °C.

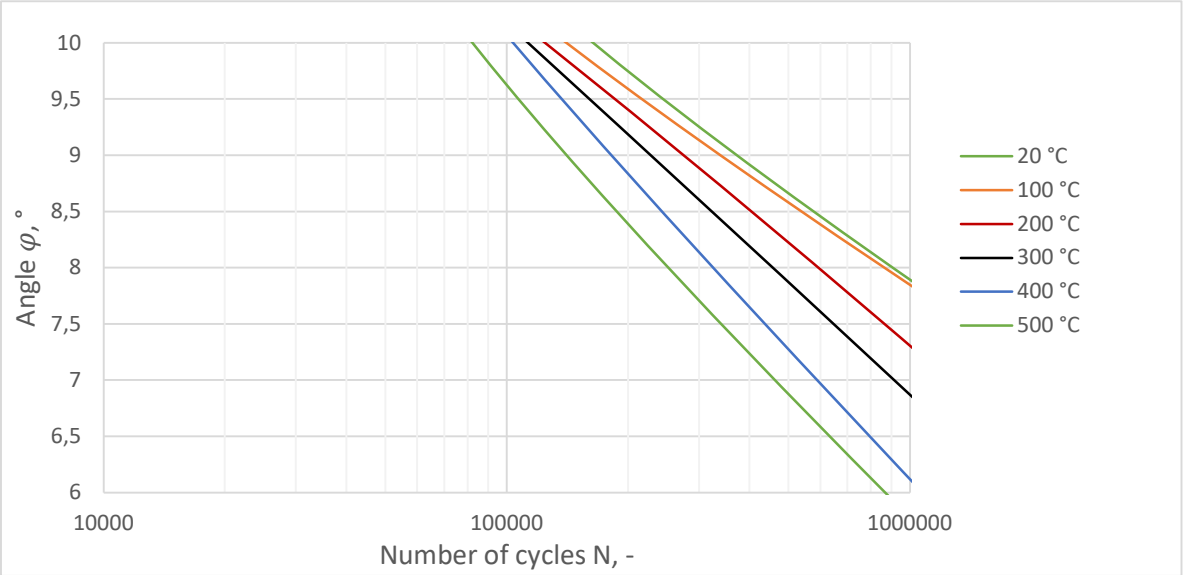

Figure 6.28: FE analysis of fatigue life of the investigated two-ply bellows in bending case of 10 ° and temperature range at 20 °C, 100 °C, 200 °C, 300 °C, 400 °C, 500 °C

The diagram on the Figure 6.28 considered that the maximum number of cycles of the investigated two-ply bellows during normal work conditions equal to 80.000-300.000 depending on the applying temperature. That equals approximately to 12.000 cycles of closing/opening of the ball valve cross section for nominal diameter of 100 mm [1], [4].

6.3.5 FE analysis of fatigue life at maximum load condition for investigated U-shaped bellows (worst-case scenario)

As it described in subchapter 6.3.4, the bellows operate under temperature influence and bending to an angle of 10 °, which described as normal operation condition.

Table 6.19: FE analysis of fatigue live of worst-case scenario of two-ply bellows for utility model ball valve with RGM [4]

		T, °C	Number cycle, N	Opening/closing cycles, N
PN 3	0,3 MPa	20	150300	10736
		100	124800	8914
		200	104345	7453
		300	89751	6411
		400	69538	4967
		500	41297	2950
PN 6	0,6 MPa	20	28500	2036
		100	24274	1734
		200	20523	1466
		300	17811	1272
		400	16094	1150
		500	10925	780
PN 10	1 MPa	20	8754	625
		100	7929	566
		200	6851	489
		300	5845	418
		400	4921	352
		500	2495	178
PN 16	1,6 MPa	20	2250	161
		100	1973	141
		200	1714	122
		300	1352	97
		400	1021	73
		500	780	56
API 6D	2 MPa	20	1755	125
Class 150		100	1318	94
		200	985	70
		300	798	57
		400	603	43
		500	450	32

Hence, in case of leakages of sealing components in stem package, the internal pressure increases in the chamber of the RGM housing, which leads to worst-case scenario with additional internal pressure loads. The bellows was designed and investigated to such working condition that all investigated loads appeared at the same time. Therefore, the FE analysis of fatigue life of worst-case scenario for investigated two-ply bellows presented on Figure 6.29. The maximal operating internal pressure is 2 MPa, according to specification for pipeline and piping valves API 6D [51] Class 150 and EN 1333 [63] PN 20, maximal bending angle is 10 ° and temperature range at 20 °C, 100 °C, 200 °C, 300 °C, 400 °C, 500 °C.

Hence, in the case of this operation condition (worst-case scenario), when the internal pressure reaches 2 MPa, according to specification for pipeline and piping valves API 6D [50] Class 150 and EN 1333 [63] PN 20, the fatigue life decry dramatically. The Table 6.19 presents the conclusion of FE analysis of fatigue life of the worst-case scenario of the investigated two-ply bellows for utility model ball valve with RGM [4].

The Table 6.19 presented that in maximal load conditions (worst-case scenario), the maximal possible number of cycles equal to 450, which considered as 32 fully closing/opening cycles of the investigated ball valve with nominal diameter of 100 mm.

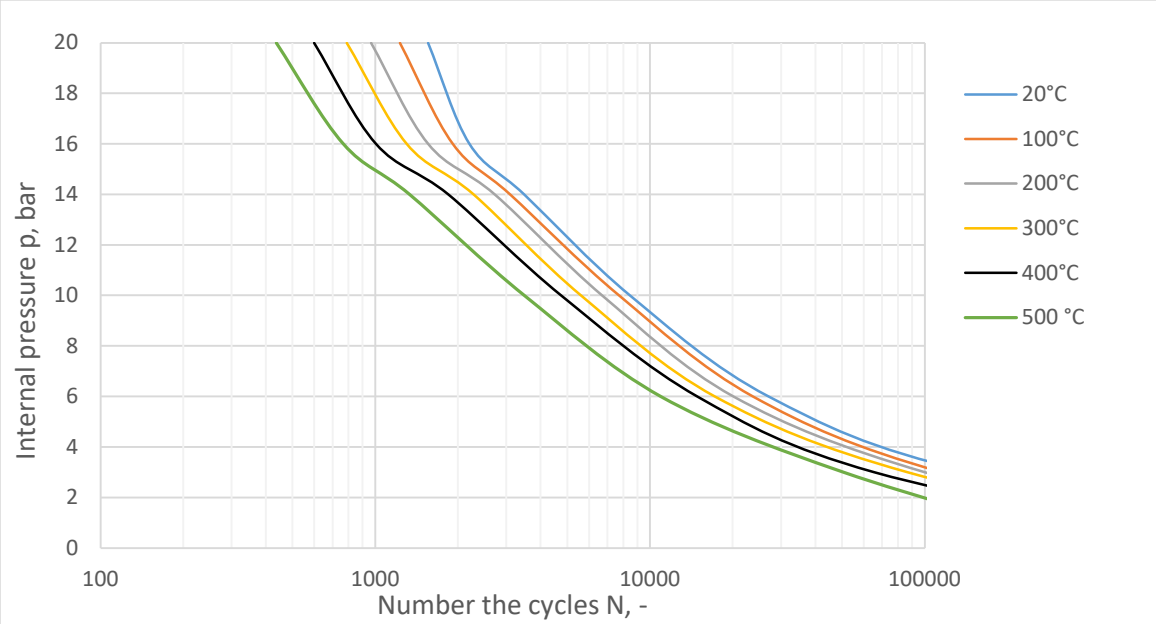

Figure 6.29: The worst-case scenario of the operation conditions of investigated two-ply bellows, at internal pressure of 2 MPa, bending angle of 10 ° and temperature range at 20 °C, 100 °C, 200 °C, 300 °C, 400 °C, 500 °C. FE analysis with Ansys® Workbench

In the case of nominal pressure 0,3 MPa, according to DIN EN ISO 1333 [63] and temperature of 500 °C the number of two-ply bellows cycles equal to 40.000, which consider 2860 fully

closing/opening cycles of the investigated ball valve with RGM and nominal diameter of 100 mm.

6.4 Conclusion of FE analysis with Ansys® Workbench

The first part of FE analysis of complex design of the RGM and it components such as ratchet wheels, pawls, housing, lever, single- and multi-ply bellows considered the analysis of equivalent stresses as well as critical areas of the mechanism. The critical components of RGM are bellows and gear wheel coupling (ratchet wheel and pawl). These two components were detailed analysed, moreover, it was determined the limit loads for these components, which helped to optimise and determine the dimensions of bellows, ratchet wheel, pawl.

Hence, it was deliberate the FEA optimization and detailed analysis for the design of RGM and ball valves for investigated nominal diameters and different pressure classes according to specification for pipeline and piping valves API 6D [51] and EN 1333 [63]. As it mentioned before, the constructive elements were comprehensive analysed with FEA, consequently, the ratchet gear coupling, housing in chapter 3; single-, and multi-ply bellows in chapter 6.

Second part of FEA represented the detailed analysis of investigated single- and multi-ply bellows critical areas under investigated loads. Consequently, these critical areas were comprehensive analysed with Ansys® Workbench FE analysis tools, which considered the limit loads of the design structure of the investigated bellows for each load case as well as for combination of the investigated loads such as internal pressure, bending and temperature influence. In addition, it considered the fatigue life of investigated two-ply bellows for normal operation condition and for worst-case scenario (maximal operation loads).

Finally, investigated two-ply bellows with U-shaped convolution cross section due to its structure performance, the valuable thickness of each individual ply and multi-ply design, provide excellent properties to withstand maximum load operation condition, which appear in investigated system during exploitation.

7. Conclusions and discussion

7.1 Conclusion of investigation of utility model ball valve with ratchet gear mechanism

The utility model № 139949 ball valve with a ratchet gear mechanism and bellows [4] was comprehensive analysed in presented doctor thesis. The investigated RGM presents a new method of solving the sealing problem of the ball valves (as well as for valves utility model № 107836 Valve 29.03.2011 [2] and utility model № 123877 Valve with bellows 10.01.2013 [3]) due to its unique design, the constructive components of RGM connected by welding (instead, for example, flanges or bolting connection). The stem of the ball valve fully sealed by welding connection between ball valve body and housing of the ratchet gear mechanism, instead of flanges or stem gland packing with O-rings and polymer sealant components. Depending on the design, the stem additionally sealed with graphite rings to withstand high temperatures up to 500 °C.

Hence, utility model № 139949 ball valve with the ratchet gear mechanism and bellows [4] designed according to DIN EN 1983 [108], EN ISO 13445-3 [21], DIN EN 12516 [107] and specification for pipeline and piping valves API 6D [50] of nominal diameter 100 mm, 150 mm, 200 mm and 300 mm. The dimensions of the ball valve, such as housing, ball, seats, and stem were also analysed. They were considered on behalf of ball valve designs of company Boehmer Ltd. [88] with nominal diameter of 100 mm, 150 mm, 200 mm, 300 mm. For investigated nominal diameters of the ball valves, there were applied the dimensions of the ratchet gear mechanism with two-ply bellows and its design elements. The investigated design elements were comprehensive analysed in chapter 3. The investigated ball valve with RGM [4] cannot be applied for larger nominal diameters due to the gear ratio of the ratchet mechanism and the dimensions of the investigated bellows. Therefore maximal applied diameter of investigated ball valve with the ratchet gear mechanism is 300 mm (DN 300) the minimal applied diameter is 100 mm (DN 100) according to DIN EN 1983 [108], EN ISO 13445-3 [21], DIN EN 12516 [107] and specification for pipeline and piping valves API 6D [50].

The investigated ball valve with RGM [4] can be applied in many industrial application cases, such as high and cryogenic temperatures, implementation with wide spectrum of different liquids, corrosive and toxic. In addition, it covers different pressure classes according to standards EN ISO 13445-3 [21], DIN EN 12516 [107], EN ISO 1333 [63] and specification for pipeline and piping valves API 6D [51]. The practical application of investigated ball valve

with RGM [4] can find in hydrogen sector due to unique and full welded design (see chapter 2.2.1.1).

The bellows considered as weakest design component of the ball valve with ratchet gear mechanism [4] due to it complex geometry and unique loading and fixing position on the RGM housing. Therefore, it was difficult to analyse bellows analytically using EN ISO 13445 Part 3 [21] or EJMA [60] standards (see chapter 3). For analytical analysis was created a new mathematical method of bellows calculation, which consider the most loaded areas of single- and multi-ply bellows with U-shaped convolution cross section (chapter 4). The new mathematical model depended on the Clark's theory of the thin toroidal shells [25].

To validate results of new mathematical method it is provided a detailed FE analysis of single- and multi-ply bellows, which presented in chapter 6. In addition, the results of new mathematical model were validated to laboratory experiment results of two-ply bellows (see chapter 5).

Depending on the operation case of investigated single- and multi-ply bellows, it considered the limit loads for ratchet gear mechanism, which detailed analysed in chapters 3 and 6.

7.2 Validation of the constructive elements of investigated ball valve with RGM

The validation of the constructive components of investigated ball valve with RGM resulting from analytical analysis with EN ISO 13445 Part 3 [21] and detailed FE analysis. The analytical validation done according to EN ISO 13445 Part 3 [21] of ratchet wheel, pawl, lever, rod end bearing, and housing (see Attachment B, sections B.2.1-B.2.7). The verification done with FE analysis of these components. The FEA provided examination of the critical areas of the design elements and more accurate results due to fine mesh, and possibilities to simulate real element geometry (see Chapter 3 and 6). During validation was concluded the minimum safety factor S = 1,5 for design elements of ball valve with RGM and S = 1,3 for investigated two-ply bellows with U-shaped convolution cross section in worst-case scenario (maximum operation load condition).

7.3 Validation of investigated two-ply bellows with U-shaped convolution cross section

The validation required representation of the fatigue life of two-ply bellows with U-shaped convolution cross section as a function of internal pressure, bending and temperature influence.

It concluded that service life decreases with increasing internal pressure, and temperature. Also, it depends on number of bending cycles, i. e. how many times the bellows can be bent with assumed maximum bending angle or how many opening/closing cycles investigated bellows can remain. As an assumption for validation of the results is that the bending during the operation of the two-ply bellows remain constant with maximal bending angle of 10 °. Due to EN ISO 13445 Part 2 [116], EN ISO 10088-3 [147] and EN ISO 10088-2 [149] the materials properties of stainless steels 1.4571 and 1.4006 do not change in cryogenic temperatures ranges. Therefore, it required no analysis in cryogenic temperatures ranges. Nevertheless, it significantly changes at high temperature rates.

In the case of considered bending model, the oscillating cycles of the two-ply bellows had ensured a longer fatigue life in low-pressure range and low-temperature range. The influence of different internal pressure classes, analysed according to standards EN ISO 13445-3 [21], DIN EN 12516 [107], EN ISO 1333 [63] and specification for pipeline and piping valves API 6D [51].

Consequently, in high pressure and high-temperature ranges, the two-ply bellows had an acceptable fatigue life for design of ball valve with RGM [4] (see Figure 7.1, Figure 6.29 and Table 6.18).

The validation of fatigue life resulting from FE analysis and analytical analysis with standard EN ISO 13445 Part 3 [21] presented on Figure 7.1.

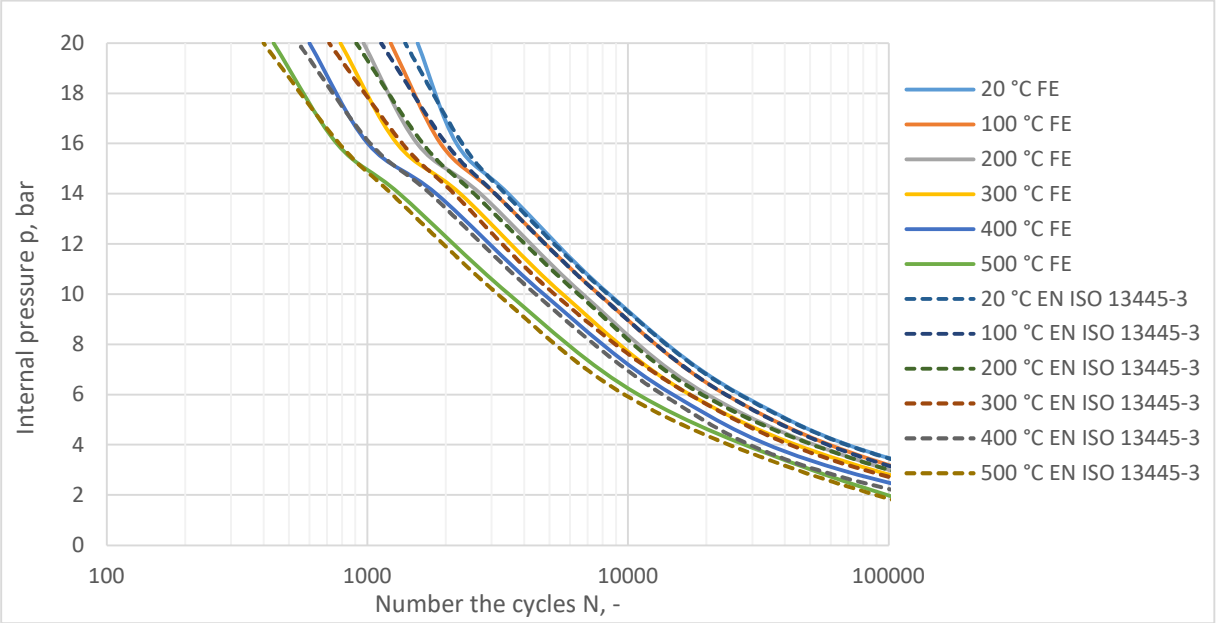

Figure 7.1: Validation of fatigue live resulting from FE analysis and analytical analysis with standard EN ISO 13445 Part 3 [21] for two-ply bellows with U-shaped convolution cross section

After validation of fatigue life, it concluded that the fatigue lifetime of FE analysis is 5 - 7 % higher than that analysed by the standard EN ISO 13445 Part 3 [21]. There are some possible reasons for these criteria.

Hence, as it defined in chapters 3 and 6, investigated two-ply bellows in case of FE analysis resulting from lower equivalent stresses, than according to analytical analysis with the standard. It explained that FEA provided examination of the critical areas of the design elements and more accurate results due to fine mesh, and possibilities to simulate close to real two-ply bellows geometry with imperfections. However, at analytical analysis affect many coefficients, which feature small deviation in results.

7.4 Verification of new mathematical analysis method of the single- and multi-ply bellows with U-shaped convolution cross section depended on the Clarks theory

The main objective of developing an analysis of ball valve with RGM has been achieved. That enable the identification and analysation of constructive elements of ball valve and RGM, as well as single- and multi-ply bellows limit loads, equivalent stresses at critical areas and fatigue life.

For example, most critical constructive element of the ball valve with RGM [4], the single- and multi-ply bellows with U-shaped convolution cross section analysed for different load cases such as internal pressure, bending and temperature influence according to the standard EN ISO 13445 Part 3 [21], subsequently, the corresponding critical areas comprehensive analysed by FEA with Ansys® Workbench software. Depended on these validation methods, the limit loads as well as fatigue life of the single- and multi-ply bellows were determined.

However, considered analysis of investigated single- and multi-ply bellows with U-shaped convolution cross is difficult and long procedure. For significantly reduction of computational efforts and more accurate analysation of the single- and multi-ply bellows was developed new mathematical method depended on the Clarks theory (see chapter 4).

The new modified mathematical method, based on Clark's theory of thin toroidal shells [25], analyse the equivalent stresses of single-and multi-ply bellows with U-shaped convolution cross section at any points of its defined geometry and the critical areas of corrugations, accordingly at the cavity, crest, and side wall (shell) section with the internal pressure load case.

In addition, the new mathematical method was validated and confirmed by laboratory

experiments (chapter 5), analytical analysis with the standards EN ISO 13445 Part 3 [21], EJMA [60] (chapter 3) and FE analysis (chapter 6).

Hence, further development of the new calculation method will provide significantly reduction of computational efforts and more accurate analysation possibilities compare to existing analysis methods (such as EN ISO 13445 Part 3 [21] and EJMA [60]). For instance, it could consider the influence of production-related factors, such as welding or specific material behaviour due to remaining stresses.

Bibliography

[1] Ivanov, V., Oleynikov, A., Deniseevich, D.: Emergency Shut-Off Valve for Pipelines. *Chemical and Petroleum Engineering*. 49 (2013), 5-6 (September), pp. 400-402.

[2] Oleynikov, A., Ivanov, V.: *Valve* – Utility Model № 107836. *Eurasian Patent Organisation,* 29.03.2011.

[3] Oleynikov, A., Ivanov, V.: *Valve with a bellows* - Utility Model № 123877. *Eurasian Patent Organisation,* 10.01.2013.

[4] Oleynikov, A., Ivanov, V.: *Ball valve with a ratchet gear and bellows* - Utility Model № 139949. *Eurasian Patent Organisation,* 03.27.2014.

[5] Oleynikov, A., Merten, C.: *Numerical Investigations of U-Shaped Metal Expansion Bellows for Fully Welded Ball Valves - CADFEM Conference,* 5.10.2018, Leipzig.

[6] Oleynikov, A., Merten, C.: *Numerical and Experimental Investigations of Geometrical Properties of U-Shaped Metal Expansion Bellows for Fully Welded Ball Valves*. *CHISA 2018 Conference*, 25-29. 08.2018, Prague.

[7] Zhu, Z., Wang, H., Sang, Y.: *The effect of environmental medium on fatigue live for U-shaped bellows expansion joint*. *International Journal of fatigue*, pp. 28-32, 2006

[8] Witzenmann GmbH. *Handbuch der Kompensatoren*, November 2012.

[9] Emiflex SPA. *EXPANSION JOINTS*, January 2014.

[10] Spiroflex. Design and manufacturing of metal bellows, expansion joints and flexible hoses. *Special application of metal bellows. Metal sealing bellows for valves.* URL: *http://www.spiroflex.hr/spezielle-verwendung-der-metallkompensatoren* (Version 12.10.2017).

[11] Richter Pumps & Valves Inc.*: Control valve.* URL: *https://www.richter-ct.com/control-valves/hv* (Version 22.06.2020).

[12] Anderson, W.: *Analysis of stresses in bellows*. Canoga Park, California: Atomics International, 15.10.1964.

[13] Richter Chemie-Technik GmbH. *Richter Chemie Regelventile*, Februar 2016.

[14] Witzenmann Ltd. *Handbuch der Metallbälge*, Januar 2010.

[15] BOA: Holding GmbH. Kompensatoren. URL: *http://www.boagroup.com/de/produkte/industrie-produkte/kompensatoren.html* (Version 11.11.2019).

[16] HKS Unternehmensgruppe. ERV-Gummikompensatoren und PTFE-Kompensatoren. URL: *http://www.hks-kompensatoren.de/Gummikompensatoren.40.html* (Version

11.10.2017).

[17] Stenflex Ltd. Stahl Kompensatoren. URL: *http://www.stenflex.com/de/produkte/stahl-kompensatoren.php* (Version 12.10.2017).

[18] Overhoff Verbindungstechnik GmbH. Legierungselemente: Einfluss der Legierung auf Stahl. URL: *https://www.overhoff.de/Daten/Legierungselemente.pdf* (Version 11.10.2017).

[19] Metallschlauchfabrik Pforzheim Unternehmensarchiv Witzenmann GmbH. Biegebalken geteilt Skizze. URL: *https://commons.wikimedia.org/wiki/-Category:Bending_of_beams#/media/File:Biegebalgen_geteilt.tif* (Version12.10.2017)

[20] Gebhardt, C.: *Praxisbuch FEM mit ANSYS Workbench: Einführung in die lineare und nichtlineare Mechanik*. Carl Hanser Verlag GmbH & Co. KG, 13.01.2011.

[21] ISO EN 13445: *Unfired pressure vessels – Part 3: Design,* 05.2018.

[22] Structural stress. *Introduction to PV Design by Analysis* URL: *http://personal.strath.ac.uk/j.wood/CCOPPS_DBA/Notes/dba_intro_content_1.htm* (Version 12.10.2017).

[23] Basar, Y., Itskov, M., Eckstein, A.: *Composite laminates: nonlinear interlaminar stress analysis by multi-layer shell elements. Computer Methods in Applied Mechanics and Engineering*, 26.03.1999.

[24] Läpple, V.: *Einführung in die Festigkeitslehre*. Springer Vieweg, 2016.

[25] Clark, R. A.: On the theory of thin elastic toroidal shells. *Journal of mathematics and physics*, 1950.

[26] Narasimham, S., Paliwal, D., Upadhyaya, A.: Stress analysis of v-shaped expansion joints under internal pressure. *International Journal of Pressure Vessels and Piping*, 01.05.1996.

[27] Harvard Computional Laboratory. *Tables of the Modified Hankel Functions of Order One-Third and their Derivatives*. Cambrigde, Mass., Harvard University Press, 1945.

[28] Vick, M., Gramoll, K.: Finite element study on the optimization of an orthotropic composite toroidal shell. *Journal of Pressure Vessel Technology*, 27.08.2012.

[29] Transport von gasförmigem Wasserstoff via Pipelines. *Mannesmann Line Pipe Ltd*., 2018.

[30] API 5L: *Specification for Line Pipe*, *American Petroleum Institute*, 46th edition, 04.2018.

[31] Gräfen, H., Pöpperling, R., Schlecker, H., Schlerkmann, H., Schwenk, W.: Zur Frage der Schädigung von Hochdruckleitungen durch Wasserstoff und wasserstoffhaltige

Gasgemische. *Gas Erdgas gwf*. 130, pp. 16-21, 1989.

[32] Kußmaul, K., Deimel, P., Sattler, E., Fischer, H.: *Einfluss von Wasserstoff auf ausgewählte Werkstoffe für den Einsatz bei Transport und Speicherung von Wasserstoff. In: Wasserstoff als Energieträger:* SFB 270 Universität Stuttgart, Abschlussbericht 1998.

[33] Xu, K., Rana, M.: *Tensile and Fracture Properties of Carbon and Low Alloy Steels in High Pressure Hydrogen. In: Effects of Hydrogen on Materials. Proceedings of the 2008 International Hydrogen Conference, B. Somerday, P. Sofronis, R. Jones (Ed.)*, (2009), pp. 349-356.

[34] Briottet, L., Moro, I., Lemoine, P.: *Quantifying the hydrogen embrittlement of pipeline steels for safety considerations. International Journal of Hydrogen Energy*, pp. 17616-17623, 2012.

[35] Savannah River National Laboratory: *Management of leaks in hydrogen production, delivery, and storage systems*. G. B. Rawls, 2006.

[36] Brogioli, D., Vailati, A.: *Diffusive mass transfer by no equilibrium fluctuations: Fick's law revisited. Phys. Rev. E*. 63 (1–4). 2001.

[37] Wurster, R., Schmidthchen, U.: *Wasserstoff Sicherheit Kompendium*, *DWV*, 2011

[38] Tröger, M., Bosch, C., Brauer, H.: *Untersuchungen zur Beständigkeit hochfester HFI-geschweißter Rohre für den Wasserstofftransport*. *Oldenburger Rohrleitungsforum*, pp. 40-45, 2014.

[39] Brauer, H., Simm, M., Wanzenberg, E., Henel, M.: *Transport von gasförmigem Wasserstoff via Pipelines? Aber sicher! H2 by Mannesmann*. 3R, Ausgabe10-11, 2018.

[40] Brauer, H., Simm, M., Wanzenberg, E., Henel, M.: *Wasserstoff im Erdgasnetz sicher transportieren. Forschungsvorhaben. H2-PIMS*, Ausgabe 03.2019.

[41] Wasserstoff. Diffusion und Versprödung: URL: *Wasserstoff | enXpress (energienovum.de)*. (Version 21.10.2019).

[42] Geitmann, S.: Wirkung von Wasserstoff auf Werkstoffe. 2nd September 2019. URL: *Wirkung von Wasserstoff auf Werkstoffe (hzwei.info)* (Version 19.11.2019).

[43] Benac, D., McAndrew, P.: *Reduction the risk of High Temperature hydrogen Attack (HTHA) Failures. Journal of Failure Analysis and Prevention*, volume 12, pp. 624-627, 14 August 2012.

[44] EIGA Richtlinie IGC Doc 121/14: *Hydrogen pipeline systems*, 2014.

[45] Nederlandse Gasunie: *Hydrogen gas in pipelines, CEN TC 234 WG 3*, 22nd January 2019.

[46] ASME B31.12. *Hydrogen piping and pipelines*, 2014.

[47] DIN EN ISO 3183: *Petroleum and natural gas industries – Steel pipe for pipeline transportation systems*, 09.2018.

[48] DIN EN 1993: Bemessung und Konstruktion von Stahlbauten. Teil 1-6. *Festigkeit und Stabilität von Schalen*, 2017.

[49] Briottet, L., Moro, I., Lemoine, P.: Quantifying the hydrogen embrittlement of pipe steels for safety considerations, *4th International Conference on Hydrogen Safety*, San Francisco, 2011.

[50] Fergin, M., Dr.-Ing. Radisch, W.: *Prüfbericht für BBF Kugelhahn DN 150 PN 40* (Infraserv-Begutachtung), Boehmer GmbH, 15 Mai 2019.

[51] API 6D/ ISO 14313: *Specification for pipeline and piping valves*, 10.2015.

[52] NACE Standard MR0175: *Sulfide Stress Cracking Resistant Metallic Materials for Oilfield Equipment*, *Standard Material Requirements*, 08.2017.

[53] ASME B16.34: *Valves – Flanged, Threaded, and Welding Ends, an American National Standard*, 2013.

[54] Gebhardt, C.: Praxisbuch FEM mit ANSYS Workbench: *Einführung in die lineare und nichtlineare Mechanik*, 2014.

[55] RBS Kompensator GmbH: Metallkompensatoren und Metallbälge. URL: *https://www.rbs-kompensator.at/de/produkte/metallkompensatoren/* (Version 14.07.2020).

[56] Flexomat GmbH: Lateralkompensator mit Zuganker und Kugelgelenken zur Aufnahme von allseitigen lateralen Bewegungen. URL: *https://www.flexomat.de/de/anwendungen/rohrleitungstechnik/* (Version 14.07.2019).

[57] Reissner, E.: *On the theory of thin elastic shells, Reissner Anniversary Volume: Contributions to Applied Mechanics*, p. 231-247, ANN Arbor, Erdwards 1949.

[58] Narasasimham, S.: *Stress analysis of V-shaped expansion joint under internal pressure. International Journal of pressure vessels and piping 71*, pp. 35-45, 1997.

[59] Krovvidi, K.: *Design and analysis of formed bellows for nuclear applications, 2nd International conference on Structural Integrity and Exibition 2018, Process Structual Integrity 14,* pp. 855-863, 2019.

[60] EJMA: *Standards of Expansion Joint Manufactures Association*, 10th Edition, 2015

[61] RCC-MR Section-I, *Design and construction rules for mechanical components of nuclear installations for high temperature structures*, Subsection-B, 2007.

[62] Sotoodeh, K.: *The importance of maximum allowable stem torque in valves. SN applied*

Science, 9 April 2019.

[63] EN 1333: *Flansche und ihre Verbindungen, Rohrleitungsteile*, *Definition und Auswahl von PN*; 2006.

[64] Finite Element Analysis of Braided Corrugated Hoses with Multiple Layers of Individual Braid Wires Using an ANSYS Implicit Solver, URL: *https://www.ansys.com/-/media/ansys/corporate/resourcelibrary/whitepaper/wp-braided-corrugated-hose.pdf* (Version 09.05.2020).

[65] Laupa, A., Weil, N.: *Analysis of U-Shaped Expansion Joints*. *ASME. J. Appl. Mech*. 1962; 29 (1):115-123. doi:10.1115/1.3636442.

[66] Rial, D., Tiar, A., Hocine, K., Roelandt, J., Wintrebert, E.: *Metallic Braided Structures: The Mechanical Modeling. Adv. Eng. Mater., 17*: p. 893-904, 2015.

[67] US Hose Corporation: *Engineering Guide No. 350, 8th Edition, Flexible Metallic Hose, Braid and Assemblies*. pp. 6-8, 2018.

[68] Material data sheet 1.4571: *Deutsche Edelstahlwerke, Nichtrostender Austenitischer Stahl.* 12.2015.

[69] Normal Approximation to Poisson distribution, *Stat.ucla.edu. Retrieved*, March 3th 2017.

[70] Distance of Two Normal (Gaussian) Probability Distributions, Allisons.org. December 5th 2007.

[71] Jordan, M.: *Bayesian Modelling and Inference. The Conjugate Prior for the Normal Distribution.* February 8th 2010.

[72] Knyazev, B., Cherkaskiy, V.: *The beginnings of processing experimental data.* Novosibirsk, 1996. – Б. Князев, В. Черкаский: *Начало обработки экспериментальных данных*. Новосибирск, 1996.

[73] Ansys® Help, Ansys Mechanical APDL, Workbench. Reference. Ansys, Inc. 2011.

[74] Wang, Y.: FEM *Simulationen von mehrlagigen Kompensatoren und deren Validierung*, *Master Thesis*. University of Stuttgart, 2019.

[75] Ninzeko, L.: *Load analysis of a gear mechanism for a ball valve test setup, Master Thesis*. University of Stuttgart, 2019.

[76] Konstantin, M.: *Neue Berechnungsmethode für mehrschichtige Kompensatoren und deren Verifikation anhand von Experimenten und Simulationen, Bachelor Thesis*. University of Stuttgart, 2017.

[77] EN ISO 3990: *Calculation of load capacity of cylindrical gear, introduction and general influence factors,* 2019.

[78] Andreeva, L., Beseda, A.: *Bellows. Calculation and design. Moscow: machine engineering*, 1975 - 156 pp. – Л. Андреева, А. Беседа. *Сильфоны. Расчет и проектирование. Москва: машиностроение*, 1975 г. – 156 с.

[79] Oleynikov, A., Ivanov, V.: *Emergency gate valve for main pipelines, Technical sciences - from theory to practice*. Proc. XVIII International scientific conf. (Novosibirsk, February 20, 2013) / NP "Siberian Association of Consultants (SibAC)". Novosibirsk. pp. 39-45, 2013. – Олейников А.В., Иванов В.В.: *Задвижка аварийного назначения для магистральных трубопроводов, Технические науки – от теории к практике*. матер. XVIII междунар. заоч. науч.-практ. конф. (г. Новосибирск, 20 февр. 2013 г.) / НП «Сибирская ассоциация консультантов (СибАК)». - Новосибирск, 2013. - С. 39-45.

[80] Oleynikov, A., Ivanov, V.: *Emergency gate valve for pipelines, Mashinostroitel.* - 2014. № 3. pp. 24-27. – Олейников А.В., Иванов В.В., *Шиберная задвижка аварийного назначения для трубопроводов, Машиностроитель*. - 2014. - № 3. - С. 24-27.

[81] Oleynikov, A., Ivanov, V.: *Emergency gate valve for main pipelines. Proceedings of VolgGTU*. Series "Rheology, processes and devices of chemical technologies". Vol. 7 : interuniversity collection of scientific papers. VolgGTU. Volgograd, 2014. № 1 (128). pp. 66-69. – Олейников, А.В. Иванов В.В.: *Шиберная задвижка для магистральных трубопроводов. Известия ВолгГТУ.* Серия «Реология, процессы и аппараты химической технологии». Вып. 7 : межвуз. сб. науч. ст. ВолгГТУ. Волгоград, 2014. № 1 (128). С. 66-69.

[82] Richter pumps and valves Inc. Control valve with bellows. URL: *https://pdf.directindustry.com/pdf/richter-chemie-technik/bellows-sealed-shut-off-control-valves/20616-721931-_3.html* (Version 22.06.2020).

[83] JCS Valve Manufacture. Knife gate valve. URL: *http://www.jcs-valve.com/productlist/list-104-1.html?gclid=CjwKCAjw3cSSBhBGEiwAVII0Z-crykE-lvWOZzcoZTFhazebXub9ul0Yc3bd8QaY44mCbZcjognoxxoC0B8QAvD_BwE* (Version 09.04.2022).

[84] AWK Valves Co. Ltd. Wedge gate valve. URL: *https://www.avkchina.com/en/product-finder/gate-valves/resilient-seated-gate-valves/21-46-001* (Version 22.06.2020).

[85] Schlumberger Ltd. Cameron T30 series fully welded ball valve. URL: *https://www.products.slb.com/valves/ball-valves/cameron-t30-series-fully-welded-ball-valve?webSyncID=e395594c-763e-7884-9b65-bc90ab29d045&-session-GUID=2c2dc984-5770-a551-6c33-847aa83de1d9* (Version 22.06.2020).

[86] Kaehle Ltd. Saunders straight through Type KB, Diaphragm valve. URL: *https://www.armaturen-schulte.de/en/diaphragm-valves-type-kb* (Version 22.06.2020).

[87] Buerkert Ltd. Fluid control systems. Butterfly valve. URL: *https://www.burkert.com/en/type/2671* (Version 22.06.2020).

[88] Boehmer Ltd. Ball valve designs. URL: *http://www.boehmer.de/en/applications/* (Version 22.06.2020).

[89] Global supply line: Total valve and actuator project solutions. Explosive decompression of the O-rings in trunnion ball valves. URL: *https://globalsupplyline.com.au/blog-post/explosive-decompression-of-o-rings-in-trunnion-ball-valves/* (Version 22.06.2020).

[90] HBM Ltd. Stain gages: The first choise for your strain measurement. URL: *https://www.hbm.com/de/0014/dehnungsmessstreifen-/?gclid=CjwKCAjwltH3BRB6EiwAhj0IUClZqbf4Bd6U_BZ_Z9NXq23krZdqxoqcgEqY8gn9RD2xYFKC9hogCxoCHPoQAvD_BwE* (Version 22.06.2020).

[91] Hoffman, K.: *Eine Einführung in die Messung mit Dehnungsmessstreifen.* Strain gauges (HBM). pp. 289. 1989.

[92] Gantner Instruments. URL: *https://www.gantner-instruments.com/blog/strain-gauge-rosettes-with-gantner-instruments/* (Version 22.06.2020).

[93] Witzenmann Hydra. *BE 356230-bb 68 bellows*. URL: *https://online.flippingbook.com/view/267448/8/* (Version 22.06.2020).

[94] Calvert, J., Farrar, R.: *Hooke's law. An Engineering Data Book*. Chapter 13-1. 2019.

[95] Butser Rubber Ltd. Rubber bellows. URL: *https://www.butserrubber.com/products/rubber-bellow/* (Version 22.06.2020).

[96] Belman Ltd. Expansion joints, bellows: *https://www.belman.com/project/what-is-an-expansion-joint/* (Version 22.06.2020)

[97] Hartmann Ltd. Wasserstoff Kugelhahn URL: *https://www.hartmann-valves.com/ zh-hans/blog/2018/07/13/wasserstoff-kugelhahn-fda-konform-und-rein-metallisch-dichtend/* (Version 15.09.2020)

[98] Samson Ltd. High temperature ceramic floating ball valve. URL: *https://www.samsoncontrols.com/product/kst-ht-ceramic-lined-floating-ball-valve-high-temp* (Version 15.09.2020)

[99] Richer Process Pumps & Valve Ltd. KNR. Heavy duty control ball valve, Bellows Sealed. URL: *https://www.richter-ct.com/ball-valves/knr* (Version 21.09.2020)

[100] Market and Market TM. Strategic insights. Global valve market analyzation. URL:

https://www.marketsandmarkets.com/Market-Reports/industrial-valve-market-256097136.html (Version 21.09.2020)

[101] Allied Market research. Global industrial valve market. URL: *https://www.alliedmarketresearch.com/industrial-valves-market#:~:text=The%20global%20industrial%20valves%20market,liquids%2C%20vapors%2C%20and%20others.* (Version 21.09.2020)

[102] Industrial valve market. URL: *https://www.mordorintelligence.com/industry-reports/industrial-valves-market* (Version 21.09.2020)

[103] Global valve demand. URL: *https://www.globenewswire.com/news-release/2020/01/22/1973503/0/en/Global-Industrial-Valve-Market-is-Expected-to-Reach-USD-93-79-Billion-by-2026-Fior-Markets.html* (Version 21.09.2020)

[104] Industrial valve market. URL: *https://www.grandviewresearch.com/industry-analysis/industrial-valves-market* (Version 21.09.2020)

[105] NIKOCHEM Group. URL: *https://www.kaustik.ru/en/index.php/about/about-nikochem-group* (Version 21.09.2020)

[106] 2014/68/EU: *Richtlinie des Europäischen Parlaments und des Rates vom 15. Mai 2014 zur Harmonisierung der Rechtsvorschriften der Mitgliedstaaten über die Bereitstellung von Druckgeräten auf dem Markt*. 05.2014.

[107] DIN EN 12516: *Industriearmaturen – Gehäusefestigkeit*, Teil 1, Teil 2. 2014.

[108] EN 1983: *Industriearmaturen – Kugelhähne aus Stahl*, 2013

[109] Nesbitt, B.: *Handbook of valves and actuators.* London, 2007

[110] Zion Market research: *Industrial Valves Market (Gate, Butterfly, Ball, Check, Globe) for Oil & Gas, Chemical, Power, Water & Wastewater and Other Applications: Global Industry Perspective, Comprehensive Analysis, Size, Share, Growth, Segment, Trends and Forecast, (2015-2021*), 2016.

[111] Cryogenic ball valve: *Red Point* ®. URL: *https://www.redpoint-valves.com/cryogenic-valve-applications* (Version 09.11.2020)

[112] Habonim Ltd. URL: *Cryogenic ball valve https://www.habonim.com/wp-content/uploads/2020/02/A3-Habonim_Catalog_Cryogenic_v26_Interactive.pdf* (Version 09.11.2020).

[113] BS6364: *Valves for cryogenic serves*. British standard. 2018.

[114] Industrial valves: *Isolating valves for low-temperature applications*. Part 1: Design, manufacturing and production testing; German version EN ISO 28921-1:2017.

[115] Valves for Cryogenic Service Including Requirements for Body. *Bonnet Extensions*.

MSS SP-134. USA 2019.

[116] DIN EN ISO 13445: *Unfired pressure vessels – Part 2: Materials*. 12.2017.

[117] DIN EN ISO 10028: *Flat production made of steel for pressure purposes – Part 3: Weld able fine grain steels, normalized.* 2017.

[118] EN ISO DIN 867: *Basic rack tooth profiles for involute teeth of cylindrical gears for general engineering and heavy engineering*. 1986.

[119] Maedler Ltd. URL: *https://www.maedler.de/product/1643/1618/sperrraeder* (Version 27.11.2020).

[120] Oleynikov, A., Ivanov, V.: *Emergency valve for pipelines. XV Regional Conference of Young Researchers of Volgograd region (Volgograd, 9-12 November 2010)*: theses of reports. VSTU. Volgograd: pp. 104-105 2011. – Олейников А.В., Иванов В.В.: Задвижка аварийного назначения для трубопроводов. XV региональная конференция молодых исследователей Волгоградской области (Волгоград, 9-12 ноября 2010 г.): тез. докл. ВолгГТУ. Волгоград, с. 104-105. 2011.

[121] Oleynikov, A., Ivanov, V.: *Emergency gate valve for pipelines. Theses of reports of review-contest of scientific, design and technological works of Volgograd State Technical University*, Volgograd, May 10-13, 2011. Volgograd State Technical University, Council SNTO. Volgograd, pp. 139-140, 2011. – Олейников, А.В., Иванов В.В.: *Задвижка аварийного назначения для трубопроводов. Тезисы докладов смотра-конкурса научных, конструкторских и технологических работ студентов ВолгГТУ*, Волгоград, 10-13 мая 2011 г. / ВолгГТУ, Совет СНТО. - Волгоград, С. 139-140. 2011.

[122] Oleynikov, A., Ivanov, V.: *Emergency gate valve for pipelines. XVII Regional Conference of Young Researchers of Volgograd region*, Volgograd, 6-9 November 2012. Theses of reports. VSTU. Volgograd, pp. 61-62. 2013. – Олейников, А.В., Иванов В.В.: *Задвижка аварийного назначения для трубопроводов. XVII региональная конференция молодых исследователей Волгоградской области*, Волгоград, 6-9 нояб. 2012 г. : тез. докл. ВолгГТУ. Волгоград, С. 61-62. 2013.

[123] Oleynikov, A., Ivanov, V.: *Emergency gate valve for pipelines. Creative youth of Kamyshin city*. V Regional Conf. of students, dedicated to the 50th anniversary of the first man space flight (Kamyshin, 14-15 apr. 2011). KTI VSTU. Volgograd. T. 5, pp. 128-130. 2011. – Олейников, А.В., Иванов В.В.: *Задвижка аварийного назначения для трубопроводов. Городу Камышину – творческую молодёжь : матер.* V регион. н.-пр. студ. конф., посвящ. 50-летию первого полёта человека в космос

(Камышин, 14-15 апр. 2011 г.). КТИ (филиал) ВолгГТУ. Волгоград, Т. 5. С. 128-130. 2011.

[124] Oleynikov, A., Ivanov, V.: *Emergency gate valve for pipelines. Creative youth to the lower Volga region*: VI Regional Conf. of students, Kamyshin, May 17-18, 2012. In 6 vols. T. 5. KTI VSTU. Kamyshin, pp. 57-58. 2012. – Олейников, А.В., Иванов В.В.: *Задвижка аварийного назначения для трубопроводов. Нижнему Поволжью – творческую молодёжь:* матер. VI регион. науч. практ. студ. конф., г. Камышин, 17-18 мая 2012 г. В 6 т. Т. 5 КТИ (филиал) ВолгГТУ. Камышин, С. 57-58. 2012.

[125] Oleynikov, A., Ivanov, V.: *Emergency gate valve for pipelines. Abstracts of reports of the review-contest of scientific, design and technological works of students of Volgograd State Technical University*, Volgograd, May 15-18, 2012. Volgograd State Technical University, Council of SNTO. Volgograd, pp. 137, 2012. – Олейников, А.В., Иванов В.В.: *Задвижка аварийного назначения для трубопроводов. Тезисы докладов смотра-конкурса научных, конструкторских и технологических работ студентов Волгоградского гос. техн. ун-та*, Волгоград, 15-18 мая 2012 г. ВолгГТУ, Совет СНТО. Волгоград, С. 137. 2012.

[126] Oleynikov, A., Ivanov, V., Denisevich, D.: *Theses of reports of anniversary review-contest of scientific, design and technological works of Volgograd State Technical University*, Volgograd, May, 11-14, 2010. Volgograd State Technical University, Council of SNTO. Volgograd, pp. 147-148, 2010. – Олейников, А.В., Денисевич Д.С., Иванов В.В.: *Запорное устройство аварийного назначения для трубопроводов. Тезисы докладов юбилейного смотра-конкурса научных, конструкторских и технологических работ студентов ВолгГТУ*, Волгоград, 11-14 мая 2010 г. ВолгГТУ, Совет СНТО. Волгоград, С. 147-148. 2010.

[127] Oleynikov, A., Ivanov, V., Sokolov, D.: *Shiber gate valves for main oil and gas pipelines. Creative youth to Russia: I All-Russian Scientific-Practical Student Conference*, Kamyshin, May 22-23, 2013. In 4 vol. T. 4. VSTU, Volgograd, pp. 42-43. 2013. – Олейников А.В., Соколов Д., Иванов В.В.: *Шиберные задвижки для магистральных нефтегазопроводов. России – творческую молодёжь : матер. I всерос. науч.-практ. студ. конф.*, г. Камышин, 22-23 мая 2013 г. В 4 т. Т. 4 ВолгГТУ, КТИ (филиал) ВолгГТУ. Волгоград, С. 42-43. 2013.

[128] Oleynikov, A., Ivanov, V.: *Ball valve with actuator absolutely isolated from working body and external environment.* VII International Scientific and Practical Conference of Young Scientists "Actual problems of science and technology - 2014", 18-20 November

2014, Ufa. – В.В. Иванов, А.В. Олейников: *Шаровой кран с приводом, абсолютно изолированным от рабочего тела и внешней среды*. VII Международная научно-практическая конференция молодых ученых «Актуальные проблемы науки и техники - 2014» 18 – 20 ноября 2014, г. Уфа.

[129] EN 12449: *Copper and copper alloys - Seamless, round tubes for general purposes*: CW508L - 2.0321. 2019.

[130] EN 10297: *Seamless circular steel tubes for mechanical and general engineering purposes – Part 1: Non-alloy and alloy steel tubes*. 06.2003.

[131] DIN 17100: *Hot rolled products in non-alloy steels for general structural applications.* 1987.

[132] EN 10028: *Flat products made of steels for pressure purposes- Part 3: Weldable fine grain steels, normalized* (P355NL1/1.0566). 2017.

[133] Gomeringer, R.: *Tabellenbuch Metall: mit Formelsammlung.* Haan-Gruiten. 2019

[134] Hoischen, H.: Technisches Zeichnen. Düsseldorf, 2020.

[135] Rewolinska, A., Perz, K., Kinal, G.: *Experimental Tests of Static Friction Coefficient for Selected Material Combinations of Expanded Graphite - Steel Used in Sealing Nodes*. ISSN 1392-1207. MECHANIKA. Volume 26(2): pp. 103-107, 2020.

[136] C. Otto Gehrckens GmbH & Co. KG. *Das O-Ring 1x1 ALLES RUND UM DIE O-RING DICHTUNG.* Seal Technology. Pinneberg. 2016.

[137] EN ISO 12240: *Spherical plain bearing – Part 4: Spherical plain bearing rod ends*, 07.1999.

[138] DIN EN 10028: *Flat products made of steel for pressure purposes – Part 7: Stainless steel*, 10.2016.

[139] DIN EN 10222: *Steel forgings for pressure purposes – Part 5: Martensitic, austenitic and austenitic-ferritic stainless steels*, 06.2017.

[140] DIN EN 10272: *Stainless steel bars for pressure purposes,* 10.2016.

[141] DIN EN 10216: *Seamless steel tubes for pressure purposes – Part 5: Stainless steel tubes*, 03.2014.

[142] AD 2000: *Ausrüstung, Aufstellung und Kennzeichnung von Druckbehältern*, 12.2020.

[143] ASME-BPVC-Section-II: *Materials. ASME Boiler and pressure vessels code (an international code). Part A – Ferrous Materials Specification*, 01.2015.

[144] ASME-BPVC-Section-II: *Materials. ASME Boiler and pressure vessels code (an international code). Part D – Properties (Metric)*, 07.2019.

[145] DIN EN 10083: *Steels for quenching and tempering – Part 2: Technical delivery*

conditions for non alloy steels, 10.2006.

[146] EN 10025: *Hot rolled products of structural steels – Part 2: Technical delivery condition for non-alloy structural steels*, 02.2005.

[147] DIN EN 10088: Stainless steels – Part 3: *Technical delivery conditions for semi-finished products, bars, rods, wire, sections and bright products of corrosion resisting steels for general purposes*, 12.2014.

[148] DIN EN 10216: *Seamless steel tubes for pressure purposes – Part 3: Alloy fine grain steel tubes*, 03.2014.

[149] DIN EN 10088: Stainless steels – Part 2: *Technical delivery conditions for sheet/plate and strip of corrosion resisting steels for general purposes*, 12.2014.

[150] ISO 9000: Quality management systems – Fundamentals and vocabulary, 2015.

[151] DIN EN 13445 Teil 3, Anhang C (normativ): *Verfahren der Spannungskategorien für die Auslegung mit Analyseverfahren.* 2018.

[152] Dietmann, H., Kockelmann, H.: *Verwendung der Gestaltänderungsenergiehypothese im Anwendungsbereich der KTA-Regeln*. VGB Kraftwerkstechnik 74 (1994), Heft 6.

[153] Sahu, J., Krupp, U., Ghosh, R., Christ, H.: *Effect of 475 ° C embrittlement on the mechanical properties of duplex stainless steel.* Materials Science and Engineering: Volume 508, Issues 1-2, pp. 1-14, 20 May 2009.

[154] R. Williams: *Further studies of the iron-chromium system.* Trans. TMS-AIME. 1958, vol. 212, pp. 497-502.

[155] El-Batahgy, A., Zaghloul, B.: *Fatigue failure of an offshore condensate recycle line in a natural gas production field. Materials Characterization.* Volume 54, Issue 3, March 2005, pp. 246-253.

[156] Cojocaru, E., Raducanu, D., Nocivin, A., Cinc, I., Vintila, A., Serban, N., Angelescu, M., Cojocaru, V.: *Influence of Aging Treatment on Microstructure and Tensile Properties of a Hot Deformed UNS S32750 Super Duplex Stainless Steel (SDSS) Alloy*. MDPI, Metals, 8 March 2020, pp. 353-368.

[157] Morris, J.: *Steels for low temperatures Applications: Materials and Chemical Science Division*. Lawrence Barkeley Laboratory. University of California, 1993, pp. 16

[158] Engineering ToolBox, (2004). *Friction - Friction Coefficients and Calculator*. URL: https://www.engineeringtoolbox.com/friction-coefficients-d_778.html (Version 21.10.21).

[159] Ingenieurbüro Andreas Hanke GmbH. *Singularitäten in der FEM. Ursachen und Bewertung*. 2019. URL:https://www.ing-hanke.de/know-how/singularitaeten-in-der-fem-ursachen-und-bewertung/ (Version 21.10.21).

[160] Welsch, M.: *Bewertung von Spannungsspitzen und Singularitäten in FEM Rechnungen*. Institut für Maschinenelemente und Rechnergestützte Produktentwicklung, Helmut-Schmidt-Universität. 11. Norddeutsches Simulationsforum. 10.2015.

[161] Richard, H., Sander, M.: *Ermüdungsrisse: Erkennen, sicher beurteilen, vermeiden*. 1. Aufl., Vieweg + Teubner, Wiesbaden, 2009.

[162] Broeckmann, C., Beiss, P.: *Werkstoffkunde I*. Institut für Werkstoffanwendungen im Maschinenbau der RWTH Aachen, Aachen 2014, pp. 88-101.

[163] Neuber, H.: *Theory of Stress Concentration for Shear-Strained Prismatical Bodies With Arbitrary Nonlinear Stress-Strain Law*. *Journal of Applied Mechanics*. 1961, pp. 544

[164] Seeger, T., Heuler, P.: *Generalized application of Neuber's rule*. *Journal of Applied Mechanics*. 1980, pp. 199-204.

[165] Schmied, B., Kurman, S.: *Statischer Festigkeitsnachweis von Schweißnähten mit örtlichen Spannungen. Schmied Engineering GmbH, Schmied Engineering GmbH.* - Manuskript zum Vortrag am Schweizer Maschinenelemente Kolloquium (SMK2010). 9. / 10. Nov. 2010 an der Hochschule für Technik Rapperswil, Schweiz.

[166] Von Mises, R.: *Mechanik der festen Körper im plastisch-deformablen Zustand. Nachrichten von der Gesellschaft der Wissenschaften zu Göttingen. Mathematisch-Physikalische Klasse.* 1913. pp. 582-592.

[167] Altenbach, H., Bolchoun, A., Kolupaev, V.: *Phenomenological Yield and Failure Criteria. Plasticity of Pressure-Sensitive Materials*, Serie ASM, Springer, Heidelberg, 2013. pp. 49-152.

[168] Rosendahl, P., Kolupaev, V., Altenbach, H.: Extreme *Yield Figures for Universal Strength Criteria. State of the Art and Future Trends in Material Modeling*, Advanced Structured Materials StructMat, Springer, Cham, 2019. pp. 259-324.

[169] ISO 20486 Part 1: *Non-destructive testing - Leak testing - Calibration of reference leaks for gases.* 2017.

[170] Bo-Hua Sun: *On symmetrical deformation of toroidal shell with circular cross-section. Institute of Mechanics and Technology & School of Civil Engineering, Xi'an University of Architecture and Technology.*7th of May 2020.

[171] Subramanian, R.: *Heat transfer in flow through conduits.* Department of Chemical and Biomolecular Engineering. Clarkson University. 2000.

[172] Welty, J., Wicks, C., Wilson, R., Rorrer, G.: *Fundamentals of Momentum, Heat and Mass transfer* (5th ed.). John Wiley and Sons. ISBN 978-0470128688. 2007.

[173] Zingoni, A., Enoma, N., Govender, N. *Equatorial bending of an elliptic toroidal shell.* Thin-Walled Structures 96, 2015. pp. 286-294.

[174] Zingoni, A., Mokhothu, B., Enoma, N.: *A theoretical formulation for the stress analysis of multi-segmented spherical shells for high-volume liquid containment.* Engineering Structures 87, 2015. pp. 21-31.

[175] Burton, J., Taborek, P., Rutledge, J.: *Temperature dependence of friction under cryogenic conditions in vacuum.* Department of Physics and Astronomy, University of California, USA. Tribology Letters, Vol. 23, No. 2, August 2006. pp. 131-141.

[176] Watson, G.: A *Treatise on the theory of Bessel Functions*, University of Cambrige, 1922. pp. 345-352.

[177] Kolesnikov, A.: *Large bending deformations of pressurized curved tubes*, Theory of Elasticity Department, Arch. Mech., 63, 5-6, Warsaw 2011. pp. 507-516.

[178] Sauer, R., Thang Duong, X., Roohbakhshan F.: *A new rotation-free isogeometric thin shell formulation and a corresponding continuity constraint for patch boundaries.* RWTH Aachen University. Computer Methods in Applied Mechanics and Engineering, 2016. pp. 1-48.

Attachment A

The numerical algorithm for investigation of single-ply bellows with U-shaped convolution cross section loaded with internal pressure of 1,6 MPa, with variables: negative curvature from 0 ° till 180 ° (cavity section), positive curvature from 180 ° till 270 ° (crest section) and side wall (shell):

```
%single-ply bellows
format compact;
%for values of x(T) the following asyptotic expantions of functions
%T_r(x), T_dr(x), T_i(x), T_di(x) are tabulated according to Clark's numerical
%integrations for investigated bellows with U-shaped convolution cross section:
xT =0:0.05:5;
Tr=[-1.288, -1.287, -1.283, -1.277, -1.268, -1.257, -1.244, -1.228, ...
    -1.21, -1.19, -1.168, -1.144, -1.118, -1.09, -1.061, -1.03, -0.998, ...
    -0.965, -0.931, -0.896, -0.86, 0.823, -0.786, -0.749, -0.711, -0.673, ...
    -0.636, -0.599, -0.562, -0.525, -0.489, -0.454, -0.419, -0.385, -0.352, ...
    -0.32, -0.29, -0.261, -0.232, -0.204, -0.178, -0.153, -0.130, ...
    -0.108, -0.088, -0.069, -0.051, -0.035, -0.02, -0.006, 0.006, 0.017, ...
    0.027, 0.036, 0.044, 0.05, 0.056, 0.061, 0.065, 0.068, 0.07, 0.071, ...
    0.072, 0.073, 0.073, 0.072, 0.071, 0.069, 0.067, 0.065, 0.063, 0.06, 0.058,
...
    0.056, 0.053, 0.05, 0.047, 0.044, 0.041, 0.038, 0.035, 0.032, 0.029, ...
    0.027, 0.024, 0.022, 0.02, 0.018, 0.016, 0.014, 0.012, 0.011, 0.009, ...
    0.008, 0.007, 0.006, 0.005, 0.004, 0.003, 0.003, 0.002]; %Tr
Tdr=[0, 0.05, 0.1, 0.149, 0.197, 0.245, 0.292, 0.337, 0.38, 0.422, ...
    0.462, 0.5, 0.535, 0.568, 0.599, 0.627, 0.652, 0.675, 0.695, 0.712, ...
    0.726, 0.737, 0.745, 0.75, 0.753, 0.753, 0.75, 0.745, 0.737, 0.727, 0.715, ...
    0.7, 0.683, 0.664, 0.644, 0.623, 0.601, 0.578, 0.554, 0.529, 0.503, ...
    0.476, 0.449, 0.421, 0.394, 0.336, 0.339, 0.312, 0.286, 0.26, 0.235, ...
    0.211, 0.188, 0.165, 0.144, 0.123, 0.104, 0.086, 0.069, 0.053, 0.038, ...
    0.024, 0.011, 0, -0.01, -0.019, -0.027, -0.034, -0.04, -0.045, -0.05, ...
    -0.053, -0.056, -0.058, -0.059, -0.059, -0.059, -0.059, -0.058, -0.057, ...
    -0.056, -0.054, -0.052, -0.05, -0.048, -0.046, -0.043, -0.04, -0.038, ...
    -0.035, -0.032, -0.03, -0.027, -0.025, -0.022, -0.02, -0.018, -0.016, ...
    -0.014, -0.012, -0.01]; %Tdr
Ti=[0, 0.047, 0.094, 0.14, 0.186, 0.231, 0.276, 0.32, 0.362, 0.403, ...
    0.443, 0.482, 0.519, 0.554, 0.588, 0.619, 0.649, 0.677, 0.702, 0.726, ...
    0.747, 0.767, 0.784, 0.799, 0.812, 0.822, 0.830, 0.836, 0.841, 0.844, ...
    0.846, 0.845, 0.842, 0.837, 0.831, 0.823, 0.814, 0.804, 0.793, 0.78, ...
    0.766, 0.751, 0.736, 0.72, 0.703, 0.686, 0.669, 0.651, 0.633, 0.615, ...
    0.597, 0.579, 0.561, 0.543, 0.525, 0.508, 0.491, 0.475, 0.459, 0.443, ...
    0.428, 0.413, 0.399, 0.386, 0.373, 0.36, 0.348, 0.337, 0.327, 0.317, 0.307,
...
    0.298, 0.29, 0.282, 0.275, 0.268, 0.261, 0.255, 0.25, 0.246, 0.242, ...
    0.238, 0.234, 0.23, 0.226, 0.223, 0.22, 0.218, 0.215, 0.213, 0.21, 0.208, ...
    0.206, 0.205, 0.203, 0.201, 0.2, 0.198, 0.197, 0.195, 0.194]; %Ti
Tdi=[0.939, 0.937, 0.932, 0.924, 0.913, 0.899, 0.882, 0.862, 0.839, ...
    0.813, 0.785, 0.755, 0.723, 0.688, 0.652, 0.614, 0.574, 0.534, ...
    0.493, 0.45, 0.407, 0.364, 0.321, 0.278, 0.235, 0.193, 0.151, ...
    0.11, 0.07, 0.031, -0.007, -0.043, -0.078, -0.111, -0.142, -0.171, ...
    -0.198, -0.222, -0.244, -0.264, -0.282, -0.298, -0.313, -0.326, ...
    -0.337, -0.346, -0.353, -0.358, -0.361, -0.362, -0.362, -0.361, ...
    -0.358, -0.354, -0.349, -0.342, -0.335, -0.327, -0.318, -0.308, ...
    -0.298, -0.287, -0.276, -0.264, -0.253, -0.241, -0.23, -0.218, -0.206, ...
    -0.195, -0.184, -0.173, -0.163, -0.152, -0.142, -0.132, -0.123, -0.114, ...
    -0.106, -0.098, -0.09, -0.083, -0.077, -0.071, -0.066, -0.061, -0.057, ...
```

```
    -0.053, -0.049, -0.046, -0.043, -0.04, -0.038, -0.036, -0.034, -0.033, ...
    -0.031, -0.03, -0.029, -0.029, -0.028]; %Tdi
%Geometry properties of investigated bellows with U-shaped convolution
%cross section:
R_1 = 1.41212 * 10^(-3); %defined dimension of negative corrugation
R_c1 = 28.5 * 10^(-3); % defined dimension of negative corrugation
h = 0.8 * 10^(-3); % thickness of the shell
E = 2*10^11; %elastic modulus of the investigated material
v = 0.3; % v: Poisson number
nl = 1; %number of bellows plies
p = -1.6 * 10^6; % Pa, Internal pressure:
% thin toroidal shell of negative curvature from 0° till 180°:
x1 = 0:1:180;
n = length(x1);
for i = 1:1:n
y(i) = pi / 180 * x1(i)
% Equation for analysation lambda, m, omega, my, fx:
lambda = R_1 / R_c1;
m = sqrt(12 * (1 - v^2));
%Equation of omega with integration limits from 0 to pi:
omega = ((m * R_1 * R_c1 * p) / (E * h.^2)) *(nl *(((lambda * x1(i)) / 2 +
cos(y(i)) + lambda *  cos(y(i)) * sin(y(i)) + 0.25 * lambda * cos(y(i)) *
sin(y(i)))));
my = m * (R_1)^2 / (R_c1 * h);
fx = my^(1/3) * y(i);
P_H = (m * (R_1 * sin(y(i)) + R_c1)* R_1 * p * sin(y(i))) / (E * h.^2);
P_V = (m * (R_1 * sin(y(i)) + R_c1)* R_1 * (p * cos(y(i)))) / (E * h.^2);
% for negative curve according to Clark considered T_r(-x) = T_r(x), T_dr(-x) = -
T_dr(x), T_i(-x) = -T_i(x), T_di(-x) = T_di(x)
%Interpolation in 2-Dimension
 T_r=interp1(xT,Tr,fx,'spline')
 T_dr=interp1(xT,Tdr,fx,'spline')
 T_i=interp1(xT,Ti,fx,'spline')
 T_di=interp1(xT, Tdi, fx,'spline')
% stress resultants, stress couples and the rotation in the no dimensional form N,
Q, M:
% stress resultant in meridional direction:
N_phi = (E * h.^2 / (m * R_c1)) * ( my.^(1/3) * (-T_i) * (cos(y(i))).^2 +
sin(y(i))) / (1 + lambda * sin(y(i))) * omega;
% transverse shear stress resultant:
Q = (E * h.^2 / (m * R_c1)) * ( (- my.^(1/3) * (-T_i) * sin(y(i)) * cos(y(i))) +
cos(y(i))) / (1 + lambda * sin(y(i))) * omega;
% stress resultant tangential to parallel circle:
N_teta = ((E * h.^2) / (m * R_c1)) * ((my.^(2/3) * (T_di) * (cos(y(i))).^2 -
my.^(1/3) * (-T_i) * sin(y(i))) * omega + P_H + P_V);
% stress couple in meridional direction:
M_phi = (E * h.^3 / (m.^2 * R_1)) * ( my.^(2/3) * (T_dr) * (cos(y(i))).^2 -
my.^(1/3) * (-T_r) *sin(y(i))) * omega + (v * lambda * my.^(1/3) * (-T_r)
*(cos(y(i))).^2 * omega) / (1 + lambda * sin(y(i)));
% stress couple in direction tangential to parallel circle:
M_teta = (E * h.^3 / (m.^2 * R_1)) * (v * (my.^(2/3) *  (cos(y(i))).^2 - my.^(1/3)
* (-T_r) *sin(y(i)))) * omega + (lambda * my.^(1/3) * (-T_r) *(cos(y(i))).^2 *
omega) / (1 + lambda * sin(y(i)));
% Stress resultants and deformations at investigated point on the bellows
corrugation (crest, side shell, or cavity:
% h: Wall thickness, p: Internal pressure:
sigma_tetaD = N_teta / h;
sigma_phiD = N_phi / h;
sigma_tetaB = 6 * M_teta / h.^2;
```

```
sigma_phiB = 6 * M_phi / h.^2;
sigma_tau = Q / h;
%membrane and bending stresses at investigated point on the bellows corrugation:
sigma_phi = abs(sigma_phiD) + abs(sigma_phiB);
sigma_teta = abs(sigma_tetaD) + abs(sigma_tetaB);
% Shape change energy hypothesis (two-dimensional):
sigma_GEH(i) = sqrt(0.5 * ( (sigma_phi - sigma_teta).^2 + (sigma_phi).^2 +
(sigma_teta).^2) + 3*sigma_tau.^2)%sigma_GEH
%results negative curvature:
end
%single-ply bellows
%Geometry properties of positive curvature for investigated bellows
%with U-shaped convolution cross section:
R_1p = 1.41212 * 10^(-3); %defined dimension of positive corrugation
R_c1_p = 38.1 * 10^(-3); % defined dimension of positive corrugation
p1 = 1.6 * 10^6; % Pa, Internal pressure:
% thin toroidal shell of positive curvature from 180° to 360°:
x2 = 180:1:360;
n = length(x2);
for i = 1:1:n
y_p(i) = 2* pi / 360 * x2(i)
% Equation for analysation lambda, m, omega, my, fx:
lambda_p = R_1p / R_c1_p;
m_p = sqrt(12 * (1 - v.^2));
%Equation of omega with integration limits from pi to 2*pi:
omega_p = (m_p * R_1p * R_c1_p * p1 / (E * h.^2)) * (nl *(((lambda_p * x2(i))/2 +
cos(y_p(i)) + 0.5 * lambda_p *  cos(y_p(i)) * sin(y_p(i)) + 0.25 * lambda_p *
sin(y_p(i))*cos(y_p(i)))));
my_p = m_p * (R_1p).^2 / (R_c1_p* h);
fx_p = my_p.^(1/3) * y_p(i);
P_H_p = (m_p* (R_1p * sin(y_p(i)) + R_c1_p)* R_1p * p1 * sin(y_p(i))) / (E *
h.^2);
P_V_p = (m_p* (R_1p * sin(y_p(i)) + R_c1_p)* R_1p * ( - p1 * cos(y_p(i)))) / (E *
h.^2);
% for positive curve according to Clark considered T_r(x) = T_r(x), T_dr(x) =
T_dr(x), T_i(x) = T_i(x), T_di(x) = T_di(x)
%Interpolation in 2-Dimension
 T_r_p=interp1(xT,Tr,fx_p,'spline')
 T_dr_p=interp1(xT,Tdr,fx_p,'spline')
 T_i_p=interp1(xT,Ti,fx_p,'spline')
 T_di_p=interp1(xT, Tdi,fx_p,'spline')
% stress resultants, stress couples and the rotation in the no dimensional form N,
Q, M:
% stress resultant in meridional direction:
N_phi_p = (E * h.^2 / (m_p * R_c1_p)) * ((my_p.^(1/3) * (T_i_p) * (cos(y_p(i))).^2
+ sin(y_p(i))) / (1 + lambda_p * sin(y_p(i)))) * omega_p;
% transverse shear stress resultant:
Q_p = E * h.^2 / (m_p * R_c1_p) * (- (my_p.^(1/3) * (T_i_p) * sin(y_p(i)) *
cos(y_p(i))) + cos(y_p(i))) / (1 + lambda_p * sin(y_p(i))) * omega_p;
% stress resultant tangential to parallel circle:
N_teta_p = ((E * h.^2) / (m_p * R_c1_p)) * ((my_p.^(2/3) * T_di_p *
(cos(y_p(i))).^2 - my_p.^(1/3) * (T_i_p) *sin(y_p(i)))  * omega_p + P_H_p +
P_V_p);
% stress couple in meridional direction:
M_phi_p = (E * h.^3 / (m_p.^2 * R_1p)) * (my_p.^(2/3) * (T_dr_p) *(cos(y_p(i))).^2
- my_p.^(1/3) * T_r_p *sin(y_p(i))) * omega_p + (v * lambda_p * my_p.^(1/3) *
T_r_p *(cos(y_p(i))).^2 * omega_p) / (1 + lambda_p * sin(y_p(i)));
% stress couple in direction tangential to parallel circle:
```

```
M_teta_p = (E * h.^3 / (m_p.^2 * R_1p)) * (v * ( my_p.^(2/3) * (T_dr_p) *
(cos(y_p(i))).^2 - my_p.^(1/3) * T_r_p *sin(y_p(i)))) * omega_p + (lambda_p *
my_p.^(1/3) * T_r_p *(cos(y_p(i))).^2 * omega_p) / (1 + lambda_p * sin(y_p(i)));
% Stress resultants and deformations at investigated point on the bellows
corrugation (crest, side shell, or cavity:
% h: Wall thickness, p: Internal pressure:
sigma_tetaD_p = N_teta_p / h;
sigma_phiD_p = N_phi_p / h;
sigma_tetaB_p = 6 * M_teta_p / h.^2;
sigma_phiB_p = 6 * M_phi_p / h.^2;
sigma_tau_p = Q_p / h;
%membrane and bending stresses at investigated point on the bellows corrugation:
sigma_phi_p = abs(sigma_phiD_p) + abs(sigma_phiB_p);
sigma_teta_p = abs(sigma_tetaD_p) + abs(sigma_tetaB_p);
% Shape change energy hypothesis (two-dimensional):
%sigma_GEH_p(i) = sqrt(0.5 * (sigma_phi_p - sigma_teta_p).^2 + (sigma_teta_p -
sigma_tau_p).^2 +  ( sigma_tau_p - sigma_phi_p).^2 )
sigma_GEH_p(i) = sqrt(0.5 * ( (sigma_phi_p - sigma_teta_p).^2 + (sigma_phi_p).^2 +
(sigma_teta_p).^2) + 3*sigma_tau_p.^2)%sigma_GEH
%results:
end
%single-ply bellows
% thin toroidal shell, side wall:
% Geometry properties of investigated bellows side wall ...
%with U-shaped convolution cross section as a function of internal pressure:
R = 28.1:0.5:38.1;
n = length(R);
for i = 1:1:n
R_c1_sw = R(i)* 10^(-3);
z=180;%degree at which the side wall B-C located between negative and positive
curvature
y_sw = pi / 180 * z;
% Equation for analysation lambda, m, omega, my, fx:
lambda_sw = R_1p / R_c1_sw;
m_sw = sqrt(12 * (1 - v^2));
%Equation of omega with integration limits at pi:
omega_sw = (m_sw * R_1p * R_c1_sw * p1 / (E * h.^2)) * (nl *(((lambda_sw * z)/2 +
cos(y_sw) + 0.5 * lambda_sw *  cos(y_sw) * sin(y_sw) + 0.25 * lambda_sw *
sin(y_sw)*cos(y_sw))));
my_sw = m_sw * (R_1p).^2 / (R_c1_sw* h);
fx_sw = my_sw.^(1/3) * y_sw;
P_H_sw = (m_sw * (R_1p * sin(y_sw) + R_c1_sw)* R_1p * p1 * sin(y_sw)) / (E *
h.^2);
P_V_sw = (m_sw * (R_1p * sin(y_sw) + R_c1_sw)* R_1p * ( - p1 * cos(y_sw))) / (E *
h.^2);
% for negative curve according to Clark considered T_r(-x) = T_r(x), T_dr(-x) = -
T_dr(x), T_i(-x) = -T_i(x), T_di(-x) = T_di(x)
%Interpolation in 2-Dimension
 T_r_sw=interp1(xT,Tr,fx_sw,'spline')
 T_dr_sw=interp1(xT,Tdr,fx_sw,'spline')
 T_i_sw=interp1(xT,Ti,fx_sw,'spline')
 T_di_sw=interp1(xT, Tdi,fx_sw,'spline')
% stress resultants, stress couples and the rotation in the no dimensional form N,
Q, M:
% stress resultant in meridional direction:
N_phi_sw = (E * h.^2 / (m_sw * R_c1_sw)) * (my_sw^(1/3) * (T_i_sw) *
(cos(y_sw)).^2 + sin(y_sw)) / (1 + lambda_sw * sin(y_sw)) * omega_sw;
% transverse shear stress resultant:
```

```
Q_sw = E * h.^2 / (m_sw * R_c1_sw) * ((my_sw^(1/3) * (T_i_sw) * sin(y_sw) *
cos(y_sw)) + cos(y_sw)) / (1 + lambda_sw * sin(y_sw)) * omega_sw;
% stress resultant tangential to parallel circle:
N_teta_sw = ((E * h.^2) / (m_sw * R_c1_sw)) * ((my_sw.^(2/3) * T_di_sw *
(cos(y_sw)).^2 - my_sw.^(1/3) * (T_i_sw) *sin(y_sw))  * omega_sw + P_H_sw +
P_V_sw);
% stress couple in meridional direction:
M_phi_sw = (E * h.^3 / (m_sw.^2 * R_1p)) *  (my_sw.^(2/3) * (T_dr_sw)
*(cos(y_sw)).^2 - v * my_sw.^(1/3) * (T_r_sw) *sin(y_sw)) * omega_sw + (v *
lambda_sw * my_sw.^(1/3) * (T_r_sw) *(cos(y_sw)).^2 * omega_sw) / (1 + lambda_sw *
sin(y_sw));
% stress couple in direction tangential to parallel circle:
M_teta_sw = (E * h.^3 / (m_sw.^2 * R_1p)) * (v * ( my_sw.^(2/3) * (T_dr_sw)
*(cos(y_sw)).^2 - my_sw.^(1/3) * (T_r_sw) *sin(y_sw))) * omega_sw + (lambda_sw *
my_sw.^(1/3) * (T_r_sw) *(cos(y_sw)).^2 * omega_sw) / (1 + lambda_sw * sin(y_sw));
% Stress resultants and deformations at investigated point on the bellows
corrugation (crest, side shell, or cavity:
% h: Wall thickness, p: Internal pressure:
sigma_tetaD_sw = N_teta_sw / h;
sigma_phiD_sw = N_phi_sw / h;
sigma_tetaB_sw = 6 * M_teta_sw / h.^2;
sigma_phiB_sw = 6 * M_phi_sw / h.^2;
sigma_tau_sw = Q_sw / h;
%membrane and bending stresses at investigated point on the bellows corrugation:
sigma_phi_sw = abs(sigma_phiD_sw) + abs(sigma_phiB_sw);
sigma_teta_sw = abs(sigma_tetaD_sw) + abs(sigma_tetaB_sw);
% Shape change energy hypothesis (two-dimensional):
sigma_GEH_sw(i) = sqrt(0.5 * ( (sigma_phi_sw - sigma_teta_sw).^2 +
(sigma_teta_sw).^2 + (sigma_phi_sw).^2 ) + 3 * sigma_tau_sw.^2)%sigma_GEH
%results:
end
plot(x1,sigma_GEH,'r--o',x2,sigma_GEH_p,'r--o',z,sigma_GEH_sw,'b--o')
xlabel('degree of revolution, °')
ylabel('Equivalent stress, sigma eq MPa')
title('Internal pressure analysis')
legend('sigma eq')
grid
```

Attachment B

B.1 Design validation of investigated ball valves with RGM

This document is the design calculation according to requirements of EN 13445 Part 3

Scope: - calculation of pressure-containing components according to EN 12516 Part 2

- stem calculation requirements EN 13445 Part 3

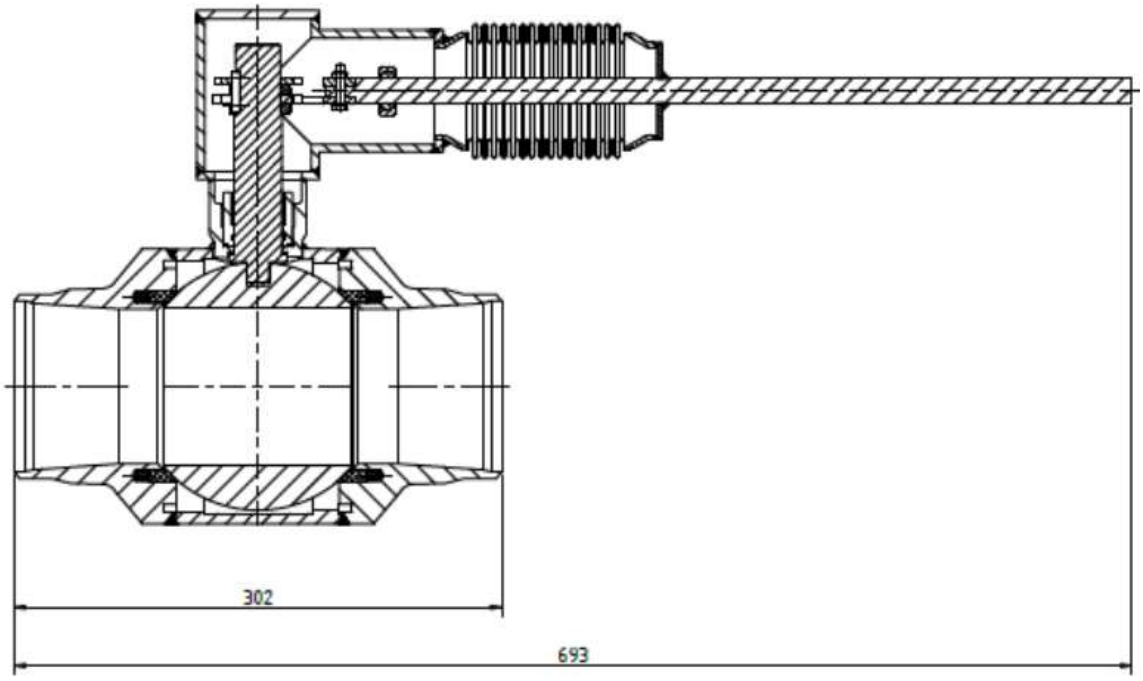

Figure B.1- Sketch of investigated ball valve DN 100 with RGM (utility model) [4]

B.1.1 Calculation of required torque for investigated ball valve

Design data	Dimensions		
Diameter of the seat	d_{seat}	[mm]	118,4
Diameter of seat contact to ball	$d_{seatcontact}$	[mm]	106,3
Area of the seat	$A_{seatarea}$	[mm]	2135
Radius of the stem bearing	$R_{bearing}$	[mm]	15,0
seat contact to ball width	$b_{Seat\ u}$	[mm]	3
specific preloading - spring	c_{spf}	[N/mm²]	1,5
Friction on the contact of stem and bearing	$\mu_{stem\text{-}bearing}$	[-]	0,030
Friction on the contact seat to ball	$\mu_{seat\text{-}ball}$	[-]	0,058
Internal pressure	P	[MPa]	2,0
Diameter of the ball (obturator)	D_{ball}	[mm]	154,0
Torque/Moment appeared on the top section of the stem due to bending of the stem	M_{stem}	[N·m]	8,0
Torque/Moment appeared on the top section of the stem due to influence the internal pressure on the seat	M_{seat}	[N·m]	13,8
Total torque/moment appeared on the top section of the stem	M_{total}	[N·m]	26,6

Seat contact angle: $\alpha_{seat} = \sin^{-1}(d_{seat\ Contact}/D_{ball}) =$ 44 °

Seat preload force: $F_{us} = \pi \cdot d_{seat\ contact} \cdot b_{seat\ u} \cdot c_{spf} =$ 1503 N

Seat preload force - x-direction: $F_{usx} = F_{us} \cdot \cos \alpha_{seat} =$ 1087 N

Friction torque – seat preload force: $M_{us} = F_{uvx} \cdot \mu_{seat/ball} \cdot \frac{R}{\cos \alpha_{seat}} =$ 4,86 N·m

Force from internal pressure on ball: $F_1 = d_{seat}^2 \cdot \frac{\pi}{4} \cdot P =$ 17749,51 N

Force from internal pressure on seat: $F_2 = A_{seatarea} \cdot P =$ 4270,79 N

Pressure influencing area of the seat: $A_{seat\ area} = \frac{\pi}{4} \cdot \left(d_{seat}^2 - d_{seat\ contact}^2\right) =$ 2135,40 mm²

Moment appeared on top section of stem due to influence of the bearing friction:

$$M_{stem} = F_1 \cdot \mu_{stem-bearing} \cdot R_{bearing} = \quad 7{,}99 \quad \text{N·m}$$

Moment appeared on top section of stem due to influence the internal pressure on the seat:

$$M_{seat} = R \cdot F_2 \cdot \mu_{seat-ball} = \quad 13{,}80 \quad \text{N·m}$$

Radius of attachment point of seat to ball:

$$R = \sqrt{\left(\frac{D_{ball}}{2}\right)^2 - \left(\frac{d_{seat\ contact}}{2}\right)^2} = \quad 55{,}71 \quad \text{mm}$$

Total torque/moment appeared on top section of the stem, due to internal pressure:

$$M_{total} = M_{stem} + M_{seat} + M_{us} = \quad 26{,}64 \quad \text{N·m}$$

MAST required, with safety factor $S_t = 1{,}5$:

$$M_{required} = M_{total} \cdot S_t = \quad 39{,}97 \quad \text{N·m}$$

B.1.2 Validation of stem based on requirement breakaway torque for ball valve with RGM

Part name:	Stem - DN100, PN20, API Class 150		
Design data	Dimensions		
Material	1.4006		
max. torque	M_{total}	[Nm]	26,6
Number of keys	n_P	[-]	1
Diameter of shaft section 1	d_1	[mm]	28,1
Diameter of shaft section 1 without keys	d_{1r}	[mm]	25,1
Diameter of shaft section 2	d_2	[mm]	29,95
Diameter of shaft section 3	d_3	[mm]	36,0
Width across of 2-flat-end	s_4	[mm]	13,9
Diameter of 2-flat-end	d_4	[mm]	36,0
Surface length of 2-flat-end	f_4	[mm]	33,2
Ratio of section 4	f_4/s_4	[-]	2,59
Square shape torsion factor 1	c_1	[-]	0,263
Square shape torsion factor 2	c_2	[-]	0,977
Safety factor for stem according to API 6D and PED	f_S	[%]	67
max. Temperature	T	[°C]	500
Yield strength at room temperature RT	$R_{p0,2/RT}$	[N/mm²]	500
Specified minimum yield strength - stem	$R_{R0,2T}$	[N/mm²]	255
Allowable design stress	$\sigma_m=R_{R0,2T}\cdot f_S$	[N/mm²]	171
Allowable average primary pure shear stress for keys, etc.	$\sigma_{SK}=\sigma_m\cdot 0,6$	[N/mm²]	103
Allowable maximum primary shear stress for circular solids	$\sigma_{SC}=\sigma_m\cdot 0,8$	[N/mm²]	137

Polar section modulus:

$$W_{t,i} = \frac{\pi \cdot {d_i}^3}{16} \qquad W_{t,i} = \frac{c_{1i}}{c_{2i}} \cdot d_i \cdot {s_i}^2$$

$$\tau_i = \frac{M}{W_{t,i}}$$

Max. torsion stress:

Area	Polar section modulus	Max. torsion stress	Result
i [-]	$W_{t,i}$ [mm³]	$t_{t,i}$ [N/mm²]	
1 - Key	3105	9	**OK**
2 - circ.	5275	5	**OK**
3 - circ.	9161	3	**OK**
4 - 2Flat	1872	14	**OK**

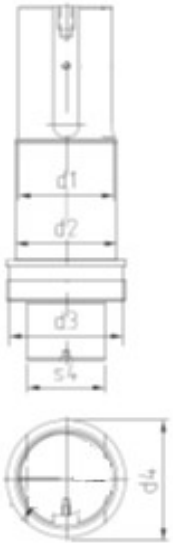

Figure B.2 - Sketch of investigated stem

Validation of stem sections: $M_{(MAST\ existing)}$ = 319,9 N·m

B.1.3 Cylindrical body under internal pressure

Calculation analysis:	DIN EN 12516-2 : 01-2015 EN 13445-3: 12-2018		
Part name: Valve body - DN100, PN20, API Class 150			
Design data	Dimensions		
Material	1.4571		
Internal Pressure	P	[MPa]	2
max. Temperature	T	[°C]	500
Material reference	EN 10216-5		
Yield strength at room temperature RT	$R_{p0,2/RT}$	[N/mm²]	210
Yield strength at investigated temperature T	$R_{p0,2/T}$	[N/mm²]	129
Tensile strength ~20°C	$R_{m/20}$	[N/mm²]	500
Weld joint efficiency factor	k_c	[-]	1,00
max. body internal diameter	d_i	[mm]	157
min. body outer diameter	d_o	[mm]	171,0
min. body shell thickness $e_p = (d_o-d_i)/2$	e_p	[mm]	7
Tolerance coefficient	c_1	[mm]	0
Corrosion and wear surcharge	c_2	[mm]	1
Safety factor (design conditions)	S	[-]	1,5
Safety factor (test conditions)	S_{test}	[-]	1,575

Allowable tensile stress - design condition: $f = min.\left(\frac{R_{p0,2,T}}{S}; \frac{R_m}{2,4}\right)$ = 86 N/mm²

Allowable tensile stress - test conditions: $f_{test} = \frac{R_{p0,2,RT}}{S_{test}}$ = 133 N/mm²

Requirement: $1{,}7 \geq \frac{d_o}{d_i} =$ 1,09 OK.

Required shell thickness - design condition: $e_c = \frac{d_i \cdot p}{(2 \cdot f - p) \cdot k_c} + c_1 + c_2 =$ 2,8 mm

Required shell thickness - test conditions: $e_{test} = \frac{d_i \cdot p}{(2 \cdot f_{test} - p) \cdot k_c} + c_1 =$ 1,2 mm

Results: **OK**

B1.4 Wall thickness calculation of nozzle under internal pressure

Part name:	Body DN100, PN20, API Class 150		
Design data	Dimensions		
Material	1.4571		
Internal Pressure	P	[MPa]	2
max. Temperature	T	[°C]	500
Material reference	EN 10216-5/EN 10222-5		
Yield strength at room temperature RT	$R_{p0,2/RT}$	[N/mm²]	210
Yield strength at investigated temperature T	$R_{p0,2/T}$	[N/mm²]	129
Tensile strength ~20°C	$R_{m/20}$	[N/mm²]	500
max. body internal diameter	di,s	[mm]	158
Body shell thickness	es	[mm]	6,5
Nozzle internal diameter	di,b	[mm]	54,1
Nozzle shell thickness	eb	[mm]	3,2
Weld Joint Efficiency Factor	k_c	[-]	1,00
Safity factor (design conditions)	S	[-]	1,5
Safity factor (test conditions)	S_{test}	[-]	1,575
Throat of welding seam	m	[mm]	5

Allowable tensile stress - design condition: $f = min.\left(\frac{R_{p0,2,T}}{S}; \frac{R_m}{2,4}\right) =$ 86 N/mm²

Allowable tensile stress - test conditions: $f_{test} = \frac{R_{p0,2,RT}}{S_{test}} =$ 133 N/mm²

Effective lenght: Body $l_{S0} = \sqrt{(d_{i,S} + e_S) \cdot e_S} =$ 32,7 mm

Nozzle $l_{b0} = \sqrt{(d_{i,b} + e_b) \cdot e_b} =$ 13,5 mm

Valve body - effective Area: $A_{f,S} = e_S \cdot l_{So}$ 212,55 mm²

$A_{p,\,S} = 0{,}5 \cdot d_{i,S} \cdot (l_{So} + 0{,}5 \cdot di,_h)$ 4720,20 mm²

Diameter ratio - Nozzle: 0,34 < 0,7

$$\frac{d_{i,S}}{d_{i,b}} =$$

Nozzle - effective Area:	$A_{fb} = e_b \cdot (l_{bo} + e_S)$			64,13	mm²
				542,11	mm²
	$A_{p,\,b} = 0{,}5 \cdot d_{i.b} \cdot (l_{bo} + e_S)$				
Weld Seam effective Area:	$A_{fW} = 2 * m^2$			50	mm²
$p \cdot \left[\frac{A_{pS} + A_{p,b}}{A_{fS} + A_{fW} + A_{fb} \cdot k_c} + \frac{1}{2}\right] \leq f$	33	N/mm²	≤	86	N/mm²
$p \cdot \left[\frac{A_{pS} + A_{p,b}}{A_{fS} + A_{fW} + A_{fb} \cdot k_c} + \frac{1}{2}\right] \leq f_{test}$	33	N/mm²	≤	133	N/mm²
			Results:	**OK**	

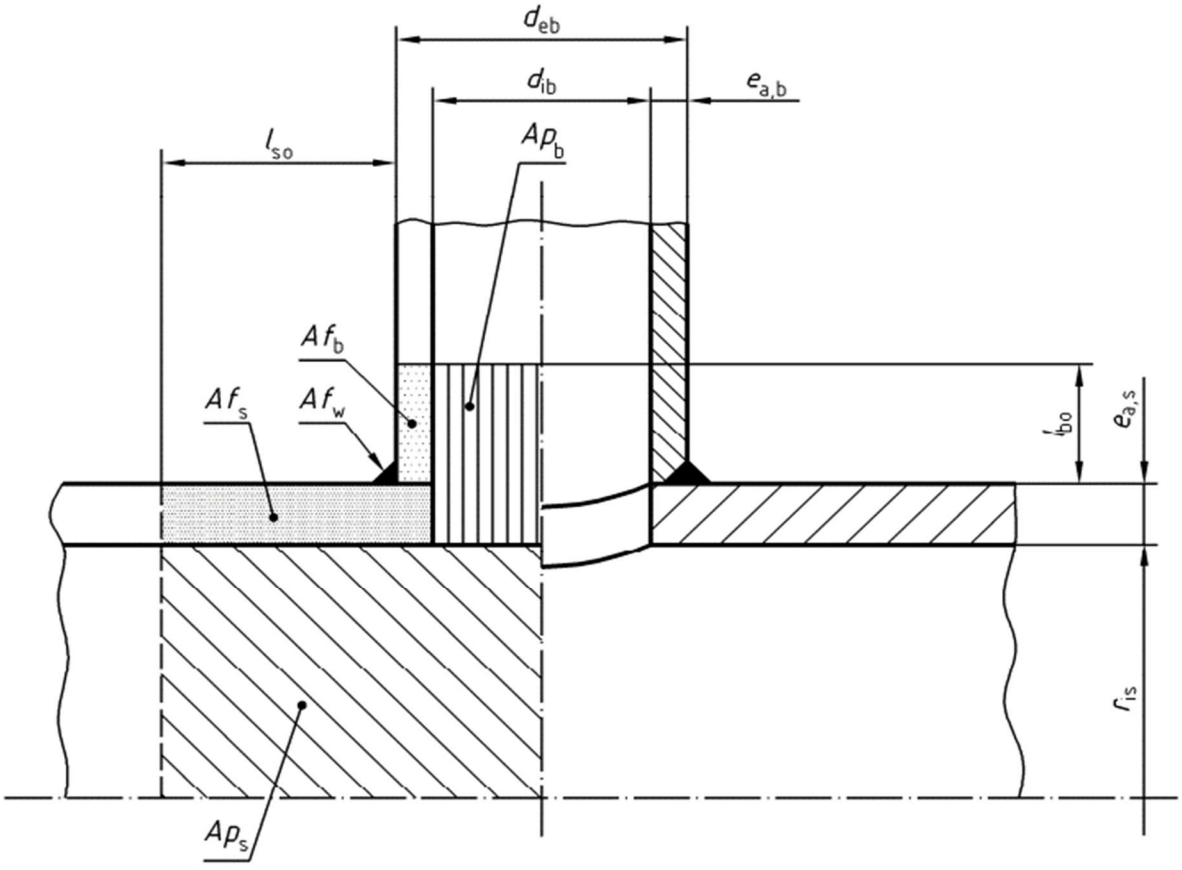

Figure B.4 - Nozzle shell thickness validation

B.1.5 Conical body under internal pressure

Part name:	Body closure DN100, PN20, API Class 150			
Design data		Dimensions		
Material		1.4571		
Internal Pressure		P	[MPa]	2
max. Temperature		T	[°C]	500
Material reference		EN 10216-5/EN 10222-5		
Yield strength at room temperature RT		$R_{p0,2/RT}$	[N/mm²]	210
Yield strength at investigated temperature T		$R_{p0,2/T}$	[N/mm²]	129
Tensile strength ~20°C		$R_{m/20}$	[N/mm²]	500
Weld Joint Efficiency Factor		k_c	[-]	1,0
max. internal diameter body		d_i	[mm]	157,0
min. outer diameter body		d_o	[mm]	171,0
min. shell thickness body	$e_a = (d_o-d_i)/2$	e_a	[mm]	7,0
min. shell thickness conical side part		e_{cK}	[mm]	6,5
Radius		r	[mm]	10
Conical side angle		j	[°]	60
Kegel - Berechnungsbeiwert		b	[-]	2,2
Tolerance coefficient		c_1	[mm]	0
Corrosion and wear surcharge		c_2	[mm]	1
Safety factor (design conditions)		S	[-]	1,5

Allowable tensile stress - design condition: $f = min.\left(\frac{R_{p0,2,T}}{S}; \frac{R_m}{2,4}\right) =$ 86 N/mm²

$e_a/d_o > 0,005$

$0,005 < \frac{e_a}{d_o} =$ 0,041

$\frac{r}{d_o} =$ 0,06

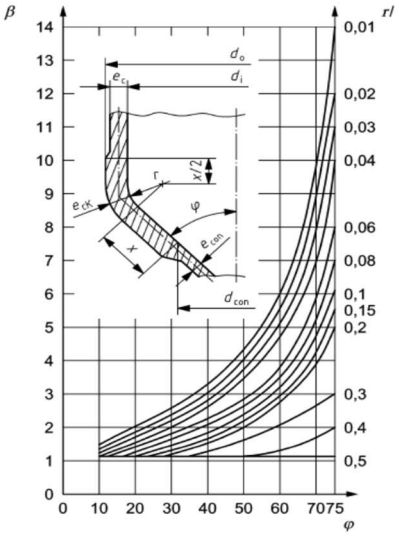

Winkel φ	β bei Verhältnis r/d_o												cos φ
	0,01	0,02	0,03	0,04	0,06	0,08	0,10	0,15	0,20	0,30	0,40	0,50	
10	1,4	1,3	1,2	1,2	1,1	1,1	1,1	1,1	1,1	1,1	1,1	1,1	0,985
20	2,0	1,8	1,7	1,6	1,4	1,3	1,2	1,1	1,1	1,1	1,1	1,1	0,940
30	2,7	2,4	2,2	2,0	1,8	1,7	1,6	1,4	1,3	1,1	1,1	1,1	0,866
45	4,1	3,7	3,3	3,0	2,6	2,4	2,2	1,9	1,8	1,4	1,1	1,1	0,707
60	6,4	5,7	5,1	4,7	4,0	3,5	3,2	2,8	2,5	2,0	1,4	1,1	0,500
75	13,6	11,7	10,7	9,5	7,7	7,0	6,3	5,4	4,8	3,1	2,0	1,1	0,259

Figure B.5 - Conical body under internal pressure EN 13445 Part 3

minimum wall thickness:	$e_{ac} = e_a - c_1 - c_2 =$	6,0	mm
Distance variable:	$x = \sqrt{d_o \cdot e_{ac}} =$	32,0	mm
Wall thickness brim - design condition:	$e_{cK} = \frac{d_o \cdot p \cdot \beta}{4 \cdot f \cdot k_c} =$	2,2	mm
Relevant diameter:	$d_{con} = d_o - 2 \cdot (e_{cK} + r \cdot (1 - cos\varphi) + x \cdot sin\varphi) =$	101,1	mm
Required cone shell thickness:	$e_{con} = \frac{p \cdot d_{con}}{(2 \cdot f - p) \cdot k_c} \cdot \frac{1}{cos\varphi} + c_1 + c_2 =$	3,4	mm

Results: **OK**

B.2 Design Calculation of investigated RGM for ball valve

This document is the design calculation according to requirements of EN 13445 Part 3

Scope:

- calculation of pressure-containing components of RGM and bellows according to standard EN 13445-3

- ratchet gear calculation according to standard DIN 3990-3

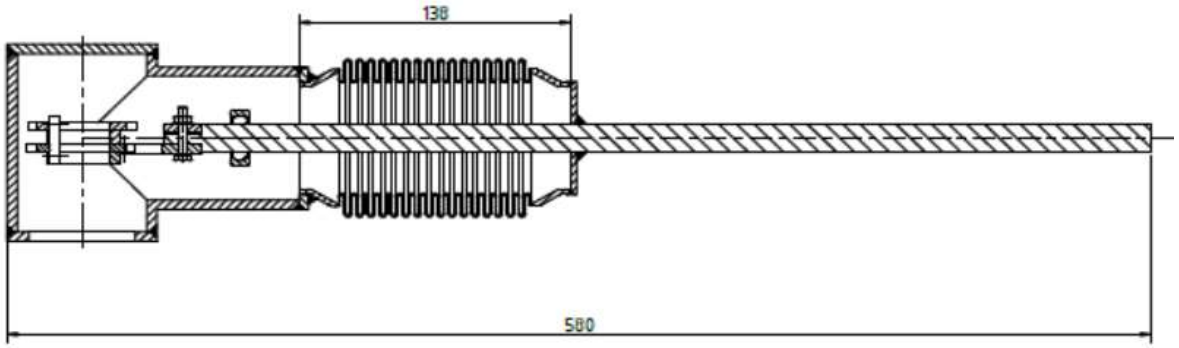

Figure B.6 - Ratchet gear mechanism drawing of ball valve DN 100

B.2.1 Validation of Ratchet Gear housing

	Ball valve with RGM (utility model)		
Design data	Dimensions		
Material	1.4571		
Diameter of vertical body	D_1	[mm]	76
Diameter of horisontal body	D_2	[mm]	76
Height of vertical body	H_1	[mm]	122
Height from weld seam of vertical shell to middle point of horizontal shell	H_2	[mm]	60
Thickness of vertical shell	t_1	[mm]	5
Thickness of horisontal shell	t_2	[mm]	5
Thickness of vertical body cover	t_3	[mm]	7
max. Temperature	T	[°C]	500
Material reference	EN 10216-5 / EN 10028-7		
Yield strength at room temperature RT	$R_{p0,2/RT}$	[N/mm²]	210
Yield strength at investigated temperature T	$R_{p0,2/T}$	[N/mm²]	129
Tensile strength ~20° C	$R_{m/20}$	[N/mm²]	500
Weld joint efficiency factor	k_c	[-]	1,00
Internal pressure	P	[MPa]	2,0
Horizontal length of ratchet gear body	L	[mm]	154,0
Length from middle line of vertical body to welding point of rod and bearing	LS	[mm]	78,0
Safety factor (design conditions)	S	[-]	1,5
Tolerance coefficient	c_1	[-]	0
Corrosion and wear surcharge	c_2	[-]	1
Throat of welding seam	m	[mm]	3

Allowable tensile stress - design condition: $f = min.\left(\frac{R_{p0,2,T}}{S}; \frac{R_m}{2,4}\right) =$ 86 N/mm²

Allowable tensile stress - test conditions: $f_{test} = \frac{R_{p0,2,RT}}{S_{test}} =$ 140 N/mm²

Requirement: $1,7 \geq \frac{d_{i,HS}}{d_{i,VS}} =$ 0,87 **OK**

required shell thickness - design condition: $e_c = \frac{d_i \cdot p}{(2 \cdot f - p) \cdot k_c} + c_1 + c_2 =$ 1,9 mm

required shell thickness - test conditions: $e_{test} = \frac{d_i \cdot p}{(2 \cdot f_{test} - p) \cdot k_c} + c_1 =$ 0,5 mm

Effective length: Vertical Body $l_{VS0} = \sqrt{(D_1 + t_1) \cdot t_1} =$ 18,8 mm

Horizontal body $l_{Hb0} = \sqrt{(D_2 - t_2) \cdot t_2} =$ 18,8 mm

RGM vertical shell - effective Area: $A_{f,VS} = t_1 \cdot l_{VSo} =$ 94,21 mm²

$A_{p,\,S} = 0{,}5 \cdot (D_1 - 2 \cdot t_1) \cdot (l_{VSo} + 0{,}5 \cdot (D_2 - 2 \cdot t_2)) =$ 1875,77 mm²

Nozzle - effective Area: $A_{fb} = t_2 \cdot (l_{Hbo} + t_1) =$ 119,21 mm²

$A_{p,\,b} = 0{,}5 \cdot (D_2 - 2 \cdot t_2) \cdot (l_{Hbo} + t_2) =$ 786,77 mm²

Weld seam effective Area: $A_{fW} = 2 * m^2 =$ 18 mm²

$$p \cdot \left[\frac{A_{pS} + A_{p,b}}{A_{fS} + A_{fW} + A_{fb} \cdot k_c} + \frac{1}{2}\right] \leq f$$ 24 N/mm² ≤ 86 N/mm²

$$p \cdot \left[\frac{A_{pS} + A_{p,b}}{A_{fS} + A_{fW} + A_{fb} \cdot k_c} + \frac{1}{2}\right] \leq f_{test}$$ 24 N/mm² ≤ 140 N/mm²

Results: **OK**

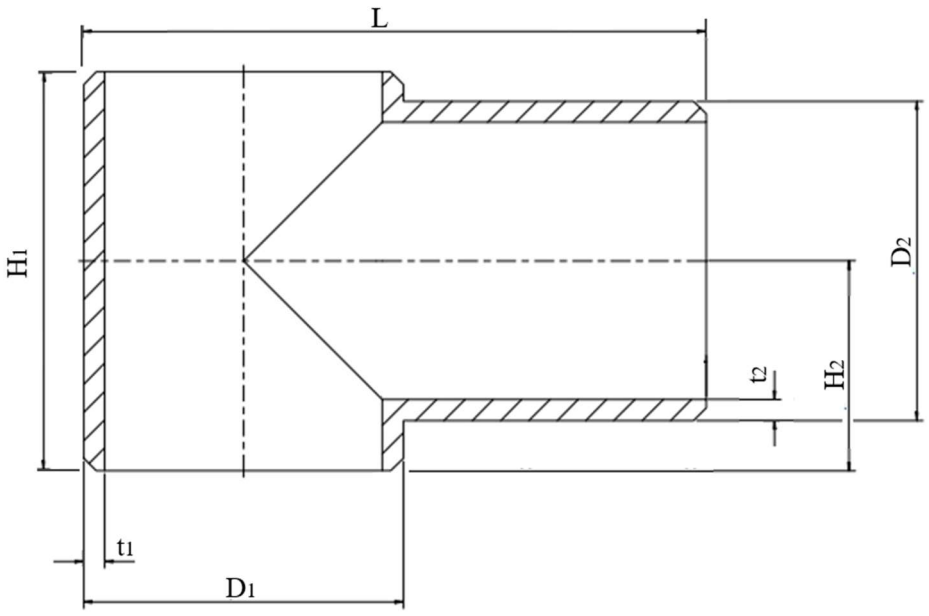

Figure B.7 - Ratchet gear mechanism housing

B.2.2 Validation of ratchet wheel

Part name:	Pawl for RGM of ball valve PN20, API Class 150		
Design data	Dimensions		
Material	1.4006		
Material reference	DIN EN 10088-3		
Diameter of wheel	D_G	[mm]	60
Diameter of wheel's hole	D_{Gh}	[mm]	28,1
Length of the key's pass	L_{GK}	[mm]	8
Width of the key's pass	b_{GK}	[mm]	3,3
Width of the ratchet wheel	b_G	[mm]	6
Number of ratchet wheel teeth	z	[mm]	40
max. Temperature	T	[°C]	500
Yield strength at room temperature RT	$R_{p0,2/RT}$	[N/mm²]	500
Yield strength at investigated temperature T	$R_{p0,2/T}$	[N/mm²]	255
Tensile strength ~20°C	$R_{m/20}$	[N/mm²]	700
Max. required stem torque	M_{total}	N·mm	26644,2
Length of the ratchet tooth	a_G	mm	6
Height of the ratchet tooth	h_G	mm	2,5

Module *m* of the ratchet wheel: $m = \frac{D_G}{z} =$ 1,5 mm

Tagential force: $F_G = \frac{M_{total}}{m \cdot z} =$ 444,07 N

The moment of resistance of pawl: $W = \frac{\omega \cdot (1{,}5 \cdot m)^3}{6} =$ 7,59 mm³

Coefficient characterizes the ratio of the width of the ratchet wheel to the module: $\omega = \frac{b_G}{m} =$ 4

Cross section of ratchet wheel tooth: $A_G = b_G \cdot a_G =$ 36 mm²

Maximal stress on ratchet wheel: $\sigma_G = \frac{F_G \cdot h_G}{W} + \frac{F_G}{A_G} =$ 158,53 N·mm²

Stress comparison: $\sigma_G < \sigma_{R0,2T}$ **OK**

Safety factor: $S = \frac{\sigma_G}{\sigma_{R0,2T}} \approx 1{,}6$

Validation of ratchet wheel: M (MAST ratchet wheel existing) = 42,86 N·m

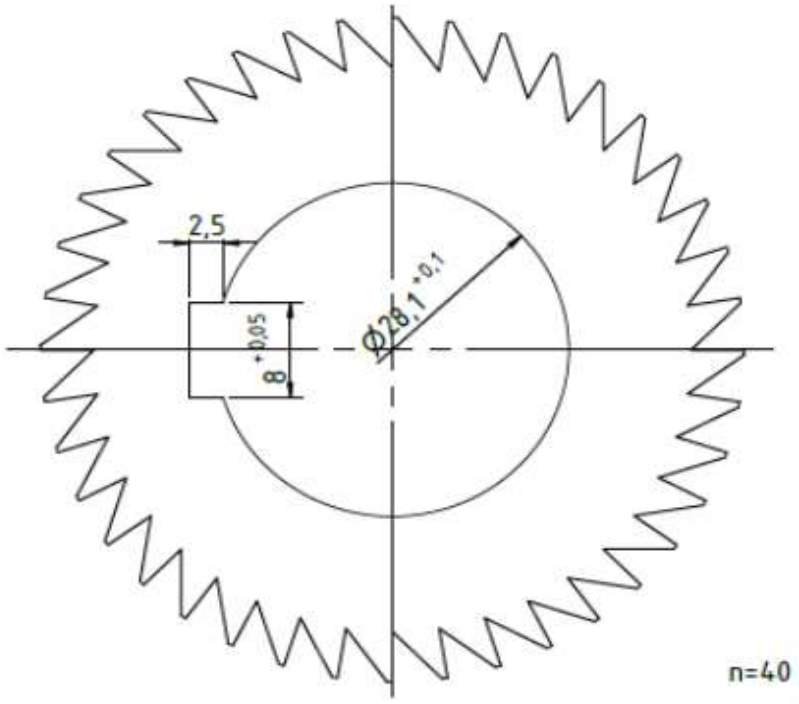

Figure B.8 - Sketch of ratchet wheel for RGM

B.2.3 Validation of pawl

Part name:	Pawl for RGM of ball valve PN20, API Class 150		
Design data	Dimentions		
Material	1.4006		
Length	L_P	[mm]	49,5
max. Temperature	T	[°C]	500
Material reference	DIN EN 10088-3		
Diameter of pawl	Dc	[mm]	18
Diameter of pawl's hole	Db	[mm]	5
Angle of pawl's body	Ab	[mm]	10
Angle of pawl's tooth	At	[mm]	15
Radius of pawl's tooth	Rh	[mm]	4
High of the pawls teeth	h_P	[mm]	6
max. Temperature	T	[°C]	500
Yield strength at room temperature RT	$R_{p0,2/RT}$	[N/mm²]	500
Yield strength at investigated temperature T	$R_{p0,2/T}$	[N/mm²]	255
Tensile strength ~20 °C	$R_{m/20}$	[N/mm²]	700
Circumferential force at the pawl's tooth	F_P	[N]	444,07
Length of the pawl's tooth	a_G	[mm]	4,5
Width of the pawl	b_G	[mm]	6

Moment on the tip of pawl's tooth:	$M_P = F_P \cdot h_P =$	2664,42	N·mm
Polar moment of resistance:	$W = \frac{b_P \cdot a^2}{6} =$	20,25	mm³
Maximal stress on pawl:	$\sigma_P = \frac{M_P}{W} =$	131,58	N/mm²

Stress validation: σ_G < $\sigma_{R0,2T}$ **OK**

Safety factor: $S = \frac{\sigma_G}{\sigma_{R0,2T}} \approx 1{,}9$

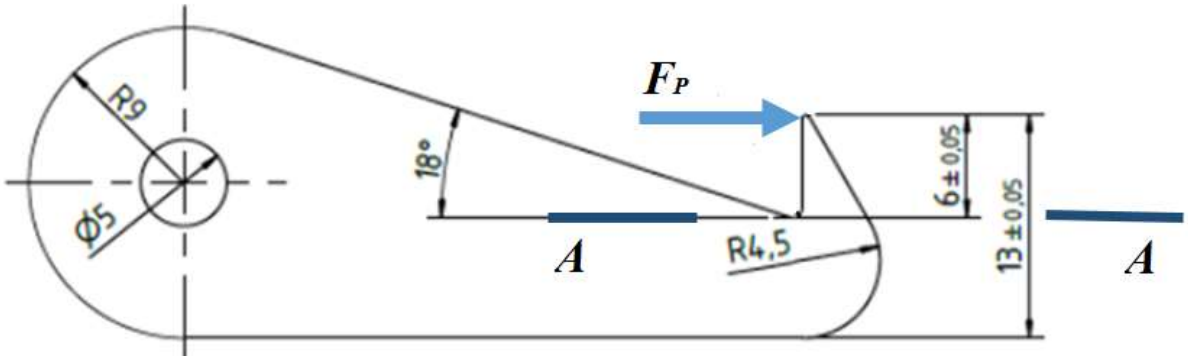

Figure B.9 - Sketch of pawl

B.2.4 Lever validation

Part name: Lever for RGM of ball valve PN20, API Class 150			
Design data	Dimentions		
Material	1.4006		
Material reference	DIN EN 10088-3		
max. Temperature	T	[°C]	500
Yield strength at room temperature RT	$R_{p0,2/RT}$	[N/mm²]	500
Yield strength at investigated temperature T	$R_{p0,2/T}$	[N/mm²]	255
Tensile strength ~20 °C	$R_{m/20}$	[N/mm²]	700
Max. force at the pawl from torsion of the ratchet wheel	F_P	N	444,07
Moment on the lever	M_L	N·mm	12868,14
Polar section modulus of lever cross section	W_L	mm³	98,17
Length from rod end bearing to the point of applied force	l_{L1}	mm	461
Length of lever from pawl to rod end bearing	l_{L2}	mm	30
Angle of pawl connection to lever	$sin\alpha$	°	75
The maximal allowable hand force	F_{Allow}	N	360
Diameter of the lever	D_L	mm	10

$$F_L \cdot l_{L1} = F_p \cdot sin\alpha \cdot l_{L2}$$

$$F_L = \frac{F_P \cdot sin\alpha \cdot l_{L2}}{l_{L1}} = \quad 27{,}91 \quad \text{N}$$

The maximal hand force required at the lever to apply the breakaway torque shall not exceed 360 N according to API 6D and 400 N according to EN 12570

F_L < F_{Allow} **OK**

Strength calculation:

sinα 0,96593

Moment at the bolt joint point of lever: $M_L = F_p \cdot sin\alpha \cdot l_{L2} =$ 12868 N·mm

Axial moment of resistance: $W_L = \frac{\pi \cdot D_L^3}{32} =$ 98,17 mm³

Maximal stress: $\sigma_{bL} = \frac{M_L}{W_L} =$ 131,07 N/mm²

Stress validation: σ_{bL} < $\sigma_{R0,2T}$ **OK**

Safety factor: $S = \frac{\sigma_{bL}}{\sigma_{R0,2T}} \approx 1{,}9$

Validation of lever: M (MAST existing lever) = 51,84 N·m

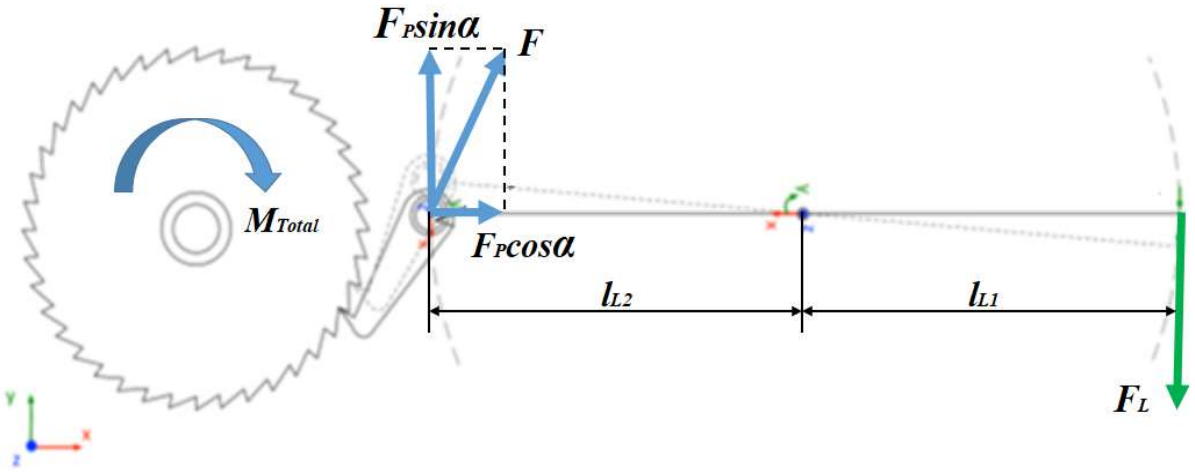

Figure B.10 - Analysation model of RGM

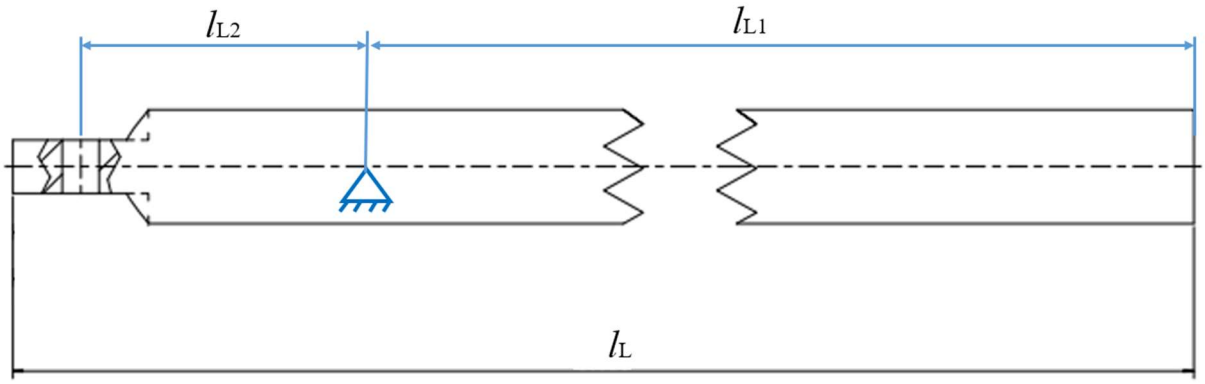

Figure B.11 - Sketch of investigated lever

B.2.5 Validation of stem key. Pressing and shearing - ISO 5211, DIN 6885

Design data	Dimensions		
Material reference	EN 10216-5 / EN 10028-7		
max. Temperature	T	[°C]	500
Yield strength at investigated temperature T- stem (1.4006)	$R_{p0,2TS}$	[N/mm²]	255
Yield strength at investigated T - ratchet wheel (1.4006)	$R_{p0,2TRG}$	[N/mm²]	255
Yield strength at investigated temperature T- key (1.1191)	$R_{p0,2TK}$	[N/mm²]	230
Moment on the key	M_{Total}	[N·mm]	25680
Diameter of top section of the stem	D_{ST}	[mm]	28
Hub depth - stem	t_S	[mm]	4
Key depth - stem	t_1	[mm]	4
Key depth - ratchet wheel	t_2	[mm]	3
Hight of the key	h	[mm]	7
Hub depth - ratchet wheel	t_{RG}	[mm]	3,3
Length of the key - stem	l_{1S}	[mm]	25
Length of the hub - ratchet wheel	l_{2RG}	[mm]	6
Number of keys	n_K	-	1

Pressing stem:

$$h_{SK} = \frac{D_S}{2} - t_1 + \frac{t_S}{2} = \quad 12 \quad \text{mm}$$

$$\sigma_{SK} = \frac{M_{total}}{l_{1S} \cdot t_1 \cdot h_{SK} \cdot n_K} = \quad 22{,}20 \quad \text{N·mm}^2$$

$$\sigma_{SK} \quad > \quad R_{P0,2TS} \quad \textbf{OK}$$

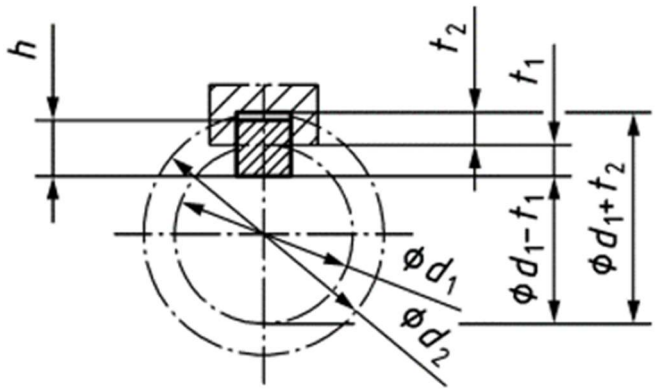

Figure B.12 - Investigated sketch of stem with a key

Pressing key:

$$h_{KRW} = \frac{D_{ST}}{2} - t_1 + h - \frac{t_2}{2} = \quad 15{,}5 \quad \text{mm}$$

$$\sigma_{RGK} = \frac{M_{Total}}{l_{2RW} \cdot t_2 \cdot h_K \cdot n_P} = \quad 95{,}50 \quad \text{N·mm²}$$

$$\sigma_{RGK} \quad > \quad R_{P0,2TRG} \quad \textbf{OK}$$

Shearing of key:

max. bending stress:

$$\sigma_{bK} = F_S \cdot h_K \cdot \frac{32}{\pi \cdot D_{STK}{}^3} = \quad 10{,}60 \quad \text{N/mm²}$$

$$F_S = \frac{2 \cdot M_{Total}}{D_{STK}} = \quad 1903{,}15 \quad \text{N}$$

max. shear stress:

$$\tau_{qL} = F_x \cdot \frac{4}{\pi \cdot d_{sko}{}^2} = \quad 3{,}09 \quad \text{N/mm²}$$

max. equivalent stress:

$$\sigma_{vS} = \sqrt{\sigma_{bL}{}^2 + 3 \cdot \tau_{qL}{}^2} = \quad 11{,}87 \quad \text{N/mm²}$$

$$\sigma_{vS} \quad > \quad R_{P0,2TK} \quad \textbf{OK}$$

Validation of stem sections: M (MAST key existing) = 71,15 N·m

Safity factor: $S_{xS} = \frac{R_{p0,2}}{\sigma_{RGK}} =$ 2,7

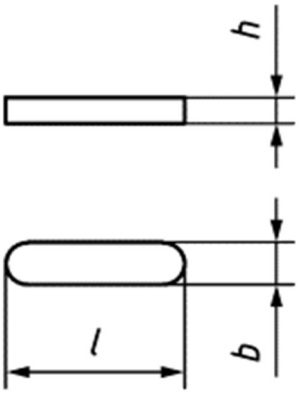

Figure B.13 - Round-faced key: (with hole for a retaining screw above the step line DIN 6885-1)

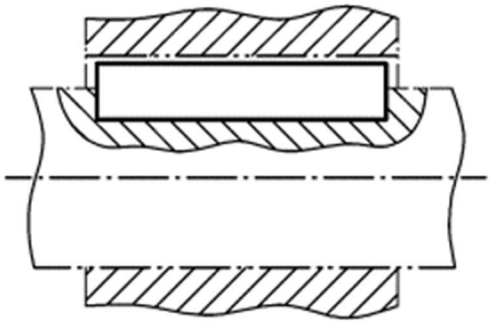

Figure B.14 - Cross-section through a feather key connection DIN 6885-1

B.2.6 Validation of the bold joint for shearing and pressing

Part name:	Bolt joint on the coupling lever and pawls, DN100, PN20, API Class 150		
Design data	Dimensions		
Material	1.4301		
Material reference	DIN EN ISO 3506-1		
max. Temperature	T	[°C]	500
Yield strength at room temperature RT	$R_{p0,2/RT}$	[N/mm²]	450
Yield strength at investigated temperature T	$R_{p0,2/T}$	[N/mm²]	240
Tensile strength ~20°C	$R_{m/20}$	[N/mm²]	700
Max. force at the pawl from torsion of the ratchet wheel	F_P	N	444,07
Number of bolt joints	n_S	-	1
Diameter of the bolt	d_S	[mm]	5
Width of the pawl	t_1, t_3	[mm]	6
Width of the end of the lever	t_2	[mm]	5

Validation of the bold joint for shearing:

$$F_{s\,max} = R_{R0,2T} \cdot A_S \cdot n_S = \quad 4712{,}39 \quad \text{N}$$

$$A_S = \frac{\pi \cdot d_S^2}{4} = \quad 19{,}63 \quad \text{mm}^2$$

$$F_{Smax} \quad < \quad F_P \quad \textbf{OK}$$

Validation of the bold joint for pressing:

$$F_{Cmax} = \sigma_{R0,2T} \cdot d_S \cdot \sum t \quad 13200 \quad \text{N}$$

$$F_{Cmax} \quad < \quad F_P \quad \textbf{OK}$$

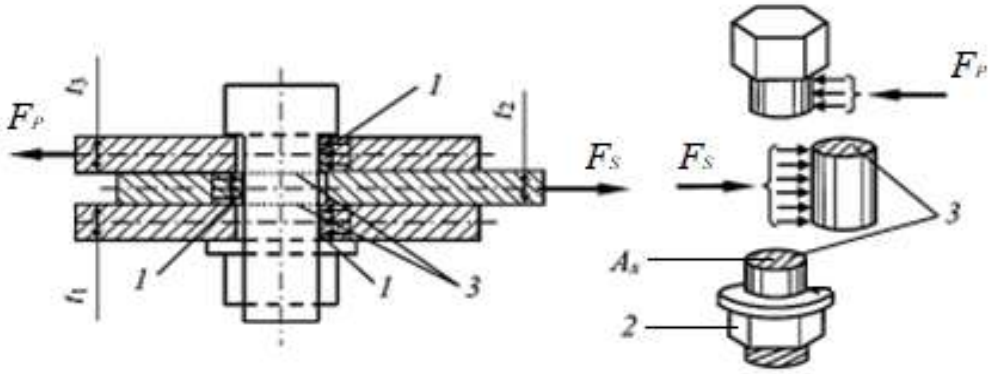

Figure B.15 - Cross section of bolt joint of pawl-lever-pawl

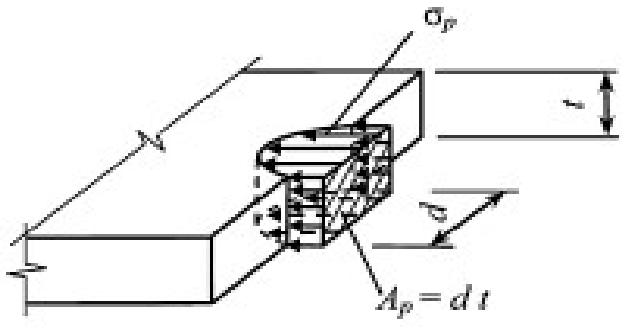

Figure B.16 - Area of pressing of the bolt joint

B.2.7 Validation of rod and bearing

Part name:	Rod end Bering 10, DN100, PN20, API Class 150		
Design data	Dimensions		
Material	1.4301		
Material reference	DIN EN ISO 3506-1		
max. Temperature	T	[°C]	500
Yield strength at room temperature RT	$R_{p0,2/RT}$	[N/mm²]	450
Yield strength at investigated temperature T	$R_{p0,2/T}$	[N/mm²]	240
Tensile strength ~20°C	$R_{m/20}$	[N/mm²]	700
Rod end bearing ball hole diameter	d	[mm]	10
Inner ring width	B	[mm]	9
Width of the rod end head	$C_{1\ max}$	[mm]	7
Rod end bearing ball diameter	dK	[mm]	16
Thread dimensions	Greb	[mm]	M10x1,5
Rod end head diameter	d_2	[mm]	29
Height of rod end bearing to middle point of ball	h_1	[mm]	48
Length of rod end bearing tread	l_3	[mm]	26
Length of rod end bearing	l_4	[mm]	62,5
Length from beginning of tread to middle point of ball	l_7	[mm]	15
Force on lever	$F_P \cdot sin\alpha$	[N]	428,94
Force on lever	$F_P \cdot cos\alpha$	[N]	114,93

Rod end bearing maximal possible angle of tilt (α):

$$\alpha_{reb} = sin^{-1}\left(\frac{B}{d}\right) - sin^{-1}\left(\frac{C_1}{d}\right) = \quad 19{,}73 \quad °$$

Race material compressive strengths:

$$F_{Preb\,max} = d_K \cdot C_1 \cdot R_{p0,2/T} = \quad 26880 \quad N$$

$$F_{Preb\,max} \quad > \quad F_P \cdot sin\alpha \quad \textbf{OK}$$

Rod end head strength insert construction:

$$F_{reb\,max} = (d_2 \cdot (d_K + 0{,}176 \cdot C_1)) \cdot C_1 \cdot R_{p0,2/T} = \quad 839543{,}04 \quad N$$

$$F_{reb\,max} \quad > \quad F_P \cdot sin\alpha \quad \textbf{OK}$$

Shank strength threaded rod end: $F_{tread\,max} = (R_{tread}^2 \cdot 0{,}78) \cdot R_{p0,2/T} = \quad 1591{,}2 \quad N$

$$F_{tread\ max} \quad > \quad F_P \cdot cos\alpha \quad \textbf{OK}$$

Axial strength: $F_{Axial\ reb\ max} = 0{,}78 \cdot ((d_K + 0{,}176 \cdot C_1)^2 - d_K^2) \cdot R_{p0,2/T} =$ 7664,31 N

$$F_{Axial\ reb\ max} \quad > \quad F_P \cdot cos\alpha \quad \textbf{OK}$$

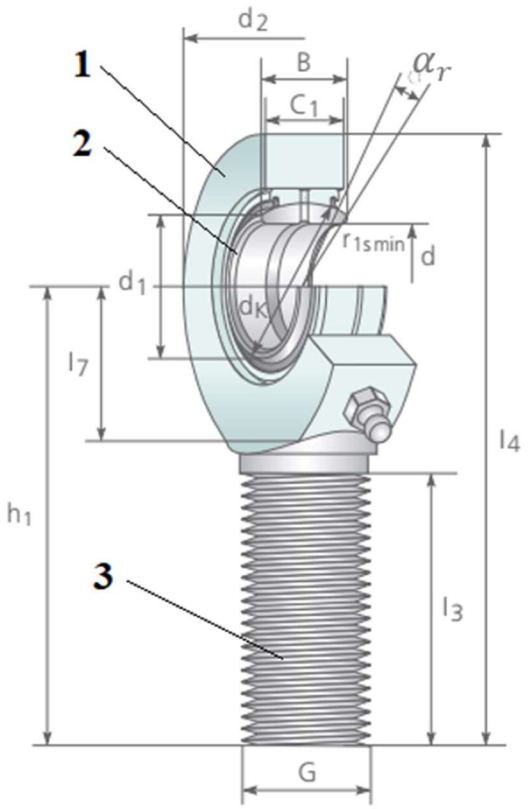

Figure B.17 - Rod end bearing investigated design

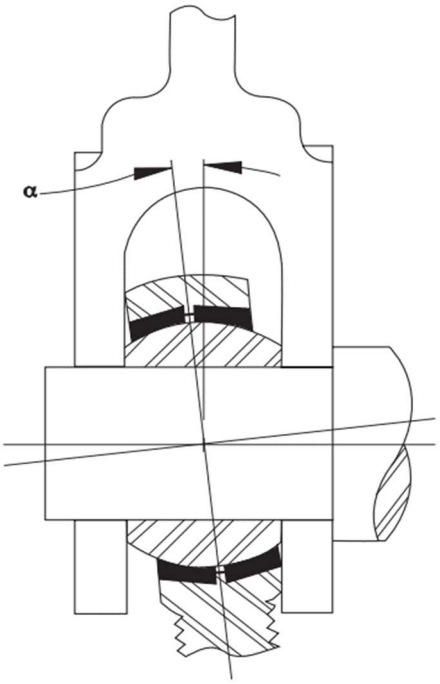

Figure B.17 - Rod end bearing angle of tilt (α)

Attachment C

Technical drawings of investigated ball valve with the ratchet gear mechanism of nominal diameter 100 mm (DN 100, PN 16, Class 150) [4]

26	1	Bellows cover	EN 13445-3	1.4571
25	1	Horisontal housing cover	EN 13445-3	1.4571
24	1	Rod end bering (10 mm)	ISO 12240-4	1.4301
23	1	Nut	DIN 934	A2-70
22	1	Screw	DIN 7984	A2-70
21	1	Feather key	DIN 6885-1	1.4301
20	1	Lever	-	1.4006
19	2	Pawl	EN ISO 3183	1.4006
18	2	Ratchet wheel	EN ISO 3183	1.4006
17	1	Bellows Hydra BE 356230-bb 68	EN 13445-3	1.4571
16	1	Horisontal housing (Pipe)	EN 13445-3	1.4571
15	1	Upper vertical housing cover	EN 13445-3	1.4571
14	1	Vertical housing (Pipe)	EN 13445-3	1.4571
13	1	Down vertical housing cover	EN 13445-3	1.4571
Ratchet gear mechanism part list				
12	1	Stem seal gasket	-	Graphite
11	1	Stem seal ring	-	Graphite
10	1	Stem sliding ring	-	1.4571
9	1	Stem Bearing	-	1.4571
8	24	Spring	EN ISO 2162-1	1.4301
7	1	Stem Packing	-	1.4571
6	1	Peg (housing)	EN 13445-3	1.4571
5	1	Stem	EN 13445-3	1.4006
4	2	Seat (ball seat)	-	1.4571
3	1	Ball (DN 100)	EN 13445-3	1.4571
2	2	Body closure	EN 13445-3	1.4571
1	1	Ball valve housing	EN 13445-3	1.4571
Ball valve part list				
Pos.	Quantity	Part Name	Standard	Material

	Date:	Name:	Material:	Material certivicate:	
Draw	01.05.2022	Oleynikov			
Check					
Note protection notice according to DIN ISO 16016		General tolerances according to DIN ISO 2768-mk		Drawings Nr.:	
Ball Valve with ratchet gear mechanism (Part List)				Article Nr.:	
				Status:	
				Language: EN	Sheet: 1/3

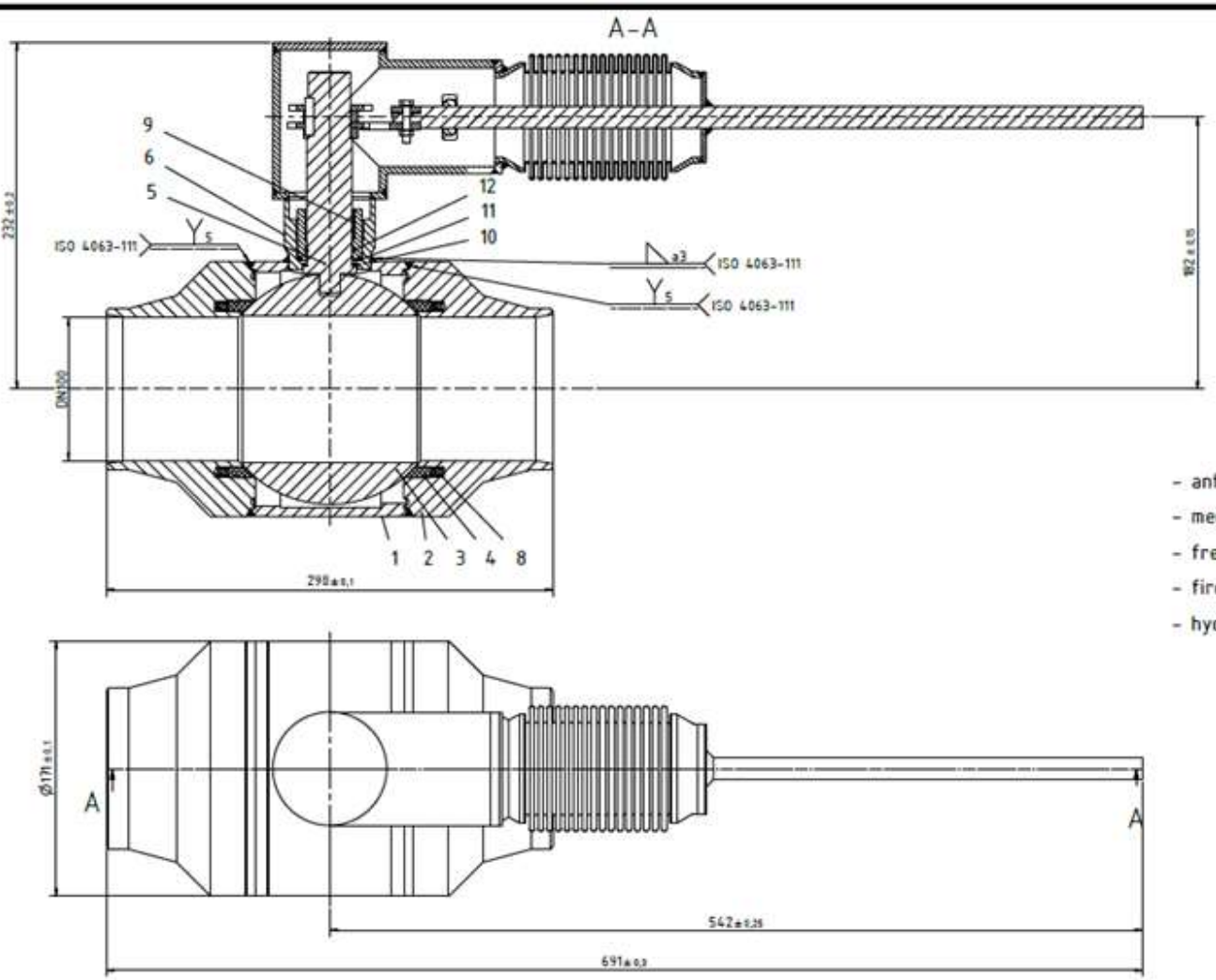

- anti-static-design-
- medium temperature = -271 °C up to +500 °C -
- free of non-ferrous metals -
- fire-safe-design -
- hydrogen design -

	Datum	Name	Werkstoff:	Werkstoff-Abnahme:	
Gez.	01.05.2022	oleynikov			
Gepr.					
Schutzvermerk nach DIN ISO 16016 beachten		Allgemeintoleranzen nach DIN ISO 2768-mK		Gewicht: N/A	Zeichnungs-Nr.: 0100001

Benennung:

Ball Valve
with ratchet gear mechanism

Artikel-Nr.: 1010-0100001

Rev.: | Status:

Maßstab	Sprache	Blatt
1:4	DE	2/3

A-A

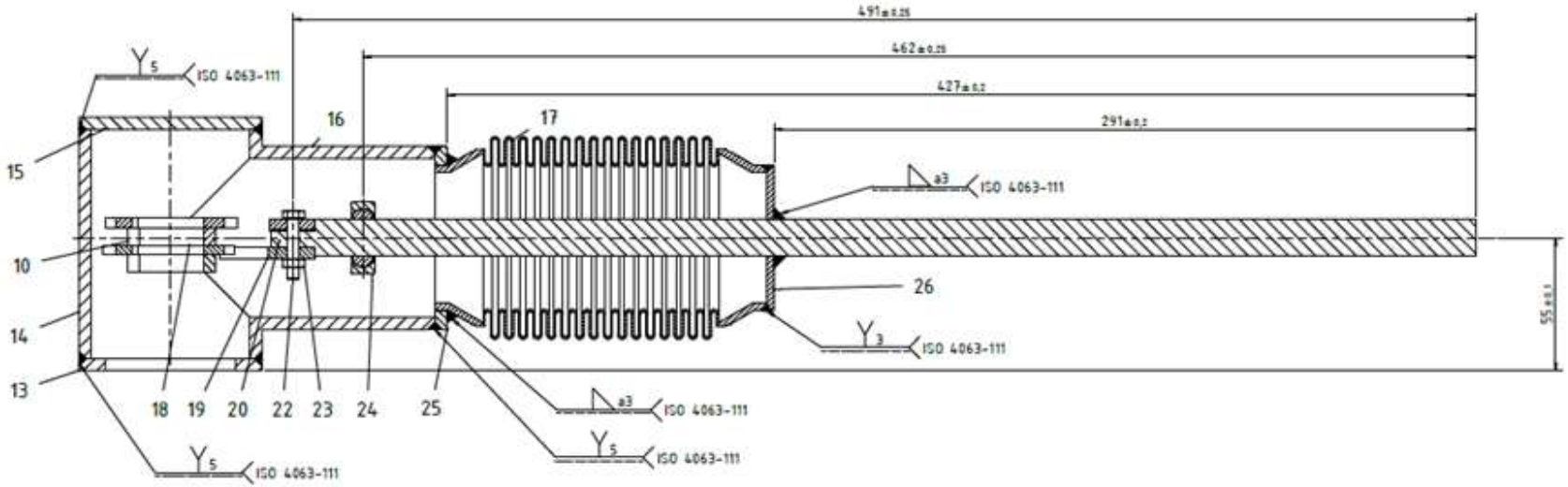

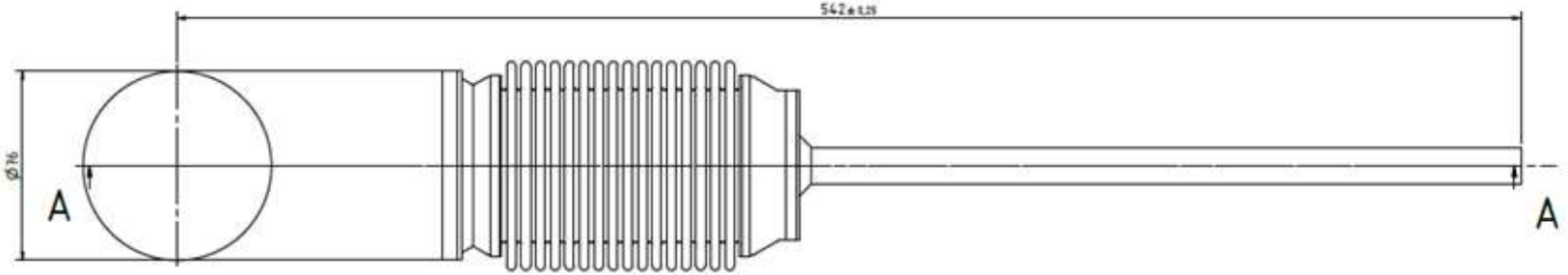

- medium temperature = -271 °C up to +500 °C -
- free of non-ferrous metals -
- fire-safe-design -
- hydrogen design -
- ratchet gear mechanism assembling all parts and weld, before installation on the ball valve -

	Datum	Name	Werkstoff:	Werkstoff-Abnahme:	
Gez.	01.05.2022	oleynikov			
Gepr.					
Schutzvermerk nach DIN ISO 16016 beachten		Allgemeintoleranzen nach DIN ISO 2768-mK		Gewicht: N/A	Zeichnungs-Nr.: 0100002
Benennung: Ratchet gear mechanism with bellows					Artikel-Nr.: 1020-0100002
					Rev.: Status:
				Maßstab: 1:2	Sprache: DE	Blatt: 3/3

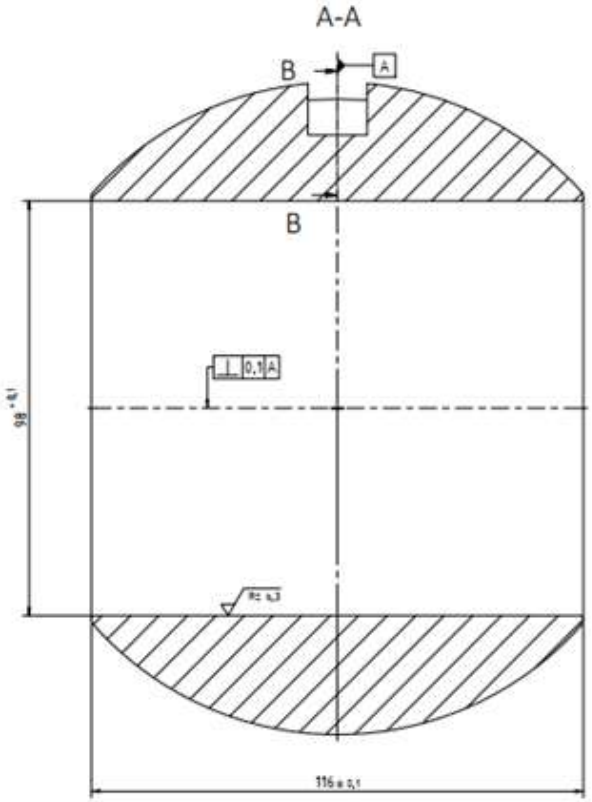

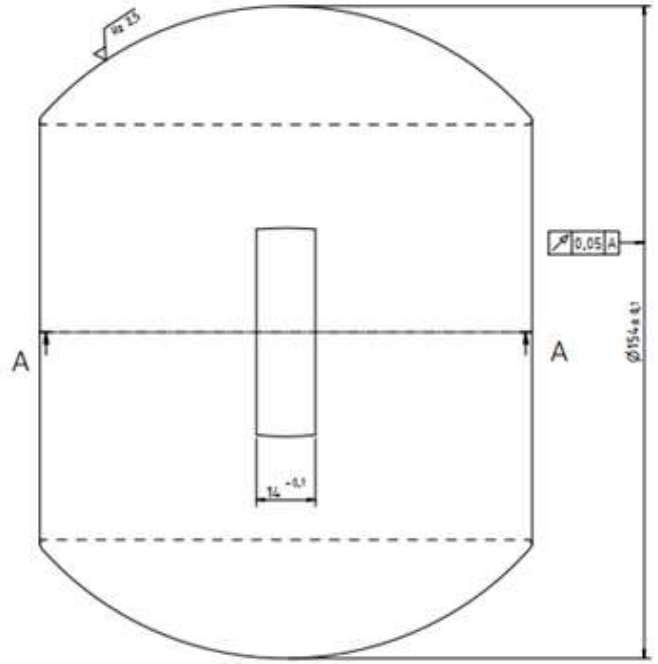

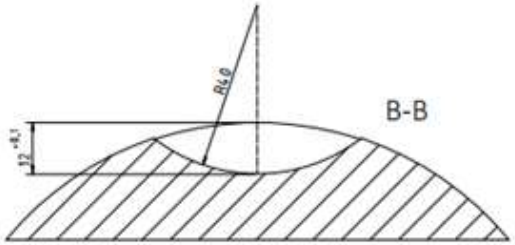

- All sharp edges grinded -

- Ball roundness tolerance according DIN 5401 = 35 𝒜m -

	Datum	Name	Werkstoff:	Werkstoff-Abnahme:	
Gez.	10.06.2020	oleynikov	1.4006		
Gepr.					
Schutzvermerk nach DIN ISO 16016 beachten: ©Böhmer GmbH			Allgemeintoleranzen nach DIN ISO 2768-mK	Gewicht: 6,883 kg	Zeichnungs-Nr.: 0100964
Benennung: Ball					Artikel-Nr.: 3060-0100963
Bezeichnung:					Rev.: 00 Status:
					Maßstab: 1:2 Sprache: DE Blatt: 1/1

A-A

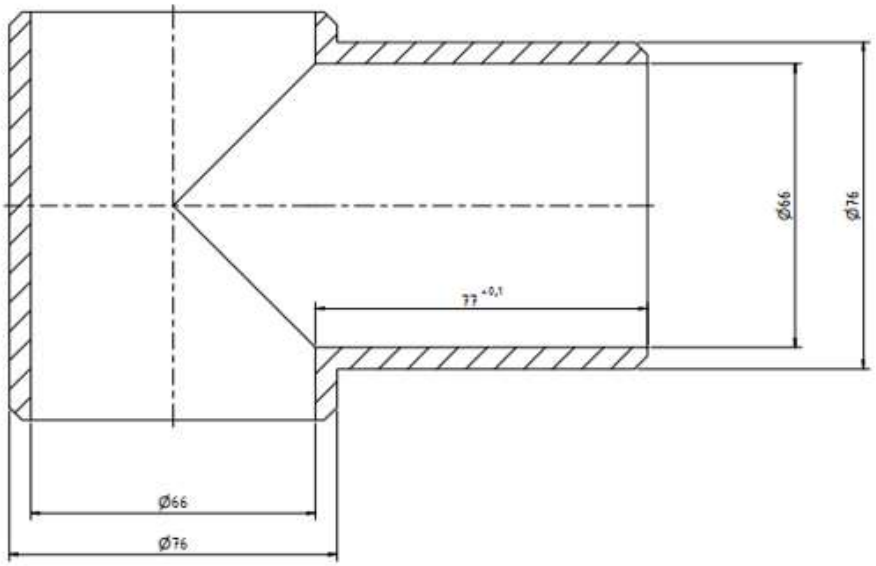

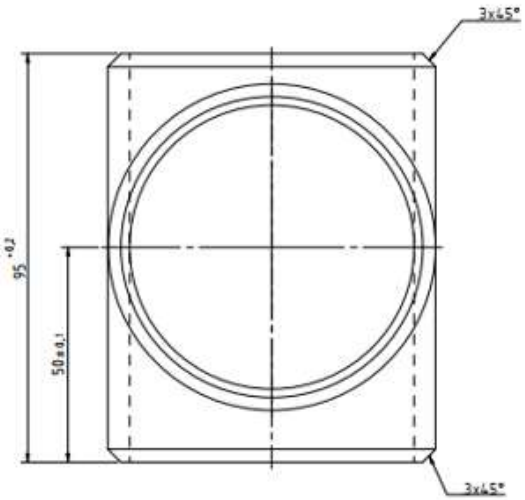

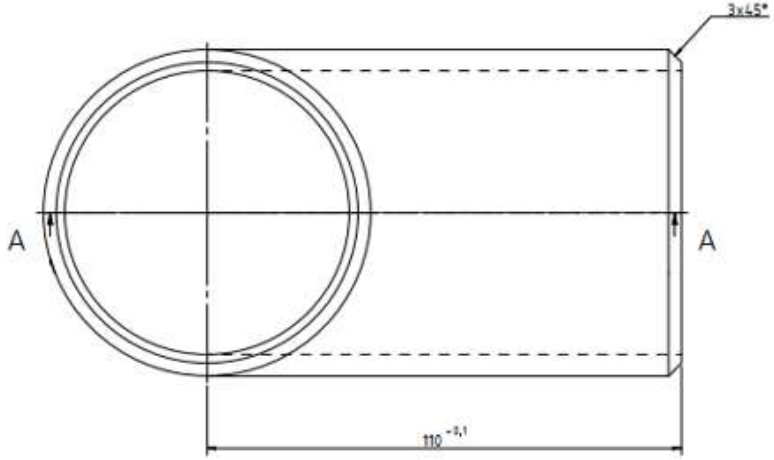

- Weld preparation according to EN ISO 9692-4 -

- All sharp edges grinded -

	Datum	Name	Werkstoff:	Werkstoff-Abnahme:	
Gez.:	10.06.2020	oleynikov	1.4571		
Gepr.:					
Schutzvermerk nach DIN ISO 16016 beachten: ©Böhmer GmbH			Allgemeintoleranzen nach DIN ISO 2768-mK	Gewicht: 1,382 kg	Zeichnungs-Nr.: 0100102
Benennung: Ratchet gear mechanism housing					Artikel-Nr.: 3010-0100102
Beschreibung:					Rev.: 00 / Status: In Bearbeitung
					Maßstab: 1:1,5 / Sprache: DE / Blatt: 1/1

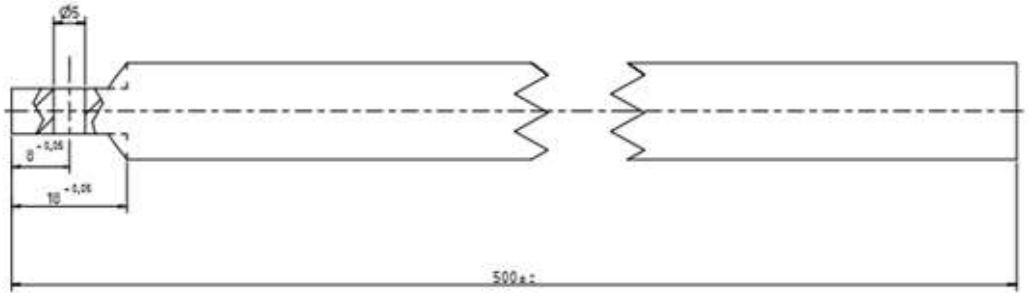

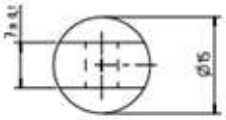

- Primary material: rod 15 mm -

- Material: stainless steel 1.4006 -

- Saw size: 502 mm -

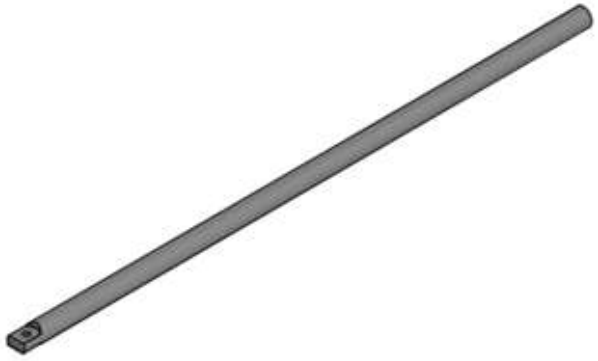

- All sharp edges grinded -

	Datum	Name	Werkstoff	Werkstoff-Abnahme	
Gez.	10.06.2020	oleynikov	1.4006		
Gepr.					
Schutzvermerk nach DIN ISO 16016 beachten: ©Böhmer GmbH		Allgemeintoleranzen nach DIN ISO 2768-mK	Gewicht 0,687 kg	Zeichnungs-Nr.: 0200020	
Benennung: Lever				Artikel-Nr.: 3020-0200020	
Bezeichnung:				Rev.: 00	Status:
				Maßstab: 1:1	Sprache: DE	Blatt: 1/1

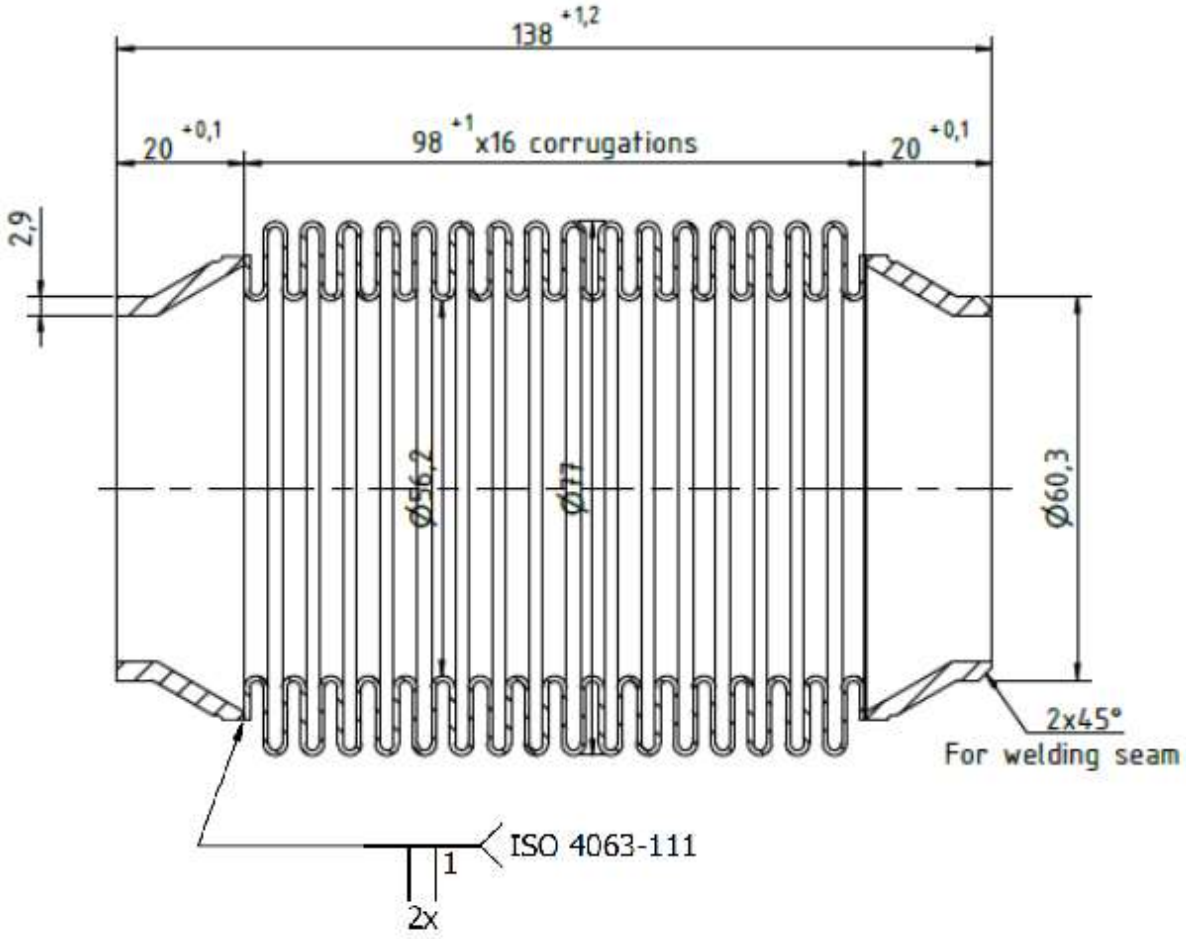

Produced from the bellows company Witzenmann
Hydra Bellows type BE 356230-bb

-All sharp edges grinded-
-Oil free finish, for weldig according to ISO 4063-111

	Datum	Name	Werkstoff	Werkstoff-Abmessung
Dez.	09.06.2020	olesynikov	Steinless steel 1.4571	
Gepr.				
Schutzvermerk nach DIN ISO 16016 beachten ©Bühner GmbH		Allgemeintoleranzen nach DIN ISO 2768-mK	Gewicht: 0,806 kg	Zeichnungs-Nr.
Benennung: Bellows				Artikel-Nr.
Bezeichnung:				Rev.: 00 Status:
				Maßstab: 1:2 Sprache: DE Blatt: 1/1

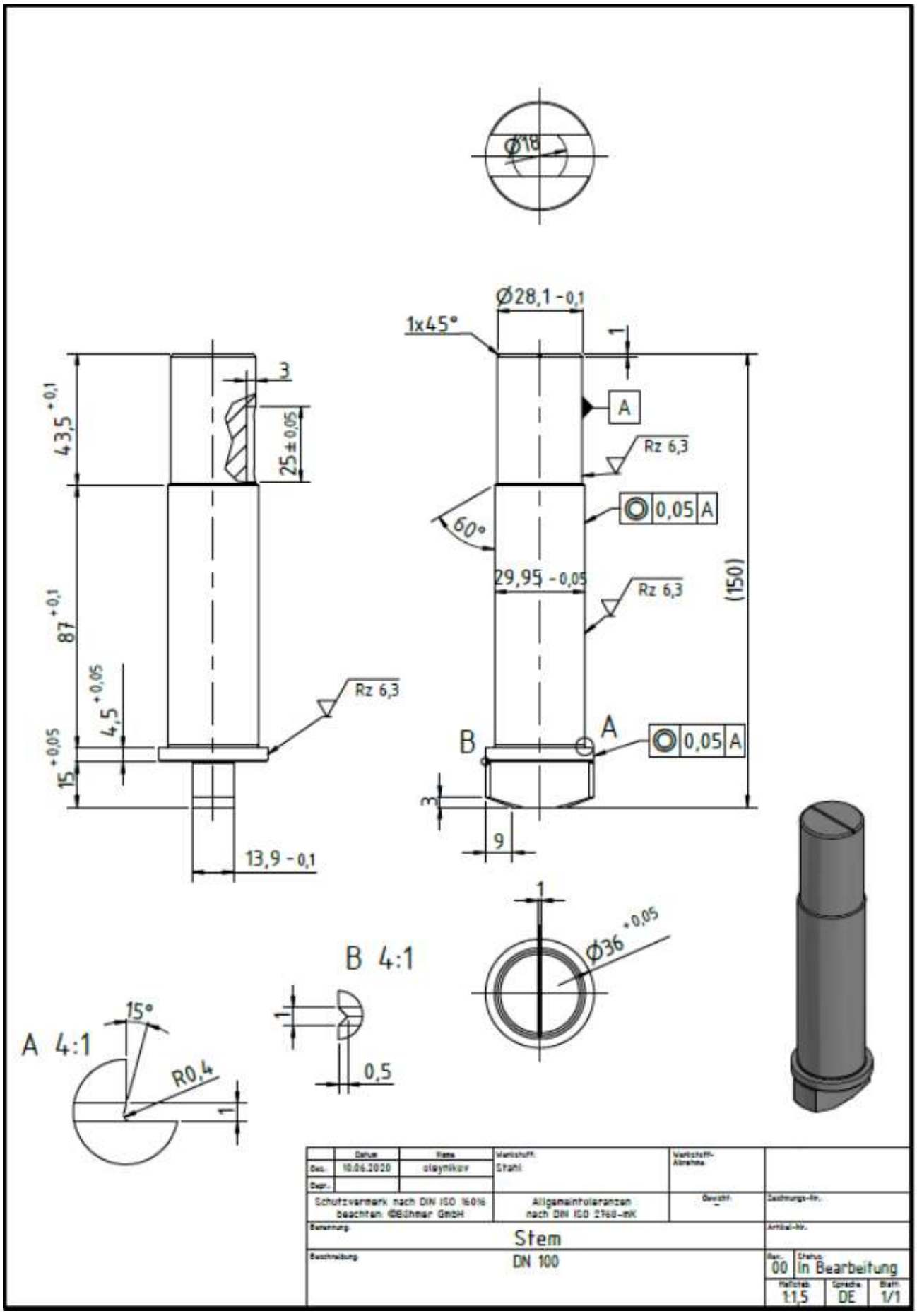
Ø18
Ø28,1 -0,1
1x45°
1
3
43,5 +0,1
25±0,05
A
Rz 6,3
0,05 A
60°
29,95 -0,05
Rz 6,3
(150)
87 +0,1
4,5 +0,05
15 +0,05
Rz 6,3
B
A
0,05 A
3
9
13,9 -0,1
B 4:1
1
Ø36 +0,05
A 4:1
15°
R0,4
1
1
0,5
Datum
Name
Gez.
10.06.2020
olaynikov
Werkstoff:
Stahl
Werkstoff-Abnahme
Schutzvermerk nach DIN ISO 16016 beachten: ©Bühler GmbH
Allgemeintoleranzen nach DIN ISO 2768-mK
Gewicht:
Zeichnungs-Nr.
Benennung
Stem
Artikel-Nr.
Bezeichnung
DN 100
Rev.
00
Status
In Bearbeitung
Maßstab
1:1,5
Sprache
DE
Blatt
1/1

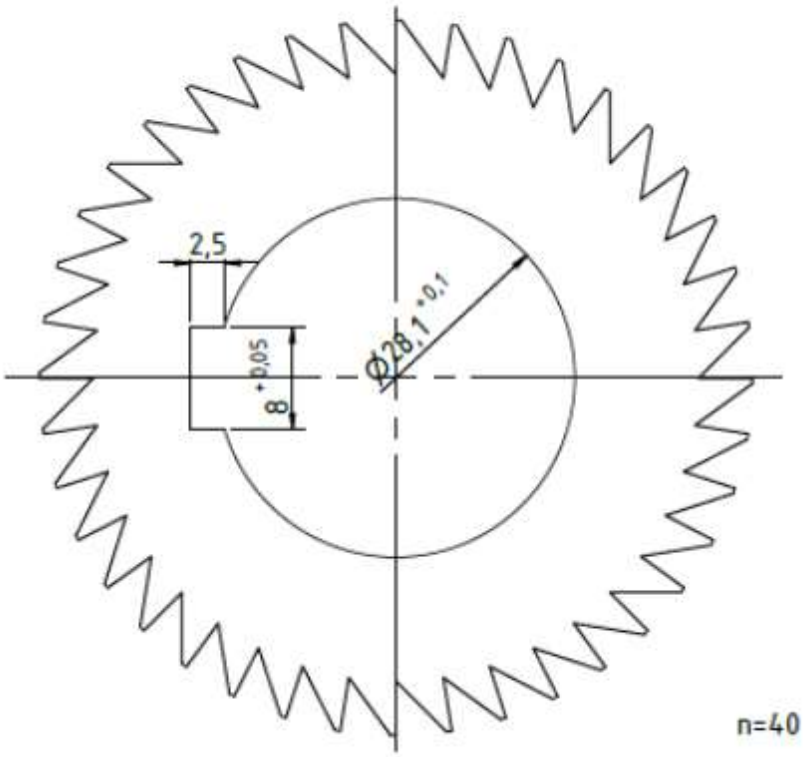

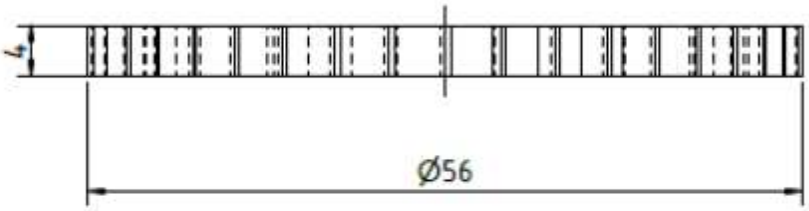

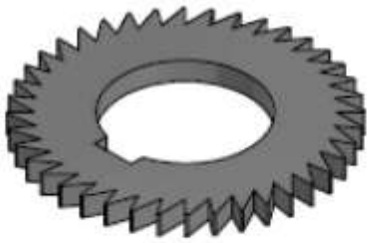

	Datum	Name	Werkstoff	Werkstoff-Abnahme	
Ges.	10.06.2020	olaynikov	Stahl		
Bearb.					
Schutzvermerk nach DIN ISO 16016 beachten: ©BÜhner GmbH			Allgemeintoleranzen nach DIN ISO 2768-mK	Gewicht 0,047 kg	Zeichnungs-Nr.
Benennung: Ratchet wheel					Artikel-Nr.
Beschreibung:					Rev. 00 Status: In Bearbeitung
					Maßstab 2:1 Sprache DE Blatt 1/1

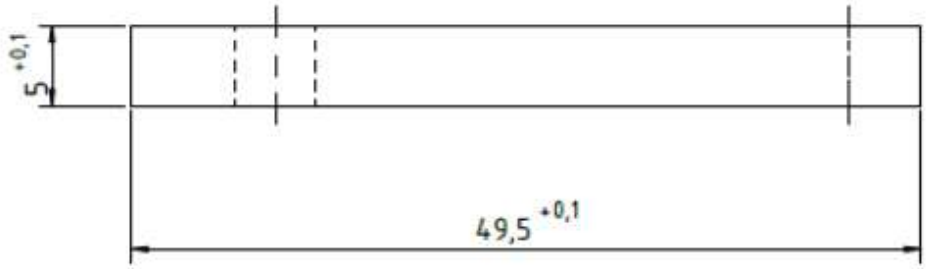

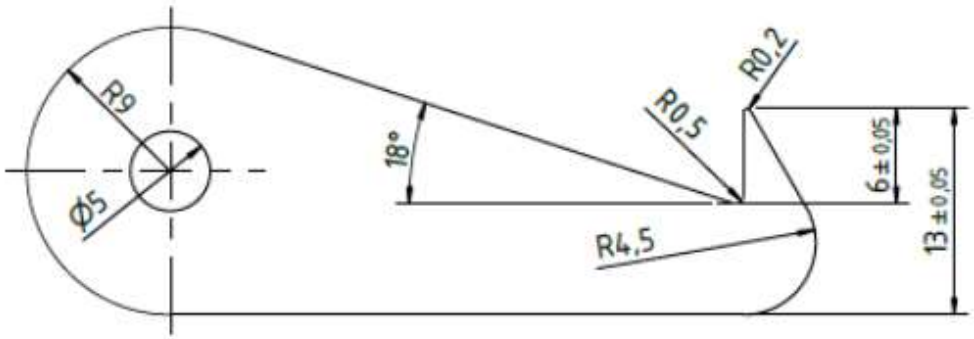

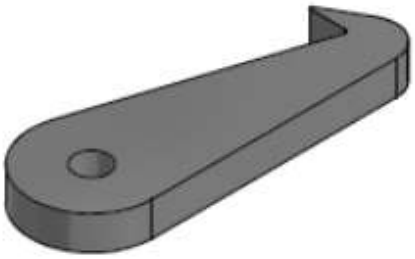

	Datum	Name	Werkstoff	Werkstoff-Abnahme	
Ges.	10.06.2020	olaynikov	Stahl		
Gepr.					
Schutzvermerk nach DIN ISO 16016 beachten. ©Bühmer GmbH		Allgemeintoleranzen nach DIN ISO 2768-mK	Gewicht 0,024 kg		Zeichnungs-Nr.
Benennung: Pawl					Artikel-Nr.
Bezeichnung					Rev. 00 Status: In Bearbeitung
					Maßstab 2:1 Sprache DE Blatt 1/1